University of Glasgow

Development of Fast Multi-System Simulation Models for Permanent Magnet Synchronous Motor and Generator Drive Systems

by

Peter Obongha Ohiero
M. Tech (Electrical Engineering)

Submitted to the School of Engineering, College of Science and Engineering, The University of Glasgow in fulfilment of the requirements for the Degree of

Doctor of Philosophy

in

Electronics and Electrical Engineering

July 2015

Abstract

This research project investigates the development and validation of alternative simulation models for voltage source inverter fed permanent magnet synchronous machine drive systems which can rapidly and accurately analyse and evaluate the performance of PM machine drives and associated control system designs.

Traditionally simulations have been conducted using switching models and state space average value methods. The simulation of switching models is time consuming and that of state space averaging involves complex mathematical transformation to d-q axis, with additional circuitry and this limits their application in a time critical design process. Even if the complex calculations of state space are overcome, the proposed model can still achieve better results.

This thesis presents the development of fast multi system simulation models for permanent magnet synchronous motor and generator drive systems. The fast simulation model: Average Voltage Estimation Model (AVEM) was developed for two-level, three phase VSI-fed PMSM drive systems and two-level three phase full-scale back-back VSI incorporated in a PMSG wind energy conversion system. The method uses the principle of control strategy and switching function to derive the average phase voltage in one switching period and then uses the average voltages to drive piecewise-linear voltage sources across the terminals of the permanent magnet synchronous machine and three phase system. A voltage source inverter loss model was also developed and incorporated into the AVEM to simulate the drive system power flow and its performance evaluated. The average voltage estimation model is also used to estimate and simulate the energy output of the variable speed PMSG wind energy conversion system. Practical implementation of this technique is achieved using a DSP based controller and validation made through comparison of the DSP AVEM energy estimation method with calculated energy.

The study also presents the development of detailed VSI switching models for a variable speed PMSM and a PMSG wind energy conversion system which serve as benchmarks for the proposed AVEM models. A detailed description of both models will be presented. Since models require a control strategy: these control strategies were also developed using the carrier-based sinusoidal (SPWM) and implemented with PI regulators. In the

permanent magnet synchronous generator wind energy conversion system application, the SPWM is applied to control the speed of the generator side converter to track maximum power as wind speed varies using the developed passive MPPT control technique and controls the AC load side converter to maintained constant DC link voltage. The sinusoidal PWM control provides a simplified control suitable for the variable speed PMSM drive system and the PMSG wind energy conversion system.

Lastly, this thesis presents a detailed development of an experimental test rig. The test rig is developed to provide flexibility for the validation and comparison of the results of both simulation models against real practical implementations for PMSM drive system and PMSG wind energy conversions system.

Several simulation case studies were performed using the PORTUNUS simulation package to validate and analyse the steady state accuracy of the proposed average voltage estimation model and control system against the switching model. Experiments were also carried out to validate the results of the simulation models. The simulation models results are presented and compared with experimental results. Suitable steady state performance analysis of two-level, three phase voltage source inverter fed permanent magnet synchronous motor and two-level three phase full scale back-back voltage source inverter with permanent magnet synchronous generator drive simulation and experimental performance are also carried out. The results show good agreement of the proposed average voltage estimation model with the switching model and experimental data, and where necessary the reasons for differences are discussed. The simulation of the AVEM is approximately 50 times faster than the switching model. The limitation of the proposed model is also discussed; mainly it cannot be used for the study and analysis of the internal dynamics of the voltage source inverter.

The results from the proposed modelling method utilising the average voltage estimation confirm that this method can be used as an alternative to the detailed switching model for fast simulation and steady state analysis of PM machine drive systems given the advantages of speed, simplicity and ease of implementation. Note that the proposed model is only used for steady state performance analysis; however, in future its application can be extended to transient analysis. In addition, the model is not about maximium power point tracking techniques but it can accommodate maximium power point tracking techniques. It should also be highlighted that exactly the same digital

control block is used in both the switching and AVEM models thus allowing a true comparison of controller behaviour.

The model developed in this research project has application beyond PMSM drive system and PMSG wind energy conversion system. It can be applied to modelling, simulation and control of other electrical machine drives such as induction machines, switched reluctance machines and three-phase VSI-fed systems.

Acknowledgement

To begin with, my biggest thanks go to my supervisor Calum Cossar who accepted to and supervised me throughout this research project after my first supervisor: Prof Enrique Acha had left the University of Glasgow. Calum Cossar, whose wealth of experience and immense expertise in the field of Electrical machine drives, power electronic converters and controls, helped me through all the challenges in the course of my research project. He is not only my supervisor but someone who always cares about my personal welfare and renders help during tough times.

I would like to thank Dr Joseph Melone for his support and advice during my research. I would also like to show appreciations to Dr Graham Morton who gave me the initial support and advice on how to use PORTUNUS simulation package. I also acknowledged the advice and support of Prof Nigel Schofield. I would also like to thank technical staff, Ian Young and Peter Miller for all the help and technical support in setting up the laboratory test rig. I owe a great thank to the mechanical workshop staff, Denis Kearns and Cameron Millar for the expertise in fabrication of the machine and test bed.

I could not have done this doctoral research without the support of my lovely wife Mrs Margaret Agbo Ohiero and children Lydia Yengwra Ohiero Jr, Favour Lehiowo Ohiero, John Woduowo Ohiero and Margaret Agbo Ochoga. I thank them immensely for the courage they show and the support during the programme. My special thanks to my loving mother Mrs Lydia Yengwra Ohiero for her love, words of encouragement, understanding and prayer.

To all my brothers and friends, Joseph Onah Okpache, Emmanuel O. Ohiero, Engr. Joseph Ukpata, Pst. Sunday Mbang, Barr. Fidelis I. Akra, Engr. Etim, Archibong Archibong, John Ogar Iyaji, Michael Oko Ibu and others to mention a few, I say thank you all for your prayers, support and encouragement.

I would also like to thank all my friends and colleagues in the University of Glasgow, Dr Andrea Montecucco, Dr Jonathan Siviter, Dr Okara Ikpe, who made life enjoyable and entertaining especially during Friday Lunch.

Finally, a big thank to the Tertiary Education Trust Fund (TETFund), Nigeria and Cross River University of Technology, Calabar, Nigeria for the funding.

Contents

List of Figures

List of Tables

Nomenclature

AVEM	Average Voltage Estimation Model
PM	Permanent Magnet
PMDC	Brushless PM DC machine
PMAC	Brushless PM AC machine
PMSM	Permanent Magnet Synchronous Motor
PMSG	Permanent Magnet Synchronous Generator
SCIG	Squirrel Cage Induction Generator
DFIG	Doubly Fed Induction Generator
EESG	Electrically Excited Synchronous Generator
WRIG	Wound Rotor Induction Generator
VSC	Voltage Source Converter
VSI	Voltage Source Inverter
IGBT	Insulated Gate Bipolar Transistor
BJT	Bipolar Junction Transistor
SCR	Silicon Controlled Rectifiers
MOSFET	Metal Oxide Silicon Effect Transistors
GTO	Gate Turn-Off Thyristors
AC	Alternating Current
DC	Direct Current
PWM	Pulse Width Modulator
SVPWM	Space Vector Pulse Width Modulation
SPWM	Sinusoidal Pulse Width Modulation
PI	Proportional Integral
K1	Proportional Gain
K2	Integral Gain
EMF	Electromotive Force
GSC	Generator Side Converter
LSC	Load Side Converter
HEV	Hybrid Electric Vehicle
WECS	Wind Energy Conversion System
MPP	Maximium power point
MPPT	Maximium power point tracking

ω_{ract}	Actual Rotor angular speed (rad/sec)
ω_{rref}	Speed reference (rad/sec)
$i_{A,}\, i_B, i_C$	Generator side phase currents
$i_{Aact}\,,\ i_{Bact}\,,\ i_{Cact}$	Actual Generator phase; A, B, C current
$i_{Aref}\,,\ i_{Bref}\,,\ i_{Cref}$	Reference Generator phase; A, B, C current
$d_{A,}\, d_B, d_C$	Generator side controller duty cycles
$Td_{A,}\, Td_B, Td_C$	Length of time Generator side phase are connected to the positive terminal of DC voltage
$T1, T2, T3, T4, T5, T6$	Time active voltage vectors are applied
$T0, T7$	Time zero voltage vectors are applied
T_{sw}	Switching period
V_{avg}	Average Voltage
VDR	Voltage Divider Rule
Z_k	Phase winding impedance
Z_T	Total impedance
$V_{A,}\, V_B, V_C$	Generator side phase voltages
$i_{aact}\,,\ i_{bact}\,,\ i_{cact}$	Actual AC Load phases; a, b, c current
$i_{aref}\,,\ i_{bref}\,,\ i_{cref}$	Reference AC Load phases a, b, c current
$d_{a,}\, d_b, d_c$	AC load side controller duty cycles
$Td_{a,}\, Td_b, Td_c$	Length of time AC load side phase are connected to the positive terminal of DC voltage
$V_{a,}\, V_b, V_c$	AC load side phase voltages
$i_{a,}\, i_b, i_c$	AC load side phase currents
$V0, V7$	Zero voltage vectors
$V1, V2, V3, V4, V5, V6$	Active voltage vectors
V_R	Resultant Voltage Vector
V_{DC}	DC link Voltage
V_{DCact}	Measured DC link Voltage
V_{DCref}	Reference DC link Voltage
I_{DC}	DC link current
I_{DCgen}	Generator side DC current
I_{DCload}	AC Load side DC current
DSP	Digital Signal Processor

FCIV	Flexible Controller Fourth Edition
FACTS	Flexible AC Transmission System
PV	Photovoltaic
GB	Gear Box
FOC	Field Oriented Control

Chapter 1 Introduction

This chapter introduces permanent magnet synchronous machines drives and presents the advantages of the permanent magnet synchronous machine over alternative AC machines used in variable speed drives. The chapter also highlights the objectives and contributions of the thesis as well as the thesis outline and the necessity for reducing the simulation execution times in the design process of permanent magnet synchronous machines and other electrical machine drives.

1.1 Background

Permanent magnet synchronous machine drives are the most widely used electrical machine drive systems in recent times due to the attractive features of permanent magnet synchronous machine such as high energy density, low torque ripple, higher efficiency, higher reliability, lower cost of maintenance and operation at low rotational speed. The permanent magnet synchronous machine is combined with power electronic converters and the operating characteristics of the permanent magnet machine are controlled by the power electronic converters. In many applications it has provided solutions to the challenges such as the problems of unreliability and poor performance due to excessive heat and losses, gearbox failures, excessive vibrations and noise, wears, high cost of maintenance and increased in the weight of the drive system associated with the traditional mechanical drive and other electrical machines drive systems [1][2]. The technologies involve conversion and processing of electrical energy to mechanical energy or vice versa. Generally, when power electronic converters are combined with electrical machines, it enables energy efficient variable speed operation. The power electronic converters are used with the appropriate control technique to control the motion and operating characteristics of electrical machines such as induction machines, DC machines, switched reluctance machines and permanent magnet synchronous machines. Among the electrical machines used for variable speed drive, permanent magnet synchronous machine are increasingly being used in many industries and renewable energy conversion for variable speed drive applications due to the various advantages and the fact that PM machine can use high performance rare-earth permanent magnets, e.g. Samarium Cobalt (SmCo5) and Neodymium-Iron-Boron-NdFeB in the

rotor and as a result do not require electrical excitation [3]. Another advantage is that PM machines have a simplified structure with reduced size, reduced maintenance and significant improvement in reliability compared to other electrical machines which use commutation, slip rings, and field windings. They also have high torque to weight ratio and high power density which makes them a preferred option in a large number of industrial and power generation applications. The number of poles and diameter of permanent magnet synchronous machines can be varied to obtain various rotational speeds to meet the requirements of many modern applications where operation at low speed is required to optimise energy savings and reduced cost. These advantages make the PM machine an attractive alternative and are used for varieties of applications. Usually, they are used for low and medium power applications such as refrigerators, freezers, computer and office equipment, air conditioning units, robotics, pumps, compressors, washing machines, elevators, ship propulsion, but now they are increasingly used in advanced adjustable speed drives such as electric vehicles, electric hybrid vehicles and variable speed renewable energy conversion applications such as wind, wave and tidal systems.

These wide areas of applications of permanent magnet synchronous machines are due to the development and advancement of power electronic semiconductor devices and control techniques. Power electronic devices are combined with permanent magnet synchronous machines and are used to enhance the performance and operating characteristics of the machines. The PM machine is controlled by the power electronic converters to achieve the desired performance. The role of power electronic converters depends on the machine applications. In adjustable speed electric motor drive applications, the power electronic converters control the operating speed and torque of the electric machine by supplying variable current and frequency to the machine [4]-[6] while in variable speed renewable energy conversion system the power electronic converters control the generator speed to track maximum power and stabilise DC link voltage and deliver a fixed voltage and frequency to the load or connection to grid [7]. Power electronic devices such as the insulated gate bipolar transistor (IGBT), MOSFET, thyristor, bipolar junction transistor (BJT), silicon controlled rectifiers (SCR), Gate Turn-Off thyristor (GTO) are used to control the speed and torque of electrical machines. Their ability to control the speed of the machine is based on switch mode operation provided by the control strategy usually from PWM control techniques [8]. Switch mode operation

requires bidirectional power flow and in order to implement bidirectional power flow characteristics, power electronic devices are arranged in a given topology. Several power electronic converter and inverter topologies have been proposed and developed, regarding the control of the speed, torque and current of permanent magnet synchronous machines in order to obtain variable speed operation, enabling choices to be made of the most efficient and reliable configuration for effective control. Power electronic converters such as current source inverters, voltage source converters (inverters), matrix converters, and cycloconverters can be used to obtain variable speed operation. In industrial PM machine drives, the voltage source inverters are commonly used and IGBTs are commonly used to implement the voltage source inverters. This is because IGBTs have the ability to handle high current, power and switching frequency compared to other presently available power electronic devices. They are basically single phase, three phases or multi-phase voltage source converter. Although, there is recent development and advancement of machine drives and converter topologies towards multiphase system [9][10], the three-phase PM machine drive and voltage source converter topology is widely used in industries for variable speed applications. The two-level three phase voltage source converters produce sinusoidal current and provide bidirectional power flow enabling control of PM machine drive systems.

Over the years, there have been growing interests in permanent magnet synchronous machine drive as a result of the numerous advantages and applications of the PM machines has over other electrical machines such as DC machines, induction machines and the conventional synchronous machines as mentioned above. This has led to a lot of research interest on the behaviour and performance of the PM machine drive system and control strategies [11]-[29]. Recently, there has been an increase in the market demand for three-phase variable speed PM machine drives due to the increasing demand for energy conservation, maximisation of power, improvement in efficiency, ease of controllability and reliability. There has also been high interest in designs, control, analysis and production of permanent magnet synchronous machine drives. Different designs and configurations of three-phase PM machine drive systems and control techniques are being proposed and investigated [30]-[38]. Extensive research has recently been carried out on the variable speed motor drives and generator drives using voltage source inverters to obtain improved efficiency, improved performance, and improved power handling capability, high reliability and better control at reduce cost for

permanent magnet synchronous motors and generators. Most Recently researchers, manufacturers, and designers of the adjustable speed electric motor drives and variable speed generator drives are focussed on developing a new generation of three phase, multiphase permanent magnet synchronous motor and generator based on variable speed with one inverter and dual parallel motor drive reported in [39][40], multiphase PM machines [41] and multilevel and multilevel modular voltage source converters [42].

The design and analysis of a variable speed permanent magnet synchronous machine drive and control e.g. EHV and wind power generation is a complicated task due to the high number of design parameters and requirements such as low cost, high power density, low maintenance, ruggedness, good quality of output power, torque, fast dynamic characteristics and improvements in efficiency. Traditionally the investment involved to achieve these is also high. It involves a lot of time, and associated cost, to design and develop a reliable test rig which will allow adequate and accurate investigation of the different machines, power electronic converters, load parameters, control techniques and performance effectiveness and build confidence on the results. Therefore, a reliable simulation model of PMSM drives and PMSG driven renewable energy power conversion is required in order to study/test the operating interactions between the mechanical, electrical components, control techniques and their outputs response before actual design and implementation. Further to this, the recent trend of variable speed permanent magnet synchronous machine designs, for example the design of one inverter with dual parallel motor drive, multiphase PM machines and multilevel and multilevel modular voltage source converters designs targeted at achieving higher voltage and power levels, have created a chance, where the simulation execution time of voltage source converters with permanent magnet synchronous motor or generator drive system becomes an important factor to consider in adjustable speed motor drive and variable speed generator drive design process.

Several studies to develop cost-effective designs of variable speed PMSM or PMSG drives and control system within the shortest possible time requiring the use of modelling and simulation tools have been explored. The most commonly used model is a detailed VSC switching model with the PMSM [43][44] and with PMSG [45]-[48]. The detailed VSI switching model is very useful in the design process of a PMSM or PMSG drive system. It is used to verify the different stages of design as well as accurate evaluation, investigation and validation of the system and control technique performance because it

represents and predicts results similar to the actual circuit configuration. However, the simulation of the switching model of power electronic converters in a drive system presents significant challenges. Severe constraints emerge with systems involving large number of power electronic switches, high power and high voltages, such as a multilevel VSI or multiple inverters. This is because the switching models are characterised by very small minimum time steps (<100ns) as determined by the required resolution of the Pulse-Width Modulation (PWM) control (e.g.: 12bit resolution @ 20kHz), and once incorporated into the complete PM machine drive mechanical system and under realistic adjustable speed conditions, simulation lengths in the region of minutes if not hours are required for accurate evaluation of the system. The simulation execution times become frustratingly long because of the non-linear switching devices, and very short simulation step lengths in the region of hundreds of nanoseconds are required for accurate results. The reduction of the simulation execution time is an important goal in the design process and analysis of any variable speed machine drives. A method of reducing the simulation time is therefore necessary. It was found that the best approach is a method that will eliminate the VSC or VSI switching circuit from the PMSM or PMSG drive simulation model.

An alternative method to modelling of the VSI in variable speed PMSM and PMSG drives is the use of the proposed Average Voltage Estimation Model (AVEM) technique. In this approach, the voltage source inverter is totally replaced with a model which reproduces the functionality of the VSI. The method is based on an analytical estimation of the 'average' voltage across each phase of the PMSM, PMSG or electric AC load during each PWM switching period and then using these average values as piecewise-linear voltage sources for each phase of the motor, generator and electric load. The advantages of the AVEM is that it simplifies the simulation model of electrical machine drive system, its simulation is faster and it is an accurate alternative model of voltage source inverter that will reproduce the functionality of the VSI and control of variable speed PMSM or PMSG drives to supply and/or produce sinusoidal three-phase AC currents based on the existing PMSM and PMSG digital controller models such that machine and controller performance/limitations can still be evaluated and optimised. A limitation with AVEM is that it cannot be used for the analysis of the internal dynamics of the voltage source inverter. However, this is only one aspect compared to the numerous studies of variable speed drives that the AVEM can be used for.

The presented research project will benefit electric motor drive manufacturers, industries and wind energy conversion designers and operators as well as researchers and students to improve the efficiency and resultant time in the development of new designs of adjustable speed motor drive and variable speed wind energy conversion system and control techniques. The resultant simulation model keeps stable operation, controls current and torque, tracks maximium power points and maintains constant DC link voltage over the required speed range. Based on performance analysis, the results for the proposed average voltage estimation model and detailed switching model are closely similar to the experimental results for a 1kW, 16-poles small fractional horsepower PM machine. This research has shown that this model though developed for small kilowatts can be applied to several hundred kilowatts as an alternative to the detailed switching model in the design process of not only wind energy conversion system but other renewable energy conversion systems where there is need to reduce the time, cost of design and final product.

1.2 Thesis Objectives

Modelling and simulation are very important processes that enable the efficient design and verification of drive systems and control strategies. Due to the fast switching of the voltage source inverter devices compared to the slow dynamics of the electrical machines and mechanical elements the simulation of drive systems using VSI switching models is time consuming. It will be advantageous to machine drive designers, researchers, wind energy conversion system's developers, and grid operators to model the drive system with freedom of simulation time step. In addition, to designers of PM machine drive system, the validation of new approach to modelling is necessary in order to build confidence on the degree of application and results of the model. In view of this, the objectives of the thesis are summarised by;

1. To develop a fast and cost-effective simulation model and control for PM AC motor drives that will totally eliminate the use of voltage source inverter switching, and can be used as an alternative model for further research and study on the evaluation and analysis of PM machine drives and control algorithm performance and optimisation.

2. To develop a fast and cost effective simulation model and control for variable speed PM generator drives in wind energy conversion systems that will totally eliminate the full scale back-back voltage source inverter switching network, and can be used as an alternative model for further research and study on the evaluation and analysis in the design process of variable speed PM generator wind energy conversion systems and control techniques performance and optimisation given the slow dynamics of the wind turbine PMSG.

3. To validate the performance accuracy and results of the fast simulation model for PMSM drive based systems and variable speed PMSG drives in wind energy conversion system against the equivalent VSI switching model and experimental results.

4. To build a flexible laboratory test rig to emulate a variable speed wind energy conversion system and PM motor drives to validates the predictions of the proposed fast simulation models for variable speed PMSM drives and PMSG wind energy conversion systems. The developed platform and simulation models will form the basis in which a wide range of existing and new PM machine drive designs and control strategies can be implemented and evaluated at reduced time and cost. It will further provide an important tool in which future research and study to enhance the quality of wind energy conversion and motor drives can be carried out.

5. To analyse the performance and efficiency of the PM motor drives and variable speed PMSG wind turbine using the proposed average voltage estimation model.

6. To implement the average voltage estimation modelling method (AVEM) using real time DSP controller to calculates the energy yield of the PMSG wind energy conversion system.

1.3 Thesis Contributions

The simulation of the PM machine drive systems and control strategies is generally based on a detailed VSI switching model. It is the objective of this research to develop and validate an alternative model for voltage source inverter switching circuit using a different approach and control that can be rapidly simulated.
The main contributions of the thesis are summarised as follows**;**

1. An alternative model of a three-phase voltage source inverter switching model which can be used for rapid and accurate simulation and analysis of different electrical machine drives, or any voltage source inverter fed three-phase AC load and control strategy has been developed using a more simplified approach that totally eliminates the VSI switching network, L-C filters circuits and also eliminates modelling the DC side as a current source [49]-[52]. This is a contribution towards reducing the time and cost of the design process and production of motor drives and three-phase power conversion systems. The proposed model allows freedom of choice when it comes to step time selection during simulation and reduces the computational d-q transformation burden involves in the previously developed average value model [53][54].

2. A Voltage Source Inverter loss model has been developed and incorporated into the AVEM. Most of the existing average value models based on state space averaging, transformation and linearization in literatures have not shown evidence of incorporation of losses and analysis of the Voltage Source Inverters. The incorporation of the VSI loss model into the proposed average voltage estimation model has further expanded the validation, analysis and application of averaging model to include power, power losses and efficiency of the electric machine drive system.

3. A fast averaging model of a full back-back power converter with variable speed PMSG WEC is difficult to find in literature. A detailed average voltage

estimation model of full scale back-back voltage source inverter with variable speed PMSG wind energy conversion system has been developed in this thesis. The derivation and development of the average voltage estimation model of two levels three-phase back-to-back VSI with WECS and control techniques that can rapidly and accurately simulate the characteristics of the system, in addition, the simplicity in the derivation of the average voltage model does not involve complex computational burden and reduce time of simulation and design process are contributions in the thesis.

4. The detailed analysis provided to understand the performance and validation of the proposed average voltage estimation model against the standard detailed switching model and experimental results.

5. The development of a small scale flexible test rig in the Laboratory to emulate PMSM drive and PMSG WECS to test and validate the results of the simulation models based on PM machine drive, and for use in future research projects to study existing and new designs of PMSM drive and PMSG WECS.

6. The proposed average voltage estimation model has been implemented using a real time DSP controller in the laboratory to calculate and display the energy output of the PMSG wind energy conversion system over any given length of time. Validation of the DSP controller average voltage estimation model WECS energy estimation, calculated (measured) energy and simulation AVEM energy prediction confirms the accuracy of the AVEM's in determining the energy output of WEC under varying wind speed conditions and maximium power point tracking control scheme. This provides an alternative method of calculating the energy yield of a typical wind energy conversion system.

1.4 Publications

[1] Ohiero, P.O.; Cossar, C.; Melone, J. and Schofield, N. "A fast simulation model for Permanent Magnet Synchronous Motor (PMSM) based system," 7th International Conference on Power Electronics, Machines and Drives (PEMD 2014), Manchester, pp 1-6, 8-10 April 2014.

[2] Ohiero, P. O.; Cossar, C. and Melone, J., "A fast simulation model for a Permanent Magnet Synchronous Generator (PMSG) drive system," 16th European Conference on Power Electronics and Applications (EPE'14-ECCE Europe), Lappeenranta, pp 1-10, 26-28 Aug. 2014.

Papers for Journal publication at the time of submission of this thesis

[3] Peter O. Ohiero and Calum Cossar , "Development of Alternative fast Simulation Model and Validation of Back-Back Voltage Source Converter for Analysis of Variable Speed PMSG Wind Energy Conversion System"

[4] Peter O. Ohiero and Calum Cossar, "DSP controller-based Implementation and Application of Average Voltage Estimation Model to Estimation WECS Energy Output"

1.5 Thesis Outline

Chapter 1 provides a general introduction of permanent magnet synchronous machines drives and presents advantages of permanent magnet synchronous machine over other electrical AC machines used in variable speed drives. The chapter also highlights the objectives and contributions of the thesis as well as the thesis outline and the necessity for reducing the simulation execution times in the design process of permanent magnet synchronous machines and other electrical machine drives when incorporated in a complete (mechanical/aerodynamic) simulation model.

Chapter 2 presents a brief review of the different components of permanent magnet synchronous machine drives. The different types of power electronic converter topologies used in variable speed PMSM drives and PMSG drive systems are outlined and the basic principles of the proposed Average Voltage Estimation Model (AVEM) stated. This chapter also presents brief reviews of wind energy conversion system (WECS) from fixed speed operation to variable speed as well as discussion on carrier-based sinusoidal PWM and proportional integral (PI) regulators. Chapter 2 also presents the existing approaches used in modelling and simulation of permanent magnet synchronous drive systems. These are the detailed switching model and the average value model, stating their advantages and disadvantages in terms of simulation execution time and the need to develop an alternative model of PM machine drive system based on a different approach.

Chapter 3 deals with the development of the proposed average voltage estimation model for permanent magnet synchronous motor drive system. The chapter begins with presentation of the basic theory of the voltage source converter switching functions and describes the principle and development methodology of the average voltage estimation modelling of voltage source inverter utilising IGBTs as well as its application in the modelling of variable speed motor drives. A detailed description and development of the voltage source inverter loss model and its incorporation into the AVEM is also presented. This is followed by the development of control strategy, simulation, performance analysis and comparison of the AVEM with the detail switching modelling method of permanent magnet synchronous motor drive system. Simulation results are presented to verify the performance of the AVEM.

Chapter 4 gives an in-depth description and development of the laboratory test rig, DSP controller, control strategy for PMSM drive system and wind energy conversion emulation system. It also presents experimental results used to validate the simulation models results. Experimental results such as current, torque, power and DC link voltage are presented in this chapter.

Chapter 5 provides a comprehensive validation and analysis of performance of the proposed average voltage estimation against switching model and experimental results of a VSI fed permanent magnet synchronous motor (PMSM) drive. Performance indicators such as Torque versus speed, current versus speed, power versus speed, losses and efficiency versus speed are compared. Simulation and experimental results show that the proposed AVEM achieves the same performance accuracy as the switching model compared with experimental data. The advantage being that the AVEM based model is significantly faster compared to the switching model.

Chapter 6 provides the detailed development of average voltage estimation model and switching model of full scale back-back voltage source inverter with variable speed PMSG wind energy conversion system and control strategy. Simulation and experimental results are presented to verify and validate the performance of the proposed AVEM of WECS against the comparable switching model and laboratory test rig. The benefits of the proposed model against the switching model are outlined. Chapter 5 also provides a calculation, simulation and performance analysis of energy yield of WECS and MPPT control based on AVEM. In chapter 5, it is also presented a significant contribution of the thesis, the practical implementation of the AVEM of WECS using real time DSP controller in which the DSP controller is used to calculate the energy output of WECS based on an AVEM model. It investigates and presents comparison of the proposed DSP-based AVEM energy estimation method, the standard calculation method and AVEM simulation method for variable speed constant torque and MPPT control PMSG WECS.

Chapter 7 presents the conclusions of the thesis and suggests further development and improvement of the proposed average voltage estimation model of voltage source inverter.

Chapter 2 Topologies and Modelling of Voltage Source Inverter and PM Machine Drive System

2 Introduction

The simulation of variable speed permanent magnet synchronous machine drive systems in this research project is based on the detailed VSI switching and the proposed average voltage estimation modelling method. Both the VSI switching model and average voltage estimation model are developed for a permanent magnet synchronous motor drive and variable speed wind turbine generator. The chapter begins with a brief review of the different components and topologies of permanent magnet synchronous machine drive systems. This will enable an understanding of the behaviour and operating principles of the components and of variable speed PM machine drive system. The different types of power electronic converter topologies used in variable speed PMSM drives and PMSG drive systems are outlined and the basic principles of the proposed Average Voltage Estimation Model (AVEM) stated. This chapter also presents brief reviews of wind energy conversion system (WECS) as well as discussion on carrier-based sinusoidal PWM and proportional integral (PI) regulators. Relevant literature reviews of the approaches used in modelling and simulation of permanent magnet synchronous drive systems are presented. These are the detailed switching model and the average value model, stating their advantages and disadvantages, examining the effect of each method in terms of the simulation execution time. The chapter also presents the reasons for the development of an alternative model of voltage source inverter with PM machine drive system based on a different approach with freedom of choice of simulation time step to speed simulation execution time.

2.1 Permanent Magnet Synchronous Machine Drive System

Permanent magnet synchronous machine drive refers to the energy conversion from electrical to mechanical or vice versa involving a permanent magnet synchronous machine and controlled by power electronic semiconductor devices to operate at various rotating speeds. In general, permanent magnet synchronous machine drive consists of the permanent magnet synchronous machine, the power electronic converter, electrical

power supply (DC or AC) and the controller, feedback devices and sensors as shown in Figure 2-1.

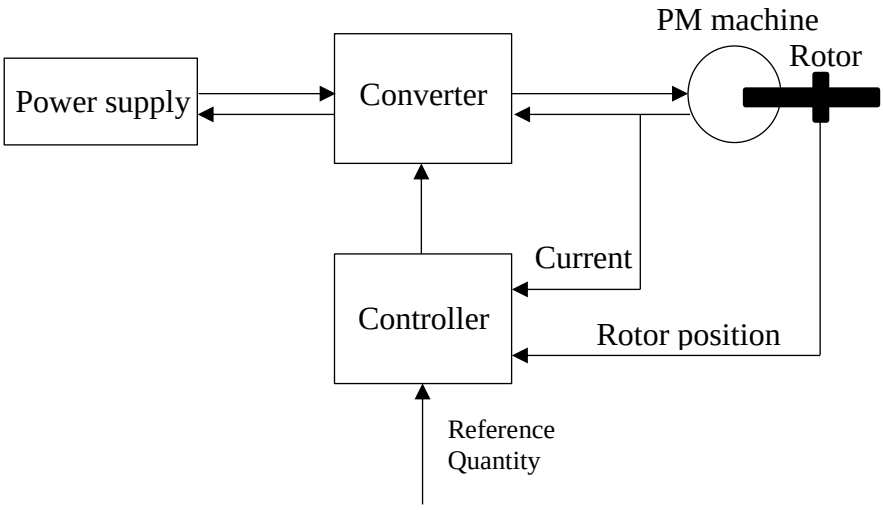

Figure 2-1: Block diagram of voltage source converter with permanent magnet synchronous machine drive system

The stator of the PM machine is connected to or is fed from the power electronic converter. The power electronic converter is an important components of the drive system where individual semiconductor devices e.g. IGBTs are arranged in a suitable topology to form the power electronic converter system. The power electronic converter considered in this research is the voltage source converter and its details are presented in section 2.3. In modelling and simulation of permanent magnet synchronous machine drive systems, the individual components are adequately represented in simulation software and the parameters or properties applied. It is important therefore to review the different components of a permanent magnet synchronous machine drive system. This will provide adequate knowledge and understanding of the behaviour and the operating characteristics of the components of the drive system.

2.2 Permanent Magnet Synchronous Machine

A permanent magnet synchronous machine consists of the outer stationary stator and the inner rotating part called the rotor made of permanent magnets. The interaction of the stator and the rotor magnetic fields generate electromagnetic torque on the shaft of the PM machine. PM machines can be used as an electric motor or generator. The physical

features of the PM motor and PM generator is the same the only difference is the mode of operation. While the rotor is always connected to the shaft of a mechanical device, the stator can be fed with or supply electrical power depending on the application. When the PM machine is fed with electrical power, it converts this electrical energy to mechanical and it is called a permanent magnet synchronous motor (PMSM) but when it converts mechanical to electrical, it is a permanent magnet synchronous generator (PMSG). In general, PM machines are classified based on the method of excitation such as direct current (DC) or alternating current (AC). There are two groups in this category, the permanent magnet direct current machine (PMDC) and the permanent magnet alternating current machine (PMAC)[55][56]. The DC excited PM machines are further divided into the permanent magnet direct current (PMDC) and permanent magnet brushless direct current (PMDC-brushless) machines. PMDC have a commutator and brushes as the traditional DC commutator machines but use permanent magnets in the place of field windings while the PMDC-brushless uses electronically controlled excitation and permanent magnets in the rotor, the brushes are absent in these machines and they have some of the advantages of PMAC machines. On the other hand, the PMAC machines use AC excitation and do not require the use of a commutator, brushes and field windings to generate the magnetic field. In the PMAC machines, the magnetic field is generated using permanent magnets mounted in the rotor. The PM machines are also classified based on the waveform of the excitation current and back EMF. In PMDC-brushless machines, a square waveform phase currents excitation is required and the resulting back EMF is trapezoidal while the PMAC machines are excited with a sinusoidal currents and a sinusoidal back EMF.

The position of the permanent magnets in the rotor also plays a significant role through which PM machines are classified. There are the surface permanent magnet machines, where magnets are mounted on the surface of the rotor e.g. surface permanent magnet synchronous motor (SPMSM) or surface permanent magnet synchronous generator (SPMSG), and the interior permanent magnet machines where magnets are mounted inside the rotor e.g. interior permanent magnet synchronous motor (IPMSM) or interior permanent magnet synchronous generator (IPMSG).

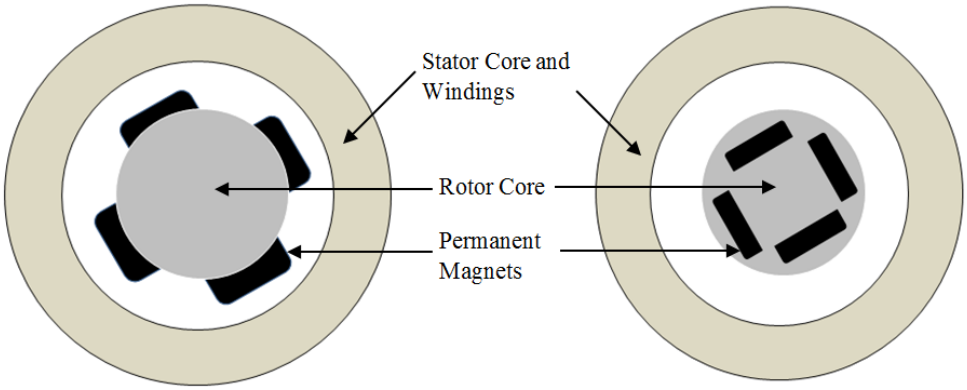

(a) Surface mounted magnet machine (b) Interior mounted magnet machine

Figure 2-2: Rotor configuration of PM machines (a) surface mounted (b) interior mounted

Figure 2-2 shows a cross section of the structure of PM machine consisting of the outer stator and the inner rotor. The stator in a conventional three phase machine has three equally distributed windings located in the slots of the stator core and permanent magnets mounted on the rotor. Figure 2-2 (a) shows a four pole PM machine design with the magnets mounted on the surface of the rotor. This type of PM machine has a simplified construction with the magnetic flux density in the permanent magnets almost similar to the flux density of the air gap. However, the location of the magnet in the air gap constitutes a disadvantage to the machine; the magnets are always exposed to the activities of the stator coils hence any harmonics in the space can easily be conducted by the magnet with resulting eddy current and losses in the magnets [57][58].

In the interior permanent magnet machine as shown in Figure 2-2 (b), the magnets are buried inside the rotor and are protected from the activities of the stator windings in the air gap and avoid the effect of possible harmonics in the space between the rotor and the stator. This allows flux concentration in the air gap with the flux density of the air gap higher than that of the magnet with resulting reluctance torque and saliency. This property of the interior mounted permanent magnet machine enables higher speed operation compared to surface mounted through field weakening. The drawback of this structure is the difficulty to obtain space on the rotor to achieve concentrated flux, since large numbers of magnet poles are required for concentrated flux. However, the proposed

average voltage estimation model is applicable to both VSI fed interior and surface mounted permanent magnet synchronous machines.

Figure 2-3 shows a torque versus speed curve with field weakening of the machine under investigation. The solid line represents the normal operation of a controlled PM machine while the dotted line represents the performance characteristics when field weakening is applied. From Figure 2-3, higher torque and wider operating range can be achieved with field weakening.

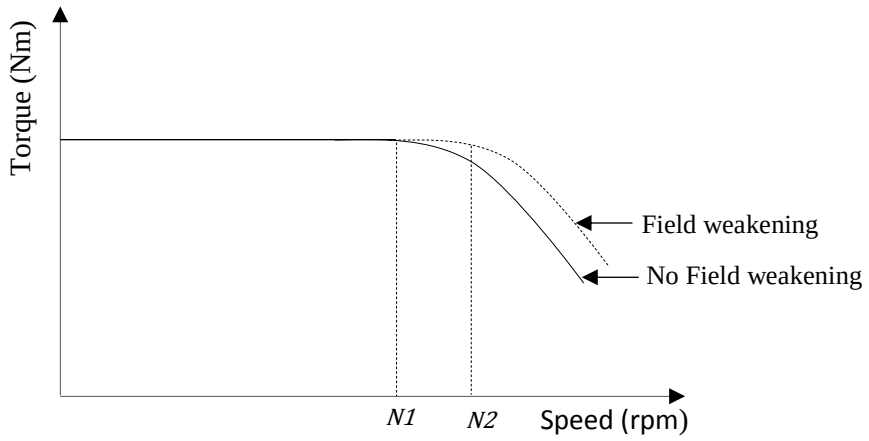

Figure 2-3: A typical torque versus speed curve with field weakening

2.3 Voltage Source Converters

Voltage source converters are an essential part of modern variable speed electric machine drives and other power conversions systems. They are used to convert and process electrical power using PWM control techniques. Current source converters can also be used to process electrical power [59][60] but most industrial applications prefers voltage source converters to current source converters because the voltage source inverter has ease of control with open loop V/Hz control, compact size, low cost, , provide higher power factor as well as lower power losses [61][62]. The block diagram of a VSC is shown in Figure 2-4. It consists of input and output terminals and allows power to flow to the load when commanded by the control block.

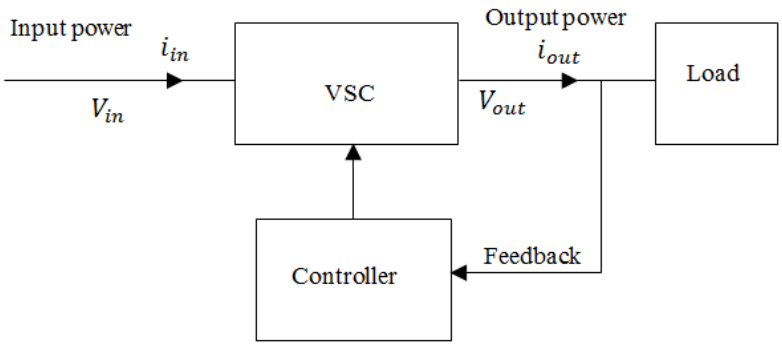

Figure 2-4: Block diagram of Voltage source converter

Depending on the application, the input power source can be DC or AC. However, a stiff or constant voltage must be applied across the terminal with the DC power source. The basic function of the VSC is to control the characteristics of electrical power such as voltage and frequency to obtain the desired form of power output. This requires a control strategy for the voltage source converter. The most commonly used control strategy in many industrial applications is the PWM control techniques such as carrier-based sinusoidal PWM [63][64] and space vector PWM [65][66]. The control strategy requires either feedback from the output, or feed forward from the input [67].

Voltage source converters are constructed using power electronic switches e.g. IGBTs and sequentially controlled to allow bidirectional power flow. They may be single-phase, three-phase or multi-phase. The single-phase VSC are applied in low power applications while the three-phase and multi-phase are used in medium and high voltage and power applications because of their suitability for rapid dynamic response and high performance. Since most industrial applications and electrical loads require a three-phase voltage supply, three-phase voltage source converters are commonly used.

2.3.1 Applications of Voltage Source Converters

Voltage source converters are used for different purposes such as providing electrical power for DC loads e.g. heater coils, furnaces, DC motors, and AC loads such as UPS, FACTS and Vars compensators. In addition, voltage source converters are used for adjustable speed drives such as hybrid vehicles, electric hybrid vehicles, conveyors, and renewable energy conversion systems e.g. wind energy conversion systems, ocean energy conversion systems, tidal energy conversion system and high voltage DC transmission systems.

2.3.2 Classification of Voltage Source Converters

Voltage source converters are classified based on the input and the desired output power as

1. DC/AC voltage source inverter
2. AC/DC voltage source converter
3. AC/DC/AC converters

2.3.3 DC/AC Voltage Source Inverter

The conventional topology for a three-phase DC/AC voltage source inverter is shown in Figure 2-5. This conversion system is commonly used to provide controlled voltage and frequency. They have been widely used to provide constant voltage and frequency for standard AC loads or integration to grid, and variable voltage and frequency for AC machine drives. The input to the VSI can be from a DC voltage source such as a battery, PV or rectified DC voltage from grid or generator and the desired output is sinusoidal voltages of constant or varying magnitude and frequency to the AC loads.

The three-phase DC/AC VSI shown in Figure 2-5 consists of two levels, six power electronic semiconductor switches (normally transistors) and six antiparallel diodes allowing bidirectional current flow and unidirectional voltage blocking capability [68]. There are three phase legs of power switches and free-wheeling antiparallel diodes, two power switches are in each phase leg of the VSI and have to be controlled to switch alternatingly in switch mode that is when the upper power converter switch in one phase leg is switch on the corresponding lower switch on the same phase leg should be switched off to avoid short circuiting (shoot through) the DC link voltage supply. To further avoid shoot through and guarantee that both switches in one phase leg of the converter do not conduct simultaneously at the same time, dead time can be introduced [69]-[72]. This is a short time neither the upper nor the lower power converter switch on a phase leg conduct but allowed between switching the upper switch off and the lower switch on and vice versa. The dead time should be as short as possible in order not to constitute output waveform distortion. Typically, dead time of 20kHz PWM is between $100ns - 1\mu s$. The switching behaviour and the quality of VSI output are based on the PWM control strategy. Various PWM control strategies either voltage or current are

available and can be used in the controlling of the power switches. Generally, there is a frequency difference between the power converters and the supply. The power switches are switched at a frequency significantly higher than the supply frequency. Such higher switching frequencies effectively reduce the harmonics content of the current waveform with smoother torque but increase the switching losses. However, a number of PWM methods have been studied in the past few decades to achieve reduced switching losses, reduced total harmonic distortion (THD) and operation over a wider linear modulation range [73]-[76].

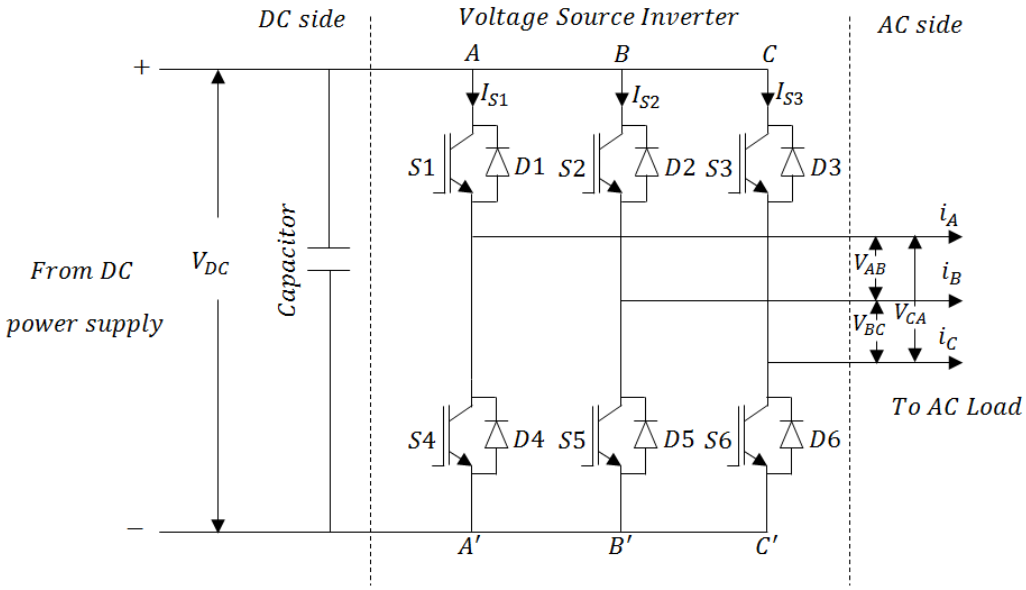

Figure 2-5: Three-phase two level 6 switches voltage source inverter

In Figure 2-5, the voltage source inverter enables the three phase AC load to be connected to the positive or negative terminal of the DC voltage supply. The output voltage as a result of the operation of the VSI is square-wave is shown in Figure 2-14.

2.3.4 AC/DC Voltage Source Converter

Figure 2-6 shows the power conversion system of AC/DC voltage source converter (VSC). The configuration of the voltage source rectifiers is the same as the DC/AC VSI but the difference lies in the mode of operation. In the case of voltage source converter (active rectifiers), the input power to the converter is from the AC power source and the desired output is DC power. Active rectification is necessary because the power is

usually from variable voltage and frequency supply source and the DC load requires a constant DC voltage or to provide DC voltage for further DC/AC conversion. However, control objective may differ between AC/DC and DC/AC, control strategies and modulation techniques for power converters switches of the AC/DC converter to operate in switch mode is the same as that of DC/AC inverters discussed in section 2.3.3. In applications where concern is given to power quality, reduction in current ripple and THD, either an inductive or inductive-capacitive-inductive filter can be added to the voltage source converter [77].

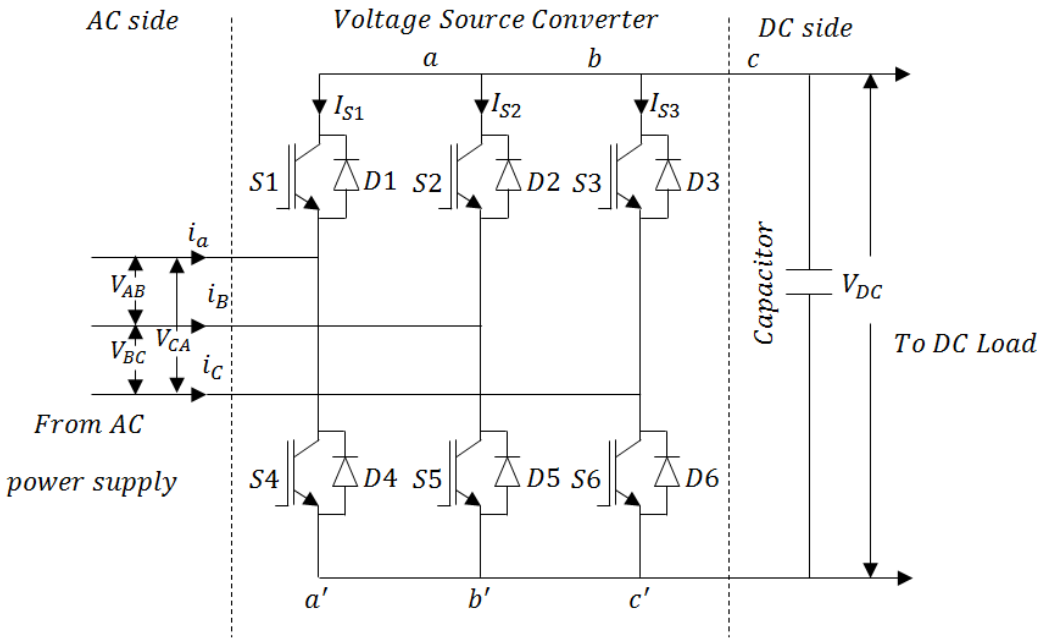

Figure 2-6: AC/DC voltage source converters

2.3.5 AC/DC/AC Voltage Source Converters

The conventional voltage source inverter and voltage source converters (rectifiers) have been discussed in section 2.3.3 and section 2.3.4. Depending on applications and the available source of power supply, two converters can be combined in cascade for AC/DC/AC conversion. A typical AC/DC/AC converter consists of AC power supply, rectifiers (passive or active), DC link and capacitor, inverter and AC load. The power supply can be from the grid or a variable speed generator driven by renewable energy sources such as wind, ocean waves and tidal while the load could be grid, R-L load

network or AC electric machines. The load side is separated from the power supply side by a DC link capacitor which acts as a filter and also decouples the grid frequency from the generator frequency. There are several advantages that can be achieve with this configuration; the number of phases can be changed between the input and output for example single phase changed to three-phase and vice versa. The voltage magnitude and frequency can also be change between the input and output. The control of the supply side voltage source converters is independent of the control of the output or AC load voltage source inverter. AC/DC/AC converters are currently used in many industrial applications such as adjustable speed electric motor drives, high voltage DC transmission, renewable energy conversion systems e.g. wind, ocean and tidal. Figure 2-7 shows the two commonly used AC/DC/AC voltage source converters.

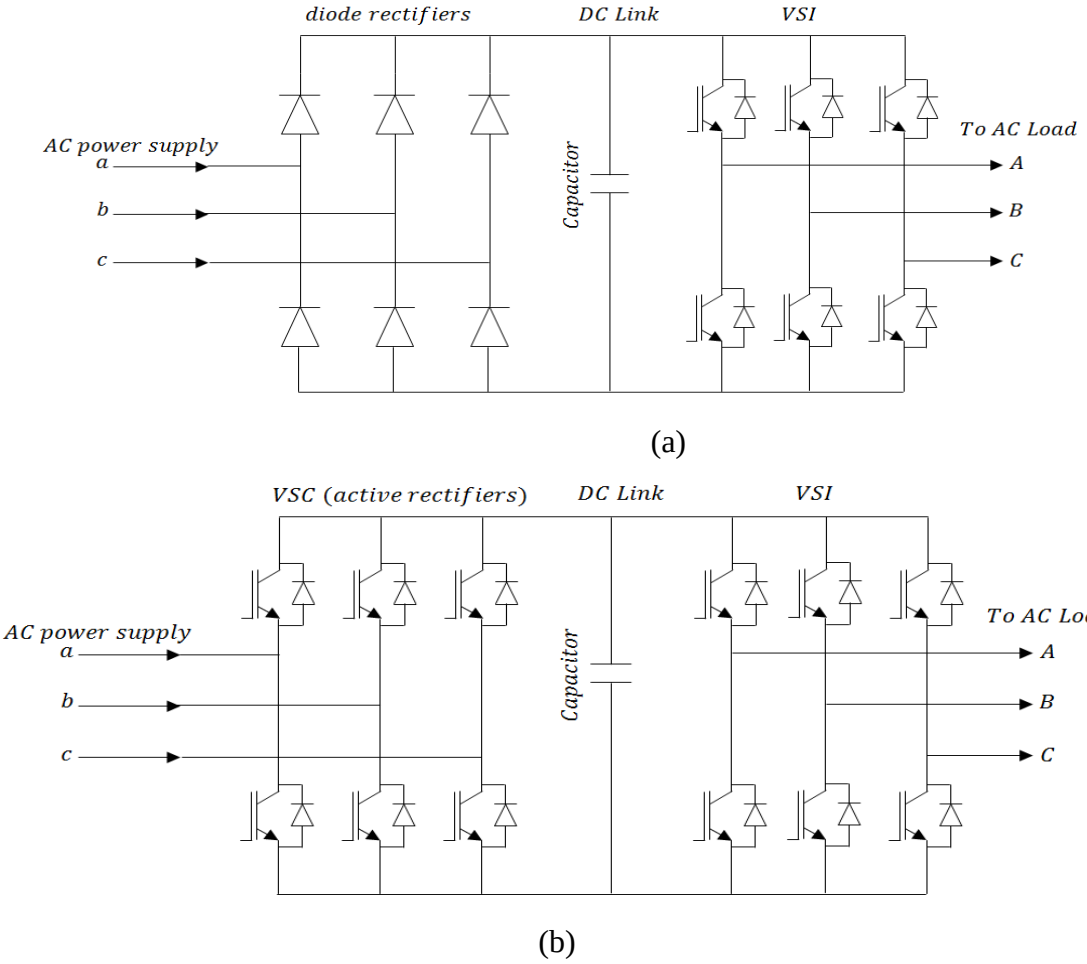

Figure 2-7: Topology of AC/DC/AC voltage source converters (a) with front end diode rectifiers (b) with front end IGBTs active rectifiers

2.4 Types of Permanent Magnet Machine Drives

Voltage source inverter fed variable speed permanent magnet machine drives in the range of hundredths to several kilowatts are generally divided into two groups, based on excitation, namely brushless DC PM Machine drives and brushless AC PM synchronous machine drives.

2.4.1 Brushless DC Permanent Magnet Machine Drives

Brushless permanent magnet DC machine (PMDC) drives use a PMDC machine with associated power electronic inverter. For the brushless DC PM motor the three phase windings are fed with rectangular current waveforms, 120^0 phase shift from one another [78]-[80]. In contrast, the brushless DC PM generator produces rectangular current waveforms, 120^0 phase shift from one another from the three phase windings [81]. In three phase brushless DC PM Machine drives, the power electronic inverter switches are controlled to excite two out of the three phase windings and the stator winding are rearranged in six possible combinations over one fundamental cycle producing rectangular current waveforms at the terminals of the PM machine which alternates from positive to negative in one electrical cycle. In order to achieve this, the stator current must be synchronised with the rotor position. The rotor position can be obtained by using a position sensor mounted on the rotor shaft, hall-effect sensor or other rotor position sensorless methods [82]-[84] aimed at reducing cost due to the sensor and improving efficiency, stability and reliability.

2.4.2 Brushless AC Permanent Magnet Synchronous Machine Drives

The brushless AC permanent magnet synchronous machine drive otherwise known as the PM AC synchronous machine drive is fed with sinusoidal current waveforms. Unlike the brushless DC PM machine drive where only two out of the three phase windings are excited, in a PM AC synchronous machine drives, all three phase windings are sinusoidally excited and conduct current at the same time. This category of PM machines is driven by an AC power source which is applied to the stator windings based on the control of the VSI. The most common topology of PM AC synchronous machine drives consists of three phase with two level three phase VSI where there are six transistors and

six anti-parallel diodes. The brushless AC permanent magnet synchronous machine drives is divided into permanent magnet synchronous motor and generator drive systems.

2.5 Permanent Magnet Synchronous Motor (PMSM) Drive System

Many industrial applications of PMSM require a wide variable speed range. With the availability of power electronic devices at improved power rating, reduced cost and reliability, voltage source inverters can be used to supply variable voltage and frequency to PMSM, for speed and torque control. PMSM drives are used in high performance and high efficiency applications from watts to several hundred of kilowatts such as servo drives, variable speed drives in electric hybrid vehicles [85].

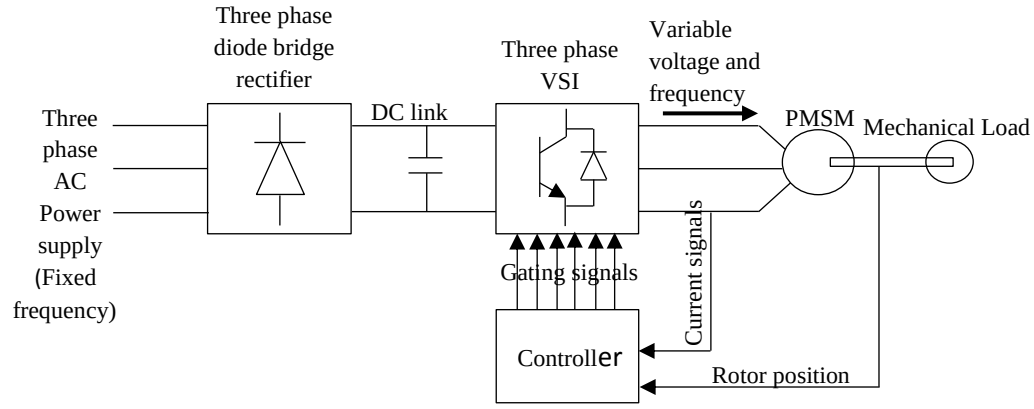

(a)

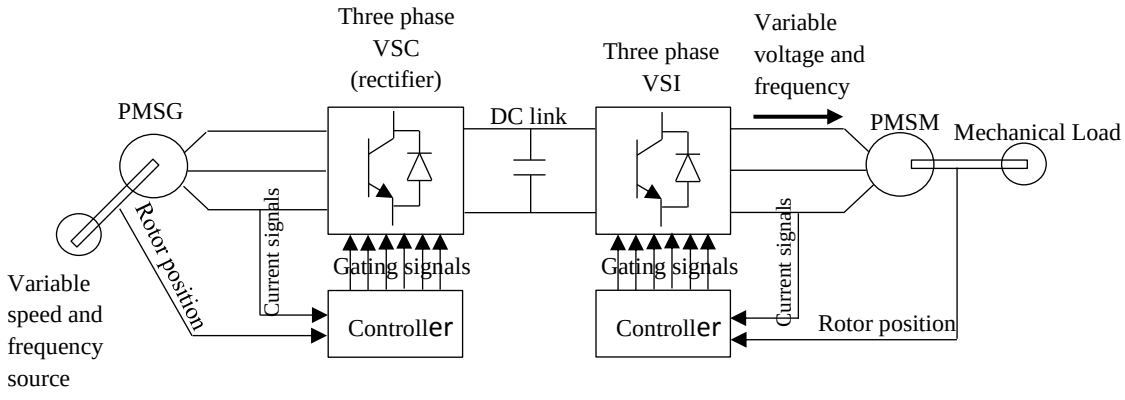

(b)

Figure 2-8: Three-phase VSI for speed control of PMSM (a) VSI with diode rectifiers (b) back-back VSC

The voltage source inverter provides variable voltage and frequency for the PMSM. The most commonly used topology for three-phase PMSM drive system is shown in Figure 2-8 (a). It consists of a constant frequency AC power supply, three-phase diode rectifier, DC link and capacitor, VSI, controller, PMSM and mechanical load. The three-phase diode rectifiers converts AC voltage to a fixed DC voltage and the VSI converts the DC voltage to AC voltage at the required magnitude and frequency. The DC link capacitor is a very important component of the drive topology. It is connected between the supply side diode rectifier and the machine side voltage source inverter. The capacitor serves as a filter to remove voltage ripple due to the pulsating DC voltage and act as a temporary energy storage or voltage source to the three-phase VSI. The PWM control is applied to the VSI which in turn supplies variable voltage and frequency to control the speed and torque of the PMSM over the required speed operation. This topology is cost effective, but has limitations when applied to variable speed drives that require regenerative braking for deceleration such as elevators, electric vehicles or other regenerative loads. Two modes of operation are possible with this configuration; motoring and regenerating. During motoring, power flows from the DC link to the motor and during regenerating power can flow from the motor to the DC link. The power flow during regenerating may accumulate as the unidirectional diode rectifiers do not allow power flow to the supply network and this can cause damage. In order to prevent damage, a parallel connected braking resistor is required in the DC link to dissipate the power as the load regenerates [86]. This configuration requires only one controller for the VSI. The controller for the VSI consists of the outer speed controller and the inner current controller. Speed feedback is required for the speed controller. Speed feedback can be obtained through measurement of speed using an encoder or speed sensor mounted on the shaft of the machine. The output of the speed controller generates the current references for the current controllers which are then compared with the measured stator currents. The resultant errors from the current controllers are compared with the carrier-based triangular waveforms and the outputs provide the gating signals of the VSI and enable the speed of the PMSM to be controlled to the desired value. If the AC power supply is from a variable voltage and frequency source the diode rectifier is replaced by a controlled rectifier as shown in Fig 2-8 (b). This application is commonly used when renewable energy conversion systems provide the power supply to the variable speed machine drives e.g. water pumping systems [87]. In this scenario, the system will need two controllers, one for the controlled rectifiers and another for the VSI-PMSM drive.

Control parameters at the variable speed and frequency source can be speed, torque, voltage, current and pulse width.

2.6 Permanent Magnet Synchronous Generator (PMSG) Drive System

Permanent magnet synchronous generator can operate over a wide speed range generating electricity with high efficiency and reliability. They are mostly applied to variable speed energy conversion system such as wind energy conversion systems, ocean wave energy conversion systems and tidal wave energy conversion systems. In such a system, the output voltage and frequency depends on the variability of the speed of the energy source. As the speed varies, the voltage and frequency also varies yet a constant voltage and frequency is required to be utilised by a standalone AC load or connected to grid. An AC/DC/AC converter is used for connecting the variable speed generator to the AC load or grid [88]-[91]. The main objective of the converters is to optimise power extraction, control the DC link voltage and transfer active and reactive power to the AC load/grid. There are two types of AC/DC/AC converter topologies used with variable speed PMSG namely;

1. The front end uncontrolled diode rectifier and DC/DC converter and VSI
2. The full scale back-back voltage source converter

2.6.1 PMSG Drive with Front End Uncontrolled Diode Rectifier, DC/DC Converter and VSI

Small energy conversion system such as wind, ocean waves, tidal waves using PMSG in the range of a few hundred watts to kilowatts that can operate at variable speed to increase the energy output, and can be connected to an independent AC load through a DC/DC converter. This is the simplest and the cheapest topology, which uses one active power electronic device (e.g. IGBT) in the DC link and controls the generator speed and torque in such a way that maximum power can be generated as the speed changes. Two type of DC/DC converter are the buck and the boost converters [92][93]. The boost DC/DC converter is widely used because it steps up the typically low output voltage of the small PMSG energy conversion systems.

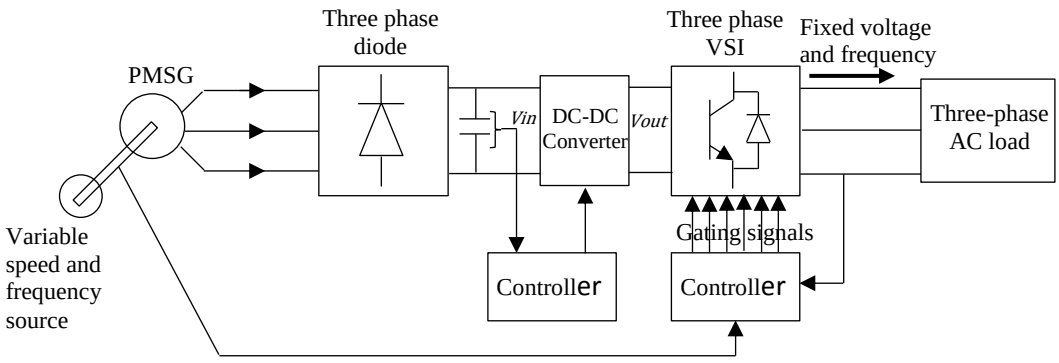

Figure 2-9: PMSG drive with front end uncontrolled diode rectifier and DC/DC converter and VSI

Figure 2-9 shows the PMSG drive system usually used for small power. It consists of a front end diode bridge rectifier (single or three-phase), a boost DC-DC converter and an inverter (single or three-phase) connected to the AC load/grid. Between the front-end diode bridge rectifier and the boost DC-DC converter is a capacitor the role of which is to reduce the voltage ripple, provides storage and isolate the generator side from the AC load side. In this topology the generator voltage output is converted into DC voltage using the diode bridge rectifier, the DC/DC boost converter steps up the DC voltage, and the AC load/grid side VSI converts the DC voltage into a constant voltage and frequency. There are two control strategies in this configuration, the DC/DC converter controller and the DC/AC inverter controller. The objective of the DC/DC converter controller is to maintain a constant DC link voltage through the duty ratio based on the conversion ratio given as:

$$\frac{V_{out}}{V_{in}} = \frac{1}{1-D} \tag{2.1}$$

Where D is the duty ratio.

Controlling the duty ratio controls the DC/DC converter switching device and the DC link voltage to the desired value and the AC load side VSI controls the operation of the generator to transfer power to the load/grid. With the correct choice of control, the generator speed can be controlled to obtain maximum power at different rotational speeds as the speed of the energy source changes. The energy source can be wind, ocean or tidal. The disadvantage of this topology is generation of current harmonics and torque ripple as a result of the operation of the diode which results in lower efficiency.

In addition, the limit in the power this topology can handle depends on the maximum power of the one stage DC/DC converter device.

2.6.2 PMSG Drive with Full Scale Back-Back Voltage Source Converter

A typical topology of a three-phase direct drive variable speed PMSG drive power conversion system is shown in Figure 2-10. This topology can be used as an isolated standalone unit or directly connected to the grid through the back-back voltage source converters. In order to obtain a higher AC voltage level and tie to the grid, a step up transformer can be used. In this concept, three-phase AC/DC and DC/AC converters are connected back-to-back between the variable speed PMSG and the AC load or grid. It consists of two-level three-phase converters; the generator side converter and the AC load/grid side converters.

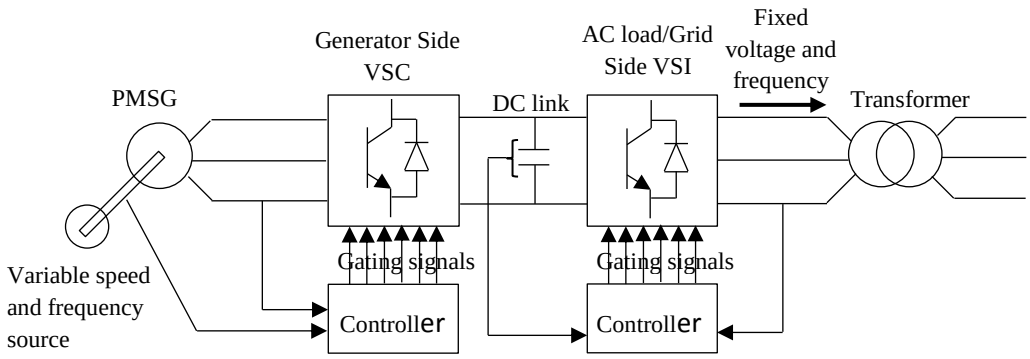

Figure 2-10: PMSG drive with full scale back-back voltage source converter

The DC Link capacitor between the generator side converter and the AC load/grid side converter serves as a storage device, filter and a point of isolation between the generator side converter and the AC side inverter decoupling the electrical frequency of the generator side from the AC load /grid side. The generator side converter converts the generated AC output voltage into DC and the AC load/grid side converter converts the DC link voltage into a constant voltage and frequency for AC load use or connection to the grid. The converters require control to effectively implement power conversion and processing. This control as earlier stated can be from any of the PWM control strategies such as carrier-based sinusoidal PWM or space vector PWM or direct torque control [94] but the control parameters depends on what needs to be controlled e.g., power, voltage,

current, torque, speed or frequency. In a grid connected situation, this configuration enables smooth grid connection and faults-ride through capability but it has disadvantages such as high cost and high power losses. Since 100% of the power generated passes through the full-scale frequency power converters, there are usually high power losses in the power converters due to the switching of the converters switches which depends on PWM switching frequency. With high PWM switching frequency, the harmonics contents at frequencies other than the fundamental frequency can be minimised but that will result in high switching losses due to the fast switching characteristics of the power electronic switches. However, with the advancement in power electronic converters technology and availability of improved permanent magnet materials, the overall efficiency of PMSG drive system is likely to improve and cost reduced in the near future.

2.7 PMSG Drive Wind Energy Conversion System

In recent years Wind Energy Conversion Systems (WECS) have seen significant development and growth, and it has certainly undergone huge transformation over the years from windmills which provided mechanical power to pump water or grind grains in the seventh century BC to producing electricity in the 19th century. The oil crises in the 1970s and the global concern over the effect on the environment and inhabitants of the greenhouse gas emissions can be viewed as the symbolic periods in the history of wind energy conversion. During this period, wind turbine generators were used to generate electricity from wind energy. The early types of wind turbine generators were made for fixed speed operation using squirrel cage induction generators (SCIG) [95]. In this concept as shown in Figure 2-11 (a), a multi-stage gearbox is used between the wind turbine and the squirrel cage induction generator to step up the low rotational wind speed and operate at near constant speed. The generator is then connected directly to the AC load/supply network (grid) through a soft starter switch and a capacitor bank to enhance grid compatibility. The capacitor bank provides reactive power and the speed of the generator is fixed by the frequency of the power supply network and maintained constant in spite of changes in wind speed over time.

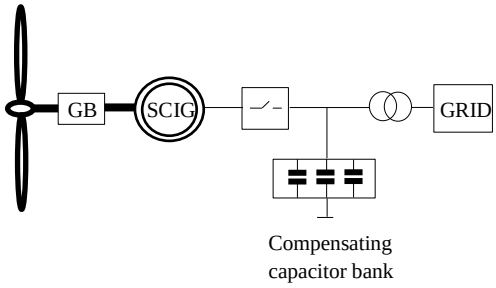

(a) Fixed speed SCIG wind turbine

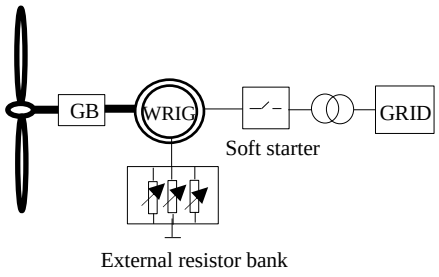

(b) WRIG wind turbine

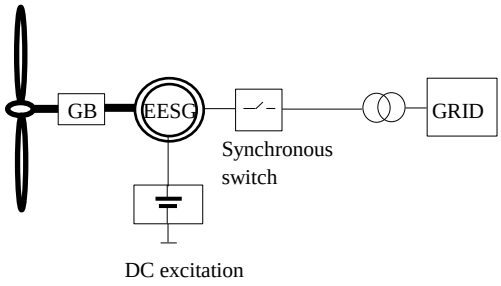

(c) Fixed speed EESG wind turbine

Figure 2-11: PMSG drive with full scale back-back voltage source converter

The fixed speed operation is simple and low cost compared to other forms of wind turbine. In addition, the squirrel cage induction generator is a cheap, rugged and simple to operate machine. However the generator rotor speed can only be varied in small amount related to the slip in the range of 1%-2% [96] as the wind speed changes. When wind speed fluctuates beyond the slip range, it results in fluctuations of the torque in the gearbox or drive train. This could lead to mechanical stress, gearbox failure and drive train fatigue. Generally Induction generators consume reactive power, cannot contribute to voltage control, and require a compensation capacitor bank to provide reactive power consumption, improve power factor and maintain a smooth grid connection. The increase in voltage fluctuation in the absence of a reactive power capacitor compensator can lead to line losses, low power quality, low power yield; reduce efficiency and reduce performance of the system. However, with the addition of a power electronic semiconductor converter, squirrel cage induction generators can now be operated at variable speed [97][98]. Another type of wind turbine generator configuration is the wound rotor induction generator (WRIG) in which the WRIG stator is connected directly to the grid as shown in Figure 2-11(b), while an external resistor bank is connected to the rotor and the rotor current controlled with power electronic converter devices enabling a small variable speed range operation [99][100]. In addition, the external resistor limits

the starting current and lock rotor current which serves as a protection to the rotor during motor starting. Compared to the doubly fed induction generator, the wound rotor induction generator has electrical connections only to the stator windings. The fixed speed wind turbine system with gearbox has been extended to synchronous generators as in Figure 2-11(c). In this concept, there is no need for the power electronic converter devices, the DC electrically excited synchronous generator is connected directly to the grid through a switch and enables the generated voltage to be regulated. Although, losses due to power electronic converter devices are absent, it has disadvantages such as the use of field windings to generate magnetic fields and a gearbox which increases losses, increases the possibilities of failure, increases cost of maintenance, and reduces reliability and efficiency.

Over the years, the need to maximise energy production in wind turbine systems has increased. In order to maximise the extracted energy, variable speed wind turbines using power electronic converters was introduced. Power electronic converters are used to process and convert varying power from the wind turbine generator to the AC load at the desired voltage and frequency or connect to the grid at fixed voltage and frequency. The power electronic converter controls the speed and torque of the wind turbine generator for maximum power extractions from the wind and transfers active and reactive power to the AC load or grid.

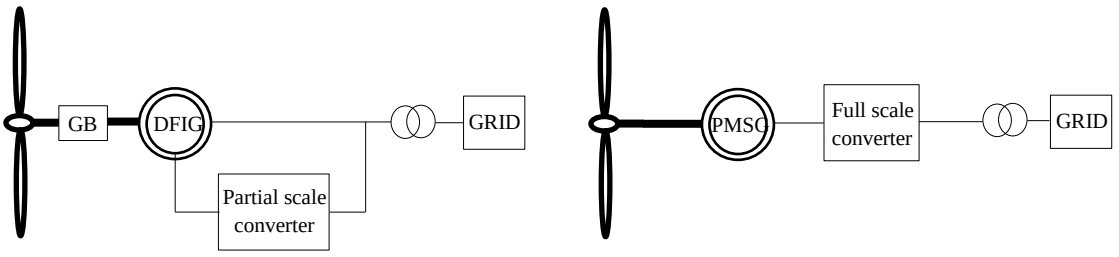

(a) DFIG wind turbine system

(b) Direct drive PMSG wind turbine system

Figure 2-12: Variable speed wind turbine systems (a) DFIG wind turbine system (b) Direct drive PMSG wind turbine system

Variable speed operation of wind turbine offers a lot of advantages such as reduced mechanical stress, reduced friction, reduced maintenance, reduced acoustic noise, improved efficiency and reliably. There are two most commonly used variable speed

wind turbine generator systems. The first wind turbine generator for variable speed is the doubly fed induction generator (DFIG). It has been widely used in wind power generation especially in high power applications (>500kW). This type of variable speed wind turbine power generation system uses a multi-stage gearbox and partial-scale power electronic converter for connection of the wind turbine generator to AC load/grid [101][102]. Figure 2-12(a) shows a variable speed wind turbine with a gearbox in which both the rotor and the stator of the DFIG are connected to the AC load or grid. While the stator is connected directly to the grid, the rotor is connected via an AC/DC/AC three phase converters, that means, the rotor power is handled by the power electronic converter, which is a fraction of the total power, normally about 30% total generator power [103][104]. The advantage is that, the losses in the power electronic converter as well as the cost of the system can be reduced when compared to a system where the converter has to handle the total generator power. But the disadvantages are that, the system uses slip rings and as current flows through these this leads to heat generation, electrical losses and possible failures and maintenance requirements. On the other hand, this concept has a limited variable speed range of approximately $\pm 30\%$ around the synchronous speed and during high voltage dip, the high voltage and current can lead to damage of the generator rotor converter. This requires additional protection of the generator and the converter usually with a Crowbar circuit [105], which means extra weight, and from an economic point of view, additional cost and maintenance is required with resulting reduction in efficiency. The DFIG is used for large power wind turbines up to several megawatts [106]. However the system is prone to faults as it uses a gearbox to connect the wind turbine to the generator to enable the slow speed, high torque of the wind turbine to be stepped up. The gearbox reduces efficiency, generates faults and requires regular maintenance- this results in additional operational costs.

The second type is the PMSG direct drive based variable speed wind energy conversion system as shown in Figure 2-12(b). It has a simplified drive train that is gearless (no gearbox) with a direct-drive PMSG connected to the grid through power electronic converters [107]. The direct-drive generator is directly connected to the wind turbine and has the capability to operate at the same low rotational speed as the wind turbine enabling power extraction even at low wind speeds. In order to utilise the low wind speed and generate particular levels of power, multi-poles generators are required with the wind

turbine. Using multi-pole generator requires larger diameter which results to large volume, weight and high cost of the system. However, to reduce generator diameter and volume, reduced cost, minimise losses and improve efficiency, the PMSG are produced with a small pole-pitch and multiple poles [108]. A PMSG drive based wind energy conversion system is an efficient and reliable concept for producing electricity from the wind energy and it is gaining wider popularity compared to other forms of variable speed wind turbine generators. Compared to the DFIG based wind turbine system, the use of PMSG drive in wind energy conversion system do not require gearbox, slip rings, and this simplifies the structure of WECs with high efficiency, reliability, reduced failures and reduced cost of maintenance. Recently, wind turbine manufacturers are exploiting the possibility of using permanent magnet synchronous generators for large power both onshore and offshore wind turbines and there is high prospect of future wind turbines employing permanent magnet synchronous generators. For example Snitchler, G. et al [109] and Leban, K. et al [110] are focused on designing megawatts PMSG for wind power generation applications. As a matter of fact presently, the world largest commercially available wind turbine, Vesta V164-8.0 with rated power of 8.0MW uses a geared medium-speed permanent magnet synchronous generator [106]. It is believed that in the near future the wind turbine industry will be dominated with variable speed PMSG wind energy conversion system.

As interest in the use of variable speed PMSG wind energy conversion system continues to grow, variable speed PMSG wind energy conversion systems have seen significant research interest in the last few decades. Many new designs of PMSGs, wind turbines and associated controllers are being proposed and developed. As more and more wind turbines of varying capacities and concepts are developed and installed, there are requirements for the next generation wind energy conversion systems. Wind energy conversion systems should be able to maximize and efficiently extract power from wind energy, it should be affordable at reduced cost (i.e. reduced cost of design and production), improve on the quality and level of power generated, simple control, reliable and stable during and after faults in order to guarantee continuous and security of power supply and most importantly should meet the grid code requirements [111]. In addition, new wind energy conversion systems should be quickly introduced into the marketplace. Considering these requirements and as various wind turbines with different capabilities are been developed, it is important to investigate the dynamic interaction and behavior of

all the components to analyze the performance of wind energy conversion system and control techniques.

2.8 Pulse Width Modulation

A desired output voltage, frequency and sinusoidal three-phase AC current can be obtained from voltage source converters through PWM switching of power electronic converter switches. The PWM allows the complementary pair of power electronic switches (e.g. IGBTs) of one phase leg of the VSC to be controlled in alternate ON and OFF mode. The control of the operation of the switches requires the gate drive signal for each switch. Pulse with modulation (PWM) control is the most commonly used method to control power switches. The type of the PWM modulation scheme used and the choice of switching frequency determine the harmonic content of the voltage and current, electromagnetic interference and losses. Lower switching frequency results to lower switching losses but higher harmonic content of the voltage and current and vice versa. Although, several modulation techniques are being proposed and developed [112]-[114], the carrier-based sinusoidal pulse width modulation (SPWM) and the space vector PWM are the most widely used PWM control techniques. Space vector PWM has been widely used because of it superior performance of reduced harmonics, reduced switching losses, better DC voltage utilisation and can be realised easily using digital processing but has the challenge of complex mathematical derivations which is time consuming and require large computer memory. This research is based on carrier-based sinusoidal PWM control techniques implementation using proportional integral (PI) regulator but the techniques developed could also be applied to Vector Control schemes.

2.8.1 Carrier-Based Sinusoidal Pulse Width Modulation

This is the simplest and the most widely used pulse width modulation. It can be applied to single phase and three-phase voltage source converters. For the carrier-based sinusoidal pulse width modulation (SPWM), the modulating signal is sinusoidal. In this method, the modulating signal which is the desired AC voltage (input or output) is compared with triangular (carrier signal) waveform to generates the ON and OFF states for the power electronic switches of the converter. When the amplitude of the modulating signal is greater than the triangular signal, the upper switch in one phase leg e.g. S1 turns

on and the lower switch e.g. S4 (see Figure 2-5) turns off. In the same manner when the amplitude of the modulating signal is less than the triangular signal upper switch S1 is off and the lower switch S4 on. When the upper switch turns on, the output is connected to the positive terminal of the DC link voltage and when it is off it is connected to the negative terminal of the DC voltage.

For the three-phase inverter shown in Figure 2-5 required to supply three-phase voltages 120^0 apart to the AC load, three-phase modulating signals of 120^0 phase displacement are used. The output of each phase of the AC load is independently controlled by the duty cycles of the corresponding switches based on the amplitude modulation ratio also known as modulation index, m_a given by

$$m_a = \frac{V_m}{V_c} \tag{2.2}$$

Where m_a represents the switching functions of the phases, $S_{A,}\, S_{B,}\, S_{C,}$, V_m is the peak of the modulating waveform, V_c is the peak of the carrier waveform. The modulation index determines the fundamental frequency component of the carrier-based PWM inverter output voltage. The output voltage varies directly with the modulation index and based on Figure 2-5, the amplitude of the fundamental component of the carrier-based PWM inverter AC output voltage is given as

$$V_{AN} = m_a \frac{V_{DC}}{2} \tag{2.3}$$

Equation 2.3 defines the relationship between the, modulation index, DC voltage and the PWM voltage output. It shows that the maximum amplitude of the fundamental AC phase voltage is a linear function of the modulation index provided $0 \leq m_a \leq 1$ is maintained. Similarly, the AC output line-line voltage in the linear modulation region is given by

$$V_{AB} = \sqrt{3}\, m_a \frac{V_{DC}}{2} \tag{2.4}$$

And at the fundamental frequency, the line –line rms voltage is given as

$$V_{AB}(rms) = \frac{\sqrt{3}}{2\sqrt{2}}\, m_a V_{DC} \tag{2.5}$$

$$V_{AB}(rms) = 0.612\, m_a V_{DC} \tag{2.6}$$

Hence, the modulation index can be varied to control the voltage. However, this relationship can become nonlinear when the amplitude of the modulating signal becomes higher than the amplitude of the carrier signal. This occurs when there is a need to increase the load voltage. When this happens, the relationship between the DC voltage and the AC output voltage becomes nonlinear and leads to over modulation [115].

The modulating signal and the carrier-based signal of the three-phase VSI in Figure 2-5 is shown in Fig. 2-13 (a) and a typical example of the switch states is shown for phase A of the VSI in Fig 2-13 (b). Fig. 2-13 (c) shows the SPWM AC output voltage of the VSI for phase A and Figure 2-14 shows the three-phase AC line voltage for SPWM. It can be seen that maximum output voltage is limited by the maximum DC voltage and the switching devices. The AC output voltage waveform of SPWM is known to contain harmonics the details of which are not dealt with in this thesis but can be found in other publications [116] – [119].

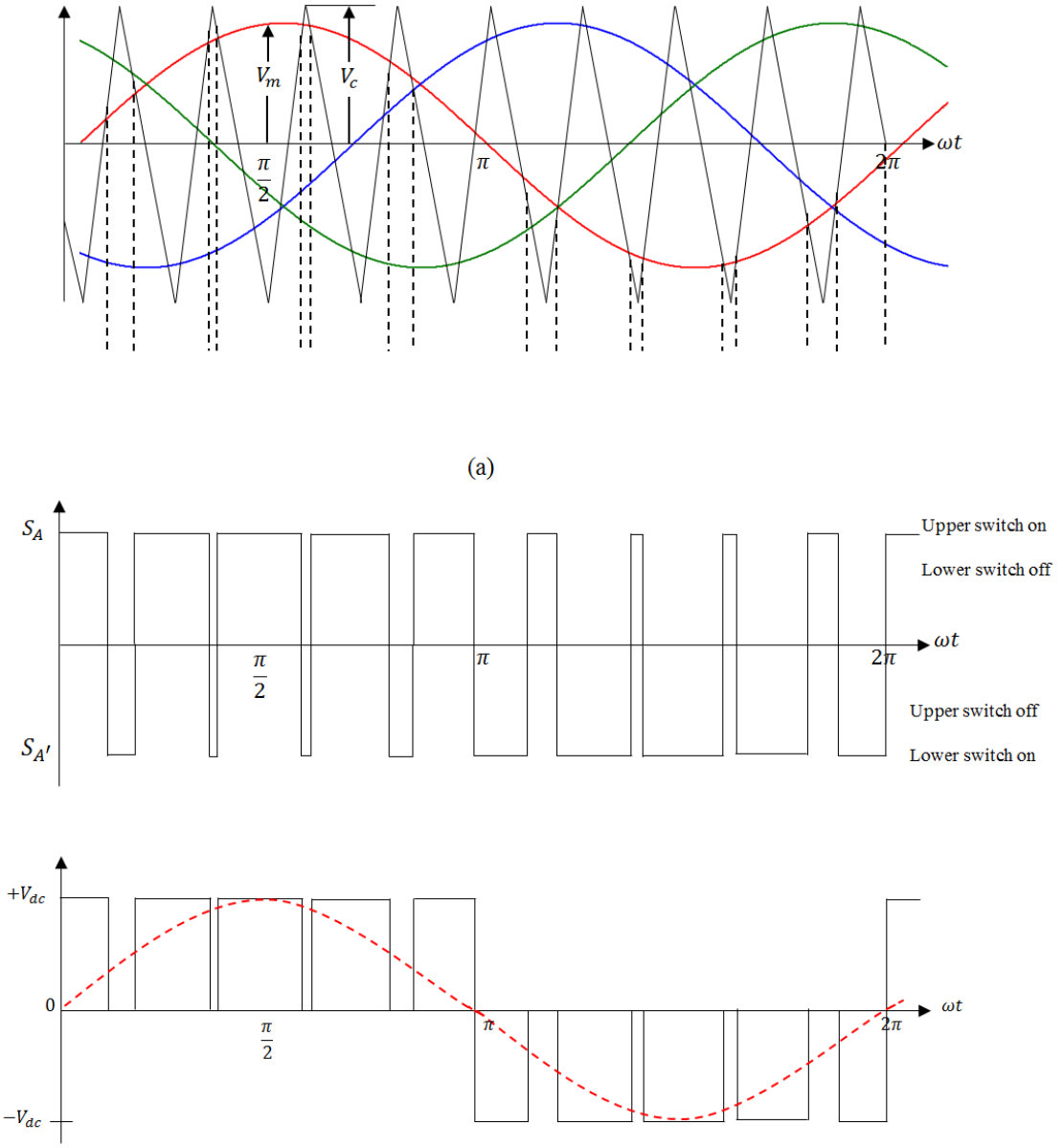

Figure 2-13: Three-phase VSI waveform for SPWM (a) modulating and carrier-based signal (b) switch states for phase A (c) ac phase (phase A) output voltage waveform

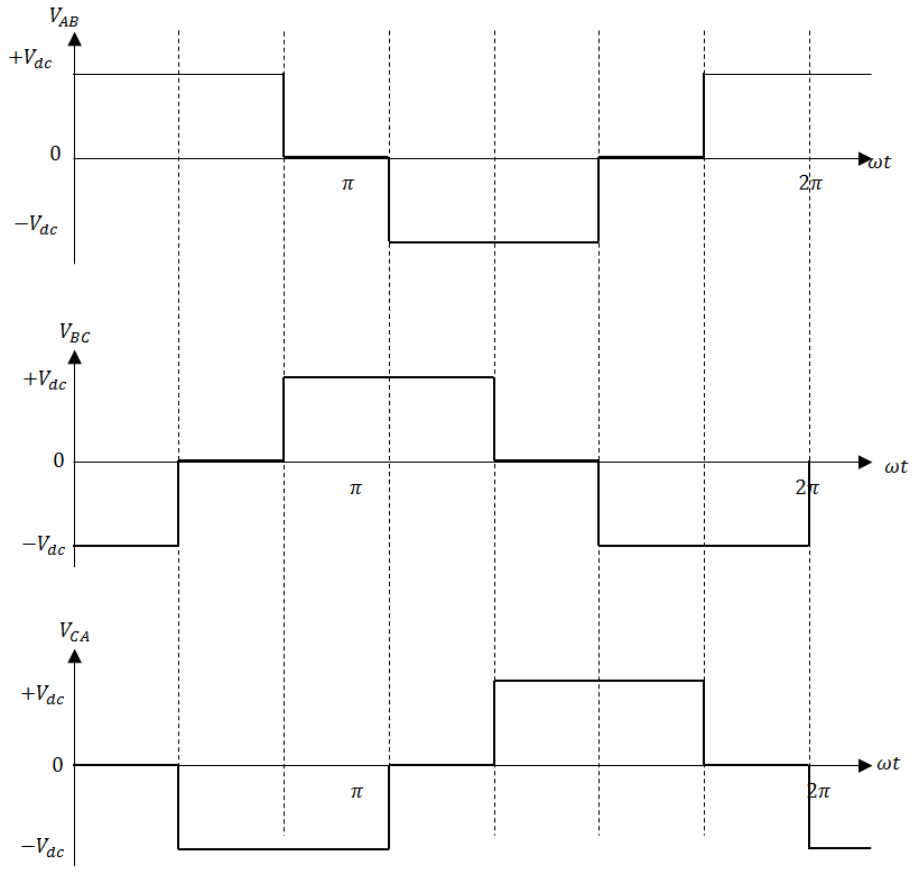

Figure 2-14: Three-phase VSI ac line voltage waveform for SPWM

2.9 Proportional Integral (PI) Controller (Regulator)

The Proportional Integral Regulator is a fundamental building block of control systems in electrical drives. It has been extensively employed in the control of magnetic flux and torque in the FOC strategy [120]. Its application is not only limited to flux and torque control but is also used to control electric motor and generator rotor speed as reported in [121][122]. PI regulators are continuously been used in industries and renewable energy conversion. Recently, PI regulators are used to control stator current, voltage, power [123].

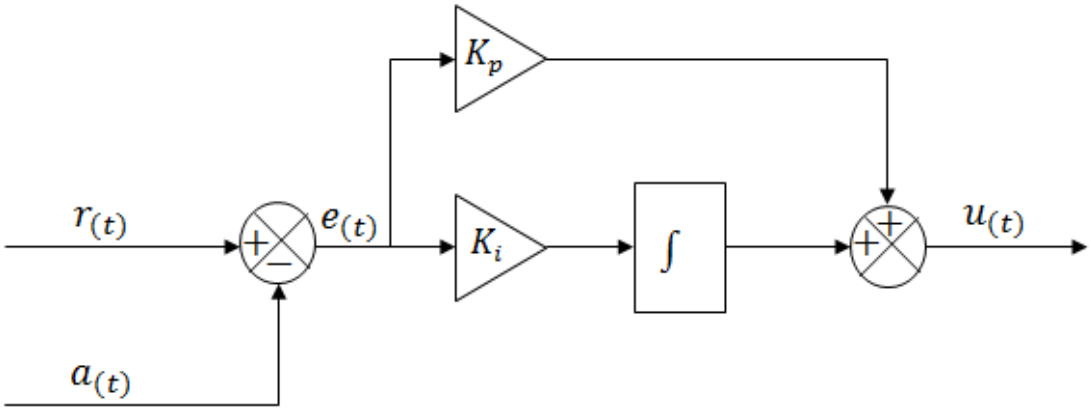

Figure 2-15: A typical proportional integral (PI) regulator algorithms

Figure 2-15 shows the structure of a typical digital PI regulator. The mathematical representation of the PI regulator in Time Domain is

$$u_{(t)} = k_p \left[e(t) + \frac{1}{T_i} \int e(t)dt \right] \tag{2.7}$$

And the transfer function in Laplace Domain is

$$\frac{u(s)}{e(s)} = k_p + \frac{k_i}{s} = k_p \left[1 + \frac{1}{T_i s} \right] \tag{2.8}$$

Where r: Reference variable
a: Actual or measured variable
e: Error signal
k_p: Proportional gain
k_i: Integral gain
u: Output signal
t: Instantaneous time
T_i: Integral time
s: Complex number frequency

The PI regulator is characterised by the two gain terms; the proportional gain k_p and integral gain k_i. With the gains, PI regulator processes the error resulting from the comparison of the measured and reference signals achieving a closed loop control in which the output signal is forced to follow the reference signal. The proportional gain regulates the output signal in direct proportion to the error signal. While the integral gain

is responsible to corrects the error. When used with a pulse width modulator, it achieves advantages such as constant switching frequency, low acoustic noise with satisfactory dynamic response and performance. In addition to these, it has a simple structure that enables easy digital and analogue implementation. The performance of the PI controller depends on the careful choice and tuning of the gains, a process which is difficult and is a major challenge in the design of the PI regulators. To overcome this challenge, different methods as presented in [124]-[126] are available through which the gains of the PI regulators can be tuned to attain satisfactory, dynamic response and performance.

2.10 Literature Reviews of VSI-PM Machine Drive Modelling and Simulation Methods

Over last number of decades, there have been extensive research and development into the design and topologies of two level three phase voltage source inverter fed electric machine drives. During this time, the market demand for electric machine drives have also increased and the requirements for electric machine drives has become more and more demanding. For example, there is an increasing demand for higher power, higher current handling capabilities, faster switching frequency, and ease in controllability, higher efficiency and reliability at reduced cost. The design, control and analysis of electric drives system have become a major concern in recent times and extensive research has been conducted and some are on-going in this area to obtained higher voltage and power levels with high efficiency, high dynamic response and performance at reduced cost.

In order to study and analyse various designs, control of electric machine drive system and the interaction between the electrical and mechanical parts of the drive, simulation tools are being extensively used by design engineers, researchers and manufacturers of electrical machine drives. This trend is expected to continue in the near future due to the continuous advancement and development in the designs and topology of power electronic devices and permanent magnet synchronous machines. Simulation tools have supported the efficient design and analysis process of electrical machine drive systems and control strategies, reduce cost, time and eliminate exposure to risk and hazards. Modern simulation programs have the capability of performing both steady state and

dynamic simulations of electrical machine drives. There are numbers of commercially available software packages which can be used in simulations such as MATLAB/Simulink, PSCAD, LABVIEW, EMTP, DigSILENT, PORTUNUS, Pspice, Saber and PSIM. In general, there are two modelling methods of voltage source inverter with permanent magnet synchronous machine drive; the detailed switching model and the average value model.

2.10.1 The Detailed VSI Switching Modelling and Simulation Method

The simulation of electric machine drive system requires accurate models which can be used to analyse both small and large machine drive systems. Various techniques and modelling methods of voltage source converters and control strategies for electric machine drive system have been developed and studied for different purposes. Some of these models and controller designs have been verified in the laboratory with digital signal processor and microcomputers [127][128]. However, the purpose for developing models differs from one author to another; the basic approach is either to use a detailed switching model or average value model of the voltage source inverter together with electrical machines. The most widely used approach is the detailed switching model. In the detailed switching model, the voltage source inverter is modelled according to the equivalent circuit topologies as described in section 2.5 and section 2.6, where the power conversion system can be represented by using component models usually available in the simulation library and the switching of the converter transistors and diode are adequately represented.

Generally, the detailed switching modelling method has been developed and used to analyse different aspects and types of electrical machine drives and control techniques. Indeed in [129]-[133], the VSI switching modeling approach is used to simulate analyses of the performance of various control techniques of induction motor drive systems. In addition the performance of DFIG wind energy conversion systems have been evaluated using the detailed VSI switching modeling method [134]-[137], taking into consideration the switch mode characteristics of the PWM converters. Similarly, the detailed switching modelling method has been used to investigate the performance of squirrel cage induction machine control techniques [138] – [145] and that of synchronous machine drive systems [146] – [149].

In the past two decades, the detailed VSI switching modelling method for electric machine drives has been developed and used for modelling and simulation of permanent magnet synchronous machine drive system. Several publications [150]-[153] have provided guidelines for modelling and simulation of PM machine drives and controller designs for which a PM machine can be represented in stationary reference frame (a, b, c) or rotating reference frame (d, q) and the voltage source inverter represented by power electronic converter switches and the control strategy providing the switching functionality.

In 1989, Pragasen Pillay et al [154][155], researched the possibility of using the VSI switching modelling method to simulate permanent magnet synchronous motor drive systems and published one of the earliest papers on the approach to a complete modelling and simulation of the permanent magnet synchronous motor (PMSM) drive. A state space model of PM motor and real time inverter switches models suitable for analysis of the PMSM drive and vector control technique was developed. This method was based on connections of the components of the PMSM drives in simulation software, which consists of the DC power supply, the three-phase voltage inverters power devices and the load. The introduction of the voltage source inverter devices in the model provide an important way of describing the switching behaviour of the voltage source inverter devices and the role of the control system. Their study outlined the step-by-step approach to the modelling and design of PMSM drive systems. However, the simulation software used was not stated, but comparison of PWM and hysteresis current control was carried out based on simulation and experimental results. In 1997, A.M Gole, et al [156] provided detailed guidelines for modelling and simulations of power electronics devices. They classified modelling considerations into two based on study objectives such as, steady state evaluations, dynamic and transient performance evaluations. The steady state evaluation enabled the power electronics converter topology to be reduced to its equivalent circuit while for dynamic and transient evaluations; a more detailed model is required. The frequency domain simulation and time domain simulation were compared as well as methods to represent semiconductor devices, power electronic sub-systems and controls were also described. Included to their study was the investigation into the effect of the time step for PMW control strategies during simulation of power electronic converters. The recommended time step of not greater than 1/5 to 1/20 of the period of the highest frequency and effects of time step on the resolution for a signal sampling for

digital control and simulation errors in time domain simulation were adequately discussed. Their study presented very useful conclusions that power electronic sub-system can be reduced and simplified depending on the purposes of the study and this has become a useful consideration upon which this research is based.

Since then, a large amount of research and analysis has investigated the development and use of the detailed VSI switching modelling method in PMSM drive design and associated control techniques. M. Azizur Rahman et al [157] presented a modelling and simulation approach to the analysis of intelligent controller for interior permanent magnet synchronous motor drive. Their method is based on three phase voltage source inverter switching model developed in MATLAB/Simulink and validated through experiment. Simulation and experimental results were presented to verify the effectiveness of the model and control strategy. The detailed switching modelling has further been applied by Liye Song et al [158] to the analyses and comparison of the stability of PI-fuzzy with PI control for permanent magnet synchronous motors. Their model was implemented in MATLAB/Simulink and the simulation results were presented to validate the effectiveness of the control and comparison with PI control strategy. However, simulation of detailed switching model is based on solution of non-linear differential equations as results of non-linear switching devices and results to long simulation execution time compared to average value model.

In some recent works on PM motor drives, the detailed switching modelling method of three-phase voltage source inverter with PMSM has been developed and used to perform analyses of PMSM drives and control strategies. Yulong Huang, et al [159], presented a detailed VSI switching model in MATLAB/Simulink to investigate the space vector pulse width modulation control as applied to operating mechanism a high voltage circuit breaker (HVCB) driven by a permanent magnet synchronous motor. In addition A.N Tiwari, et al [160], performed a simulation in MATLAB/Simulink to analyse the performance of PMSM drive and hysteresis current control using a detailed inverter switching model. Recently, the switching modelling method of a three phase voltage source inverter fed PMSM drive was developed in [161]-[163] and applied to analyse the performance of vector control and direct torque control of PMSM drive based on SVPWM. Flux weakening is another important aspect of PMSM drive that has seen use of the detailed switching modelling method. Matthias Preindl et al [164], applied the

detailed switching model in the study of a flux weakening technique for PMSM based model predictive direct torque control where the complete switching of the VSI transistors and diodes are fully represented. Several research activities aimed at developing improved control techniques and advance controllers for PMSM drive system [165]-[167] are carried out using the detailed switching model. Similarly, investigations on PMSM drive focussed on reduction of cost and number of sensors, eliminate measurement of rotor speed, speed sensorless control of PMSM drive [168]-[172] have been conducted using simulation switching models of voltage source inverters. The detailed switching model have also been applied to the study of single three phase inverter fed parallel PMSM [173]-[176], cascade two level three phase inverter fed PMSM drive, multilevel and modular multilevel [177]-[181] as well as methods to reduce losses of PMSM drive systems, increase and optimise efficiency [182][183].

Alternatively, Anca D. Hansen et al [184], developed a switching model of the three-phase full-scale back-back voltage source converter and controller design for a grid connected wind turbine with a multi-pole permanent magnet synchronous generator in DIgSILENT. The complete model consisted of the aerodynamic rotor, a two mass drive train model, PMSG and voltage source converter, pitch angle control and grid including the switching of 12 PWM IGBTs and 12 diodes. The performance of the wind turbine control technique and the effect of the variation of wind speed on the performance of the control of active and reactive power to the grid were studied. Simulation results with simulation set time of 206 seconds were presented to verify the effectiveness of the control technique. Since simulation of PWM converters depends strongly on simulation time step and the simulation time step of PWM converter is limited to a small time step, the simulation of switching models for longer times becomes difficult and time consuming. Many researchers have developed and applied the detailed modelling method to analyse and investigate the different aspects of three phase full scale back-back voltage source inverters with variable speed PMSG wind turbine systems and control techniques. In [185], a detailed switching model of a back-back voltage source inverter had been developed in PSCAD/EMTDC to compare and analyse a variable speed wind energy conversion system with DFIG and synchronous generators. Research as reported in [186][187] investigated deriving a representation that was suitable for analysis of Hysteresis band current control (HBCC), voltage oriented control (VOC) and flux oriented control (FOC) for a power variable speed PMSG wind turbine.

The mathematical model of the PMSG in d-q reference frame, the voltage source inverter model based on switching scheme for six power transistors at the generator side and six power transistors at the AC load side as well as the design of the controllers were developed in MATLAB/Simulink. Time-domain simulation results were presented to validate the model and control techniques. The model enables analysis of the system and control strategy but the drawback is the requirement for complex mathematical transformation from three-phase to stationary reference and then to rotating reference frame.

In [188]-[191], detailed switching model have been successfully developed in different simulation packages and used for the analysis of maximum power point tracking control techniques of variable speed wind energy conversion systems, speed sensorless control techniques by [192]-[197], performance analysis of flux weakening control of variable speed PMSG WECs [198]. In Youssef Errami, et al [199][200], a detailed switching model of a variable speed PMSG wind farm using back-back voltage source converters is presented. Their model consists of 5-2MW PMSG wind turbine each connected to a common DC through a three-phase voltage source converter and the common DC bus connected to the grid through filters. The PWM and MPPT control technique were used to generate the switching signals for the generator side converter and the direct power control generated switching signals for the grid side inverter. From the model, there are a total of 5x6 = 30 power electronic converter switches and antiparallel diodes at the generators side and 1x6 power electronic converter switches and antiparallel diodes at the grid side with PMSG drive system simulated in MATLAB/Simulink. Simulation results for a chosen period of 10 second were presented to validate the effectiveness of the models and control schemes. Additionally in [201], a multi-stage three-phase AC/DC PWM converter switching model was developed in SIMPLORER for the performance study of a 12-phase standalone PMSG wind turbine system for maximum power extraction. From the models, a total of 4 stages of 4x6 active power converter switches operating in switching mode were simulated and simulation results for a chosen time of 350ms were given to verify the model and control effectiveness as unity power factor was achieved. S.M. Muyeen et al [202] developed a simulation model for a fuzzy-logic controlled inverter system for grid interconnected variable speed wind generator using PSCAD/EMTDC. To analyze the dynamic and transient behavior and stability of the system, a model of three-phase variable speed PMSG wind turbine with full scale

frequency converter connected to an infinite bus through a transformer were described. The model includes the wind turbine model, the generator model in d-q reference frame, the full scale frequency converter modelled as a three-phase two-level voltage source converter with six IGBTs and antiparallel diodes at the generator side and the same at the grid side. The operation of the voltage source inverters was based on switching pulses from a fuzzy logic controller. A simulation time step of 20μs and simulation set time of 300s and 5s were used for the dynamic and transient stability analyses.

A significant amount of literature has been published on the development and uses of the detailed switching model to investigate the different aspects of a voltage source inverter fed variable speed PMSM drive and full scale back-back VSI with PMSG wind energy conversion system. Although, the detailed switching model is an established and widely used modelling approach which is adequate for the design and analysis of PMSM drives and PMSG drive wind energy conversion systems and other electrical machine drive systems and can easily be implemented, it has the drawback of long simulation execution times. The simulation of the PWM VSI detailed switching modelling method is based on a rigid numerical integration of nonlinear differential equations restricted by simulation time steps to obtain good resolution as required by the PWM control techniques. This requires a substantial length of simulation execution times and this limits its application for a time scheduled cost effective PM machine design and control process analysis. This situation gets even worse when the system to be simulated has large number of power electronic converter devices. This is because modern power electronic devices operate in switch-mode and are non-linear discontinuous system. In addition, the switching models are characterised by very small minimum simulation step lengths (<100ns) as determined by the required resolution of the Pulse-Width Modulation (PWM) control (e.g.: 12bit resolution @ 20kHz), and once incorporated into the complete rotating PM machine drive mechanical system or renewable power conversion system and under realistic adjustable speed conditions, simulation lengths in the region of minutes if not hours are required for accurate evaluation of the system. The simulation of detailed switching model results to long simulation execution times because of the non-linear switching devices involved, and very short simulation step lengths in the region of hundreds of nanoseconds are required for accurate results. This modelling approach requires high performance microprocessor computer with large memory and reasonably long simulation time to obtain accurate and reliable results.

In a time-scheduled design process, a more simplified and accurate model with the total elimination of the switching devices which takes into consideration the dynamics of the variable speed PMSM drive and PMSG wind turbine behaviour is required to rapidly simulate machine and control technique performance where adequate consideration is given to the length of the simulation execution time.

2.10.2 Average Value Model for PM Machines Drives

The simplification of modelling power conversion systems by eliminating the PWM converter components switching using averaging techniques have been pursued and researched on in the last few decades leading to the introduction of the modelling method called the Average Value Model. This modelling approach which is well established for DC/DC converters is traceable to the earliest work on average circuit models for switching converters by Wester and Middlebrooks. In 1972, Wester and Middlebrook [203] explored and introduced the possibility of using the duty cycles of PWM modulators and developed average value model for DC/DC converters. They further expanded the averaging technique to include state-space average modelling which became a generalised modelling method for DC/DC converter in 1976 [204]. The state space averaging technique provides very important tools to analysing switched mode power systems and describes the functions and behaviour of the power electronic converters and control techniques especially where detailed analysis of the switching network is not necessary. Similarly, in 1998 [205][206], V. Vorperian developed average PWM switch model for power converters and replaced a power converter switch and diode with a three terminal device from which both the average and linearized three terminals switch model was derived. Generally, there are three average modelling approaches to power electronics converters; the state-space averaging, circuit averaging and the PWM average switch model. The most widely used simplified method to modelling of PWM converters is the average value model based on state-space averaging. In 1994, Silva Hiti et al in [207][208] further developed and applied state-space averaging technique to a three phase PMSM operating at constant speed supplied by a PWM VSI. Silva Hiti et al presented a simplified average model of PMSM drive in rotating coordinates where the DC side is modelled as a current source and the AC side modelled a voltage sources in dq axis and the duty cycle as the weighting function in one switching period thus eliminating the switching functions of the power converters.

However, their models were not applied to variable speed electrical machine operation, nonlinearities and switch mode behaviour of the converters were studied. These models are viewed as outstanding contributions in the research field as it helped to eliminate the non-linearity of inverter device switching and forms the basis for subsequent average models. However, it takes a lot of computation time to derive state space averaging equations based on d-q axis as it involves a significant amount of complex mathematical transformations. Figure 2-16 shows the most widely used state-space average value model for two level three-phase voltage source converters where the current and voltage can be average over a switching cycles based on duty cycles and switching functions.

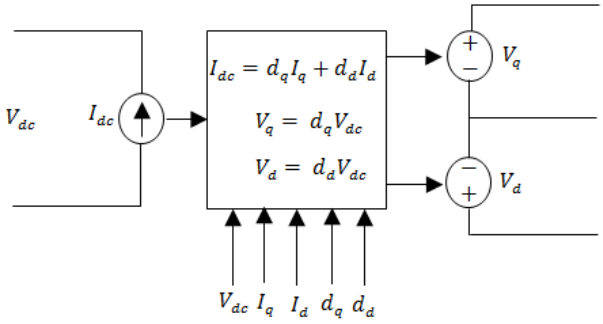

Figure 2-16: State-space average value model of VSI

Since the application of the state-space averaging techniques to three-phase VSI by Silva Hiti et al, a significant number of works on development and applications of average value models have been undertaken. In [209][210], the average modelling approach is applied to the modelling of STATCOM and active filters where a circuit average has been developed to replace switch mode shunt converters. Their approach uses a fixed and variable frequency control strategy such as PWM voltage control and hysteresis to derive average state space equation for voltages and currents based on continuous duty ratio average over a switching period. The continuous duty ratio is obtained from matrix representation of switching function and uses the average inductor currents to drive current-dependent current sources representing each converter and the average capacitor voltage drives three voltage-dependent voltage sources. This paper made significant contributions on the average value and average circuit model as the MATLAB/Simulink results presented validates the effectiveness of the model and control strategies. However the model could reduce simulation run time but it was not applied to variable speed dynamic system where the interaction between the slow dynamics of the machine and the

very fast switching of VSI is of major concern. In addition, deriving the state space equation based on AC filters presents great limitations, opposing the requirement to reduce simulation execution time. Another drawback is the requirement for additional filter circuitry. The correct design and choice of inductance and capacitance to achieve these objectives is difficult as the inductance chosen must ensure that the input current flows at all times and never equals zero. In addition, this method has a drawback in its requirement for complex mathematical computations, to produce the state equations from which an equivalent average circuit model is obtained. Several average value models have been proposed in which the average AC variables are related to the DC link variables using the duty cycles from the control strategy. The approach requires transformation of voltages and currents in dq axis and averaging over the switching period. In [211], Ahmed, S. et al developed an average model of a DC/AC three-phase voltage source inverter with additional parallel diode bridge for the converter phase-leg operations. The model could be used for the study of control strategy and reduce simulation execution time but it is not applied to a real time dynamic systems such as variable speed drive system.

Recently, the average value modelling approach has been applied to modelling of brushless DC motors with 180^0/120° voltage source inverter by Qiang Han et al [212]. Their models which take into consideration the commutation and conduction of the brushless DC motor were developed in MATLAB/ Simulink. Although, small and large signal analysis of brushless DC motor and associated control has been carried out the model is not used for variable speed dynamics where the interaction of the motor, power electronic switching, mechanical load and control requires even a more simplified model. In [213], an average value technique similar to that developed in [212] has been presented for trapezoidal back EMF machines. Significant contributions are made by [212][213], but their approach requires a very laborious computational burden and is time consuming. In addition, the accuracy of the model could have been strengthened by comparing the results of the model to an existing standard such as detailed switching model and experimental results. Most recently, a completely mathematical and analytical based average value model has been proposed. The approach requires the use of switching functions to derive the average value of voltage or current in one switching period, form differential equations or mathematical equivalence of the system from which a simulation can be carried out. Such models based on state-space equations have

been used for the modelling of a DC/AC three-phase grid connected voltage source inverters and LCL filters system by Bjarte Hoff et al. [214], where a variable DC voltage is connected to the grid through power electronic converters. However, the converters are modelled as a mathematical model and there is a need for other components e.g. DC voltage source, grid and control circuit interacts with the inverter model to demonstrate the accuracy of the model. Similarly, Junfei Chen et al [215], recently exploited the possibility of using mathematical equivalence to replace power electronics devices in a model of a directly driven wind turbine with a permanent magnet synchronous generator. The model has been successfully used in the study of grid short circuits and could reduce simulation run time. Despite the fact that the wind turbine and converters are modelled as a mathematical equivalence, it requires that the PMSG and additional passive components representing the grid should be used to implement the interaction between the mathematical model of the converters and the dynamics of the generator, control and grid system. Moreover, the publication did not include analysis of the effectiveness and accuracy of the approach as the results were not compared to existing standards such as switching models and experimental verifications.

A significant amount of works based on the averaging method of simplifying power electronic converter models has also been reviewed. Most of these averaging models are based on state-space averaging methods derived for voltage and current over one switching period using duty cycles developed separately for either an AC/DC converter or a DC/AC inverter. Deriving the state space equations based on d-q transformation, linearization, and AC filters, in which the DC side is modelled as a controlled current source and the AC side as controlled voltage sources, presents great limitations, opposing the requirement to reduce simulation execution time as it is tedious and time consuming. It involves complex mathematical computations, to produce the state equations from which an equivalent circuit model can be obtain. Note that, even if the complex calculation problem of state space average modelling method is overcome, the proposed average voltage estimation model can still achieve better results than previous average value model. In addition, the correct design and choice of inductance and capacitance to achieve these objectives is difficult as the inductance chosen must ensure that the input current flows at all times and never equals zero. In particular, the development of average

model of a three-phase back-back converter with a variable speed rotating generator as obtainable in wind power generation that will reflect the slow dynamics and the intermittence of wind speed of the variable speed system, where the supply voltage and current as well as the DC-link voltage also varies as the speed varies and need stabilisation is difficult and it is difficult to find in literature. In addition, most of the published average value models do not take into consideration validation of results against switching model and experimental results or practical implementation. A few validations against the switching models are limited to comparison of current and torque waveforms. There is also a need to further widen the validation of models by including a voltage source inverters loss model to analyse output parameters such as torque, power and energy and also validation through practical implementation. Most switching models and average voltage models for power electronic converters in power conversion systems so far reviewed and existing in literature are developed and implemented in MATLAB/Simulink and other simulation software but it is harder to find such models developed in PORTUNUS simulation package.

This research proposed an alternative Average Voltage Estimation Model (AVEM) of the voltage source inverter (VSI) which enables a PM motor and generator drive system to be rapidly and accurately simulated. The proposed method is based on an analytical estimation of the 'average' ac voltage across each phase of the PMSM during each PWM switching period and then using these average values as piecewise-linear voltage sources for each phase in a three-phase machine or three-phase AC load phase. This improved method differs from the previous methods in configuration with the total elimination of VSI switches, DC-link capacitor and LCL filters, replacing the VSI with 3 simple controlled voltage sources. In addition, for this method the approach to deriving the average voltage estimation differs significantly from the previous methods which base their averaging on a state space equation resulting in relatively complex equivalent circuit models and mathematical computations. The advantage of this method is that it significantly reduces simulation execution time, its simplicity in implementation, reduced size of the simulation model and computations time, which means reduction in the storage capacity requires of the computer and the fact that it retains the existing PM

machine and digital controller models therefore allowing machine and actual controller performances to be evaluated and optimised.

Chapter 3 Development of Average Voltage Estimation Model for PMSM Drive System

3 Introduction

The average voltage estimation model of a two level three phase voltage source inverter fed permanent magnet synchronous motor drive is presented in this chapter. Its development is based on the voltage source inverter control strategy and switching functions therefore the chapter begins with the basic theory of the voltage source converter and describes the principle, development and implementation of the average voltage estimation model and its application in variable speed electric motor drives. A key contribution of the three phase average voltage estimation model is shown in Table 3-2. A detailed description and development of the voltage source inverter loss model and its incorporation into the AVEM is also presented. This is followed by the simulation and comparison of the AVEM with the detail switching modelling method. The switching model is used as a benchmark from which the results of the newly developed average voltage model are compared. This is because the easiest ways to determine the accuracy and reliability of any new model or technique is by verification and validation against other existing trusted models, and also if possible through experimentation. The final section of the chapter presents and discusses the results of the PORTUNUS package simulation of the proposed average voltage estimation model and the detailed switching of voltage source inverter and PM machine drive systems. The main conclusion is that the average voltage model is capable of accurately simulating the PI current (torque) controller over a wide operating range and produces results closely in agreement with the standard switching model, but at significantly faster simulation times.

3.1 Theory of Voltage Source Inverter Switching Modelling

The average voltage estimation model of the voltage source inverter is based on the control strategy and switching functions of the voltage source inverter. To fully understand the process of developing the AVEM and its applications, a comprehensive theory of the switching function of the VSI is first described then the AVEM and its application in variable speed PMSM drive will be discussed. The development of an

accurate voltage source inverter model through the understanding of the general theory of the switching function is an important requirement for any type of machine control. The detailed VSI switching model is a method of analysis of electrical machines, power electronic devices, controls and loads where the power electronic semiconductor devices for voltage source inverters are represented by discrete components models which are usually available in the library of the simulation software in which their parameters can be adequately defined while the control technique is being developed.

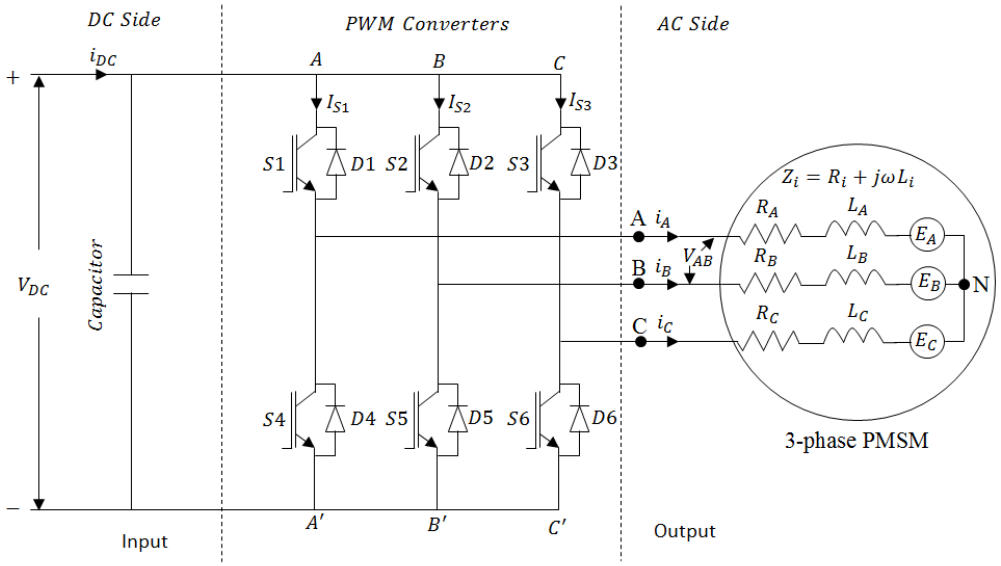

Figure 3-1: Configuration of PMSM drive detailed VSI switching model

Figure 3-1 shows the circuit configuration for a two-level three-phase VSI switching network connected to the balanced three-phase PMSM. Depending on the mode of operation, the input can be DC or AC. Considering the input to the VSI is DC voltage, V_{DC} and current I_{DC}, and expected to supply AC output voltages, ; V_A, V_B, V_C and currents i_A, i_B, i_C to the terminals of the PMSM or any three-phase AC load, the output variables can be calculated based on the input and control functions.

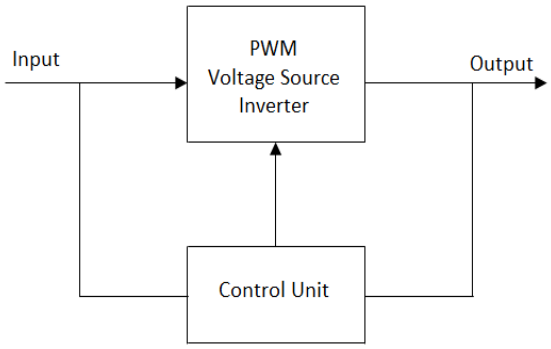

Figure 3-2: Block diagram of PWM voltage source inverter system

When a DC voltage is applied across the VSI, a DC current flow through the VSI and with the action of the control unit (see Figure 3-2), the power switches conduct as requested and the desired output voltage and current can be produced. There are three-phase legs, each phase leg has two power electronic converter switches, the upper and the lower switch and the operation of the two power switches of one-phase leg is given by

$$S_i = 1 - S_{i'} \tag{3.1}$$

$$S_i = \begin{cases} 1 \text{ upper switch ON} \\ 0 \text{ lower switch ON} \end{cases}$$

Where, the subscript i represent phase A, B, and C and S_A, S_B, S_C, are the switching functions when the upper power switches in phase A, B, C are ON and $S_{A'}, S_{B'}, S_{C'}$ are the switching functions when the lower devices in phase A, B, C are ON. This enables the PMSM to be connected to either the positive or the negative terminal of the DC power supply. Using the switching functions, a comprehensive relationship between the input and output variables can be obtained which describes the detailed function of the power electronic VSI.

3.1.1 Phase Voltage and Line-Line Voltage based on Switching Function

Phase and line-line voltages, and as a result phase currents, are the controlled outputs of the voltage source inverter. How these are generated using switching functions is important to understanding the behaviour of the control strategy. The line-line voltage and the output phase voltage across the terminals of the three-phase PMSM as a function of the switching function can be obtained by first understanding that the voltages,

V_{A0}, V_{B0}, V_{C0} between the phases and the negative terminal of the DC voltage source are given by:

$$V_{A0} = S_A V_{DC} \tag{3.2}$$

$$V_{B0} = S_B V_{DC} \tag{3.3}$$

$$V_{C0} = S_C V_{DC} \tag{3.4}$$

And (3.5) describes the relationship between the voltage at the star point of the three-phase PMSM and the negative terminal of the DC link voltage source as:

$$V_{N0} = \frac{1}{3}(V_{A0} + V_{B0} + V_{C0}) \tag{3.5}$$

From (3.2)-(3.4), V_{N0} can be expressed based on switching function as:

$$V_{N0} = \frac{1}{3}(S_A V_{DC} + S_B V_{DC} + S_C V_{DC}) \tag{3.6}$$

$$V_{N0} = \frac{V_{DC}}{3}(S_A + S_B + S_C) \tag{3.7}$$

In a three phase balanced system, the three phase voltages, V_{AN}, V_{BN}, V_{CN} are expressed as:

$$V_{AN} = V_{A0} - V_{N0} \tag{3.8}$$

$$V_{BN} = V_{B0} - V_{N0} \tag{3.9}$$

$$V_{CN} = V_{C0} - V_{N0} \tag{3.10}$$

Therefore, from (3.2) - (3.7), the three phase voltage equations for the two-level three-phase VSI as a factor of the switching function are described by:

$$V_{AN} = \frac{V_{DC}}{3}(2S_A - S_B - S_C) \tag{3.11}$$

$$V_{BN} = \frac{V_{DC}}{3}(-S_A + 2S_B - S_C) \tag{3.12}$$

$$V_{CN} = \frac{V_{DC}}{3}(-S_A - S_B + 2S_C) \tag{3.13}$$

The line-line voltages can be calculated based on (3.2) - (3.4) as:

$$V_{AB} = V_{A0} - V_{B0} \tag{3.14}$$

$$V_{BC} = V_{B0} - V_{C0} \tag{3.15}$$

$$V_{CA} = V_{C0} - V_{A0} \tag{3.16}$$

Substituting (3.2 - 3.4) into (3.14 - 3.16), the line-line voltages, V_{AB}, V_{BC}, V_{CA} can be expressed as function of the voltage source inverter switching functions as:

$$V_{AB} = V_{DC}(S_A - S_B) \tag{3.17}$$

$$V_{BC} = V_{DC}(S_B - S_C) \tag{3.18}$$

$$V_{CA} = V_{DC}(S_C - S_A) \tag{3.19}$$

3.1.2 Phase current and DC link current based on switching functions

Figure 3-3 shows a balanced three-phase PMSM drive system. The PMSM windings are represented by R-L which is connected to the three-phase VSI but neutral is not connected to the VSI. From Figure 3-3, it is possible to determine the calculation of input DC current in relation to the output AC currents using the switching functions.

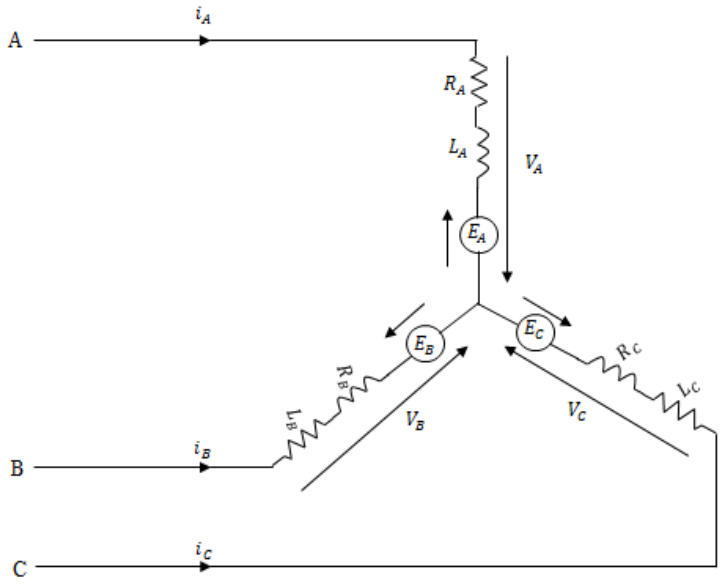

Figure 3-3: Three-phase PMSM equivalent circuit with unconnected neutral

By applying Kirchhoff voltage law in a close loop, the instantaneous phase currents i_A, i_B, i_C can be obtained from which the switching current as well as average DC current under the influence of the switching functions can be shown as:

$$\frac{di_A}{dt} = \frac{V_{AN} - i_A R - E_A}{L} \tag{3.20}$$

$$\frac{di_B}{dt} = \frac{V_{BN} - i_B R - E_B}{L} \tag{3.21}$$

$$\frac{di_C}{dt} = \frac{V_{CN} - i_C R - E_C}{L} \tag{3.22}$$

Where, E_A, E_B, E_C is the back-emfs, R is the stator resistance, L is the stator inductance.

Equation (3.20 - 3.22) can further be expressed based on the fundamental modulating frequency as follows:

$$i_A = I_m \sin \omega t \tag{3.23}$$

$$i_B = I_m \sin(\omega t - 120^0) \tag{3.24}$$

$$i_C = I_m \sin(\omega t - 240^0) \tag{3.25}$$

Applying the switching function, the switch currents, $I_{S_A}, I_{S_B}, I_{S_C},$ can be calculated as:

$$I_{S_A} = i_A S_A \tag{3.26}$$

$$I_{S_B} = i_B S_B \tag{3.27}$$

$$I_{S_C} = i_C S_C \tag{3.28}$$

Considering only the fundamental frequency component and neglecting the harmonic components, the instantaneous DC current, i_{DC} in terms of the switching frequency and the three-phase current can be determined using:

$$i_{DC} = i_A S_A + i_B S_B + i_C S_C \tag{3.29}$$

Hence, the average dc-link current over a cycle can be modelled as:

$$I_{DC} = \frac{1}{2\pi} \int_0^{2\pi} i_{DCavg} d\omega t \tag{3.30}$$

Generally, the switching circuit uses a PWM control strategy to generate the duty cycle which in turn generates the switching functions. Using the carrier-based sinusoidal PWM control strategy discussed in section 2.8.1, the duty cycles can be set as follows:

$$d_A = \frac{m_A}{V_C} \tag{3.31}$$

$$d_B = \frac{m_B}{V_C} \tag{3.32}$$

$$d_C = \frac{m_C}{V_C} \tag{3.33}$$

Where, d_A, d_B, d_C are the duty ratios and are related to the modulating signals. If the modulating signal is sinusoidal the duty ratios are sinusoidal while V_C is the peak value of the carrier waveform and m_A, m_B, m_C are the modulation index expressed based on the fundamental modulating frequency as:

$$m_A = V_m \sin(\omega t) \tag{3.34}$$

$$m_B = V_m \sin(\omega t - 120^0) \tag{3.35}$$

$$m_C = V_m \sin(\omega t - 240^0) \tag{3.36}$$

Where, V_m is the peak value of the sinusoidal waveform.

The switching operation and functions of the voltage source inverter in relation to the input DC voltage and output is summarised in Table 3-1

Table 3-1: Three phase and line-line voltages of a three-phase balanced system with inverter switching functions

Voltage Vectors	Switching state			Phase Voltage in terms of V_{DC}			Line Voltage in terms of V_{DC}		
	S_A	S_B	S_C	V_A	V_B	V_C	V_{AB}	V_{BC}	V_{CA}
$V0$	0	0	0	0	0	0	0	0	0
$V1$	1	0	0	2/3	-1/3	-1/3	1	0	-1
$V2$	1	1	0	1/3	1/3	-2/3	0	1	-1
$V3$	0	1	0	-1/3	2/3	-1/3	-1	1	0
$V4$	0	1	1	-2/3	1/3	1/3	-1	0	1
$V5$	0	0	1	-1/3	-1/3	2/3	0	-1	1
$V6$	1	0	1	1/3	-2/3	1/3	1	-1	0
$V7$	1	1	1	0	0	0	0	0	0

Table 3-1 shows the summary of inputs and outputs of a three-phase PWM VSI switching operation using a carrier-based PWM control strategy. It can be seen that the determining factors in the switching model is the DC link voltage and the switching functions. Each time a simulation exercise is conducted on switching model and with PWM control strategy, the simulation software gives output based on Equations 3.11 - 3.13. Essentially, these switching functions are usually from a high frequency (>4 kHz) PWM control strategy which requires small simulation time step to achieve the required resolution and results in long simulation run times.

3.2 Development of the Proposed Average Voltage Estimation Model (AVEM) of a Voltage Source Inverter for PMSM Drives

The detail switching model is an accurate and effective approach to modelling PMSM and other electrical machine drives as has been described and validated by several researchers [157] – [202]. However, with the increase in the complexity and requirements in the design and simulation of PMSM drive systems, a more simplified and faster model is required to eliminate the inverter circuit due to the switching operations and simulation time step effect. As a result modelling of PMSM drive systems using various average value methods have been developed for AC/DC or DC/AC constant speed, fixed frequency PMSM drive systems, as has been listed in Chapter 2. However, the method of derivation of the average value state space equation becomes more complicated if three-phase back-back voltage source inverters are involved with dynamic systems such as variable speed motors or generators. Consequently the author has investigated a more simplified and faster approach to enhance the modelling of PMSM drive systems.

Since the theory of detailed VSI switching model has been discussed in section 3.1, this section presents the principles and development of the average voltage estimation model of a three-phase voltage source inverter with an example of application to PMSM drive system. The average voltage estimation model of voltage source inverters is based on the control strategy and switching functions of the inverter. It is an analytical estimation of the ‘average’ instantaneous voltage across each phase of a three-phase AC load during each PWM switching period and then using these averages to supply a piecewise linear voltage source for each phase of the three-phase system. This proposed average voltage estimation modelling method reported by the author [216] overcomes the challenges of switching model and previous average value models. The proposed model is developed first for a PMSM drive system and is then expanded for variable speed PMSG wind energy conversion systems and also used as a generalised model for any three-phase system which requires control.

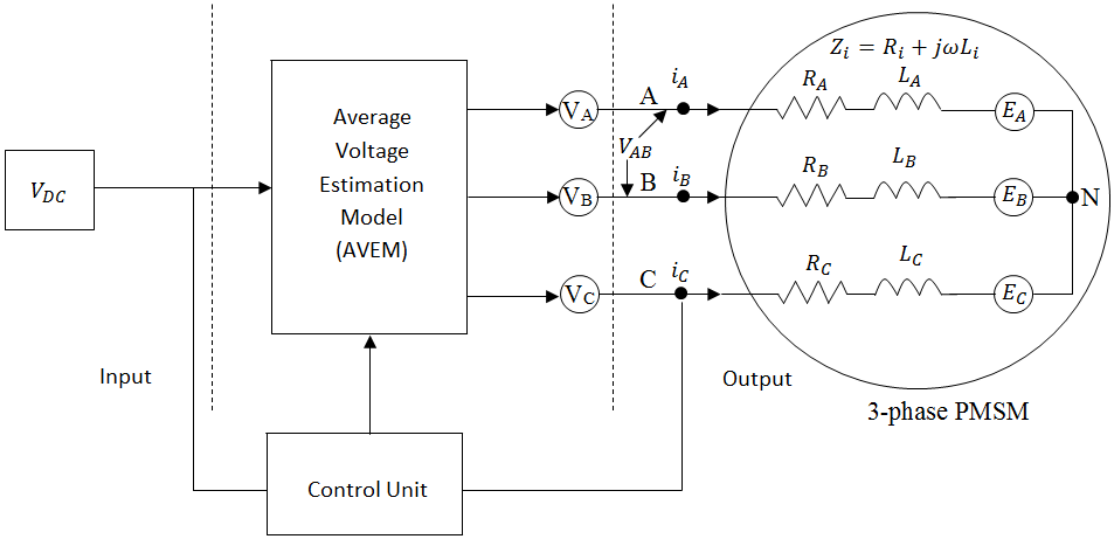

Figure 3-4: Average Voltage estimation model of VSI with three-phase balanced PMSM

Figure 3-4 shows the proposed average voltage estimation model of the VSI and control of three-phase PMSM drive system. It consists of the three controlled voltage sources for the PMSM driving a mechanical load, the control system and the average voltage estimation block. The inverter switches are totally eliminated and replaced with three voltages sources driven by a function representing the 'average' value of VSI output voltage in each phase. The advantage is that, the switching and non-ideal characteristics of the power electronic switches (IGBTs) are now removed from the configuration.

3.2.1 Equivalent Circuit of a PMSM

The single phase equivalent circuit of a typical PMSM is shown in Figure 3-5. The voltage V is applied to the stator and a back-emf E is developed in the PMSM. The stator resistance and inductance are given by R and L respectively.

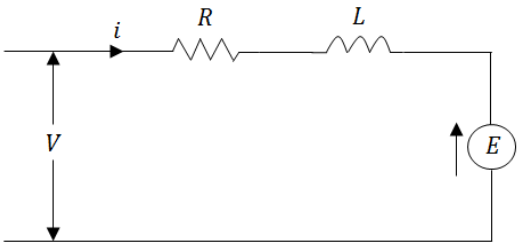

Figure 3-5: Single phase equivalent circuit of PMSM

In motoring, the applied voltage V is opposed by the back-emf E. If the voltage V is greater than the back-emf, current i flows into the stator of the PMSM. On the other hand, the PM machine generates when the back-emf is greater than the applied voltage and current flows out of the stator. The relationship between the applied voltage and back-emf is given by

$$V = E + iR + L\frac{di}{dt} \tag{3.37}$$

Where IR and $L\frac{dI}{dt}$ represent the voltage drop across the stator resistance and inductance.

In an inverter fed PMSM shown in Figure 3-6, the applied voltage V to the PMSM is supplied by the inverter under the action of the control technique. This voltage can be estimated based on principle of control strategy and switching functions when the inverter switching circuits are not needed in the simulation of PMSM drive system. In which case the voltage V can be replaced with an average value V_{avg} and equation 3.37 becomes

$$V_{avg} = E + iR + L\frac{di}{dt} \tag{3.38}$$

3.2.2 Average Voltage Calculation

The average voltage estimation model of voltage source inverters analytically estimates the 'average' instantaneous voltage across each phase of a three-phase AC load during each PWM switching period and then uses these averages to supply a piecewise linear voltage source for each phase of the three-phase system.

In order to develop the average voltage estimation model, several considerations are made as follows;

1. The PMSM (or AC load) is a balanced three-phase star connected load with equal phase impedance.
2. The role of the voltage source inverter is to connect the DC voltage to the three-phase AC load based on the control strategy at each switching period. By this it establishes the voltage across each of the phases of the three-phase PMSM (load).
3. The switching function of VSI and control results to $2^3 = 8$ VSI switching output states which give rise to PWM output voltage waveforms and voltage vectors.

4. In each sampling period, the voltage applied to the three-phase PMSM can be averaged.
5. At any particular time the average resultant voltage is located in any of the six sectors of the voltage vector hexagon.
6. The value of the average voltage can be estimated from the adjacent voltage vectors in the sector it's located in.
7. The time the adjacent voltage vectors are applied differs from one sector to the other.
8. In each switching cycle, the DC voltage supply forms a series circuit with the equal impedance windings of the three-phase PMSM.
9. Therefore using the Voltage Divider Rule (VDR) the voltage drop across each phase winding during each switching period can be estimated.

Figure 3-6 illustrates the relationship between the DC voltage supply, three phase voltage source inverter and the equivalent circuits of the three-phase PMSM where, V_A, V_B, V_C are the phase voltages, E_A, E_B, E_C are the back-emfs, i_A, i_B, i_C are the phase currents and Z_A, Z_B, Z_C are the phase impedance of the three-phase PMSM. The voltages at the terminals of the PMSM depend on the operation and states of the inverter switches which is determined by the control strategy PWM waveform. During the operation of the voltage source inverter and in a switching cycle, the control strategy generates eight combinations of three phase PWM waveform which enable the voltage source inverter to convert the DC link voltage to AC voltage and applied to the three phase PMSM windings.

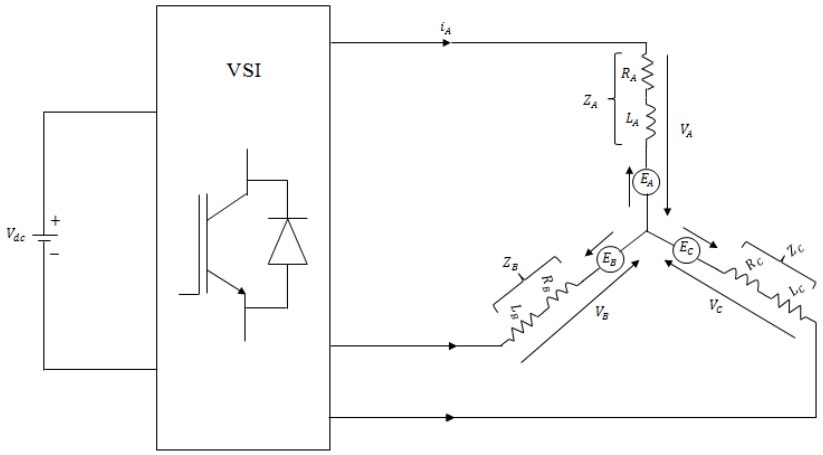

Figure 3-6: DC voltage and 3 phase star connected VSI fed PMSM equivalent

From the switching function point of view, each time the upper switches are turned on, it enables the terminals of the three-phase PMSM to be connected to either the positive terminal of the DC voltage. In each switching cycle, there are two possible states for one phase-leg of the inverter to connect the DC supply voltage to the three-phase PMSM. When the upper switch is fully ON, the lower switch on that same phase leg will be fully OFF and vice versa. When the upper switch on a phase leg is ON, the phase is connected to the positive of the DC voltage and the state of the inverter switch is 1. On the other hand when the switch on the same phase leg is OFF, the phase is connected to the negative of the DC voltage and the state of the inverter switch is 0. For the three phases, there are a total of 2^3 = 8 options resulting in 8 switching combinations and 8 voltage vectors as shown in Figure 3-7 [217].

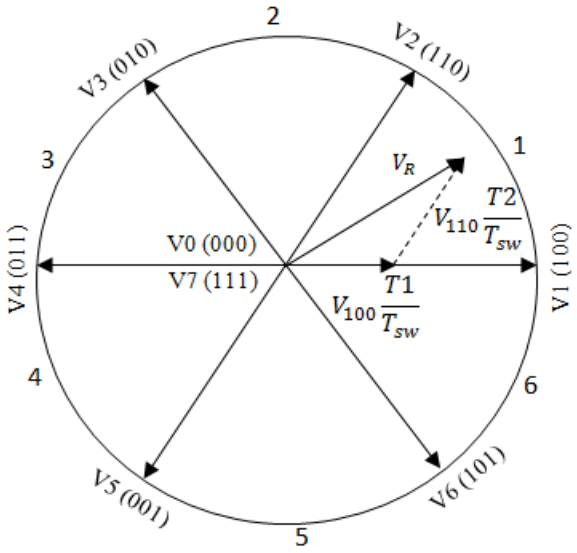

Figure 3-7: Space voltage vectors and sectors

Figure 3-7 describes the representation of the switching combinations and commanded voltage vectors in a space hexagon. There are a total of six sectors and eight voltage vectors. Six of the voltage vectors; V1, V2, V3, V4, V5, V6 are active voltage vectors and two V0, V7 are zero voltage vectors. For each of the voltage vectors the states are clearly stated. The state defines the connection of the phases of the three-phase PMSM to the terminals of the DC voltage supply. There are eight ways the DC voltage is connected to the three phase PMSM in one switching period and results to eight three-phase PMSM equivalent circuits arrangement as shown in Figure 3-8.

Each sectors has two adjacent active voltage vectors and two zero voltage vectors that are applied for a switching period, T_{SW}. In principle, there are four three phase PMSM equivalent circuits for each sector, two for the active voltage vectors and two for the zero voltage vectors. The adjacent voltage vectors and the zero voltage vectors are used to calculate the resultant voltage vector. The resultant voltage vector in one sector is different from the other sector due to the different switching states and voltage vectors. Therefore, the average phase voltage is calculated from the resultant voltage vector using the voltage drop across each of the phases and the time the voltage vectors are applied in each sectors in one switching period. The voltage drop across each phase due to the DC voltage depends on the PMSM equivalent circuits while the time the voltage vectors are applied depends on the PWM waveform over the switching period.

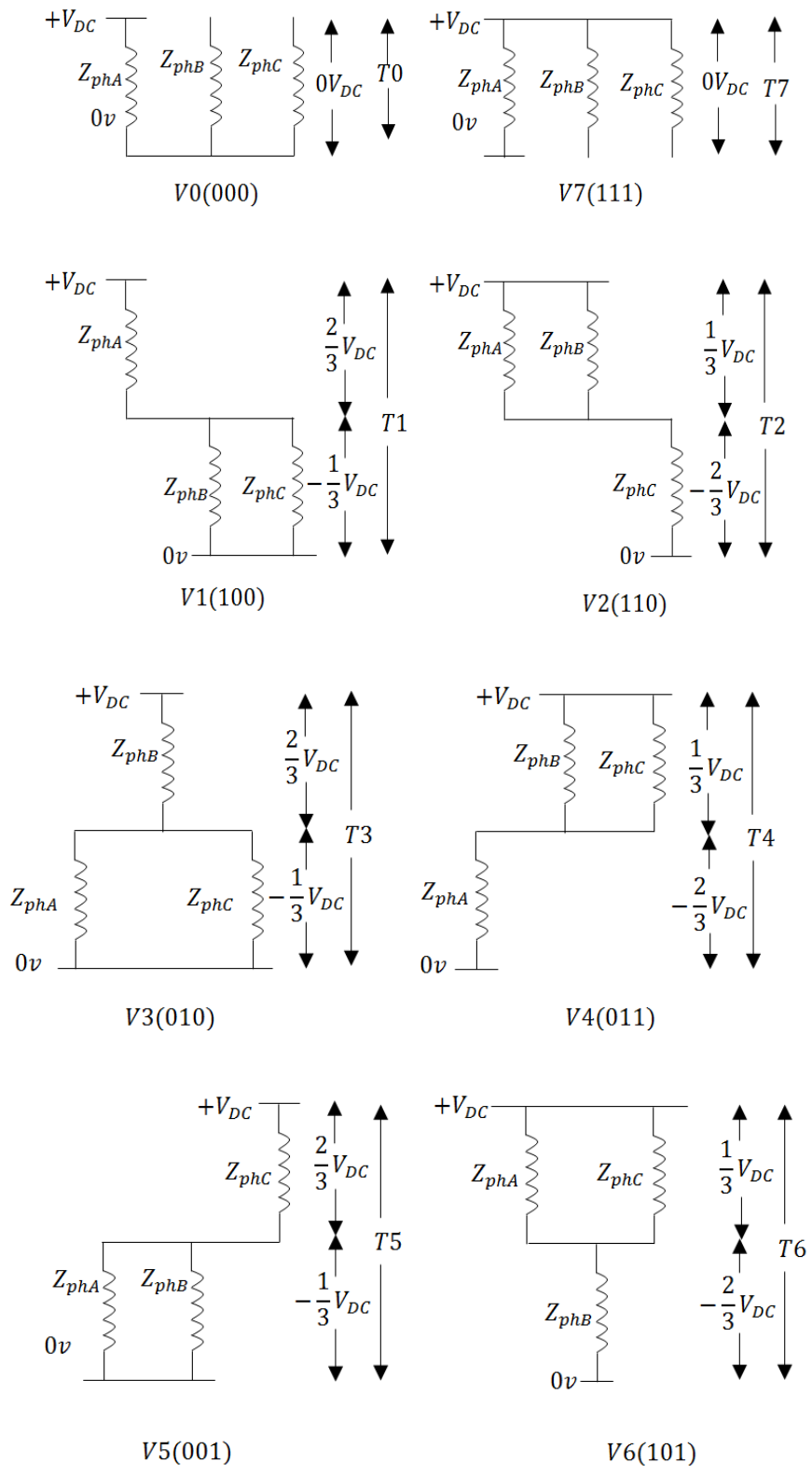

Figure 3-8: Three phase equivalent circuits of the commanded voltage vector and voltage drop across phases

In each of the PMSM equivalent circuits shown in Figure 3-8, the DC voltage forms a series circuit with the three-phase PMSM winding represented by impedance network of equal magnitude. Therefore, the voltage drops across each phase windings, Z_A, Z_B, Z_C can be calculated from DC voltage using the Voltage Divider Rule given as

$$V_k = \frac{Z_k}{Z_T} V_{DC} \qquad k \in (A, B, C) \tag{3.39}$$

Where; V_k is the voltage drop across the phases; A, B, C, Z_T is the total impedance of the series circuit, Z_k is the impedance across the phase in which the voltage drop is calculated and V_{DC} is the DC supply voltage. Using (3.39) the voltage drop across each of the phases due to the DC voltage in each of the sectors are calculated.

On the other hand, the time, T1, T2, T3, T4, T5, T6, T7 the voltage vectors are applied depends on the PWM waveform. In each commanded voltage for one switching period the PWM voltage is usually symmetrical as shown in Figure 3-9.

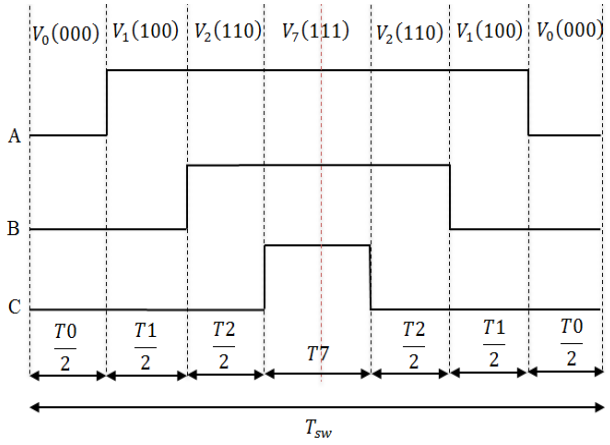

Figure 3-9: Symmetrical three phase PWM outputs

Figure 3-9 shows that the second half of the PWM waveform symmetry is a mirror image of the first and the switching operation in the first half is repeated in the second half. This made it possible to simplify the estimation of average phase voltage using half of the symmetry in a complete switching period. In order to calculate the time of adjacent voltage vectors, PWM waveform half symmetry is then formed for six sectors considering only the active voltage vectors as shown in Figure 3-10.

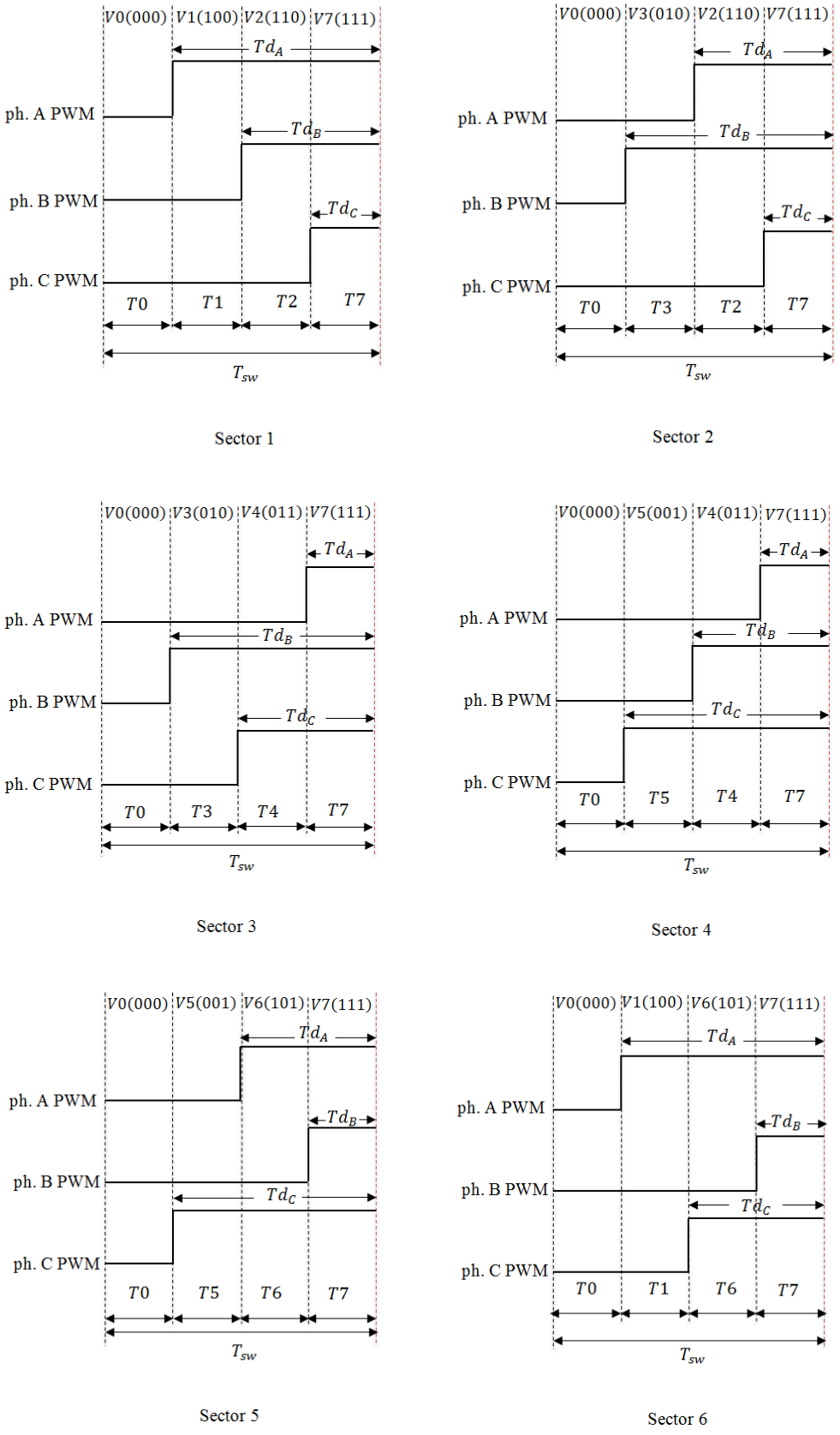

Figure 3-10: PWM voltage waveform and commanded voltage vectors

Figure 3-10 shows the half waveforms of the commanded voltage vector in each of the sectors during a switching cycle. In each of the sectors, the half PWM waveforms of the commanded voltage vector during a switching cycle consists of four voltage vectors from which the time the voltage vectors is applied and average phase voltage can be calculated.

3.2.3 Sector Calculation

The average voltage estimation depends on the sectors in which the resultant voltage vector resides during the switching cycle. Therefore, the first step is to accurately determine the sector to estimate the average phase voltage. Using the carrier-based sinusoidal PI current control strategy, there are three separate PI current controllers which independently generate duty cycles during the switching period. From the duty cycles, sectors can be calculated, timing variables can be determined and of course average voltage for each phase estimated. To determine the sector, the three phase duty cycles are compared with each other. A simplified algorithm is developed as shown in the flowchart of Figure 3-11 which gives the required sector for each particular switching period.

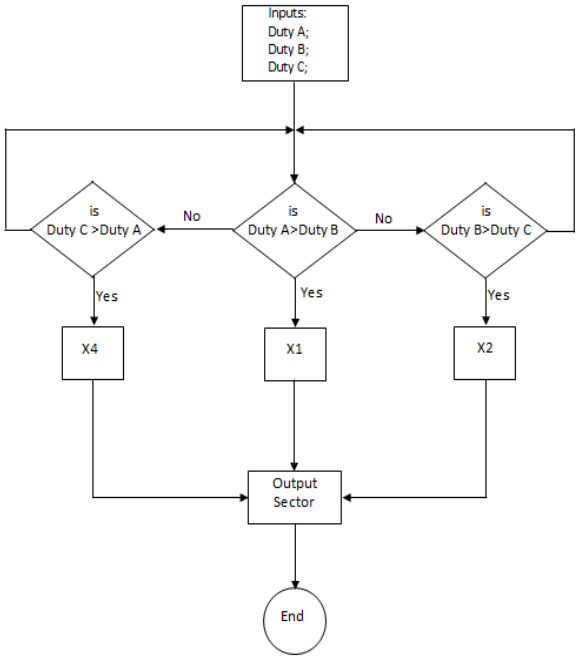

Figure 3-11: Simplified flowcharts for sector calculation and selection

The flowchart above illustrates a comprehensive description of how the commanded duty cycles are used to calculate and select a particular sector. The duty cycles per phase from

the output of the PI-regulators are read and compared. Phase *A* duty cycle is compared with the duty cycle of phase *B,* phase *B* duty cycle is compared with that of a phase *C* and that phase C compared with the duty cycle of phase *A*. If the condition in the decision box is met, output is given as 1 else the output is zero. Each comparator has multiplying factors which are carefully chosen by the author based on experience and knowledge of the operation of PWM voltage source inverter. After comparing the duty cycles, the results are multiplied by the appropriate factor. The output of phase *A* comparator is multiplied by 1, phase *B* comparator multiplied of 2 and that of phase *C* multiplied by 4. The resultant summation of the outputs of the multipliers indicates the sector at the particular time in the switching cycle.

3.2.4 Average Voltage Estimation for Sector 1

An example of how to estimate average voltage in a sector is presented for sector 1. In sector 1, there are two active voltage vector V1, V2 applied for T1 and T2 and two zero voltage vectors V0, V7 applied for T0 and T7. Therefore, the resultant voltage vector in sector 1 (see figure 3-7) is given by

$$V_R = \frac{T1V1}{T_{sw}} + \frac{T2V2}{T_{sw}} + \frac{T0V0}{T_{sw}} + \frac{T7V7}{T_{sw}} \tag{3.40}$$

$$T_{sw} = T1 + T2 + T0 + T7 \tag{3.41}$$

Where, V_R is the resultant voltage vector, T_{sw} Switching period, $T1\ and\ T2$ are the time of applying the active voltage vectors, $T0$ and $T7$ are the time of applying the zero voltage vectors. The zero voltage vectors, $V0$ and $V7$ are approximated to zero, therefore equation (3.40) becomes:

$$V_R = \frac{T1V1(100)}{T_{sw}} + \frac{T2V2(110)}{T_{sw}} \tag{3.42}$$

T1 and T2 are calculated from the PWM waveform and V1 and V2 are calculated from the voltage drop due to DC voltage.

3.2.5 Timing Calculation

The time voltage vectors are applied is known by simply identifying the length of time each of the phases of the three-phase PMSM stay connected to the DC voltage supply. The sequence is to identify and compare the relative lengths of the three phase PWM

waveform in each sector such as the long, longer and longest among the three phases PWM waveform in each sector.

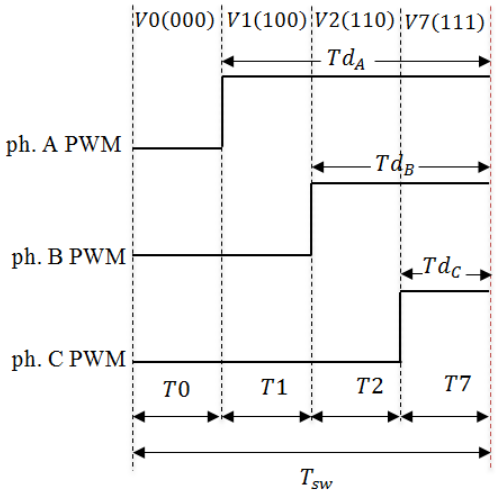

Figure 3-12: PWM waveform half symmetry of in sector 1

From the PWM waveform of sector 1 shown in Figure 3-12, $Td_A > Td_B > Td_C$ therefore, the timing variables in sector 1 are given by;

$$T1 = Td_A - Td_B \tag{3.43}$$

$$T2 = Td_B - Td_C \tag{3.44}$$

Where, $Td_A, Td_B, and\ Td_C$ are the lengths of the PWM waveform in phase A, B and C.

Then, the final step is to calculate the average voltage and this requires the three phase PMSM equivalent circuits in sector 1. Figure 3-13 shows the three phase PMSM equivalent circuits arrangement for voltage vectors V1, V2, V0 and V7 in sector 1. During the time T0, all the phase windings are connected to the negative terminal of the DC voltage and during the time T7 the three phases are equally connected to the positive terminal and does not command any voltage.

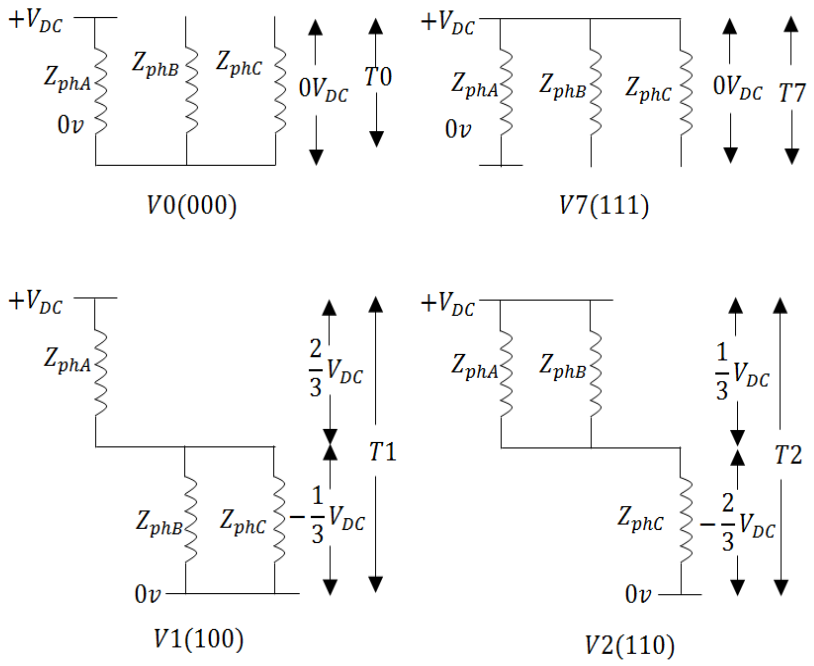

Figure 3-13: Three phase PMSM equivalent circuits and voltage drop across phases due to DC voltage of sector 1

However, during the time T1 and T2, the DC voltage forms a series circuit with the three phase PMSM windings and the corresponding voltage drop across each of the phases due to V_{DC} is calculated and replaced the voltage vector V1, V2, V0, and V7 in equation 3.42 and the average voltage for the three phases in sector 1 are given as,

$$V_{Aavg} = \frac{\frac{2}{3}V_{DC}T1 + \frac{1}{3}V_{DC}T2}{T_{sw}} \tag{3.45}$$

$$V_{Bavg} = \frac{-\frac{1}{3}V_{DC}T1 + \frac{1}{3}V_{DC}T2}{T_{sw}} \tag{3.46}$$

$$V_{Cavg} = \frac{-\frac{1}{3}V_{DC}T1 - \frac{2}{3}V_{DC}T2}{T_{sw}} \tag{3.47}$$

V_{Aavg} , V_{Bavg}, V_{Cavg} are the average voltage in phase *A*, *B* and *C* and T1, T2 calculated by equation 3.43 and 3.44.

The average voltage estimation modelling approach is sector dependent and calculates average phase voltage in every sector in a switching period independently per phase given a total of three sets of equation for each sector. This derivation relies strongly on the combination of the three phase PMSM equivalent circuit diagrams of the commanded

voltage vectors and the PWM waveform half symmetry in each sector in a switching period. Therefore, the average voltages in other sectors are estimated in a similar process to that of sector 1 and the summary of the derivations shown in Table 3-2.

Table 3-2: Summary of average voltage estimation per phase for each sector

Sectors	Commanded duty cycles configuration	Timing calculation	Average estimated voltage		
			V_A	V_B	V_C
1	$Td_A \geq Td_B$ $Td_B \geq Td_C$ $Td_A \geq Td_C$	$T1 = Td_A - Td_B$ $T2 = Td_B - Td_C$	$\frac{V_{DC}}{3T_{sw}}(2T1 + T2)$	$\frac{V_{DC}}{3T_{sw}}(-T1 + T2)$	$\frac{V_{DC}}{3T_{sw}}(-T1 - 2T2)$
2	$Td_B \geq Td_A$ $Td_A \geq Td_C$ $Td_B \geq Td_C$	$T2 = Td_A - Td_C$ $T3 = Td_B - Td_A$	$\frac{V_{DC}}{3T_{sw}}(T2 - T3)$	$\frac{V_{DC}}{3T_{sw}}(T2 + 2T3)$	$\frac{V_{DC}}{3T_{sw}}(-2T2 - T3)$
3	$Td_B \geq Td_C$ $Td_C \geq Td_A$ $Td_B \geq Td_A$	$T3 = Td_B - Td_C$ $T4 = Td_C - Td_A$	$\frac{V_{DC}}{3T_{sw}}(-T3 - 2T4)$	$\frac{V_{DC}}{3T_{sw}}(2T3 + T4)$	$\frac{V_{DC}}{3T_{sw}}(-T3 + T4)$
4	$Td_C \geq Td_B$ $Td_B \geq Td_A$ $Td_C \geq Td_A$	$T4 = Td_B - Td_A$ $T5 = Td_C - Td_B$	$\frac{V_{DC}}{3T_{sw}}(-2T4 - T5)$	$\frac{V_{DC}}{3T_{sw}}(T4 - T5)$	$\frac{V_{DC}}{3T_{sw}}(T4 + 2T5)$
5	$Td_C \geq Td_A$ $Td_A \geq Td_B$ $Td_C \geq Td_B$	$T5 = Td_C - Td_A$ $T6 = Td_A - Td_B$	$\frac{V_{DC}}{3T_{sw}}(-T5 + T6)$	$\frac{V_{DC}}{3T_{sw}}(-T5 - 2T6)$	$\frac{V_{DC}}{3T_{sw}}(2T5 + T6)$
6	$Td_A \geq Td_C$ $Td_C \geq Td_B$ $Td_A \geq Td_B$	$T1 = Td_A - Td_C$ $T6 = Td_C - Td_B$	$\frac{V_{DC}}{3T_{sw}}(2T1 + T6)$	$\frac{V_{DC}}{3T_{sw}}(-T1 - 2T6)$	$\frac{V_{DC}}{3T_{sw}}(-T1 + T6)$

Table 3-2 shows the summary of the simplified average voltage estimation in each phase in each switching period for the 6 sectors. The operation of the average voltage model is independent determined for each phase. Therefore, the sum of the average voltages estimated in all the sectors in one phase gives the total average voltage for that phase. This total average voltage per phase is then use to drive each of the voltage sources connected to the three-phase PMSM and can also be used with any three phase system where control is required. In each switching interval, this calculation requires knowledge of the DC voltage value V_{DC} and switching period T_{SW} (this depends on the switching frequency chosen). In this research a switching frequency of 20 kHz equivalents to a switching period of 50μs is used.

Applying the average voltage, the average instantaneous current can be written as

$$\frac{di_A}{dt} = \frac{V_{ANavg} - i_A R - E_A}{L} \tag{3.48}$$

$$\frac{di_B}{dt} = \frac{V_{BNavg} - i_B R - E_B}{L} \tag{3.49}$$

$$\frac{di_C}{dt} = \frac{V_{CNavg} - i_C R - E_C}{L} \tag{3.50}$$

And the developed electromagnetic torque is given as function of the rotor natural flux amplitude and the stator currents in three-phase PMSM as follows

$$T_e = p\varphi_m(i_A + i_B + i_C) \tag{3.51}$$

$$T_e = p\varphi_m I_m \tag{3.52}$$

Equations 3.51 and 3.52 describe the electromagnetic torque, T_e which drives the mechanical load. The dynamics interaction in the mechanical system between the electromagnetic torque, T_e the load torque, T_L and viscosity cause changes in the rotational speed given by

$$J\frac{d\omega_r}{dt} = T_e - T_L - C_v\omega_r \tag{3.53}$$

Where, $J =$ Rotor inertia, $\omega_r =$ Rotor mechanical speed, $C_v =$ Viscosity coefficient

From equation 3.51 and 3.52, controlling the stator current amplitude, I_m controls the electromagnetic torque and controlling the torque as in (equation 3.53) can cause either

an acceleration or deceleration. Therefore regulating the torque also controls the speed of the PMSM.

Similarly, the instantaneous average electrical power in a three phase system is given as;

$$P\ (t) = V_{Aavg} i_A + V_{Bavg} i_B + V_{Cavg} i_C \tag{3.54}$$

3.2.6 DC Link Current Estimation

An important result of the average voltage model is the ability to predict DC link current. This is useful in battery-powered three-phase PMSM drive system to know the capacity of the battery bank and to estimate the losses in order to fully utilise the energy of the battery. Also in variable speed PSMG based system with the average voltage model as will be seen in chapter 5, which is one of the main objectives pursued in this research, accurate estimation of DC current is important in the modelling of the DC link voltage. Due to the absent of DC link capacitor and the DC link between the generator side and the AC load/grid side, DC link voltage is modelled based on the DC link current. The DC link current is also estimated per sector.

An example of how DC link current is estimated using average voltage estimation model is again presented for sector 1. The basic idea is that in each commanded voltage vector, the DC voltage forms a series circuit with the three-phase PMSM. Using Figure 3-12 and Figure 3-13, during which time the zero voltage vectors is applied $T0$ and $T7$, all the phase currents are circulating around the phases and therefore the DC link current is zero. However, during, $T1$, the DC link current is equal to phase *A* current and during $T2$ the DC link current is equal to the negative of phase *C* (see Figure 3-12 and Figure 3-13). Therefore, DC link current in sector 1 is describes by

$$I_{DCgen} = \frac{T1}{T_{sw}} i_A - \frac{T2}{T_{sw}} i_C \tag{3.55}$$

Where, $i_A\ and\ i_C$ are the currents measured in phase *A* and phase *C*.

This calculation have to be carried out in each switching interval in all the sectors and the summation of the DC link current in all the sectors gives the final DC link current.

3.3 Voltage Source Inverter Loss Modelling

Variable speed drive uses voltage source inverter to connect PM machine to the electrical power source with the aim to conserve or maximise power from the source. The most efficient way to utilise the energy in variable speed drive system is to know the losses in the PM machine and the voltage source inverters. Knowing the losses helps in the right choice of power electronic devices in the voltage source inverter, minimise losses and efficiency analysis of the drive system. In a PM machine drive systems, the losses include the machine and power electronic converter losses. The machine losses include mechanical losses, windage, core and iron losses [218][219]. When detailed constituents losses in the machine are not needed, the most simplified method to calculate losses is the direct measurement of currents, voltage and power from which losses can be calculated knowing the power transfer (input and output of the individual components) in the system [220]. This of course is sufficient to calculate the total losses in the PM machine and VSI. Since in the AVEM, the VSI is absent, loss model of voltage source inverter is required to calculate the actual power input, power output and efficiency of components as well as the total efficiency of the drive system.

The section presents a loss model of two level three phase voltage source inverter using IGBTs that can be incorporated into the proposed average voltage estimation model suitable to analyse the power and efficiency of each components and overall system under different control strategies and operating points. A number of methods can be used to calculate the losses in power electronic converters. One method, utilise current and voltage to calculate the power losses in the voltage source inverter [220]. This method only predicts accurate losses in the VSI when the loss components are embedded in the VSI model. In a situation where the embedded loss components are absent, the manufacturer data sheet provides relevant information on the power electronic converters e.g. IGBTs and diodes from which the losses are calculated. In the proposed AVEM, where the VSI switching network is eliminated, the method utilising the manufacturer data sheet is used to calculate the power electronic converter losses. The losses in voltage source inverters are calculated for one phase of the inverter consisting of an IGBT and a diode and the result multiplied by the number of combination IGBT and diode to obtain total losses for three phases. Generally, there are two types of losses in inverter, namely the conduction and switching losses.

3.3.1 Conduction Losses

The conduction losses occur when the IGBTs and diodes change to on-state as current flows through them. In the on-state, voltage drop across the IGBTs and diodes. The voltage drop across IGBT due to current flowing and on-state resistance is given as [221]

$$V_{CE}(i_{CE}) = V_{CE0} + i_C r_C \tag{3.56}$$

In the same manner, the voltage drop across the diode as current flows given as

$$V_D(i_D) = V_{D0} + i_D r_D \tag{3.57}$$

Where; V_{CE0} and V_{D0} are the threshold voltage across the IGBT and diode, i_C and i_D are the current flowing through IGBT and diode, r_{CE} and r_D are the on-state resistance of the IGBT and diode. These on-state parameters listed above can be obtained from the output characteristics available in the manufacturer's data sheet as a function of the conducting current. With the on-state voltage drop across each of the device, the instantaneous conduction losses for IGBT and diode can be calculated by the product of the on-state voltage drop and the instantaneous current expressed as follows;

$$P_{condIGBT} = V_{CE}(t)i_C(t) = V_{CE0}i_C(t) + {i_C}^2(t)r_C \tag{3.58}$$

$$P_{condDiode} = V_D(t)i_D(t) = V_{D0}i_D(t) + {i_D}^2(t)r_D \tag{3.59}$$

The instantaneous conduction power losses in (3.58) and (3.59) can be averaged over one switching period as

$$P_{condIGBT} = \frac{1}{T_{sw}}\int_0^{T_{sw}}\left(V_{CE0}i_C(t) + {i_C}^2(t)r_C\right)dt \tag{3.60}$$

$$P_{condDiode} = \frac{1}{T_{sw}}\int_0^{T_{sw}}\left(V_{D0}i_D(t) + {i_D}^2(t)r_D\right)dt \tag{3.61}$$

It is important to take into considerations the type of control strategy. Since SPWM is used, the instantaneous current flowing through each phase leg of the inverter is given as

$$i_C(t) = i_m \sin \omega t \tag{3.62}$$

For three phases, the instantaneous currents are at 120^0 phase shift from each other and at a phase angle ∅. With this, (3.60) and (3.61) becomes

$$P_{condIGBT} = \frac{1}{T_{sw}}\int_0^{T_{sw}}(V_{CE0}i_m \sin\omega t + (i_m \sin\omega t)^2 r_C).\tau(t)dt \quad (3.63)$$

$$P_{condDiode} = \frac{1}{T_{sw}}\int_0^{T_{sw}}(V_{D0}i_m \sin\omega t + (i_m \sin\omega t)^2 r_D).\tau(t)dt \quad (3.64)$$

Where, i_m is the peak value of the input current, $\tau(t)$ defines the pattern of the PWM pulses, which is either 0 or 1. When the IGBT is turned ON it is 1 but it's turned OFF it equals to 0. The pattern of PWM pulses, $\tau(t)$which gives the duty cycle variation over time, can be written as a function of the modulation index and phase angle as

$$\tau(t) = \frac{1}{2}(1 + m\sin(\omega t + \emptyset)) \quad (3.65)$$

Substituting (3.65) into (3.63) and (3.64) and finding the integral, the model equations for conduction losses of the IGBT and diode can be expressed as [221]

$$P_{condIGBT} = V_{CE0}i_m\left(\frac{1}{2\pi} + \frac{m\cos\emptyset}{8}\right) + i^2{}_m r_C(\frac{1}{8} + \frac{m\cos\emptyset}{3\pi}) \quad (3.66)$$

$$P_{condDiode} = V_{D0}i_m\left(\frac{1}{2\pi} - \frac{m\cos\emptyset}{8}\right) + i^2{}_m r_D(\frac{1}{8} - \frac{m\cos\emptyset}{3\pi}) \quad (3.67)$$

Where i_m is the peak value of the input current given as, $i_m = \sqrt{2}\, i_{rms}$

m is the modulation index

$\emptyset$ is the phase angle

$\cos\emptyset$ is power factor (pf)

Equation 3.66 and 3.67 are then used to model the conduction losses for one IGBT and one diode. A combination of (3.66) and (3.67) calculates the conduction losses which can further be multiplied by the number of switches which for a three-phase VSI are 6 switches to get the total conduction losses. The threshold voltage across the IGBT,V_{CE0}, diode, V_{D0}, the on-state resistance of the IGBT r_{CE} and diode r_D are obtained from the output characteristics of the power electronic devices while the modulation index, m and power factor, $\cos\emptyset$ are can be obtained from the nameplate of the machine. Depending on the choice of the operating temperature, the on-state parameters can be obtained from the output characteristics as described in Appendix B from which the IGBT and diode conduction losses are modelled.

3.3.2 Switching Losses

The IGBT and diode switching losses can be described as the sum of the energies losses due to turn-on and turn-off of the IGBT and diode. For the diode only the losses during the reverse recovery is needed, the turn on and turn off losses are neglected. Therefore the turn-on and turn off energy losses for the IGBTs can be calculated using

$$E_{onIGBT} = \int_0^{t_1} V_{CE}(t) + i_C(t)dt \tag{3.68}$$

$$E_{offIGBT} = \int_{t_1}^{t_2} V_{CE}(t) + i_C(t)dt \tag{3.69}$$

Where, t_1 is the time the collector-emitter voltage starts to rise and t_2 is the time the collector current become zero. The switching losses in the IGBTs over a switching cycle depends on the switching frequency and the turn-on and turn-off energies given as

$$P_{swIGBT} = (E_{onIGBT} + E_{offIGBT})f_{sw} \tag{3.70}$$

For the diode, the reverse recovery energy from which the switching losses in the diode is calculated is given as

$$E_{onDiode} = \int_0^{t_1} V_D(t) + i_D(t)dt \tag{3.71}$$

$$= \frac{1}{4} Q_{rr} V_{Drr} \tag{3.72}$$

Thus the diode switching losses can be calculated as

$$P_{swDiode} = (E_{onDiode})f_{sw} \tag{3.73}$$

Where, Q_{rr} is the diode recovery charge, V_{Drr} the reverse recovery voltage across the diode and f_{sw} is the control strategy switching frequency. Calculating the switching losses in IGBTs and diode is usually a difficult task. The most simplified approach is the use of manufacture's datasheet. The datasheet provides the turn-on and turn-off energies as a function of IGBTs and diode current as shown in appendix B, Q_{rr} and V_{Drr} that can be used to calculate the switching losses.

Therefore, equations (3.66), (3.67), (3.70) and (3.73) are used to model the losses of one IGBT and diode. The total losses is the sum of the IGBTs conduction and switching multiply by the number of IGBTs in the circuits and the sum of the diode conduction and

switching losses multiply by the number of diodes in the circuits. For a three-phase VSI, the total losses is given as

$$P_{3phVSI} = 6(P_{condIGBT} + P_{condDiode} + P_{swIGBT} + P_{swDiode}) \quad (3.74)$$

3.4 Modelling of Permanent Magnet Synchronous Machine

Permanent Magnet Synchronous Machine is generally modelled based on the stator circuit equations either in d-q reference frame or the traditional a, b, c reference frame. A number of PM machines either motor or generator models already exist in literatures [222] - [224]. In addition, emphasis of this thesis is placed on developing an alternative VSI model that can be accurately and rapidly simulated, therefore PM machine model available in PORTUNUS simulation package is considered adequate for the study [225]. The PORTUNUS PM Machine model can operate with mechanical, electrical and thermal inputs. This allows the model to operate as a PM motor or generator. As a PM motor model, it is operated with electrical input (DC voltage source) and as a PM generator it is driven by a mechanical source such as speed or torque source. The PM machine model requires parameters such as stator resistance, d-q axis inductances, and flux linkage, number of pole pairs and inertia to be accurately specified in order to produce the expected mechanical torque. This makes it flexible therefore to model different types of machines by changing the parameters to match that of the machine under investigation. All that is required is to know the parameters of such machines which in most cases are stated in the datasheet or provided by the manufacturers.

3.5 Implementation and Simulation of Average Voltage Estimation Model and Detailed VSI Switching Model of Variable Speed PMSM Drive System

This section presents the implementation and simulation of the proposed average voltage estimation and switching model of a variable speed permanent magnet synchronous motor drive system using the commercially available PORTUNUS simulation package.

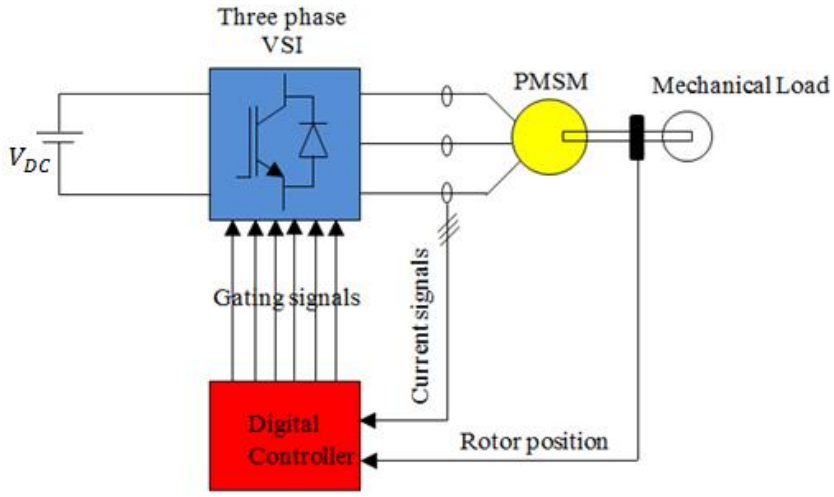

(a)

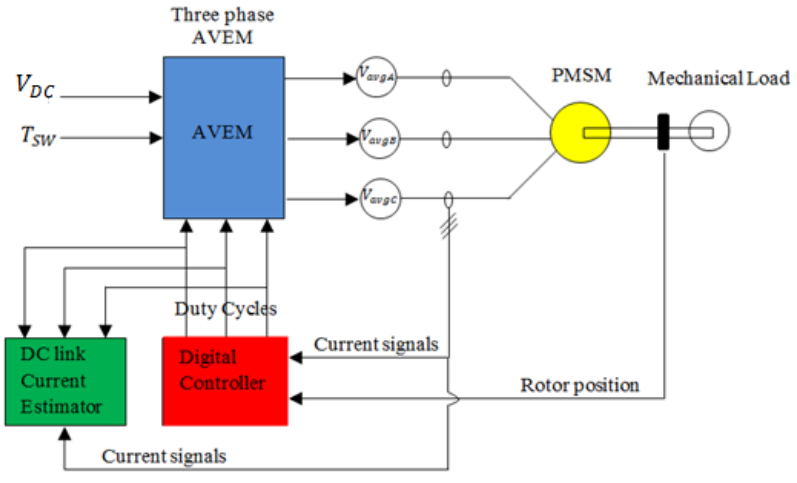

(b)

Figure 3-14: Block diagrams of PMSM drive Systems (a) switching model (b) AVEM

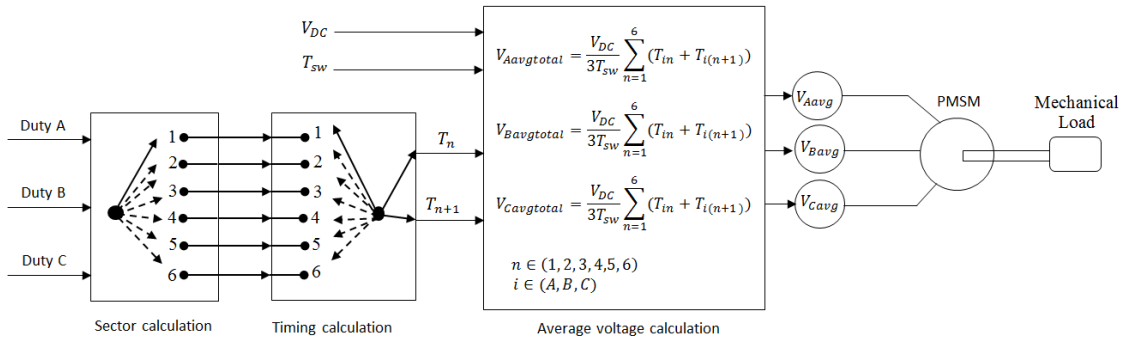

Figure 3-15: An overview of three-phase average voltage calculation

Figure 3-14 (a) and (b) shows the respective block diagram of the switching circuit and AVEM for the PMSM drive system. The switching model takes into account the switching states of all transistors (IGBTs) and diodes in the inverter, while the proposed AVEM eliminates the switching states and has been developed based on the approach described in section 3.2. Figure 3-15 shows an overview of the average voltage estimation of three-phase VSI, PMSM and mechanical load. There are three major blocks towards realising average voltage estimation that can be applied to the terminals of not only a three phase PMSM but any three phase system. The first block is where decision of the sector, the average voltage resides in is taken. This block is very important as the accuracy of average voltage estimation depends on careful and proper selection of the sector in each switching cycle. The second block calculates the length of time the phases of the PMSM or AC load stay connected to the DC link terminals and the third block does the actual calculation of the average voltage in one switching period which drives three voltage sources connected to the terminals of the PMSM. The inputs to the average voltage model as can be seen in Figure 3-14 and Figure 3-15 are the duty cycles usually from the outputs of the PI current controllers, DC voltage and switching period. Therefore the first step in the development of the average voltage model is the choice of the control strategy that is compatible with three-phase system is important. Considering that SPWM is an independent control technique in which each phase is controlled independent of the other makes it a better choice for the implementation. With the control strategy, it is possible to estimate the average voltage from the DC link voltage and the switching functions of the three-phase voltage source inverters. The conventional sinusoidal PWM, PI current controller is considered in this thesis and will be used for both the switching model and the average voltage model in order to establish an accurate

point of comparison; however it is believed that vector control can be implemented with this model with possibly similar results and benefits.

3.5.1 Control Technique for the PMSM Drive System

To implement both models, a control strategy is required. The primary objective of the PMSM control is to control the electromagnetic torque by controlling the 3 phase stator currents. These phase currents are required to be sinusoidal and synchronised with the respective motor phase back emf. The current control technique based on the sinusoidal pulse width modulation (SPWM) control strategy is applied to the models.

SPWM is a well-established independent control technique used to control voltage source inverter driven PMSMs in which each phase is controlled independent of the other. It is implemented with PI regulators generating duty cycles in each switching cycle. Figure 3-16 (b) shows the algorithm used to achieve PI regulator in this thesis and its parameters are shown in Appendix A, Table 3. In the switching model, the inverter uses the duty cycles to generate gating signals for the power switches and control the stator current while the AVEM uses the duty cycles from the control strategy to estimate the average voltage and control the stator current of the PMSM to produce mechanical torque at various rotational speeds.

The Sinusoidal PWM current control strategy relies on accurate information about the rotor position and phase currents of the PMSM for its implementation. The controller receives the rotor position from either an encoder or resolver mounted on the shaft and from this calculates the rotor electrical angular position and also speed reference if an outer speed control loop is included. However there are possibilities of estimating the rotor position and speed without measurement, but this is not an area of research in this thesis, the methods relying on rotor position measurement and speed feedback is used. The PMSM rotor angular position is measured with an encoder and the electrical rotor position calculated using the relationship,

$$\theta_e = p\theta_r \tag{3.75}$$

Changing the rotor position over time is defined as the rotor mechanical speed given by

$$\omega_r = \frac{d\theta_r}{dt} \tag{3.76}$$

From equation 3.76, it is possible to establish the relationship between the mechanical rotor speed and electrical speed as

$$\omega_e = p\omega_r \tag{3.77}$$

Where, θ_r is the rotor mechanical position, θ_e is the rotor electrical position, p is the pole pairs, ω_r is the mechanical speed of the rotor and ω_e is the electrical speed of the rotor.

In the sinusoidal PWM control strategy each PI regulator compares the sinusoidal reference with the relevant motor phase current. Therefore to have a sinusoidal reference current, the reference current is passed through a sine wave generator or a sine wave lookup table synchronised with the PMSG rotor position whose electrical angle is given by (3.75) and a phase shift of 120^0 is applied to obtain the three-phase reference currents given as follows;

$$i_{Aref} = I_m \sin\theta_e \tag{3.78}$$

$$i_{Bref} = I_m \sin\theta_e - \frac{2\pi}{3} \tag{3.79}$$

$$i_{Cref} = I_m \sin\theta_e - \frac{4\pi}{3} \tag{3.80}$$

Figure 3-16 shows the control structure for the three phase PMSM drive system. The controller consists of only the current (torque) control loop. However, an outer speed control loop can be introduced to generate the current reference when speed control is required. When this happens, the actual speed is compared with a reference speed to generate the current reference. Due to the independency in this control technique, each phase has a PI regulator and there are a total of three PI regulators.

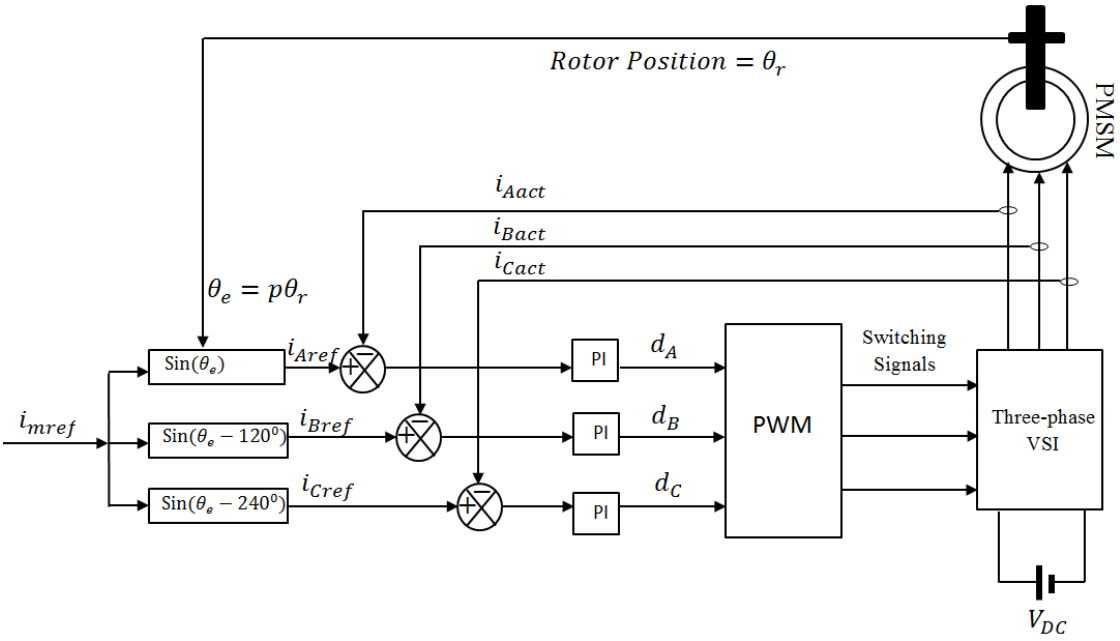

(a)

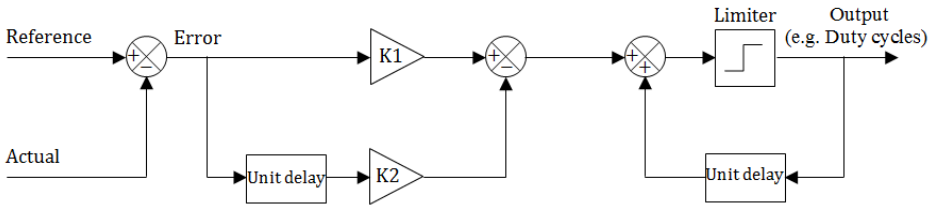

(b)

Figure 3-16: PMSM drive control structure (a) Control algorithm (b) PI regulator

The PMSM stator currents, i_{Aact}, i_{Bact}, i_{Cact} are measured per phase using current sensors and compares with the sinusoidal reference, i_{Aref}, i_{Bref}, i_{Cref}. The result of each phase comparison is fed into the relevant PI regulator. The PI regulator processed error from the comparison. For the switching model, the output of the PI regulator is compared with a triangular carrier signal and modulated at a high frequency (e.g. 20kHz as used in the models) to generates complementary gate drive signals in the relevant phase-leg. This means, when the upper switch in one phase leg is on, the lower switch in that same phase leg will be off and vice versa. This process produces a PWM voltage across the three-phase of the PMSM. Controlling the PWM voltage generates a variable voltage and frequency for adjustable speed motor drive. Alternatively, the output of the PI regulator is used by the average voltage estimation model to estimate the average

voltage that drives the three phase controlled piecewise linear voltage sources across the terminals of the PMSM.

3.5.2 Simulation and Comparison of the results of Average Voltage Estimation Model of PMSM Drive against Switching Model Full Load Current Reference

In this chapter, two methods for modelling the voltage source inverter with variable speed PMSM drive systems have been discussed and developed. The switching model, which takes into account the switching states of the inverter, and the proposed AVEM which eliminates the switching states. Since, the proposed average voltage estimation model is developed based on the switching function, it is necessary first to verify its accuracy against the detail switching model. Hence, the detailed switching model is used as reference against which the results of the proposed AVEM are compared.

Simulations of the models were conducted using the commercially available PORTUNUS simulation package for a small fractional horse power PM machine drive system ($\geq 1kW$) to demonstrate the effectiveness of the AVEM model. The choice of small fractional horse power PM machine minimises the cost of the test rig used to validate the results of both models. However, it is also envisaged that the AVEM can also be used for large machine drive systems design process. The PM machine model implemented in this simulation study is found in the PORTUNUS model library. The parameters of the PM machine model chosen for this purpose are given in Appendix A, Table 1. Both simulation models share similar input variables such as DC voltage, V_{DC} of 57V, PWM switching period T_{SW} = 50μs (switching frequency = 20 kHz). The simulation in this section is based on operating the PMSM drive at a fixed current reference while the operating speed is varied in order to see the steady state performance of the average voltage estimation model and compare the results with switching model across the complete operating speed range. In the simulation, 300rpm is used for low operating speed and 450 rpm for high operating speed.

In order to check if the proposed AVEM can potentially estimate average phase voltages in each sector, simulation were carried out to verify the accurate calculation of the sectors from the outputs of the three phase PI controller.

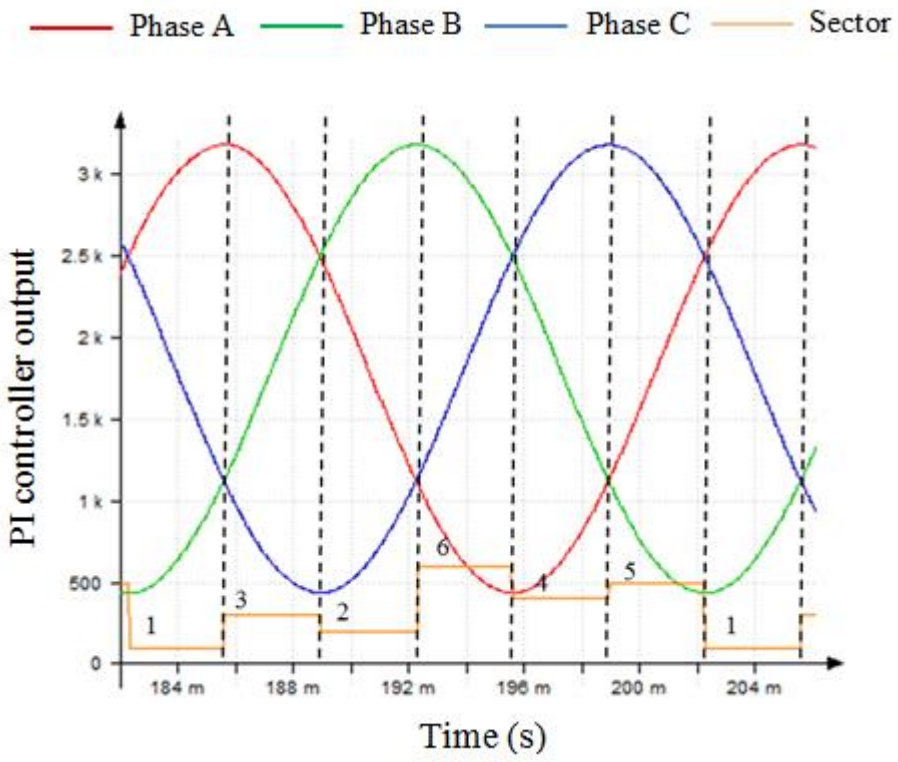

Figure 3-17: PORTUNUS results of three-phase PI controller output and sectors calculation

Figure 3-17 shows the PORTUNUS simulation results of the duty cycles and sector calculation. In the Figure 3-17, it can be seen that as the control strategy is sinusoidal, the duty cycles are sinusoidal. In addition it can be seen that the sectors are accurately calculated as described in section 3.2.3. For example, in sector 1 only one condition of $d_A > d_B$ is met and gives a 1 while others, $d_B > d_C$ and $d_C > d_A$ are not met and the results equals to a 0. This automatically indicates the sector is 1. Similarly, the results of other sector verify the accuracy of the AVEM in calculating the sector from the three phase duty cycles. After this, simulations were carried out using the detailed switching model and the AVEM of the PMSM drive and the results presented.

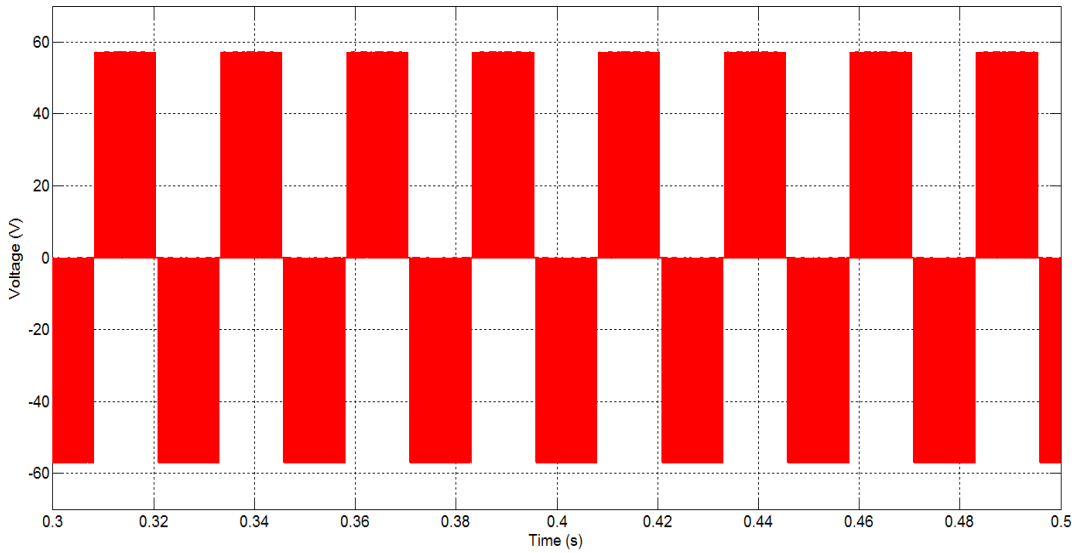

Figure 3-18: PWM line voltage at the terminals of the PMSM @ 15A current reference and 300 rpm using switching model

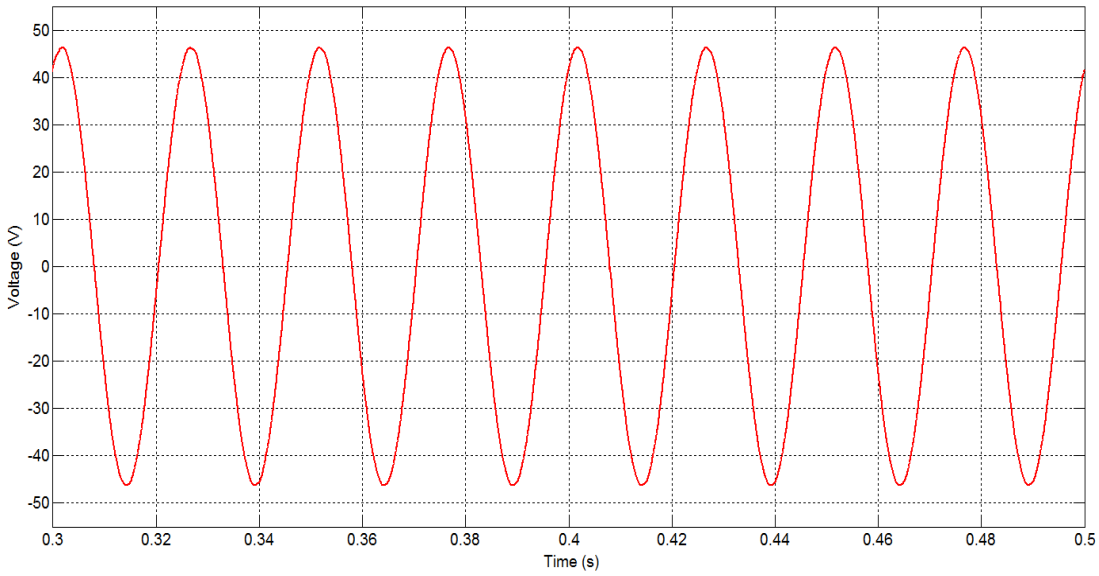

Figure 3-19: Line voltage at the terminals of the PMSM @ 15A current reference and 300 rpm using AVEM

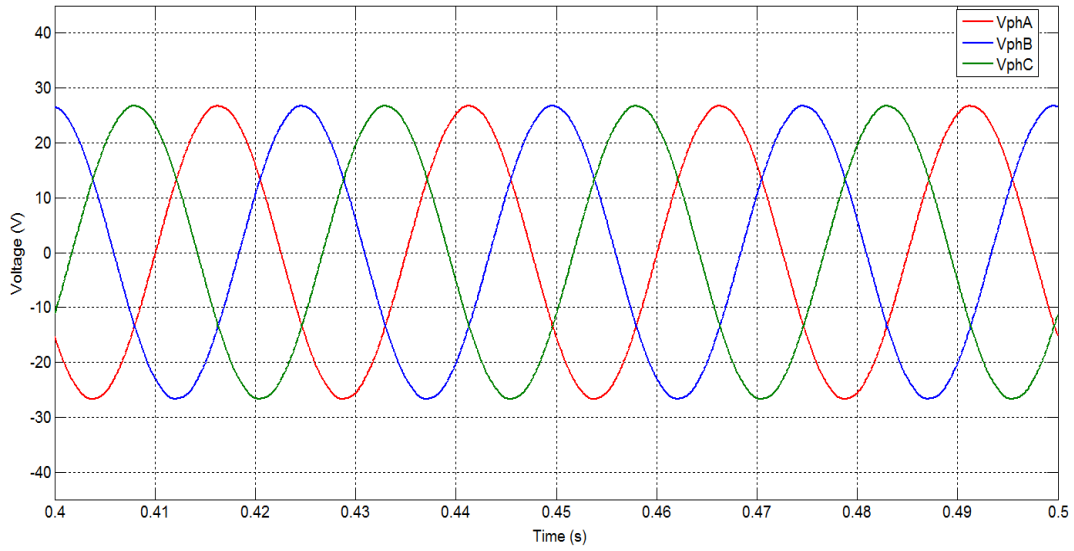

Figure 3-20: Three phase voltage at the terminals of the PMSM @ 15A current reference and 300 rpm using AVEM

Figure 3-18 shows the PORTUNUS simulation time domain output line voltage supplied by the voltage source inverter switching model to the terminals of the PMSM while Figure 3-19 illustrates line voltage supplied by the average voltage estimation model when the current reference is 15A at an operating speed of 300 rpm. In addition, Figure 3-20 shows the three phase average phase voltages using the AVEM. It can be seen that while the conventional switching model produces PWM output voltages @ +/-57V, the proposed AVEM produces sinusoidal controlled voltage at the terminals of the PMSM. Despite this difference in the waveform of the voltage at the terminals of the PMSM, there no loss of accuracy in the control of the PMSM stator current to achieve the desired torque output as will be seen in the following results.

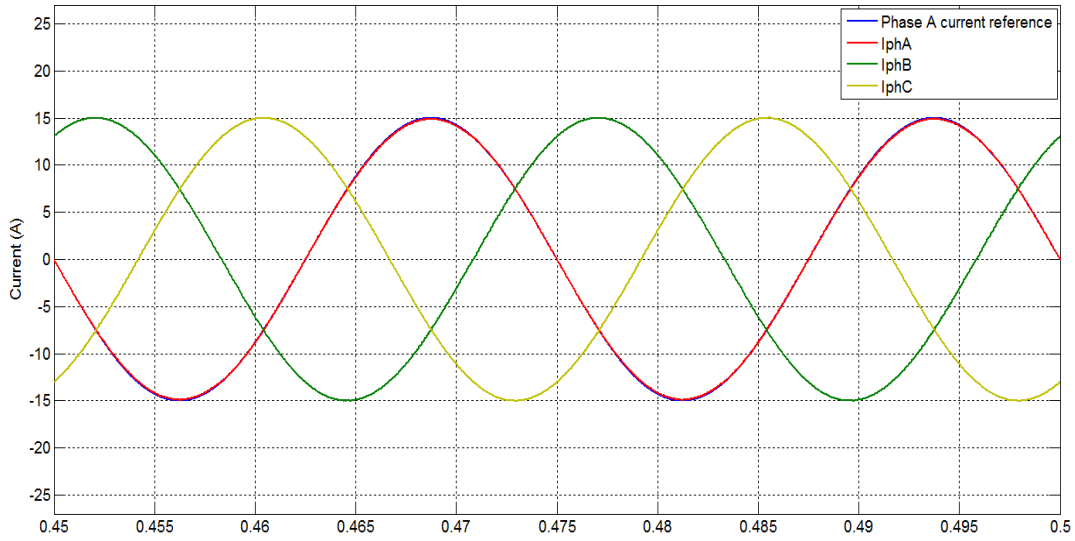

Figure 3-21: Simulation of three-phase PMSM stator current control @ 15A current reference and 300 rpm using switching model

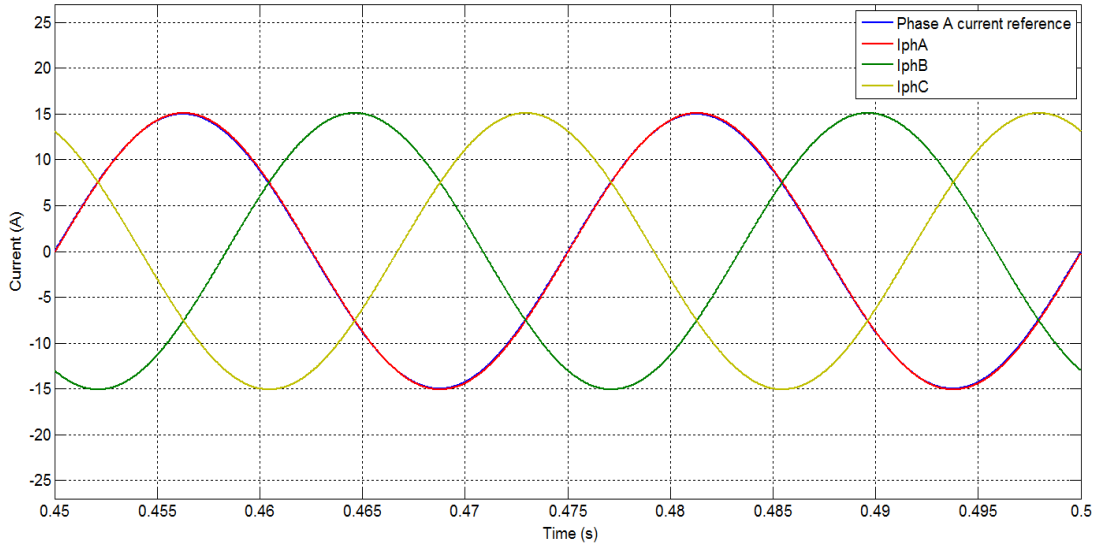

Figure 3-22: Simulation of three-phase PMSM stator current control @ 15A current reference and 300 rpm using AVEM

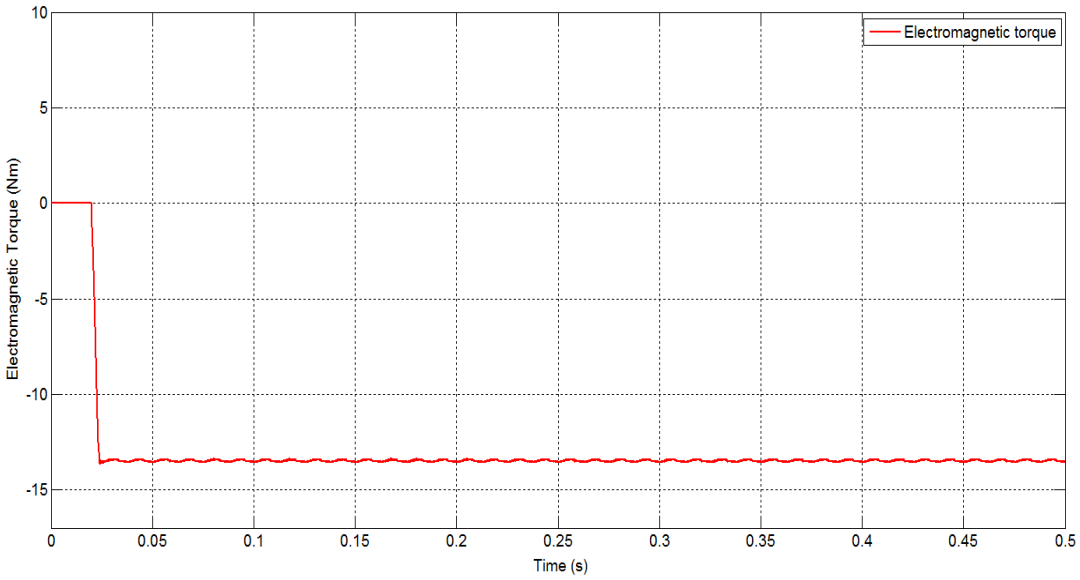

Figure 3-23: Simulation of PMSM drive generated torque @15A current reference and 300 rpm using Switching model

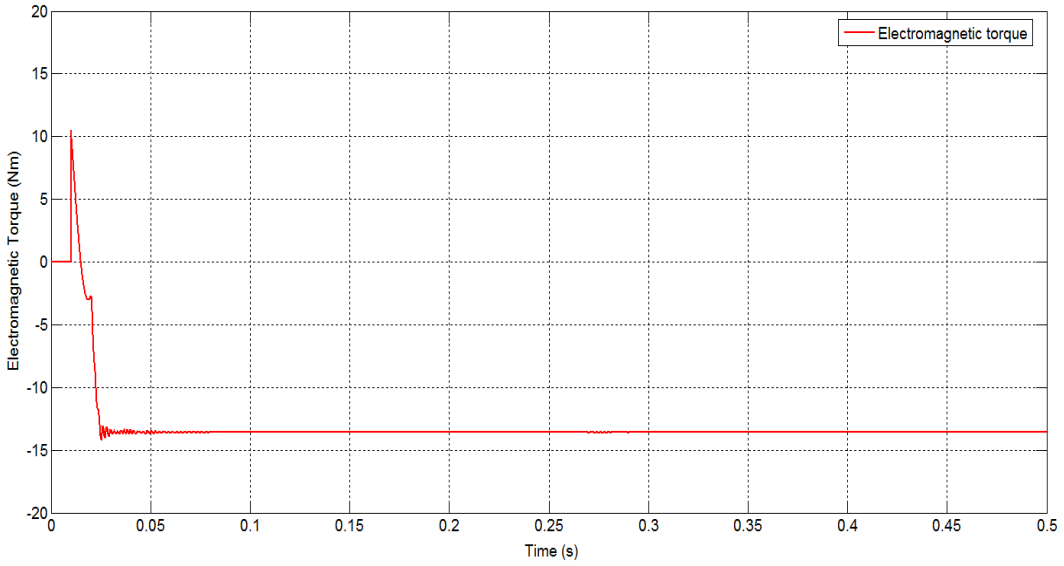

Figure 3-24: Simulation of PMSM drive generated torque @15A current reference and 300 rpm using AVEM

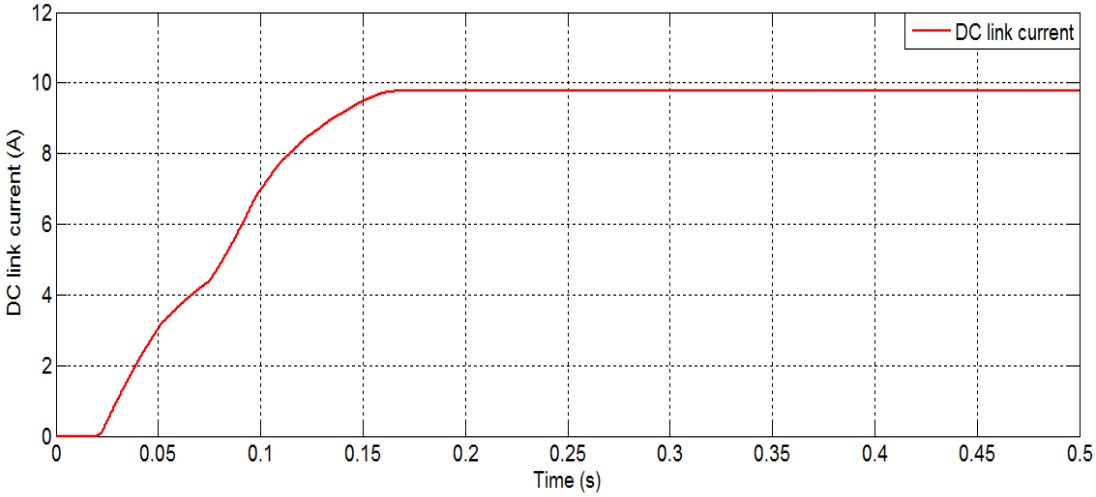

Figure 3-25: Simulated DC link current @15A current reference and 300 rpm using Switching model

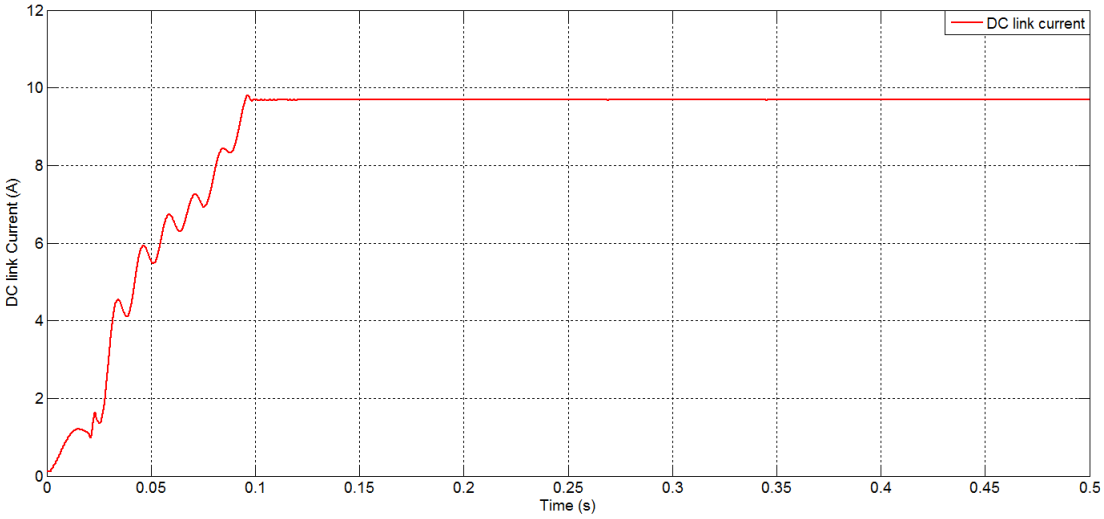

Figure 3-26: Simulated DC link current @15A current reference and 300 rpm using AVEM

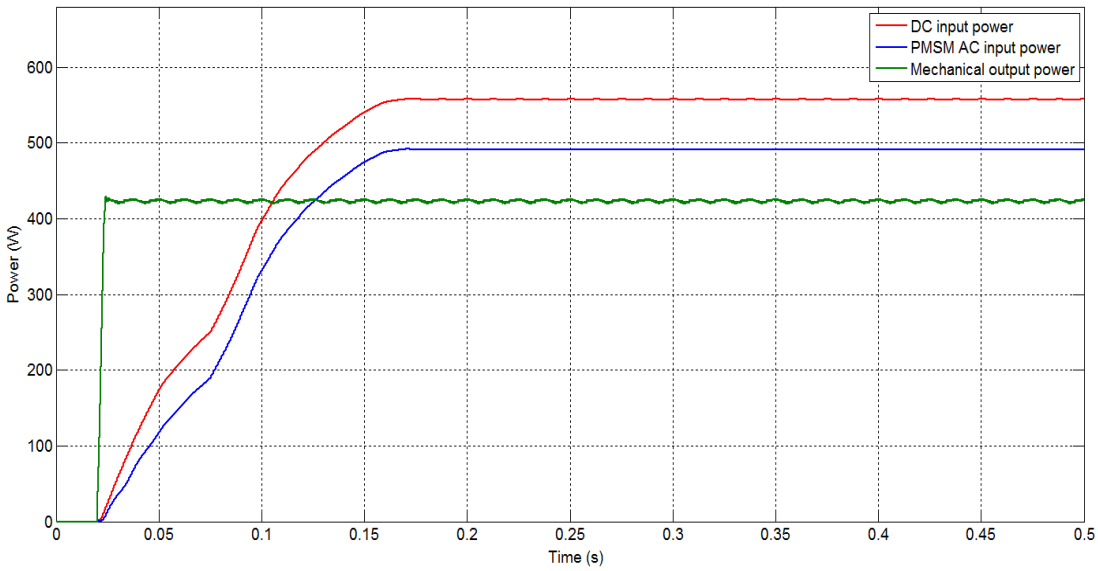

Figure 3-27: Simulation of PMSM drive power @ 15A current reference and 300rpm using switching model with VSI loss model

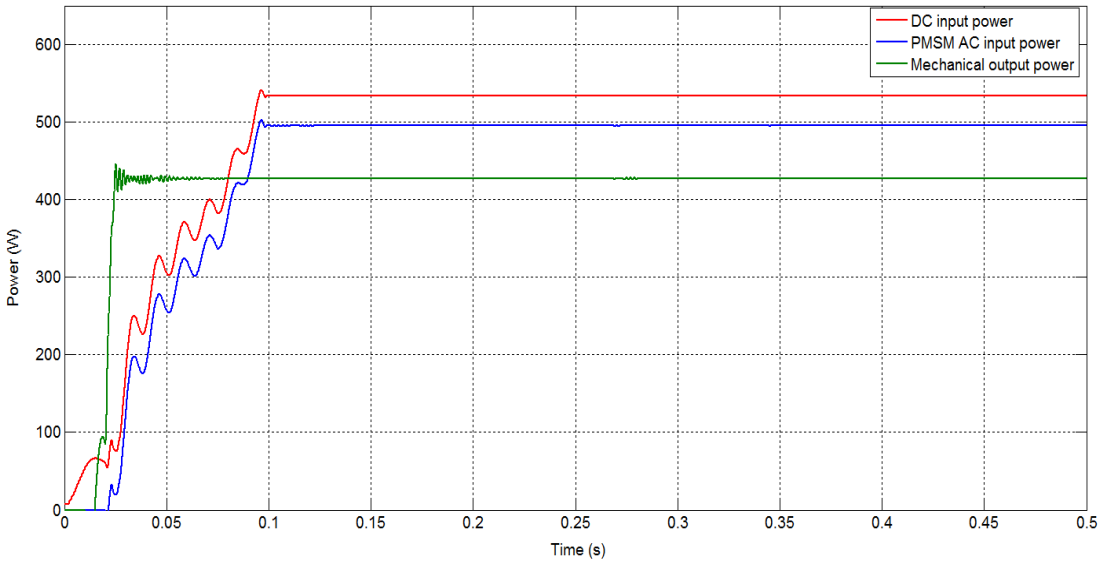

Figure 3-28: Simulation of PMSM drive power @ 15A current reference and 300rpm using AVEM with VSI loss model

The simulation results of the proposed AVEM of PMSM drive system are compared to the switching model in order to validate the performance accuracy of the proposed AVEM. Figure 3-21 – Figure 3-30 show the simulated results of the proposed AVEM and switching model at the lower operating speed while Figure 3-31 – Figure 3-37 show the simulated results at higher operating speed. Figure 3-21 and Figure 3-22 show the

time domain simulation stator current comparison between the switching model and AVEM at 15A current reference and 300 rpm using the carrier-based sinusoidal PWM PI current control strategy. It can be seen that the results of the AVEM agrees very well with the switching model in tracking the waveform of the reference current, with the same phase sequence and magnitude. Note that the AVEM model results do not include the current ripple due to the PWM switching, for the purposes of this model this is not considered a major drawback. This effectiveness and quality of the current control is reflected on the torque output of the electrical machine drive. Figure 3-23 shows the simulated torque versus time of the switching model and Figure 3-24 shows the torque versus time of the proposed average voltage estimation model. The torque predicted by the AVEM as shown in Figure 3-24 is compared with the prediction of the switching models shown in Figure 3-23 and the results shows that the switching model and AVEM predicted the same output torque and profile showing negative torque profile which is what is expected during motoring (given the Portunus sign convention). Comparing the results, the AVEM simulation torque curves are smoother than that of the switching model because of the absent of the switching actions in the AVEM. In addition, the DC link current predicted by the AVEM as described in section 3.2.6 is shown in Figure 3-26 while that of the switching model is shown in Figure 3-25. It can be seen that the DC link current predicted by the AVEM is in good agreement with that of switching model. Similarly, Figure 3-27 shows the PMSM drive power predicted using the switching model and Figure 3-28 shows the drive power predicted using AVEM where the DC input power, the AC power input to the PMSM and the mechanical output power are adequately simulated and predicted. The power flow from the DC power supply to the mechanical output simulated by the proposed AVEM agrees well with the power flow using the switching model.

In variable speed drive systems, power electronic converters control the frequency of the applied voltage. The voltage and current applied to the stator of the PMSM are obtained from the output of the three phases VSI, the frequency of which depends on the PMSM rotor speed. It is important to verify and analyse the relationship between the stator current frequency and the rotor operating speed. Theoretically, the PM machine synchronous speed is related to the frequency by

$$N_s = \frac{120f}{p} \tag{3.81}$$

Where, N_s is the synchronous speed (rpm), f is the frequency and p is the number of poles of the machine. With the 16 poles PMSM as shown in Appendix A, Table 1, two operating speed of 200 rpm and 300 rpm were considered for this verification.

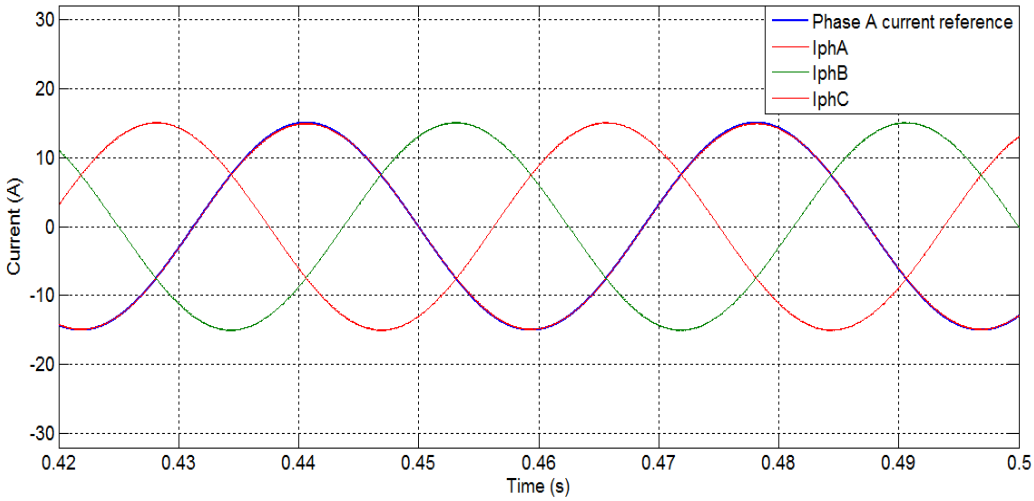

Figure 3-29: Simulation of three-phase PMSM stator current control @ 15A current reference and 200 rpm using Switching model

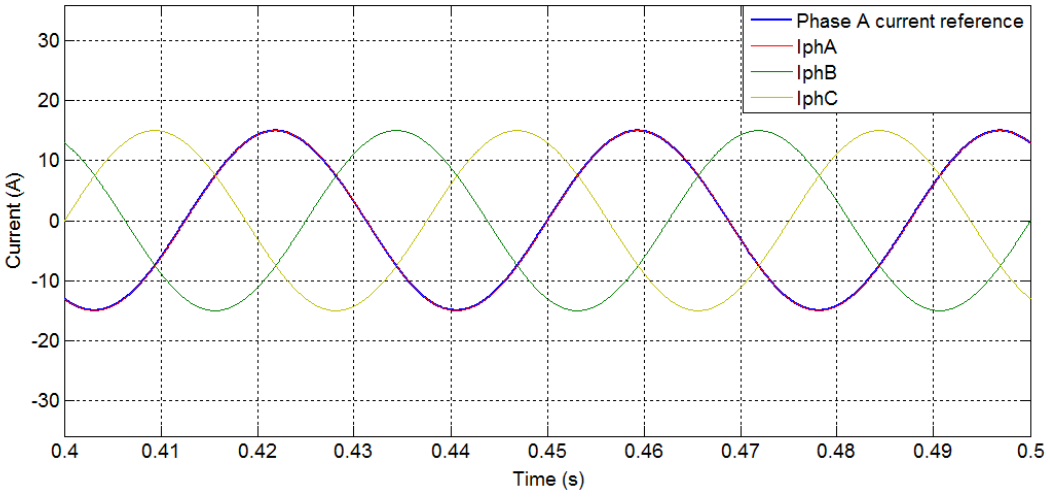

Figure 3-30: Simulation of three-phase PMSM stator current control @ 15A current reference and 200 rpm using AVEM

When the PMSM rotor shaft is rotating at a speed of 200 rpm, a low frequency stator current is supplied to the terminals of the PMSM. Figure 3-29 and Figure 3-30 show the stator current waveform when the PMSM operates at 200 rpm predicted by the switching

and AVEM and the frequency of the current is 26.67Hz. When the rotor speed is 300 rpm, the frequency of the stator current waveform is 40Hz shown in Figure 3-21 and Figure 3-22. It can be seen that when electrical machine operates at low speed, low frequency current from the voltage source inverter is applied to stator of the machine, whereas when the rotor speed is high, a high frequency stator current is applied, which is what is theoretically expected. Again, both the switching model and the proposed AVEM predicted the same frequency at each operating speeds. The good match of the results of the AVEM with the switching models validates its accuracy and can be used for further analysis.

The proposed average voltage estimation of VSI with PMSM drive system performance is further verified and compared with the detailed switching model at higher rotor speed where the current regulators can no longer produce sinusoidal currents due to high motor back emf. Simulations were also conducted at the same current reference of 15A demand from the PMSM stator driving a mechanical load but at 450 rpm to compare the simulation results of the AVEM with the switching model.

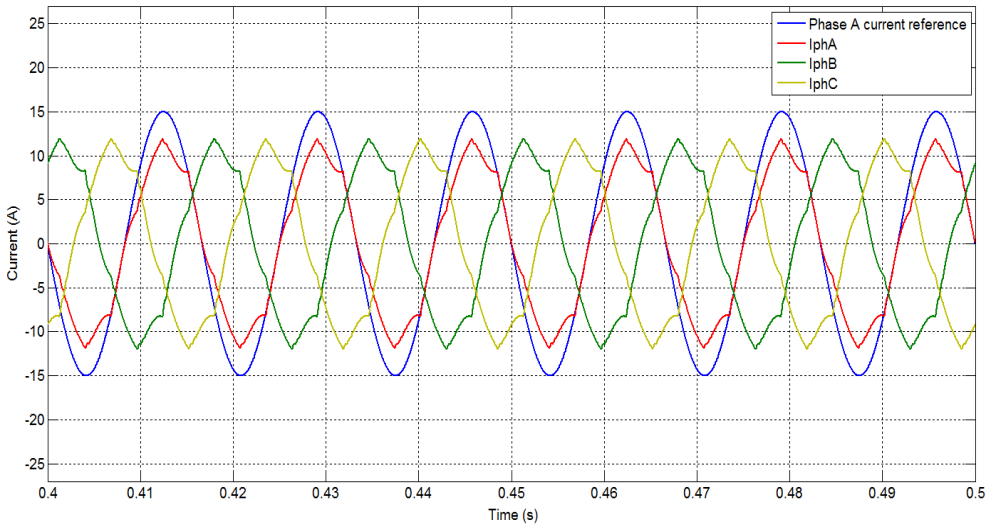

Figure 3-31: Simulation of three-phase PMSM stator current control @ 15A current reference and 450 rpm using Switching model

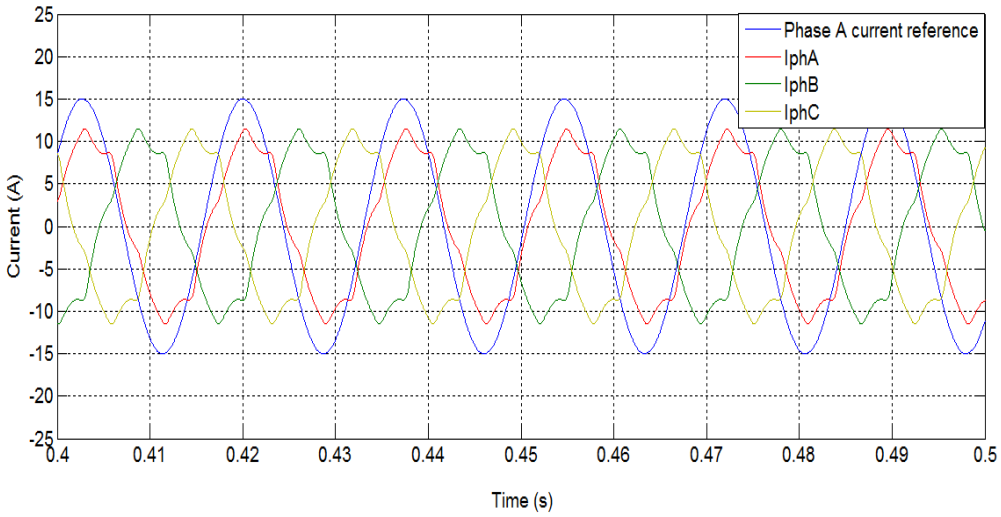

Figure 3-32: Simulation of three-phase PMSM stator current control @ 15A current reference and 450 rpm using AVEM

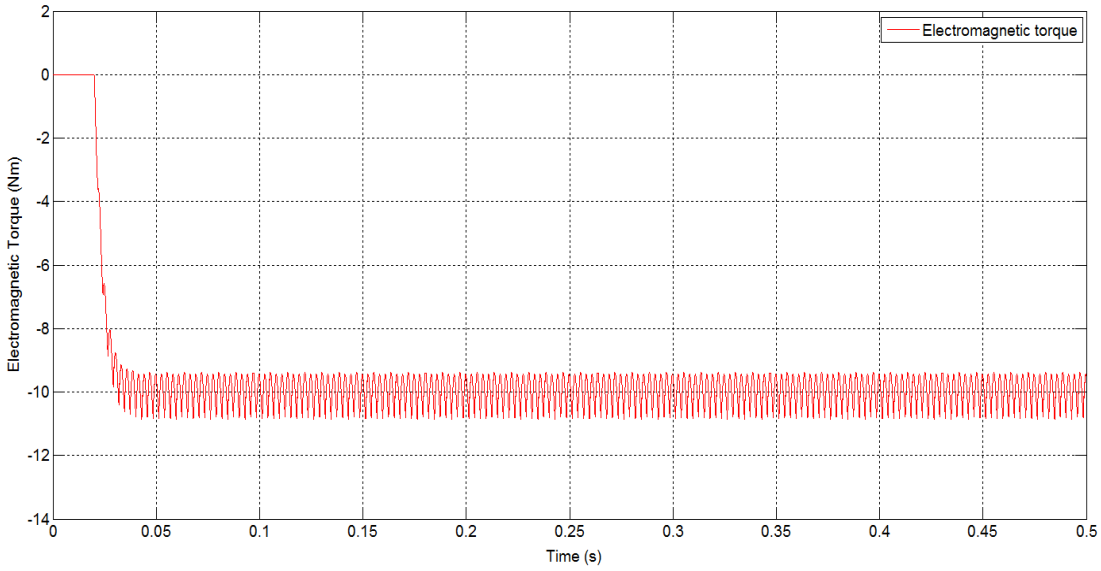

Figure 3-33: Simulation of PMSM generated torque @15A current reference and 450 rpm using switching model

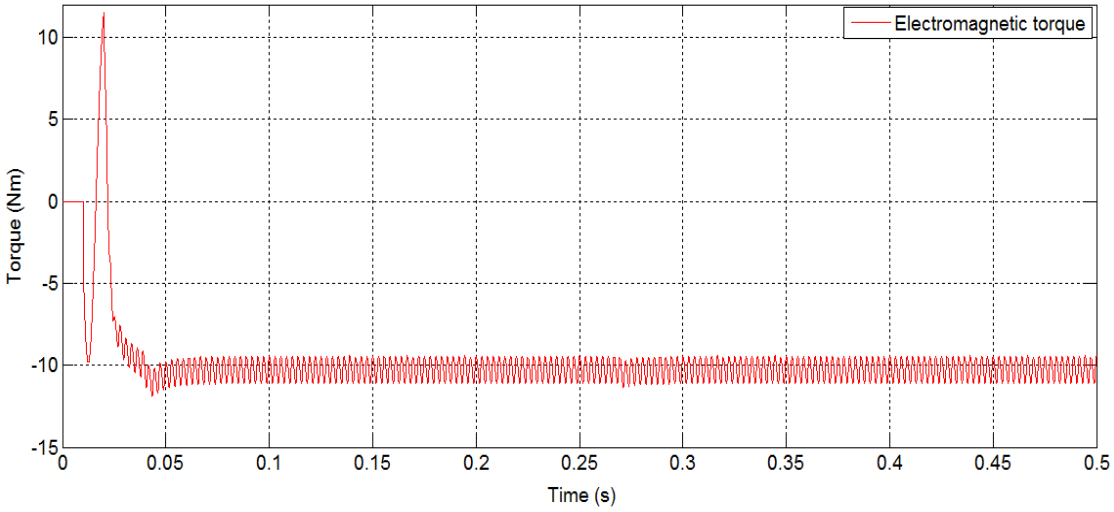

Figure 3-34: Simulation of PMSM generated torque @15A current reference and 450 rpm using AVEM

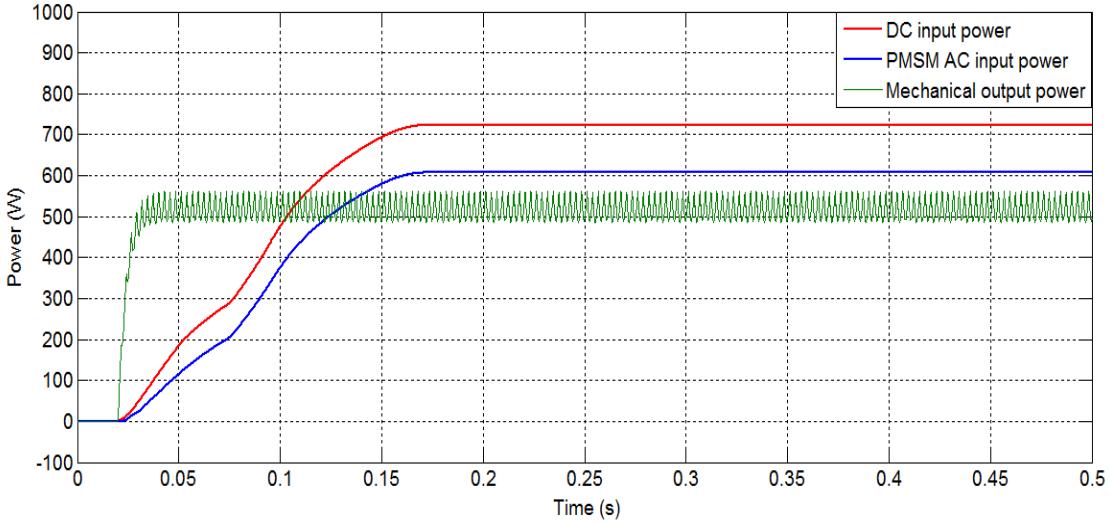

Figure 3-35: Simulation of PMSM drive power @ 15A current reference and 450rpm using Switching model with VSI losses

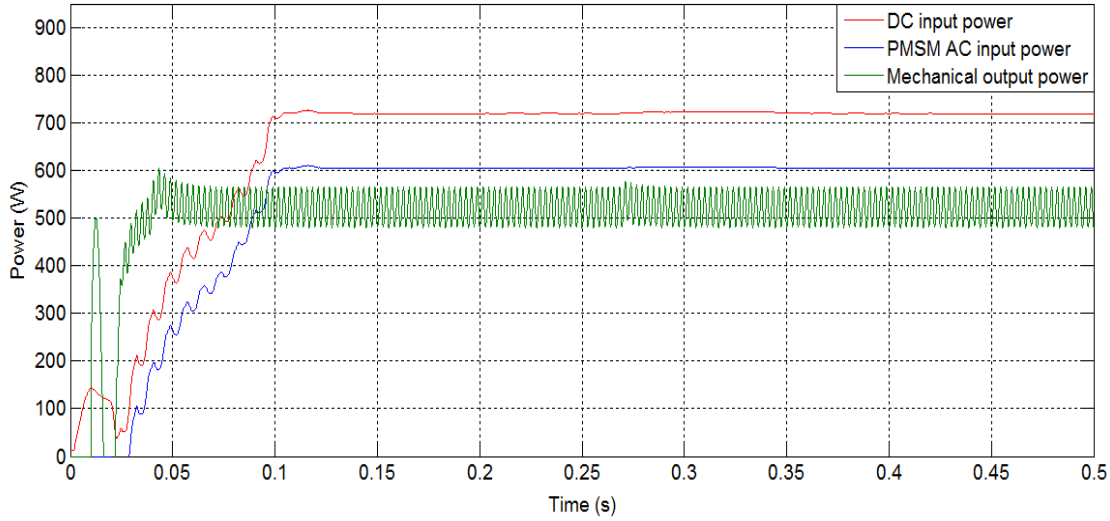

Figure 3-36: Simulation of PMSM drive power @ 15A current reference and 450rpm using AVEM with VSI losses

Figure 3-31 – Figure 3-36 show the simulated results using the AVEM and the switching model at high operating speed of the PMSM drive system. Figure 3-31 and 3-32 shows the operation of the PMSM under the PI current control at higher operating speed i.e. a speed above the constant torque region, in this particular case 450 rpm. It can be seen from the results that both the AVEM and the switching model predict the same non sinusoidal waveform of the actual motor currents. However, control of stator current is lost at this speed (higher speed). This is because, the speed of the PMSM determines the

induced voltage at the terminals of the PMSM and as the speed increases the induced voltage increased beyond the stiff DC link voltage and the DC voltage is unable to overcome the higher motor back emf and limits the current that flows into the PMSM which is characterised with diminishing and non-sinusoidal stator phase current away from the reference current. The effect of the loss of current control is shown on the predicted torque and power. Again comparing the results for torque (Figure 3-33 and Figure 3-34) and power (Figure 3-35 and Figure 3-36), the AVEM model predicts the same performance as the switching model. These results validate the performance of the AVEM against the switching model in simulating and implementing the current/torque controller and the performance of the PI current controller to control the stator current and the PMSM torque under variable speed conditions. It is important to highlight that the exact same digital current control block is used in both simulation models therefore the AVEM is very useful in analysing and optimising the performance of the chosen control strategy. It is also worth highlighting that there is no reason why a vector control strategy could not be used in both models, other than the time and effort required to implement this in Portunus. The results also show that the proposed AVEM can be used to simulate and analyse power flow in electrical machine drive systems.

3.6 Conclusion

The detailed average voltage estimation modelling (AVEM) and control of a PMSM drive has been developed and simulated. The model has been found capable of implementing the control of a PMSM drive system and it controls the operating characteristics of the PMSM both in low and high operating speed, (constant torque and field weakening region,) which has been shown in the simulation results. Since the proposed average voltage estimation model is based on PWM control and switching functions of VSI, a brief introduction of the theory of the VSI switching modelling method was first outlined. The switching modelling method takes into considerations the switching states of all the transistors and diodes during simulations and is restricted by the small minimum simulation step time. This is followed by the procedures for developing the AVEM using a different approach to the average value model which totally eliminates the switching states and gives the AVEM a far higher minimum step time which makes it significantly faster in analysing wider PMSM output parameters without a subsequent loss in accuracy.

The chapter has also included the introduction of the voltage source inverter loss model into the average value model and describes the procedures involved in modelling the conduction and switching losses of the VSI IGBTs transistors and diode using the manufacturer's datasheet approach. The VSI model is then incorporated into the AVEM, which has further expanded the scope of the average value model which enabled the analysis of powers and efficiency of the drive system. The chapter also presents the development and implementation of sinusoidal PI current control for the PMSM drive and concluded with simulation results to show the steady state performance of the AVEM model and the PI current control at low and high operating speed regions (constant torque region and the constant power region) of the PMSM drive system. The results shows the accuracy of the proposed AVEM model against the switching model in implementing a control strategy for the PMSM drive system predicting the waveforms of the motor currents and controlling the torque of the PMSM drive system at fixed reference current/torque demand and speed.

Chapter 4: A Practical Implementation of PMSM Drive and PMSG Wind Energy Conversion System

4 Introduction

A flexible laboratory test rig has been developed in order to validate the simulation results for the proposed average voltage estimation model and the detailed switching model of a three phase VSI with variable speed PMSM and PMSG drive systems.

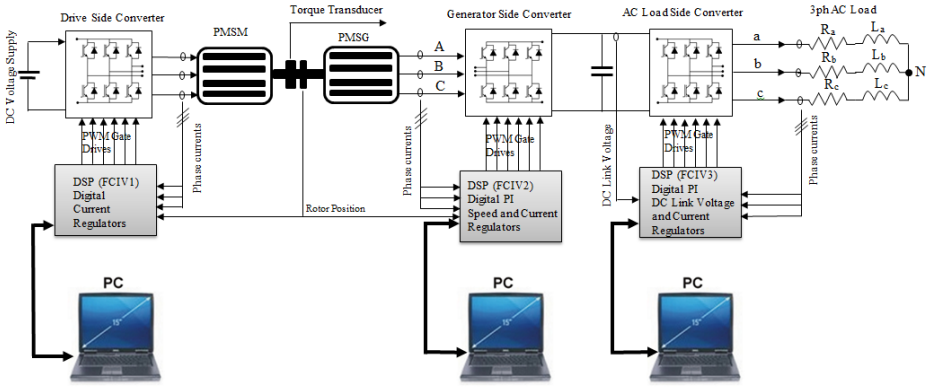

Figure 4-1: Configuration of the laboratory Test platform

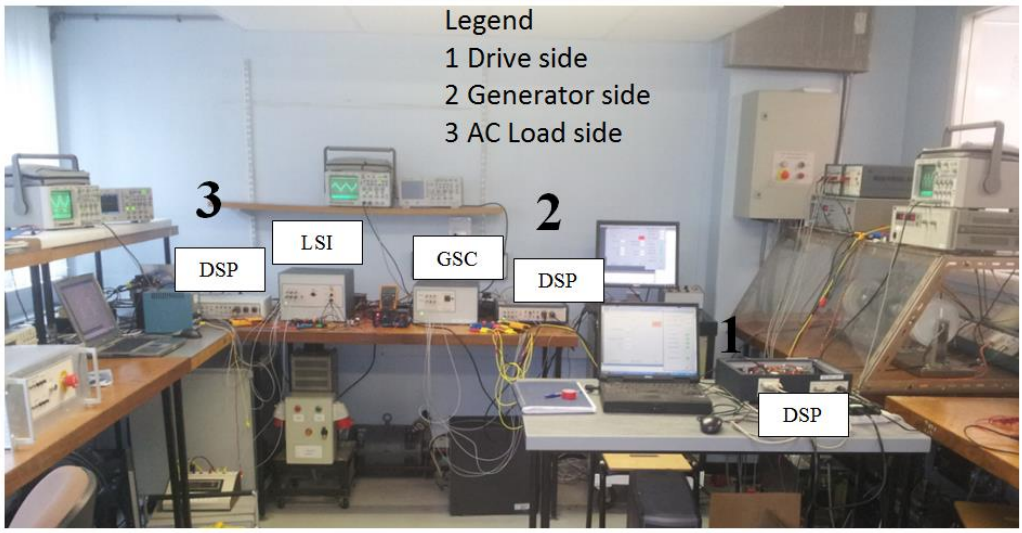

Figure 4-2: Laboratory setup of the Test platform

Figures 4-1 and 4-2 respectively show the configuration and the laboratory setup of the test platform used for the experiments in this thesis. It consists of two 1 kW permanent magnet synchronous machines whose parameters are shown in Appendix A, Table 1, with one designated as the PMSM and the other as the PMSG directly connected to each other as shown in Figure 4-3. The set-up also contains power electronic converters, sensors, feedback devices, a Digital signal control system, a three phase AC load and measuring devices. A DC voltage source is fed into the drive side converter, which converts the DC voltage to AC voltage and fed to the PMSM. The PMSM is directly connected to the shaft of the PMSG and the output of the PMSG connected to a three phase AC load through a full scale three phase back-to-back voltage source inverter.

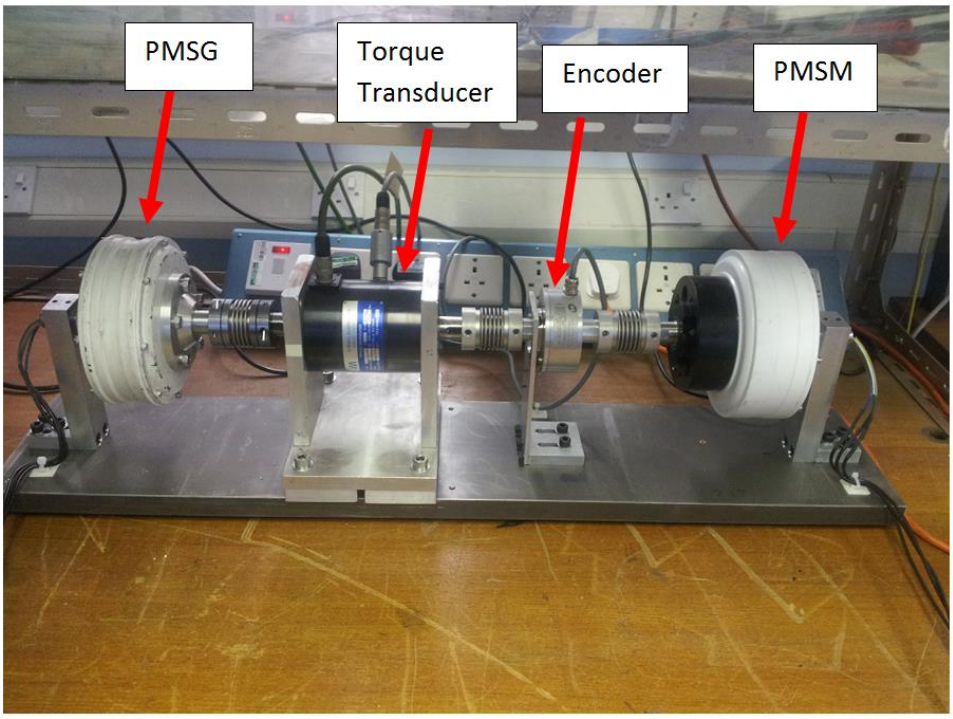

Figure 4-3: Test platform Machine setup

The test platform is constructed to serve two purposes; as a PMSM drive system and also as a PMSG wind energy conversion systems' emulator, enabling operation in two modes. This means experiments are carried out either in motoring mode or in generating mode. In motoring mode, the PMSM operates as a drive and the PMSG is controlled and used to load the PMSM. When operating as a PMSM drive system, the Load side inverter and

its control is isolated and the DC link capacitor replaced with a constant DC voltage source. In generating mode, the PMSM acts as a drive and its torque is controlled to emulate a wind turbine, which serves as a variable speed source for the PMSG. The output of the variable speed PMSG is fed into the generator side converter which connects the AC load through the DC-AC load side converter. Clearly, the drive side converter controls the current (torque) of the PMSM, while the generator side and the AC load side converter controls speed and DC link voltage respectively. PMSM and PMSG are of surface mounted rotor permanent magnet design.

4.1 Voltage Source Converters

The voltage source converters in this test rig are made up of insulated gate bipolar transistors (IGBTs). There are 3 three-phase converters; one each for the drive motor, generator and AC load. The converter at the left hand PMSM drive side (see Figure 4-1) connects DC voltage supply to a three-phase PMSM. This converter converts DC to AC on application of appropriate control signals to the gates. The second converter from the left connected to the front end of the PMSG plays a dual role, in motor mode it converts DC to AC supply to the PMSG, which then acts as load to the PMSM. In the other case, it converts AC generated from the PMSG to DC voltage when receiving suitable control signals from the DSP (FCIV 2), while the third converter changes DC to AC for the three phase AC load or connection to grid. All the converters have provisions for optical fibre cables through which the control signals supplied by the DSP controller can be applied to the gates of the IGBTs.

4.2 Digital Signal Control System

The DSP is a key component in the Test rig that provides real time calculation capability and allows the validation and testing of the existing and new control strategies associated with variable speed PM motor drives and renewable energy conversion system. The DSP used in this research is part of the Flexible Controller 4th edition (FCIV) platform. It is able to control the voltage source inverter connected to each machine. Each controller has a dedicated computer. This computer has the capability to establish connections and create software for the FCIV. This PC communicates with the FCIV for effective implementation of the control. Presently the computer used has a

development board optimized with the Texas Instruments (TI) c28 series DSP processor which can be programmed using TI's code composer software suite. The control techniques are developed using C-programing language within Code Composer and compiled on the PC before being run on the DSP. The typical control technique based on PWM using a PI control loop with a switching frequency of 20 kHz is developed. This can be downloaded and processed by FCIV to generate the required control signals to the gates of each converter when control is needed. The control signals which are developed in a way similar to those of the simulation models are supplied from FCIV to the converters through optical cables as shown in Figure 4-4.

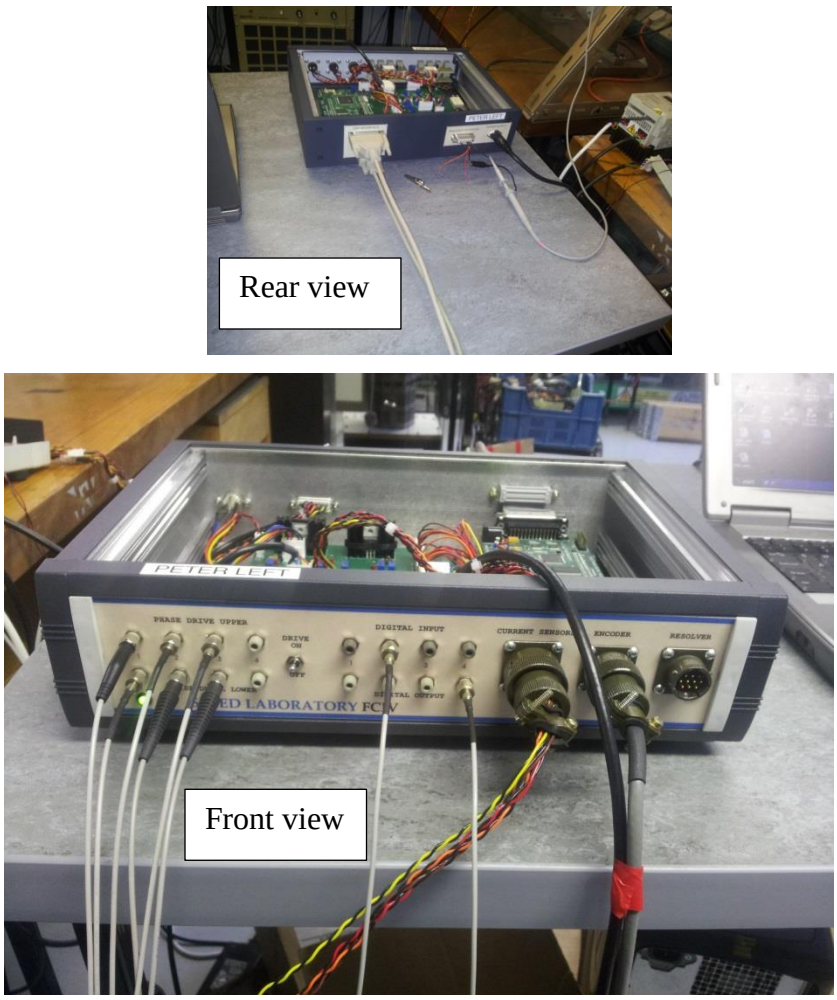

Figure 4-4: Screenshot of Digital Signal Processor

Measured quantities such as speed, phase currents, and DC link voltage are necessary for the development of the control scheme for the FCIV. Speed and rotor position are measured using a 1024 line incremental encoder, and torque with a torque transducer.

The rotor position encoder and torque transducer are mounted on the shaft between the PMSM and PMSG (see Figure 4-3). Other sensors are current and voltage sensors used to measure current and voltage respectively. A position encoder, current and voltage sensors provide established connections through which their outputs are fed into the controller. All the measured quantities are in analogue form and are required to be converted into its digital equivalent. The DSP has a built in multi-channel Analogue to Digital (A/D) converter, used in converting measured analogue signals to digital values. At each command (interrupt) for control, the digitalised values are interpreted by the FCIV to generate control signals applied to the gates of the converter. This is in consideration that in one phase leg only one converter switch will be on at a time giving rise to on/off states per phase to avoid short circuiting the DC link.

In practice, it can be seen that all the converter controllers in the test platform have an inner current control loop. Independently, current control is developed for each phase of the converter. The actual currents are independently measured and compared with their predefined reference currents to generate current errors. The predefined reference currents are synchronised with the rotor position angle and with a phase shift of 120^0 degrees from each other. The resulting current error becomes the input to the PI regulator. The PI regulator processes the current error and outputs it to the PWM modulator. The PWM modulator compares the output of the PI regulator with triangular carrier signals and modulates it at a frequency of 20 kHz to generate switching signals driving the converter gates. For the PMSM drive side, the motor electromagnetic torque is controlled through the stator current to emulate the characteristics of the wind turbine during WECS experiments. On the generator side, the current reference is produced by the outer speed control loop with a set speed reference, while for the AC load side controller; the current reference is generated by the outer DC link control loop with a set DC link voltage reference. Both the speed and DC link voltage control loop are implemented with a PI regulator.

4.3 Experimental Results

Experimental results to be used to for validating the simulation results are recorded by the measuring devices and captured with a digital sampling oscilloscope (DSO). The results are categorised based on the tests carried out, such as results for a PMSM drive

system and variable speed PMSG WECS. One important aspect of the test is the similarity in the current controller of the motor and the generator.

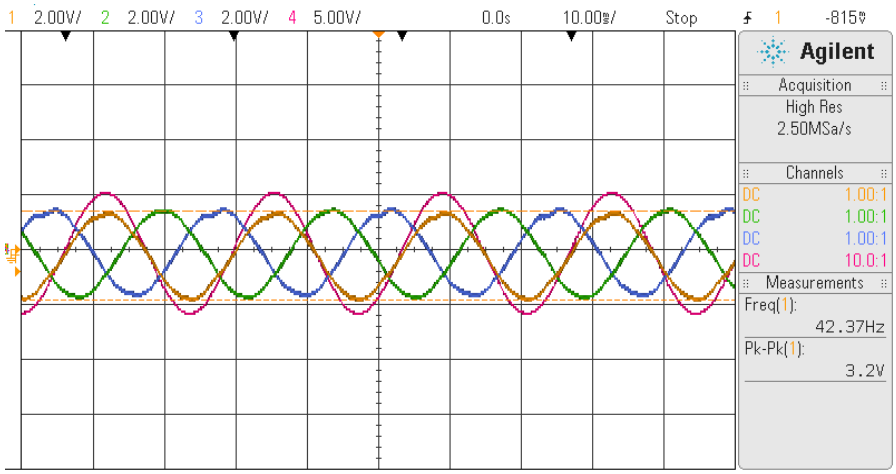

Figure 4-5: PMSM three phase stator current at 300 rpm and current reference of 15A on a current probe of 100mV/A

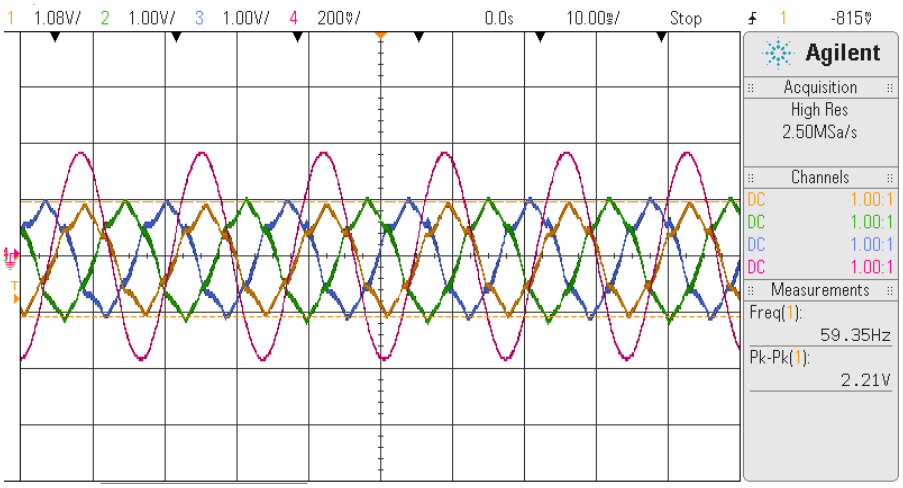

Figure 4-6: PMSM three phase stator current at 450 rpm and current reference of 15A on a current probe of 100mV/A

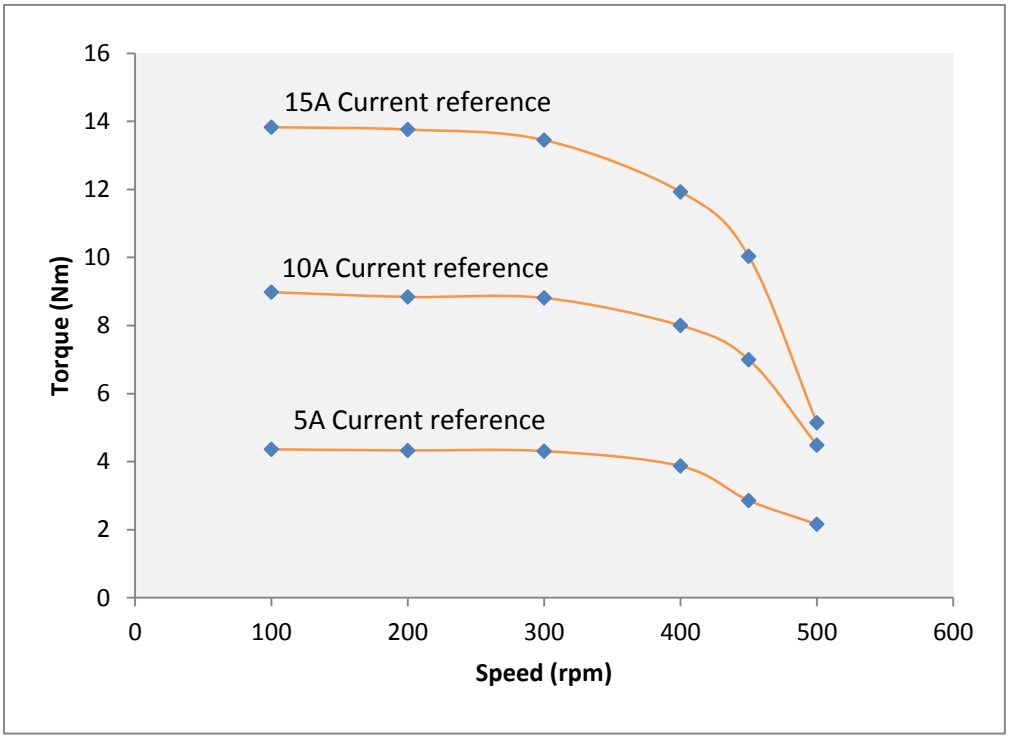

Figure 4-7: PMSM drive system Torque speed characteristics at different torque and current reference

Figure 4-5 and Figure 4-6 show the PI current control reference compared with the measured stator current, where the aim is to control the current of the PMSM drive system to obtain a desired mechanical torque. The results represent the operation of the drive at the two ends of the operating speed of the drive; the low speed region and the higher speed region. From Figure 4-5, it can be seen that at the lower speed region (e.g. ≤ 300 rpm), the stator current is controlled to its reference value (silver coloured waveform under the red coloured waveform) in waveform, magnitude, sequence and frequency. With the current probe of 100mV/A in each of the phases, the peak of the reference current of 15A is supplied by the inverter to the terminals of the PMSM and produces a mechanical load torque of 13.85Nm. On the other hand, Figure 4-6 shows the waveform of the stator three phase current at 450 rpm representing operation of the drive at a higher operating speed. It can be seen the control of stator current is lost shown by the large difference between the phase current and the reference current. The current reference demanded is still 15A peak yet a non-sinusoidal current of value less than the reference current is supplied to the stator resulting to a lower value, 10.44Nm of generated mechanical torque. This experiment is repeated at different current references

and the torque is then recorded and plotted as shown in Figure 4-7. Figure 4-7 shows the recorded torque versus speed curves of the PMSM at various current references.

4.4 Wind Energy Conversion Emulation System

A 1 kW wind energy conversion system emulator was developed to validate the predictions of simulation models and control strategy for the WECS. With the emulator, the performance of different PMSGs, converters and control strategies can be tested and analysed. In addition, it will provide a future test platform in which a wide range of variable speed wind energy conversion systems can be tested and evaluated. It consists of a permanent magnet synchronous generator (PMSG) coupled to a permanent magnet synchronous Motor (PMSM). The PMSM torque is controlled by the DSP to emulate the wind turbine. The mechanical energy of the PMSM (wind turbine emulator) is directly connected to the PMSG and the generator is connected to the AC load through a back-to-back voltage source inverter and delivers power from the wind turbine emulator-PMSG to the AC load.

This section presents results of both steady state and dynamic performance of the WECS emulator and control strategy. At first, the steady state tests are carried out for different wind speeds and different values of generator rotational speed. This involves varying the generator speed at a certain wind speed and observing the turbine power, torque, power coefficient, tip speed ratio, generator power, current, torque, DC link voltage, DC link current, AC load power, current and frequency. The second test involves applying a variable speed data and calculating the energy yield of the WECS over a period of time. The torque of the drive side PMSM is controlled to emulate a 1 kW variable speed wind turbine in a PMSG wind energy conversion system. In this concept, the rotor rotational speed is measured and with the wind speed calculates the turbine torque which generates the current references for the three phases which are compared with the actual measured phase current and generates the gating signals for the drive side inverter. Since the emulator depends on the rotational speed feedback and the PMSM drive and the generator are directly coupled, to reproduce the power versus speed of a typical wind energy conversion system, the PMSG rotational speed needs to be controlled. With a certain wind speed selected, the generator speed is indirectly controlled by controlling the generator torque. The emulator is developed using the controller to accept wind speed

as a constant value or wind speed profile. The initial challenge is how to provide the initial rotor speed the emulator requires to calculate the reference current. This problem was solved by developing two modes of operation for the emulator; the current control and the emulator mode. The emulator first starts with current control to build up rotational speed and then changes to the emulator mode. Once this is achieved, current control is applied at the generator side and DC link voltage applied to the AC load side. The steady state tests were conducted for different wind speed such as 8m/s, 10m/s and 12m/s and at each wind speed, the current; voltage and power at different points were recorded and plotted against the rotational speed. Some of the experimental results are hereby presented.

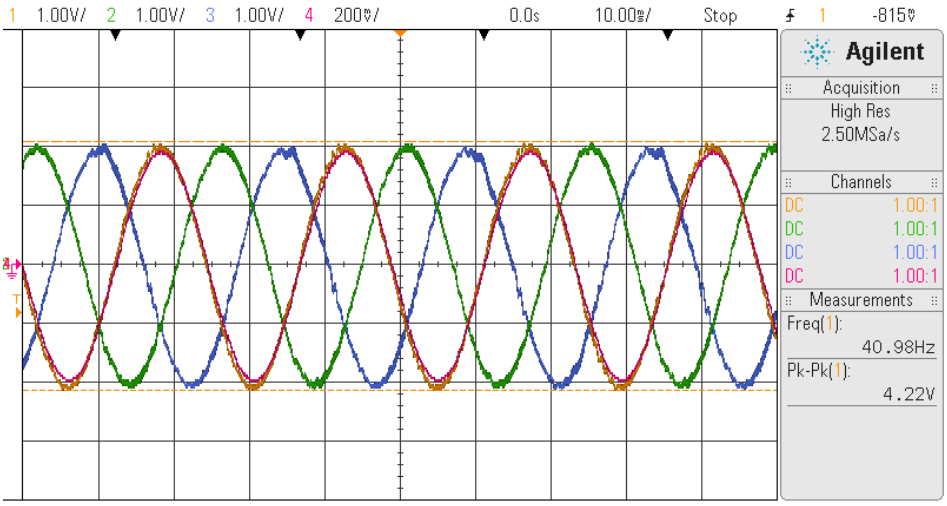

Figure 4-8: Variable speed WECS Emulator PMSG three phase stator current at 12m/s and current reference (silver colour) of 20A on a current probe of 100mV/A

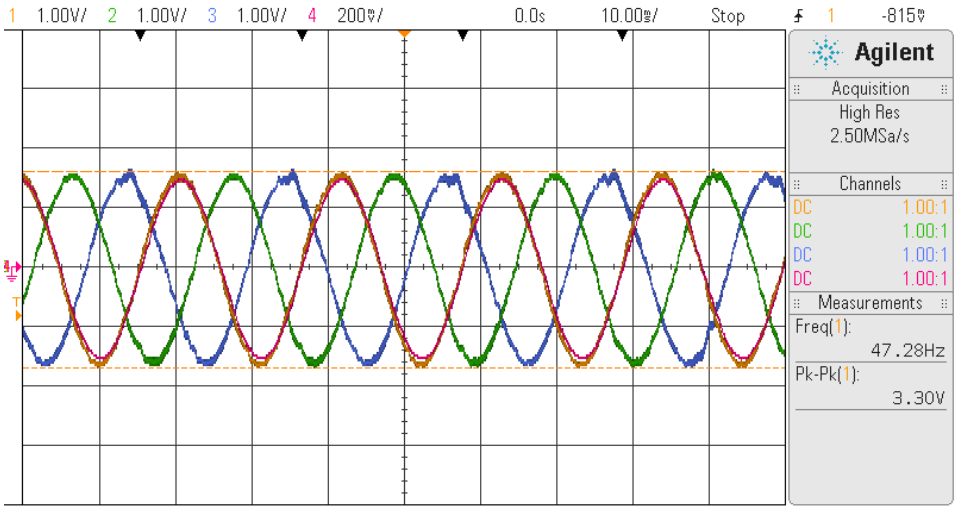

Figure 4-9: Variable speed WECS Emulator PMSG three phase stator current at 12m/s and current reference (silver colour) of 16A on a current probe of 100mV/A

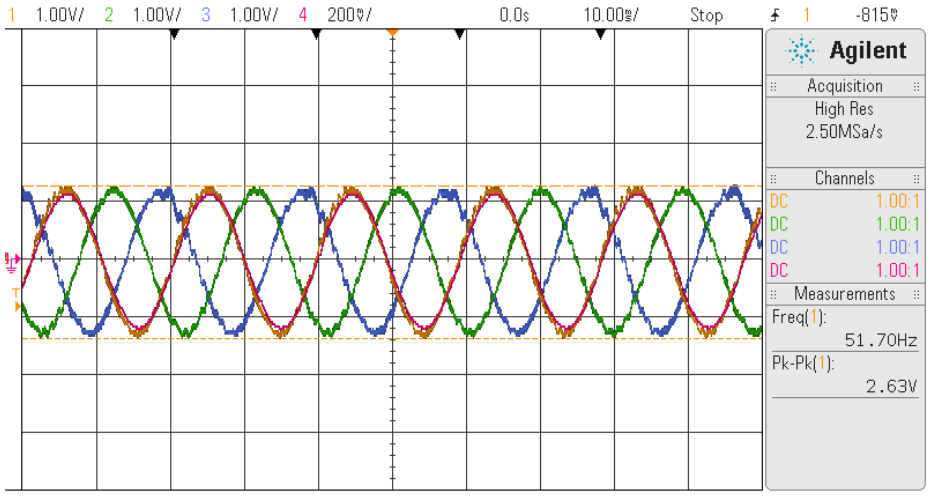

Figure 4-10: AC load three phase stator current at 12m/s and DC Link voltage reference of 57V on a current probe of 100mV/A

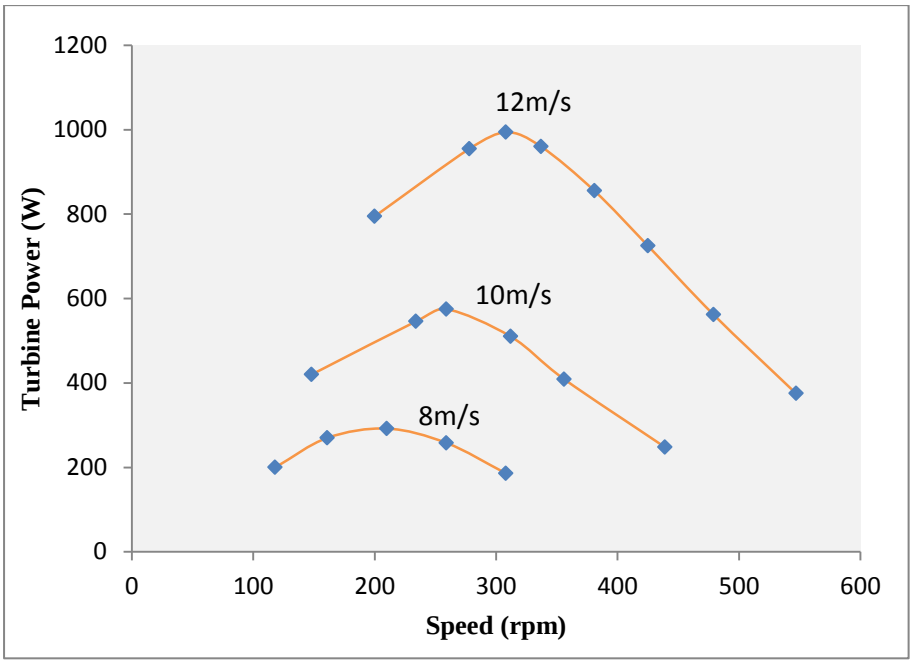

Figure 4-11: Variable speed PMSG WECS Emulator turbine power at different wind speed

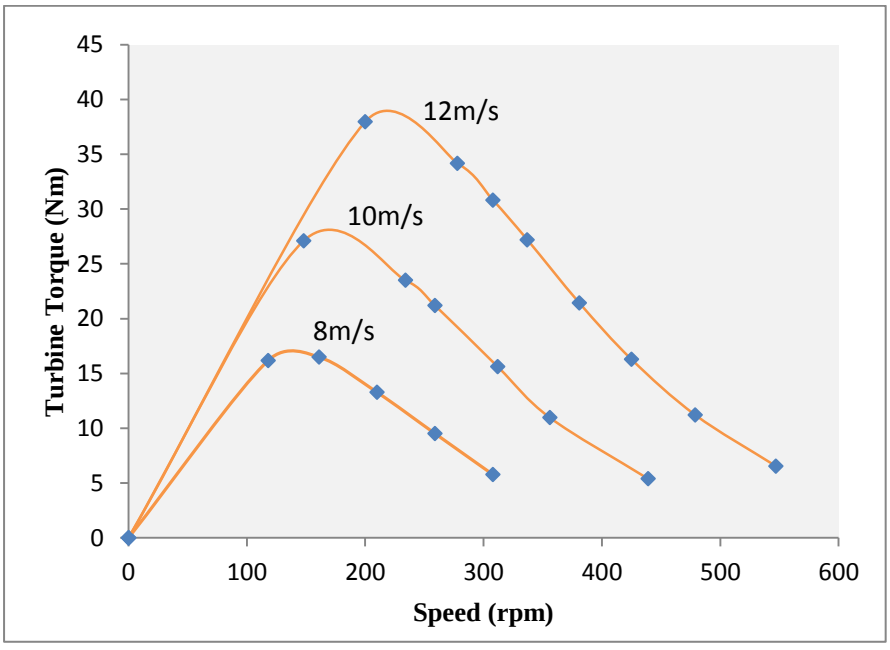

Figure 4-12: Variable speed PMSG WECS Emulator Turbine torque (for turbine only and for Lab.) at 12m/s

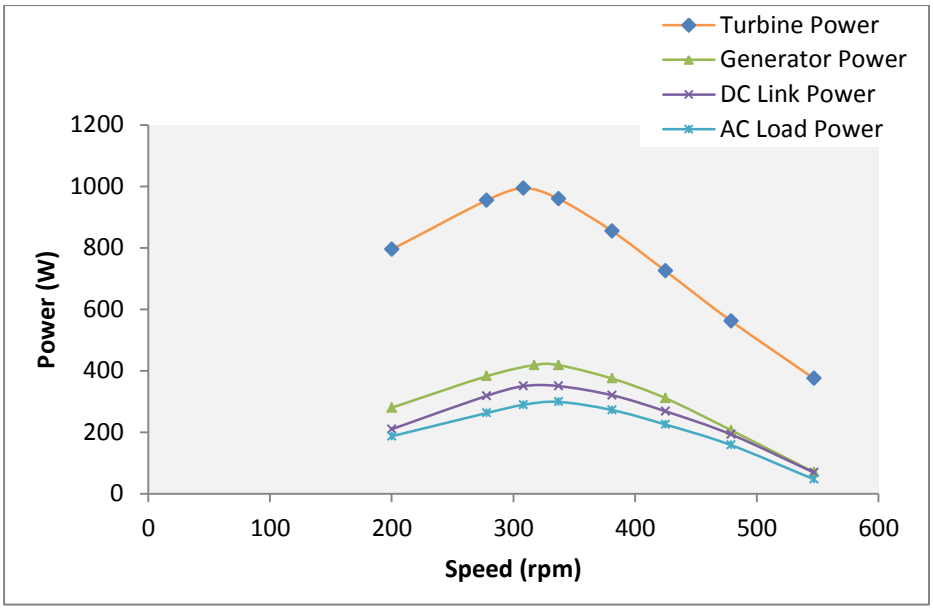

Figure 4-13: Variable speed PMSG WECS Emulator Power transfer from the wind turbine to the AC load at 12m/s

Figure 4-8 shows a screen shot of the three phase experimental current demand to control the rotational speed of the PMSG to 300 rpm for the wind turbine emulator to produce maximum turbine mechanical power of 1kW at 12m/s while Figure 4-9 shows the three phase current demand on the generator at the same 12m/s for the AC load power to have a maximum value of 299W at a rotational speed of 337 rpm. Figure 4-10 shows the three phase current supply to the AC load at which AC load power is maximum during the DC link voltage control at 12m/s. It can be seen that the AC load current is controlled to the reference value generated by the DC link voltage control. The results show that the control technique can generate a fixed frequency AC current at 50Hz to the AC load. In all cases, the actual stator current follows the profile of the current reference in magnitude, in correct sequence and frequency with all the current waveform sinusoidal except when control is lost at higher rotor speed. This validates the performance of the PMSG WECS emulator and control strategy. However, it can be seen that when 20A peak was demanded from the generator and using a current probe of 100mV/A, about 21A peak was actually produced by the generator leading to an error of 1A peak (see figure 4-8). Generally, the performance of the wind turbine emulator and control strategy depends on the accuracy of the feedback signals such as rotor speed and stator currents which also depends on the accuracy of the encoder and current sensors. This difference is consistent in all the recorded parameters and has been noted to be negligible.

The PMSG stator current reference is then varied for the generator torque to track the (Cp/tip speed ratio) curve of the wind turbine emulator and turbine torque, input power, and output power are measured by the torque transducer and 3-phase power analyser, recorded and then plotted against rotor speed. Figure 4-11 shows the turbine power versus speed at different wind speeds over the operating speed range of the generator and Figure 4-12 shows the torque versus speed curve. In Figure 4-11 and Figure 4-12, it is shown that the torque versus speed and power versus speed of the wind turbine have been reproduced by the PM machine emulator. In Figure 4-13, the power transfer characteristics of the PMSG wind energy conversion at 12m/s is shown by the power output at different points measured during the experiments. The results shown validate the correct direction of power flow and transfer from the wind turbine to the AC load by the emulator. From the results, it is observed that the turbine torque reaches a maximum point at a lower speed than the turbine power and the AC load power which is what is expected of a typical WECS. These results confirm the effectiveness of the wind energy conversion emulator and the control techniques. These performance tests are repeated for 8m/s and 10m/s and the results were used to validate the results of the simulation models as shown in chapter 6, section 6.5.4. For the dynamic performance tests of the WECS emulator and control strategy, a variable wind speed as shown in Figure 6.30 (a) was then applied to the WECS emulator and a passive maximum power point tracking control implemented. Maximum power points were recorded at each wind speed as shown in Table 6-2 and Table 6-3. In all the steady state and dynamic performance tests, the stator current, DC link voltage and powers at different points of the PMSG WECS are maintained at the desired values.

The next chapter will present a more detail validation of the steady state performance of the AVEM across the complete operating range of a small fractional horsepower PM motor against both the switching model and an actual PMSM drive laboratory test rig.

Chapter 5 Performance Validation and Analysis of the Average Voltage Estimation Model for a PMSM Drive System

5 Introduction

Two different modelling approaches for a PMSM drive have been outlined in Chapter 3 and the simulation results presented based on operation at full load current over a range of speeds. The results shown in Chapter 3 demonstrate that the proposed AVEM is suitable for the simulation and implementation of a complete PMSM drive system with faster simulation times. This chapter validates the ability of the proposed model to work under dynamic conditions with results being close to alternative methods such as the switching model and laboratory tests.

In a variable speed PMSM drive, the current load demand and the torque produced over a certain speed range is a very important operating performance characteristic. It is important that the newly developed model accuracy be validated against existing standards such as the detailed switching model and experimental results in predicting the very important characteristic; torque versus speed envelope of the PMSM drive system. There are a number of benefits to validate a model, namely to determine; the accuracy, the limit of application, any deficiencies, and any modification that need to be applied. This chapter compares the predictions for the torque/speed characteristics of the PMSM drive system using the proposed average voltage estimation modelling method with the switching modelling method and experimental results over the constant torque and field weakening regions. The details of the experimental setup based on the switching model are discussed in Chapter 4. The chapter also demonstrates the significance of the inclusion of the VSI loss model into the AVEM by the ability of the AVEM to predict power and efficiencies that are comparable with the experimental results over the complete operating range. The scope of the validation of the AVEM is further widened to include analysis of the PMSM drive system power, power losses and efficiencies and compares the simulation results with the experimental results to show its ability to predict power and efficiencies over the constant torque and field weakening regions.

The simulation setup is the same as in section 3.5.2 but the results presented in this chapter are based on different torque/current demands over a speed range of 100 rpm to 550 rpm using the switching model, the proposed AVEM and laboratory test. The PMSM parameters used in the simulation are shown in Appendix A, Table 1. The chapter also presents the benefit that can be derived using the AVEM model by comparing the simulation execution time to the switching modelling method. In the simulation in this chapter, the time step is selected to reflect the requirements of the modelling method. A minimum time step of 100ns was used for the switching model and 30μs for the AVEM.

5.1 Validation and Analysis of Current versus Speed of the PMSM Drive System

In Chapter 3, the performance comparison of the AVEM with the switching modelling in predicting the instantaneous motor phase currents was presented. The simulations at this stage were expanded to include varying operating speed and torque demand from which the steady state performance characteristics of the PMSM using the AVEM could be validated. Generally, in variable speed drives the performance characteristics depend on the applied control technique and the machine performance. Hence it is crucial to validate and analyse the prediction of the PI current control of the PMSM drive system motor currents by the proposed AVEM against the switching model and laboratory testing. In addition, DC link voltage source or battery performance is very important in knowing how to effectively utilise or conserve energy from the battery. While the DC voltage is maintained constant, it is worthwhile to validate the performance of the DC current prediction over the operating range considering the method of calculating DC link current using AVEM model as described by equation 3.55.

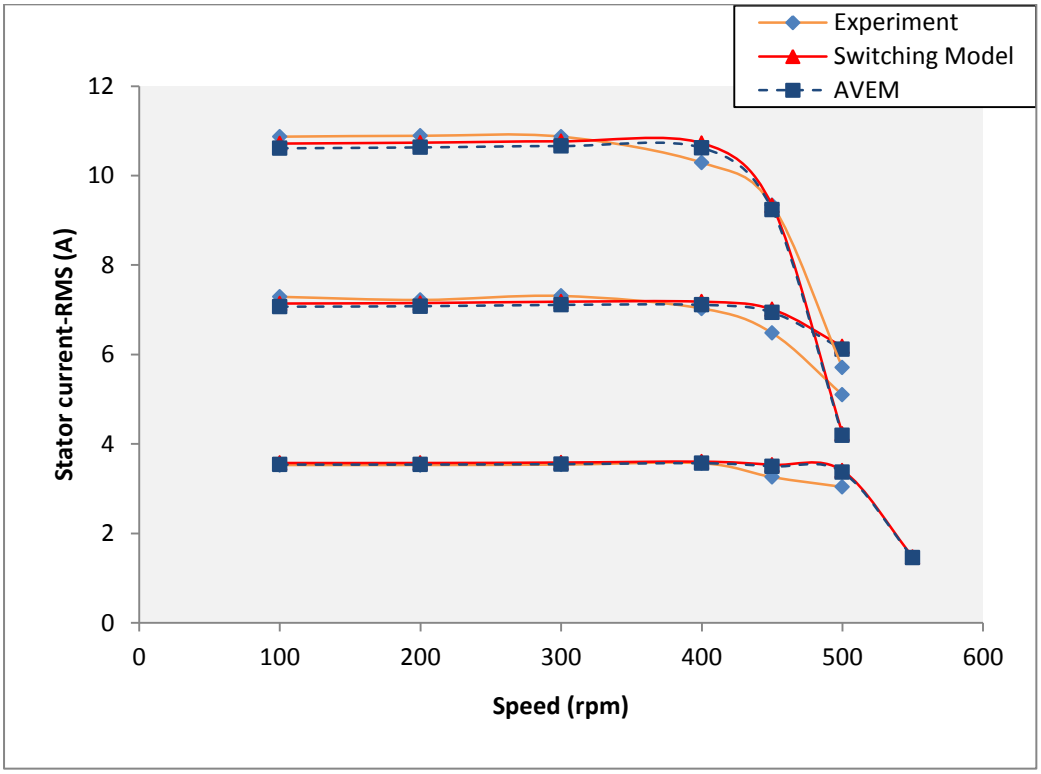

Figure 5-1: Comparison of the PMSM stator current (RMS) for AVEM, switching model and experiments

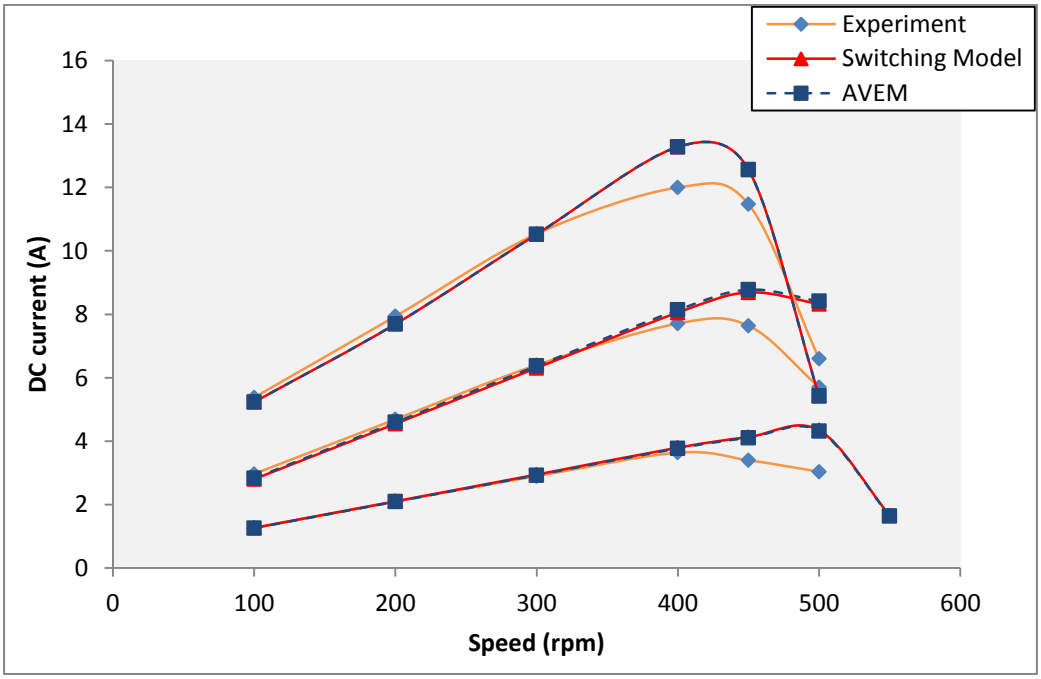

Figure 5-2: Comparison of DC link current for AVEM, switching model and experiments

Figure 5-1 shows the PMSM motor phase currents under PI current control and Figure 5-2 shows the DC current prediction over the operating speed range using the AVEM, switching model and experiment. Comparing the results of the simulation AVEM and switching models and experiment, it can be seen that the results of the AVEM and switching model agree with each other in low and high speed region and are reasonably close to the experimental results especially in the constant torque region in controlling the stator current to its reference value and predicting the DC current. It can also be seen that with the switching model and AVEM, the motor phase currents track the reference over a wider speed range than the test machine. While there is no loss of accuracy between the results of the simulation models, there is some difference in the current prediction between the simulation models and experimental results. The difference is observed to increase as the current reference increases and more significantly in high speed region. The author proposes that this difference is due to the different approach to the loss consideration and calculation between the laboratory test rig and the simulation models and also the Portunus PM machine model. In the experimental test rig, all the loss components are parts of real life equipment while the simulation models, losses are calculated. In addition, the experimental VSI module have all the components of VSI losses embedded in the modules while in the switching model and AVEM, the VSI losses are calculated using loss models developed from manufacture's datasheets and this it is suggested accounts for the difference. In general, it can be seen that in the low speed region the results validate the effectiveness and accuracy of the model, and it is proposed that future work, particularly in the Portunus PM machine model and adequate consideration by the simulation models of losses present in the laboratory test rig system, can further improve the performance in the high speed region. From an engineering perspective the AVEM are acceptable and can be used for predicting the PMSM stator current and DC link current.

5.2 Validation of Torque versus Speed Curves for the PMSM Drive System

In variable speed electric motor drives the torque versus speed curves are important output performance parameters used to evaluate the operating characteristics and applications of the electric motor. It is important to state that each electric motor has its

own particular torque versus speed profile which needs to be investigated before application and operation. This has been the focus in variable speed drive system analysis. Knowing the torque versus speed performance characteristics of any motor is the first step in any successful application and operation of such a motor. It is useful in determining the operating speed and limit of the motor, the type and the limit of the applied load torque, for example the maximum load torque that can be applied to the motor beyond which the motor will either stall or overheat. It is therefore important for simulation model to accurately predict the torque versus speed characteristics of any machine under investigation. For this particular PMSM under investigation, the torque versus speed profile predicted by the proposed AVEM, the switching model and experiment is shown in Figure 5-3.

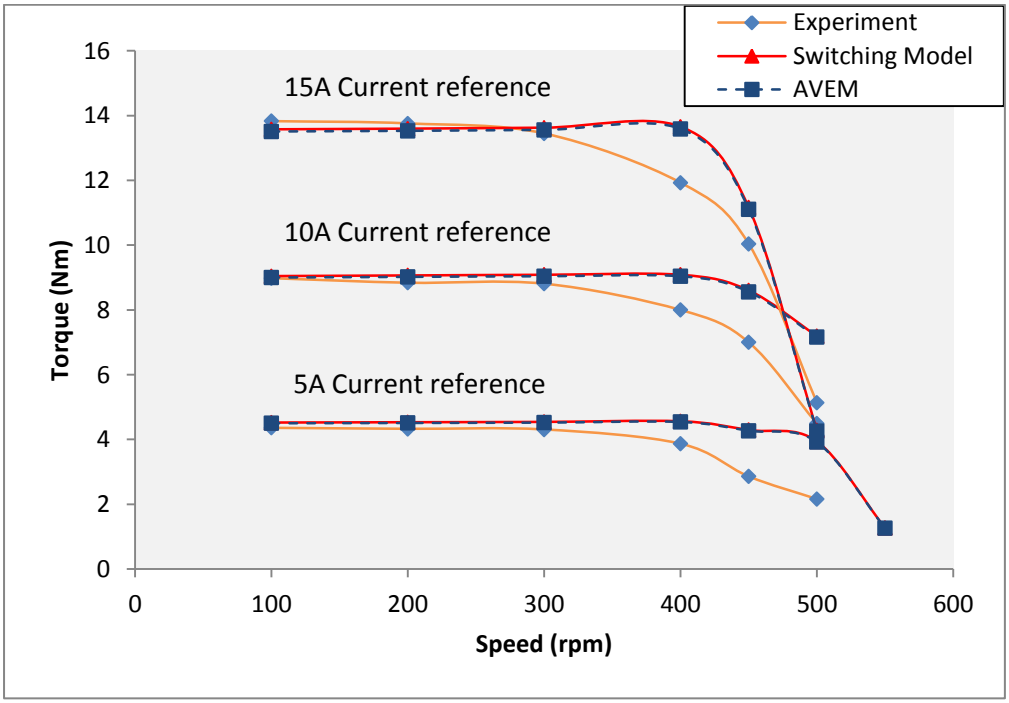

Figure 5-3: Torque-speed characteristics of the PMSM-VSI drive system

Figure 5-3 shows the comparison of the analysis of the torque produced by the AVEM, switching model and experimental test rig at different current reference demand across the complete speed range. It can be seen that the characteristics of the current control is reflected in the PMSM torque output. The torque-speed profile result of the AVEM agrees with that of the switching model over the complete operating speed range and is

very close to the experimental results in constant torque region. It is observed that at higher speed, there is a difference between the results of the simulation models and the experimental results. Generally, the torque speed characteristics of VSI fed PMSM drive systems experiences reduction in torque at speeds above the rated speed. This is because, the speed of the PMSM determines the induced voltage at the terminals of the PMSM and as the speed increases the induced voltage increased beyond the stiff DC link voltage and limits the current that flows into the PMSM which is characterised with diminishing and non-sinusoidal stator phase current away from the reference current as shown in Figure 3-31 and 3-32. However the results shows a sharp decline of the experimental results at higher speed which when compared to the simulation model, makes the prediction of the simulation models seems to overestimate torque at higher operating speed. This of course is largely due to the different approach to the loss consideration and calculation between the simulation models and experimental setup as stated in section 5.1. Another significant factor is the accuracy of the Portunus PM motor model, the improvement of which was outwith the scope of this study but the results have been fed back to the Portunus developers to assist in their future model developments. On general assessment, the results validate the performance and accuracy of the AVEM in predicting the torque versus speed profile of the PMSM drive system. However, the accuracy of the model can further be enhanced especially at higher speed region by giving some more consideration to losses which are embedded in the test rig components, and also improvements to the machine model.

5.3 Field Weakening Analysis

Field weakening is a very important technique in variable speed drive applications and is applied when there is a need to extend the operating speed range of the motor drive. It is important that the AVEM can accurately implement field weakening and is validated against experimental results. There are approaches that can be used to field weaken at higher speed in order to obtain higher torque and expand the operating speed range. One such approach is to use the d-axis current [226][227] and another is to advance the phase angle [228] between the reference current and the relevant motor back emf (note: both these techniques are essentially one and the same thing). In both these techniques the idea is to produce d axis flux which opposes the rotor flux and therefore reduces the

resultant back emf seen at the motor terminals. This in turn reduces the voltage requirements on the inverter to force the motor currents to track the reference and as a result sinusoidal current control is maintained at higher speeds. This section provides results which demonstrate the ability of the proposed AVEM to implement field weakening of PMSM drives at higher operating speeds.

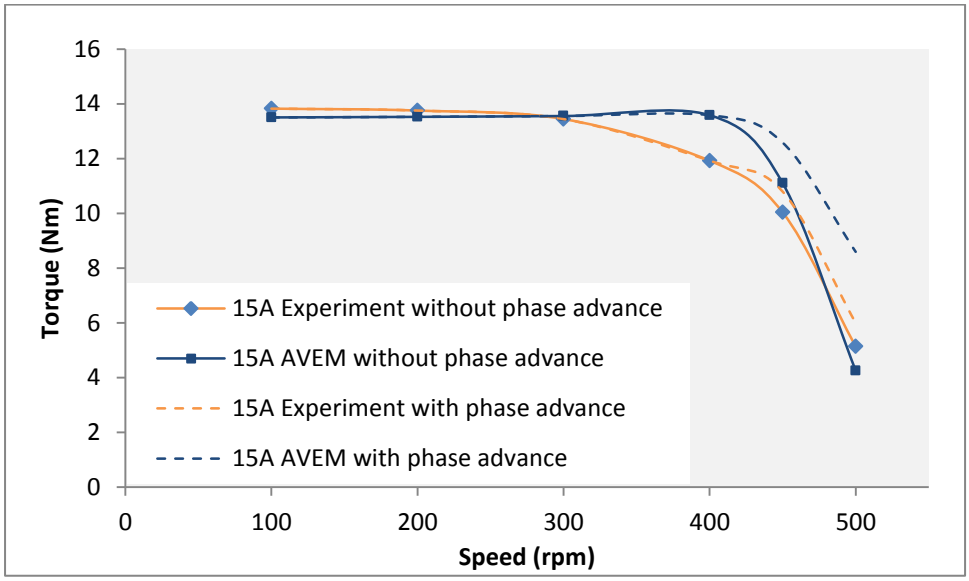

Figure 5-4: Torque-speed characteristics of average voltage estimation model and experiment of VSI- fed PMSM drive system under field weakening at 15A current reference

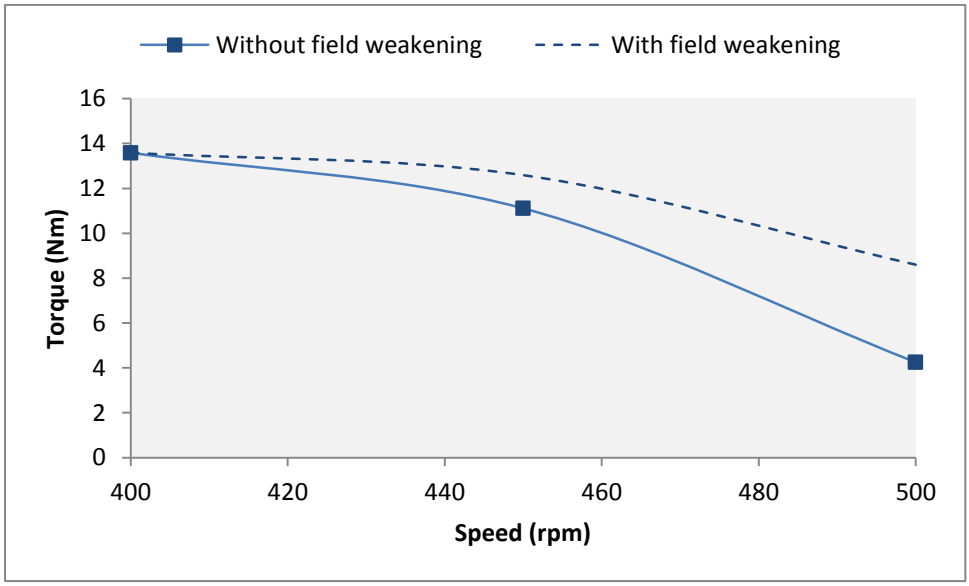

Figure 5-5: Comparison of Torque- speed characteristics with field weakening using AVEM

Figure 5-4 shows how higher torque is achieved and the operating speed of this particular machine under investigation extended using phase angle advance when the PMSM drive system operated at 15A current reference. From the point where current control is lost represented by 400 rpm, shown by the diminishing stator phase current, phase angle advance have been used to achieve higher torque (indicated by dotted lines). Figure 5-5 shows a zoomed section of Figure 5-4 showing field weakening using the average voltage estimation model. It can be seen that the AVEM predicted 13.59Nm at 400 rpm, 11.11Nm at 450 rpm and 4.25Nm at 500 rpm. However, when the phase angle is advanced higher torque up to 12.59Nm was predicted by the AVEM at 450 rpm and 8.6Nm at 500 rpm. The results validate the ability of the AVEM to implement field weakening of the PMSM drive system.

5.4 Power Validation and Analysis of the PMSM Drive System

The key outcome to any simulation model of a variable speed machine drive system is to correctly predict the input power, the losses and output power from which efficiency can be determined. The performance of the system with the AVEM and switching model in predicting power input and output is simulated and analysed and the results validated against experimental results. At constant DC link supply voltage of 57V, the DC power input, the three-phase VSI output power and the mechanical power output are recorded for different rotational speeds. The powers obtained from the AVEM were then compared with the switching model and experimental results.

In a real time PMSM drive test rig, with high performance measuring equipment such as a power analyser, ammeter, voltmeter, torque transducers and position encoder, power can be measured or calculated at different points in the drive system. Generally, the power relation in a variable speed drive utilising input DC power is given by

$$P_m = P_{DC} - P_{inverter\ electrical} - P_{losses} \tag{5.1}$$

Where P_m is the mechanical power output, P_{DC} is the DC input power, $P_{inverter\ electrical}$ is the voltage source inverter output power or power supplied by the voltage source inverter to the terminals of the PMSM and P_{losses} is the VSI losses and machine losses i.e. stator copper loss, iron loss, magnet loss and friction and windage loss. However in

the simulation model, the situation is different especially in the proposed AVEM where the VSI is eliminated. In such a situation, the losses have to be modelled and incorporated into the model. A detailed discussion on the VSI loss model is presented in section 3.3. Since the losses are modelled in the simulation models, a classical approach is used to calculate the DC link power input. The measured electrical power at the terminals of the PMSM drive is added to the VSI inverter losses from the loss model to calculate the DC input power. The resultant powers predicted at different points in the PMSM drive system from the AVEM, the switching model and experimental test rig are plotted as a function of speed.

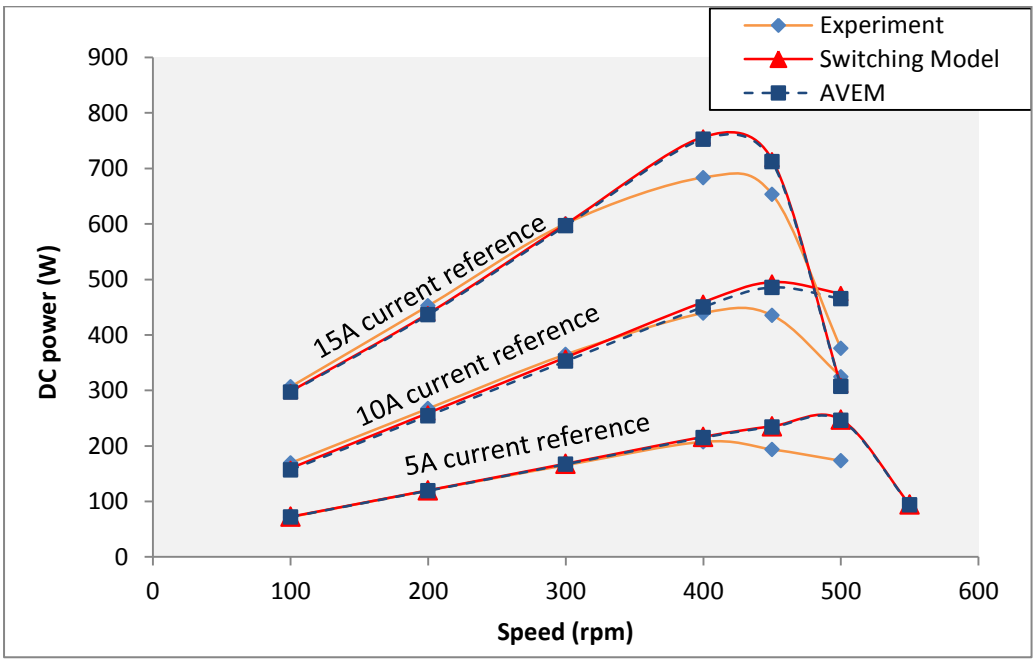

Figure 5-6: Comparison of DC input power using AVEM, switching model and experiments at different current reference

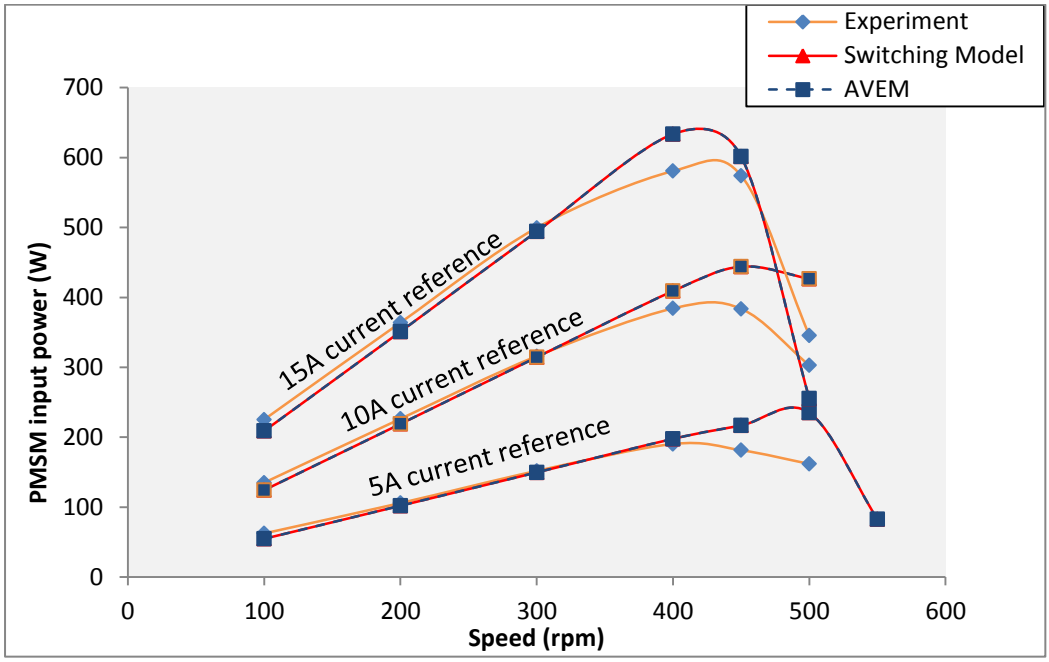

Figure 5-7: Comparison of PMSM input power using AVEM, switching model and experiments at different current reference

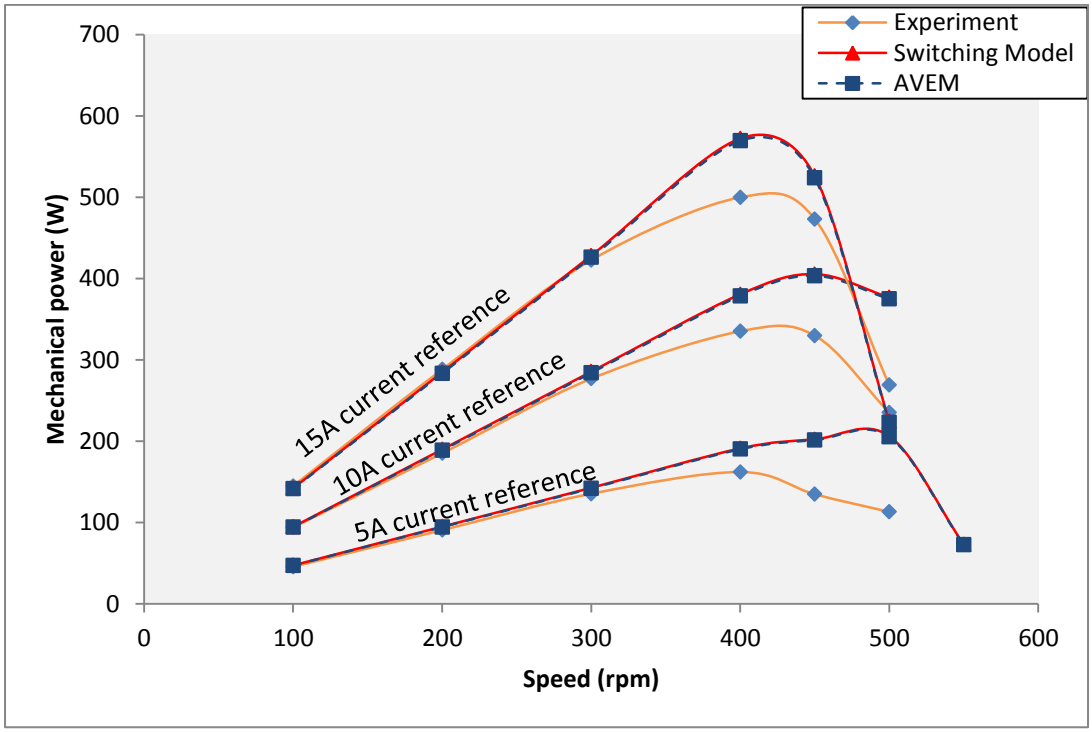

Figure 5-8: Comparison of mechanical output power using AVEM, switching model and experiments at different current reference

Figure 5-6, Figure 5-7 and Figure 5-8 show the validation of the power prediction of the PMSM drive system by the AVEM model, the switching model and experimental results. Figure 5-6 shows the DC input power to the drive system, while Figure 5-7 shows the electrical power at the terminals of the three phases PMSM and Figure 5-8 shows mechanical power output of the PMSM drive system. From the results, the same level of accuracy as demonstrated with current control and torque versus speed is shown between the predicted power of the simulation models and experimental results in the low speed region. It can be seen that the power predicted by the AVEM, the switching model and experiment follow the same profile and increase with an increase in current reference and speed. However, there are some differences between the simulation model and experimental results. The difference again increases as the current reference and speed increases. The simulation models results as shown in Figure 5-6, at low speed region, underestimates the DC link power compared to the experiment results which becomes obvious at high current reference. Contrary to this, at the higher speed region, the simulation model results can be seen to be overestimating the power compared to the experimental results. This difference is largely due to differences in the loss consideration between the experimental setup and simulation models. The results indicates that the simulation models make insufficient consideration of VSI losses and the Portunus PM machine model does not make appropriate consideration to power losses in the higher speed regions. On general assessment, from the design point of view, the results validate the accuracy of the AVEM to predict the powers versus rotor speed profile of the PMSM drive system under investigation similar to that of the experiment results and can be used for the analyses of electrical machine drive power, losses and efficiencies. However, appropriate consideration of the VSI and motor losses should be made in the simulation models to further enhance their performance.

5.5 Efficiency Validation and Analysis of the PMSM Drives System

The efficiency analysis is a significant aspect of the drive design process which determines effective utilisation of input power from the source and the power available to the mechanical load at various speeds. It is therefore necessary to validate any new simulation model's ability to be used to study and analyse the efficiency and losses of the

electric motor drive system. It is clear that not all the power supplied to the drive system gets to the mechanical load, some of the power is lost in the system. The power losses are dominant in the inverter and the motor, hence accurate prediction of losses is an important tool to efficiency analysis. Power losses can be analysed by computing the difference between the input power and the output power while efficiency is the ratio of the power output to the power input. This computation can be made for the inverter, motor and the overall system. This section presents validation of efficiencies and losses between the AVEM and the experimental results considering that the results shown from section 5.1 to 5.4 already confirms that the AVEM predict results similar to the switching modelling method.

5.5.1 Validation and Analysis of the Voltage Source Inverter Losses and Efficiency

The VSI efficiency is calculated at each current reference by comparing the inverter output power to the DC link input power and the losses determined by the difference between the inverter output power and the DC link power. With the proposed AVEM model where the VSI is eliminated, the loss model described in section 3.3 is incorporated into the model to effectively analyse power and efficiency using AVEM. Since the losses in the simulation models are modelled, a classical approach is used to analysis the efficiency. The measured electrical power at the terminals of the PMSM drive is added to the VSI inverter losses from the loss model to calculate the DC input power and the inverter efficiency is analysed. The VSI efficiency at various current references predicted by the AVEM and experiment were plotted as shown in Figure 5-9 – Figure 5-11.

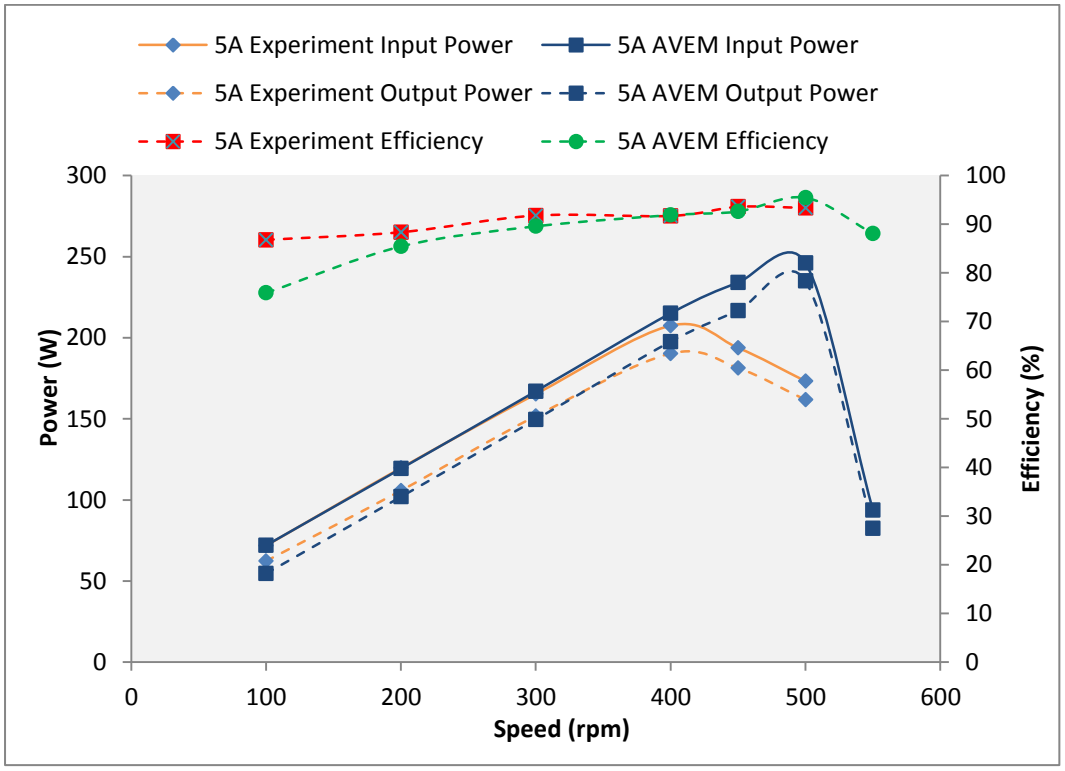

Figure 5-9: Comparison of VSI Losses and Efficiency of by AVEM and experiment at 5A current reference

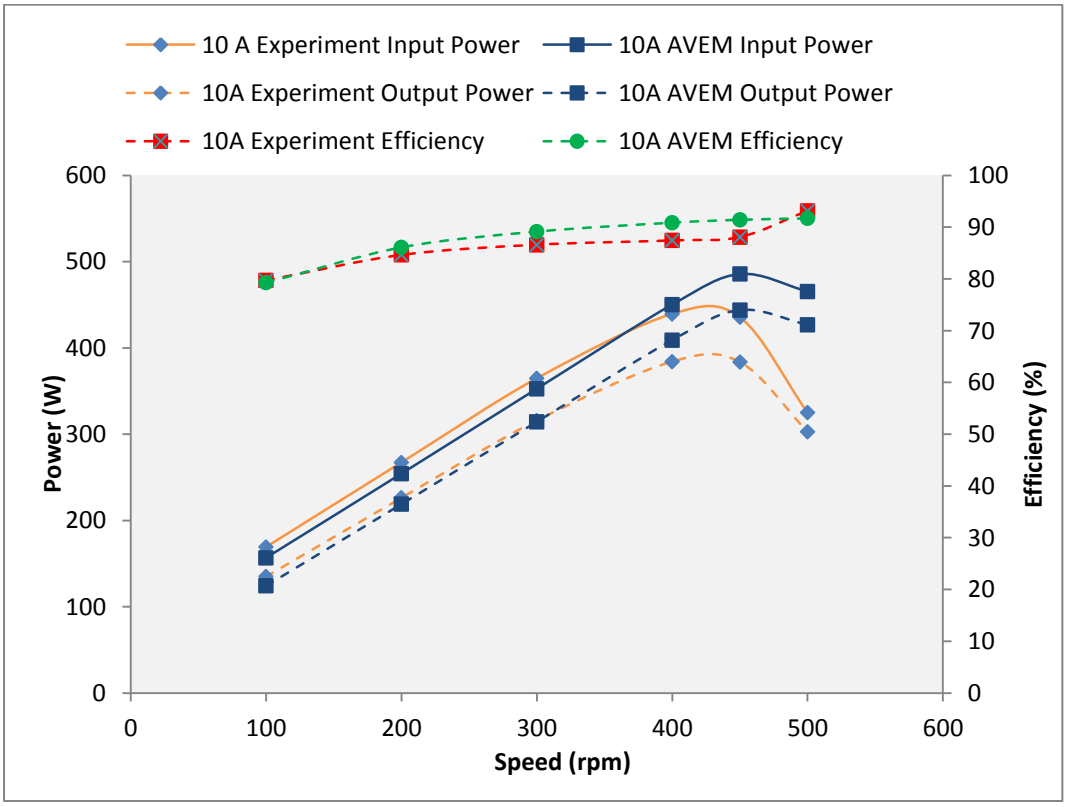

Figure 5-10: Comparison of VSI Losses and Efficiency by AVEM and experiment at 10A current reference

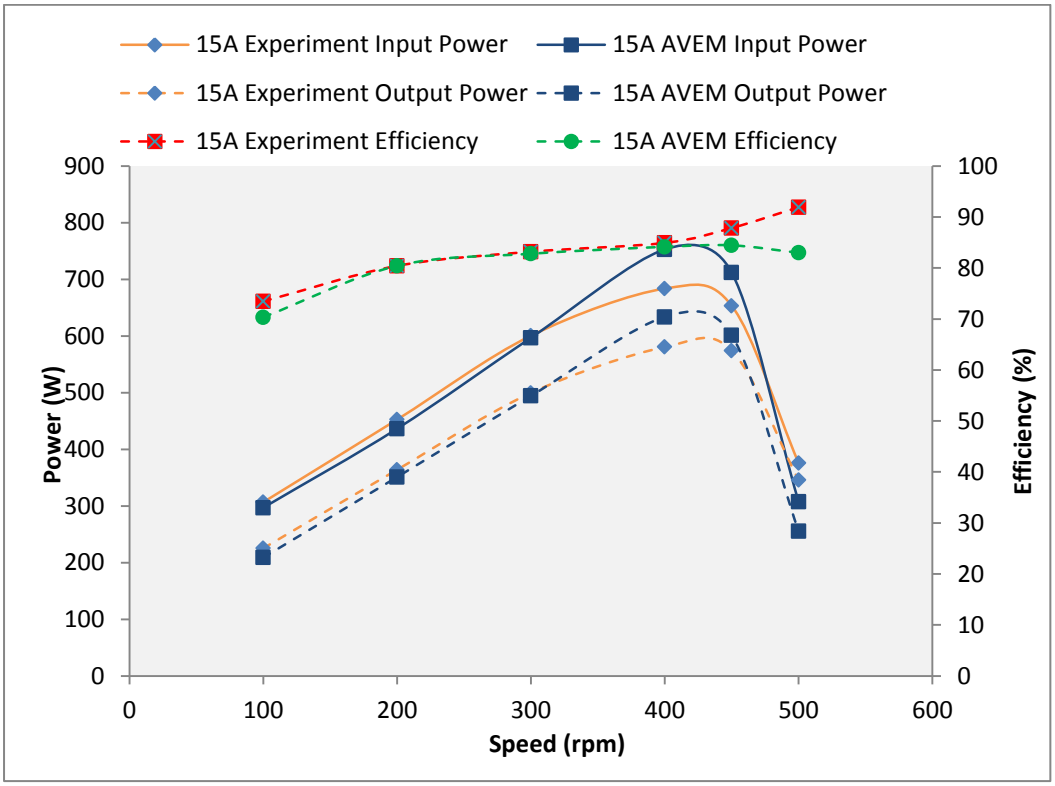

Figure 5-11: Comparison of VSI Losses and Efficiency by AVEM and experiment at 15A current reference

Figure 5-9 – Figure 5-11 show the voltage source inverter efficiency and by extension the VSI losses predicted by the AVEM and experimental results at different reference currents over the speed range. It can be seen that the efficiency and losses predicted by the AVEM follow the same distribution against speed as that of the experiment both at low current reference and higher current reference especially in the low speed region. From these results the same trend is exhibited by both the AVEM and the experimental results on VSI losses with regards to changes in the current reference. The VSI losses increases with increase in current reference, for example, at 5A current reference, the maximum VSI losses predicted by the AVEM is 18W and that of the test data is 17W while at 15A current reference, the maximum VSI losses using AVEM is 118W and that of the experiment is 103W. It can be seen that the accuracy of the efficiency prediction by AVEM improves as the current reference increase. Comparing the prediction of the AVEM and experimental results in terms of loss consideration, the AVEM needs to give more consideration to VSI losses to further enhance its accuracy.

5.5.2 Validation and Analysis of the PMSM Losses and Efficiency

Variable speed drives convert electrical power into mechanical power which is a function of the generated torque and the operating speed. The efficiency on how the electrical power is utilised to obtain mechanical power output depends on the losses present in the electric motor. This section validates and compares the PMSM losses and efficiency predicted by the AVEM with the experimental results.

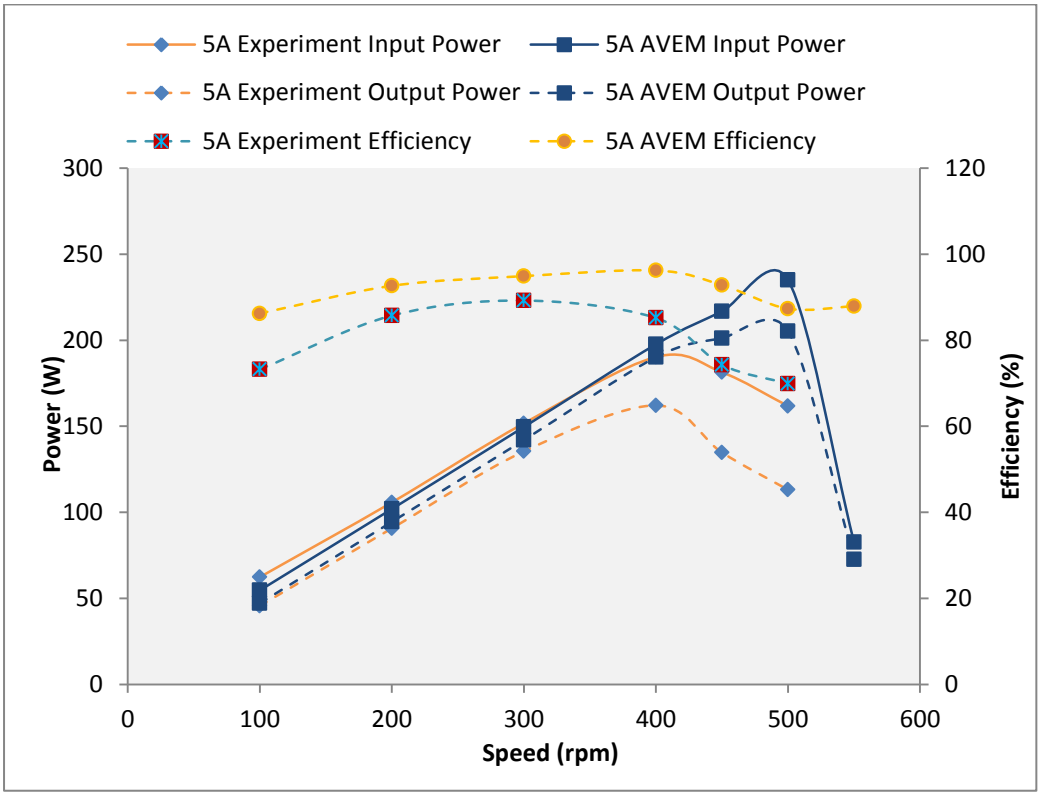

Figure 5-12: Comparison of PMSM Losses and Efficiency by AVEM and experiment at 5A current reference

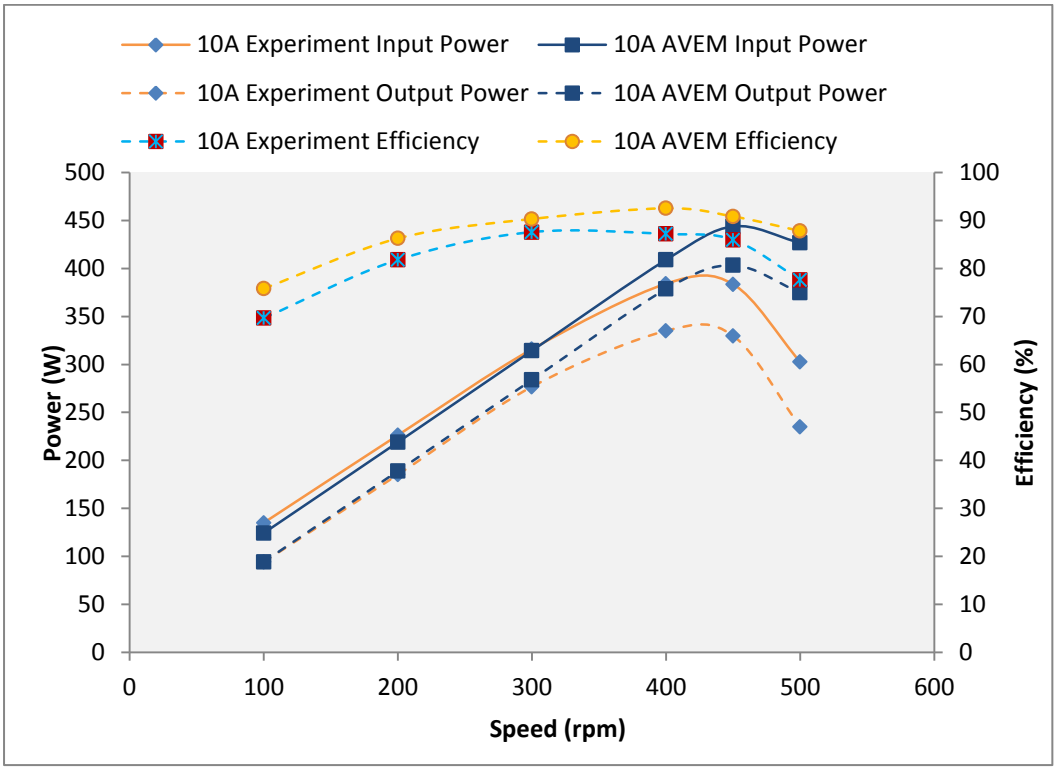

Figure 5-13: Comparison of PMSM Losses and Efficiency by AVEM and experiment at 10A current reference

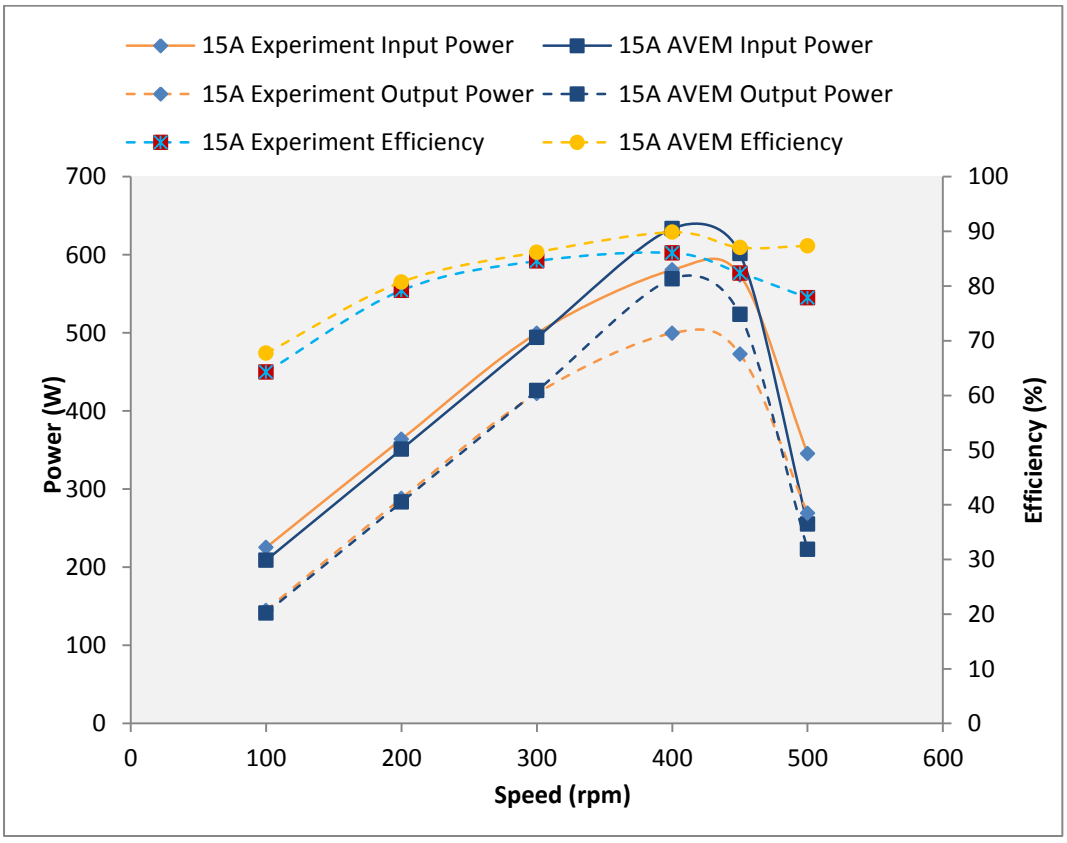

Figure 5-14: Comparison of PMSM Losses and Efficiency by AVEM and experiment at 15A current reference

Figure 5-12 – Figure 5-14 show the comparison of the PMSM losses and efficiency predicted by using the AVEM and experimental results at different reference currents over the speed range. It can be seen that the efficiency and losses predicted by the AVEM follow the same trend as that obtained with the VSI losses and efficiency seen by the same distribution of the losses and efficiency curve of the AVEM and experimental results in the low speed (constant torque) region. Again the PMSM losses increase with increase in current reference with better predicted accuracy at higher current reference. The poor prediction of the PMSM efficiency at low current reference compared to experimental results is due to the underestimation of the mechanical output through the underestimation of the torque as shown in Figure 5-3. However comparing the prediction of the AVEM and experimental results, the results validate the accuracy of the AVEM in predicting the profile of the efficiencies and losses of the PMSM drive system.

5.5.3 The PMSM Drive System Efficiency

The PMSM drive systems overall efficiency and losses based on DC link input power and mechanical output power predicted by the AVEM and experiment are potted against the operating speed as shown in Figure 5-15 – Figure 5-17.

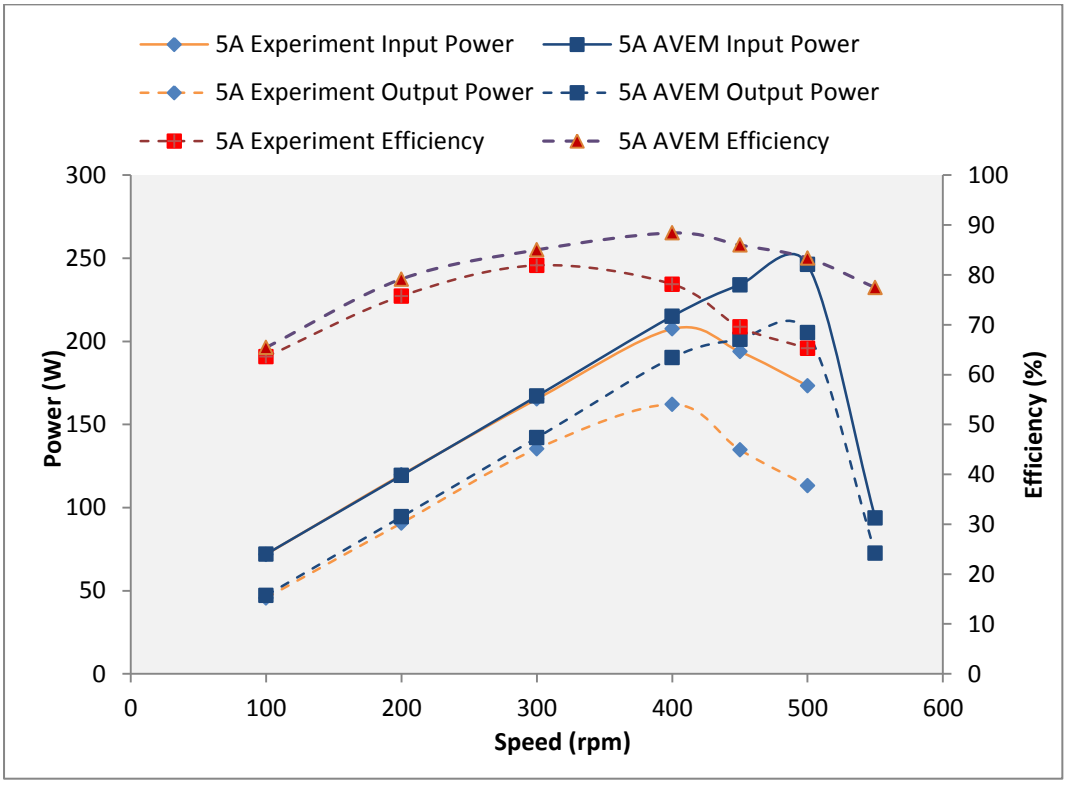

Figure 5-15: Comparison of the PMSM drive Losses and Efficiency by AVEM and experiment at 5A current reference

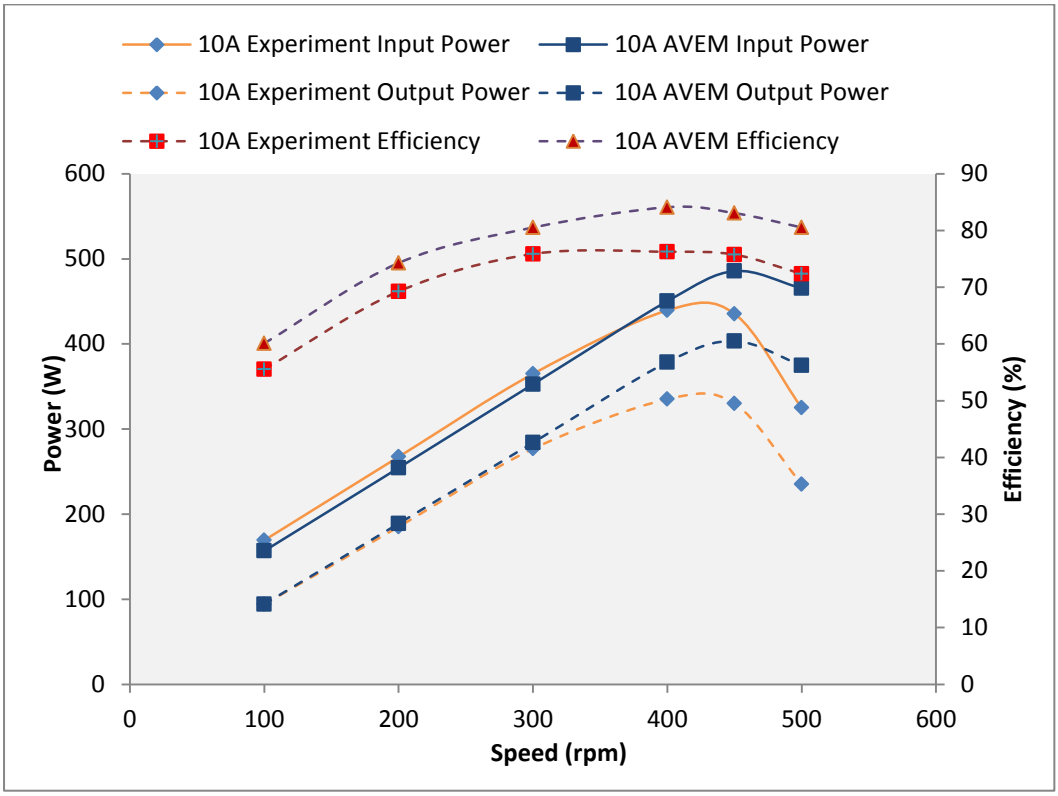

Figure 5-16: Comparison of the PMSM drive Losses and Efficiency by AVEM and experiment at 10A current reference

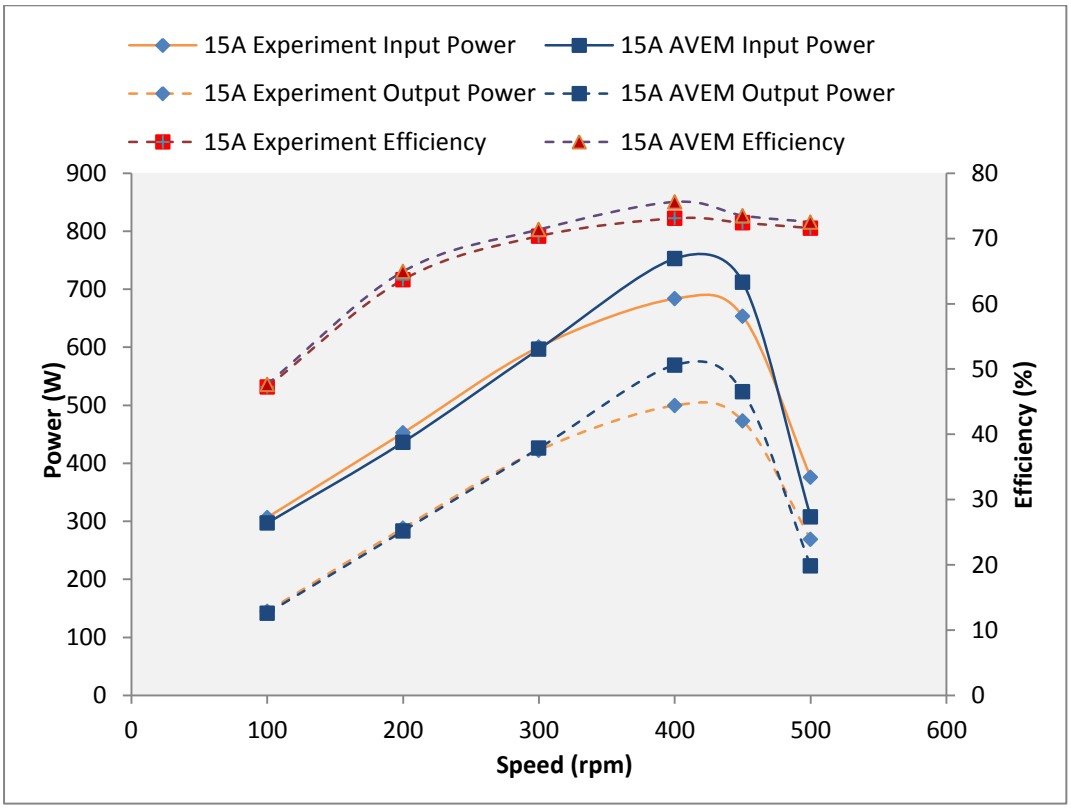

Figure 5-17: Comparison of the PMSM drive Losses and Efficiency by AVEM and experiment at 15A current reference

Figure 5-15 – Figure 5-17 shows the losses and efficiency of the PMSM drive system predicted using the AVEM and the experimental results. The curve of the efficiency and the losses predicted over the speed range by the AVEM is similar in shape to the experimental results. The losses are also seen to increase with the current reference. The differences in the numerical value of the losses and efficiency predicted between the AVEM and experiment is due to the differences in the power predicted at each level of operation. However, from the engineering point of view, the AVEM have shown promise in predicting the performance characteristics and quantities of a typical electric motor drive system.

5.6 Comparison of Simulation Execution Time

In all the simulations in this chapter, the simulation step sizes were chosen to reflect the requirements of each method. The limiting factor of the Average Voltage Estimation method is the minimum step size, which is restricted here to less than the PI loop run time of 50μs on a typical real-life DSP. For the PWM switching model, the limiting factor is minimum step size, which is set to the resolution of the PWM duty cycle, typically <1000th of the PWM switching period.

Table 5-1: Comparison of simulation completion time between switching model and AVEM

Models	Minimium time step (s)	Maximium time step (s)	Simulation set time (s)	Time taken to complete simulation
Switching model	$100e^{-9}$	$1e^{-3}$	0.5	2.5 hours
AVEM	$30e^{-6}$	$1e^{-3}$	0.5	3 minutes
AVEM	$40e^{-6}$	$1e^{-3}$	0.5	2 minutes

Table 5-1 shows the comparison of the simulation completion time between the switching model and AVEM model. It can be seen that with the simulation set time of 0.5s, completion time for the switching model with a time step of 100ns is 2.5 hours while the simulation completion time for the AVEM with freedom of time step 30μs is 3 minutes and 40μs is 2 minutes which is **50 to 70** times faster than the switching model.

5.7 Conclusion

A comprehensive validation of the AVEM model has been presented in this chapter including all aspects of steady state performance analysis of PMSM drive systems ranging from current control prediction to efficiencies. The chapter begins with the validation of both the stator current and DC current reemphasising the ability of the AVEM to implement PI current control. Further to this the chapter also presented the very important characteristic of adjustable speed drive; the torque versus speed curve. The torque versus speed profile of the PMSM under investigation was adequately validated against the corresponding switching model and experimental results and the AVEM shows a reasonable degree of accuracy.

The chapter also considered the implementation of field weakening of the PMSM drive using the proposed average voltage estimation model. In addition to this the chapter also demonstrates the benefits that can be derived with the inclusion of the VSI model into the AVEM, which enables the actual power flow to be accurately determined and compared with existing standard models such as the switching model and experimental results. The chapter extended the scope of validation to include input power, VSI output power, mechanical output power and efficiency. Adequate analysis of the simulation results and experimental results are presented stating the level of accuracies and differences which are predominantly occurring at higher speed with reasons given where there is difference and methods to enhance the performance of the simulation models suggested. The last part of the chapter which deals with the most significant benefit of the AVEM is the comparison of the simulation execution time. The models were simulated based on the time step requirements of simulation models and the AVEM is found to be **50 to 70** times faster than the switching model. The results show a good agreement between the AVEM, the switching model and experimental results and the AVEM demonstrates itself to be capable of significantly reducing the simulation time. It is hoped that this average voltage model will be adopted as an alternative model in the PM motor drive design process.

The next chapter will present an expansion and development of the proposed average voltage estimation model for a full scale back-back VSI in variable speed PMSG wind turbine systems applications.

Chapter 6 Development of an Average Voltage Estimation Model for a Full Power Electronic Converter based Permanent Magnet Synchronous Generator in a Wind Power Application

6 Introduction

Wind energy conversion systems utilising PMSG with back-back VSI are an attractive addition to renewable energy conversion systems in recent times. They are used for small power systems providing off-grid electricity for rural remote areas, as well as connection to the grid. Recently, development of PMSG WECS have advanced with increasing complexity and power capability leading to extensive research in novel wind power generation systems. Current research and development is focussed on cost effective methods of harnessing wind energy in several locations such as onshore, offshore and remote locations. In addition, the whole concept of wind energy conversion systems is also changing; generators are now designed with multiple phases, multilevel voltage source converters and in a more advance form, the emergence of modular multilevel voltage source inverter are attracting serious research interests. These modifications are geared towards achieving higher voltage level, higher power level and high efficiency. As the topologies become more and more complex with increasing numbers of power electronic devices (e.g. IGBTs), it become more important to simulate the behaviour of the WECS and control strategy under various conditions in order to develop an efficient WECS and control strategy. The simulation execution times under this circumstance will become significantly longer due to the large number of power electronic devices involved and the effect of the simulation small step time requirement of the PWM resolution for accuracy. One of the key models among the simulation models needed for the WECS is the back-back voltage source converter model. From the simulation point of view, this model can be simplified without necessarily having to include the VSCs. Hence for small, large and complex WECS, it requires a more simplified model which can enhance rapid and fast development of cost effective and efficient WECS and control strategies. The most important factor to consider is to incorporate the dynamics of the PMSG, control strategy and load into the model and it should be used to analyse within a short time scale different design changes.

The average voltage estimation modelling of voltage source inverters has been investigated and validated for PMSM drive systems in the previous chapter. It has been shown that the AVEM model is a faster method of simulating VSI in variable speed PMSM drive systems. This modelling approach which was further developed by the author for a generalised variable speed PMSG drive system [229] is expanded and its application can be extended to the simulation and analysis of variable speed PMSG wind energy conversion systems with three phase full scale back-back voltage source converters. This chapter presents one of the major contributions of this research, the development and implementation of average voltage estimation model of a three-phase back-to-back VSI fed variable speed wind turbine permanent magnet generator. It is indeed unique because average voltage estimation model of this kind is harder to find in literature. Most of the previous efforts of average value models are developed for either AC/DC or DC/AC based on fixed value DC voltage or DC link rectified voltage dedicated to motor drive or DC/AC grid connected systems. However, this can be extended to back-back VSI but can be computationally intensive and time consuming to do that. Dealing again with variable speed voltage sources e.g. wind, ocean etc., which implies variable rectified DC link voltage becomes challenging and requires a lots of knowledge to arrive at a final model that will be feasible for the study of the behaviour and characteristics of the conversion system. Therefore, a simple model of WECS based on average voltage estimation in one switching period is much faster than the switching model and requires less to model. Initially, the detailed switching model of back-back VSI with variable speed PMSG wind energy conversion system will be developed to show the switching functions and then the development of the AVEM with PMSG wind energy conversion system to compare the simplifications and the benefit in terms of simulation execution times.

6.1 Detailed Switching Model of Full Scale Back-Back Voltage Source Inverter with PMSG Wind Energy Conversion System

The block diagram shown in Figure 6-1 describes a detailed back-back voltage source inverter switching model of the variable speed PMSG wind turbine. As a configuration suitable for small scale standalone wind energy conversion systems, the variable speed

multiple pole PMSG is directly driven by a fixed pitch low power wind turbine and connected to an AC load through a two level three-phase back-back voltage source converter (VSC). The back-back VSC consists of the three-phase AC/DC voltage source converter (VSC) at the generator side and the same configuration of three phase DC/AC voltage source inverter (VSI) at the AC load side. The generator side converters is connected to the AC load side inverters through a capacitor which serves as a storage device, filters voltage ripple and a point of isolation between the generator frequency and the load side frequency. This configuration can be modified to include a transformer at the AC load side when higher voltage is needed to integrate to grid.

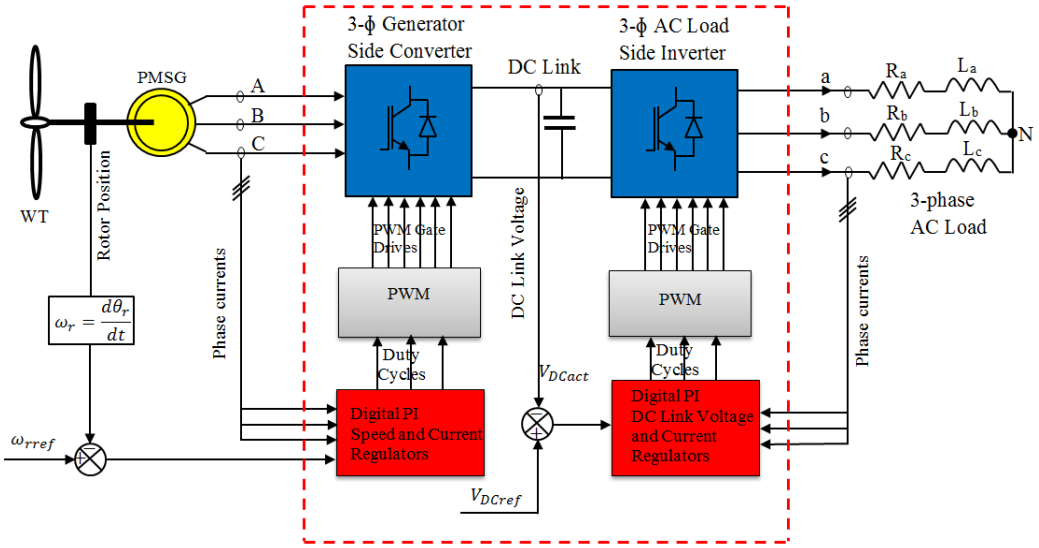

Figure 6-1: Block diagram of two level back-to-back PWM voltage source converters switching with variable speed PMSG wind energy conversion system

Compared with the configuration shown in Figure 3-1, the number of power electronic devices is now increased to a total of 12 power electronic PWM converter switches and 12 antiparallel diodes (6 at the generator side and 6 at the load side) as shown in Figure 6-2, where both the generator side VSC and the AC load side use PWM controlled IGBT switches. With the increased number of power switches and diodes, the simulation execution times due to switching behaviour of the power electronic PWM converters will become even longer due to the multiplier effect of the small step time of the PWM resolution requirement for accuracy. However, under the action of the control strategy, the generator side converts and processes variable frequency AC voltage to DC voltage while the AC load side converts and processes DC voltage to fixed frequency AC

voltage. The controller at the generator side and the AC load side depends on the choice of control parameters. In a wind energy conversion system, the aim of the control is to track as much power from the wind and delivered a constant frequency power to the load/grid. In order to achieve MPPT and DC link voltage regulation as the wind speed changes, the generator side converter is designed to control the wind turbine and generator speed to track maximum power at low speed and limit over power at high speed, while the AC load side converter matches the output power from the generator to the load by maintaining a constant DC link voltage. This enables a fixed frequency and fixed voltage to be supplied to the AC load.

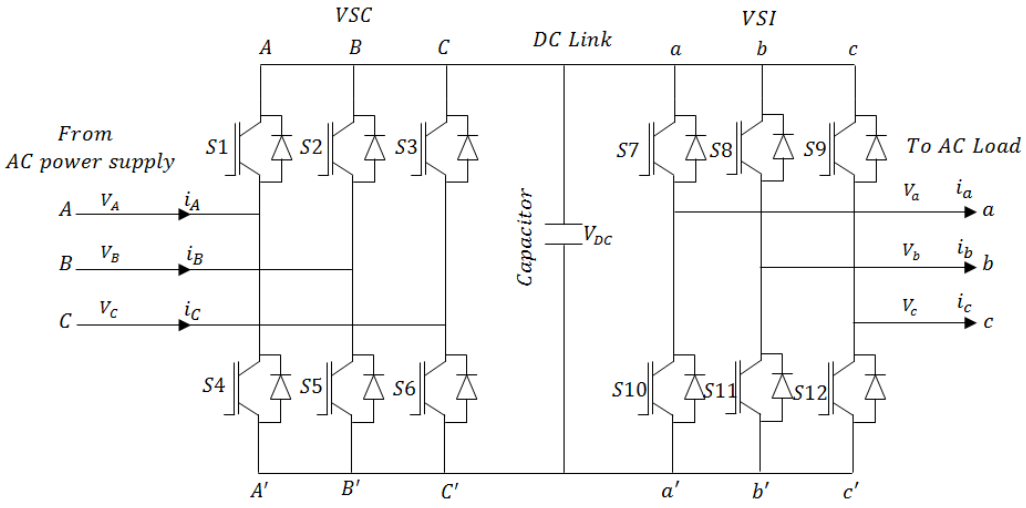

Figure 6-2: Circuit configuration of two level full scale back-back voltage source converters

From Figure 6-2, it can be seen that the generator side AC/DC converter has three phase input voltages defined as V_A, V_B, V_C which are converted to a DC voltage V_{DC} which serves as the input voltage to the AC load side DC/AC voltage source inverters. The AC load side inverter produces three phase output voltages given as V_a, V_b, V_c at the terminals of the three phase AC load. For the conversion to take place, the two complementary power electronic switches in each phase leg operate in switch mode i.e. when the upper switch on one phase leg is ON, the lower switch on the same phase leg is OFF and vice versa given by

$$S_i = \begin{cases} 1 \text{ upper switch ON} \\ 0 \text{ lower switch ON} \end{cases}$$

Where, the subscript i represent phase A, B, and C.

For the switches to operate this way, a suitable control strategy is required. The sinusoidal Pulse Width Modulation (SPWM) control is applied to generate the switching signals for each leg of the converters as described in section 3.1, therefore the three phase voltages at the generator terminals are given as a factor of DC link voltage and switching function as

$$V_A = \frac{V_{DC}}{3}(2S_A - S_B - S_C) \tag{6.1}$$

$$V_B = \frac{V_{DC}}{3}(-S_A + 2S_B - S_C) \tag{6.2}$$

$$V_C = \frac{V_{DC}}{3}(-S_A - S_B + 2S_C) \tag{6.3}$$

Where V_{DC} is the DC link voltage, S_A, S_B and S_C are the switching function when the upper switch in each phase leg of the generator side converters is on.

In a similar way, the three phase output voltages from the AC load side inverter can be expressed as a function of the DC link voltage and switching signals. From Figure 6-2, the circuit configuration of the load side inverters is the same as the generator side converters; the different is the mode of conversion. During the switching of the power converter switches as a result of the load side controller, the three phase voltages established at the terminals the three phase AC load given can be given by

$$V_a = \frac{V_{DC}}{3}(2S_a - S_b - S_c) \tag{6.4}$$

$$V_b = \frac{V_{DC}}{3}(-S_a + 2S_b - S_c) \tag{6.5}$$

$$V_c = \frac{V_{DC}}{3}(-S_a - S_b + 2S_c) \tag{6.6}$$

Where $S_a, S_b \; and \; S_c$ are switching functions when the upper switch in each phase leg of the AC load side inverters is ON.

6.2 Average Voltage Estimation Modelling of Back-Back VSI with Variable Speed PMSG Wind Energy Conversion System

In a cost-effective design process and analysis of variable speed PMSG and control system, the requirement is to deliver to the customer or market within the shortest possible time, and therefore the long simulation time is unacceptable. In view of this, an alternative average voltage estimation model of voltage source inverter that can be rapidly and accurately simulated and used in place of the detailed VSI switching model with variable speed PMSG is proposed. Figure 6-3 shows the configuration of the developed average voltage estimation model of VSI for a variable speed PMSG wind energy conversion system. It consists of the wind turbine, the PMSG, the generator side and AC load side controllers identical to the VSI switching model but compared with the detailed switching model shown in Figure 6-2, the three-phase back-back converters (VSI) and DC link capacitor are totally replaced with two-three-phase average voltage estimation functions and voltage sources, one at the generator side and another at the AC load side. In between the generator side and the load side average voltage models is a 'Virtual' DC link the voltage of which is estimated by the model.

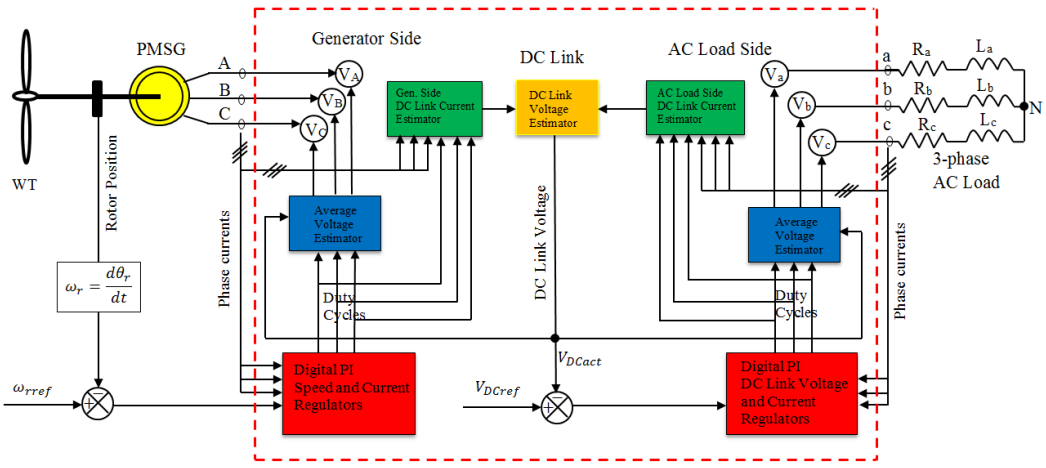

Figure 6-3: Average Voltage Estimation Model of back-back voltage source inverters with PMSG wind energy conversion system

In general, the average voltage estimation model of a full scale VSI with variable speed PMSG is developed based on the control strategy and the switching function of the VSI.

The average voltage estimation model (AVEM) of a full scale back-back VSI with variable speed PMSG wind energy conversion system similar to the detailed switching model, consists of two models, the generator side AVEM and the AC side AVEM. The generator side AVEM controls the speed of the generator and wind turbine to track maximum power below rated wind speed and limit power above rated speed while the AC load side AVEM ensures that the DC link voltage is constant in order to generate a fixed voltage and frequency to the AC load/grid. The generator side model depends on the duty cycles from the generator side controller while the AC load side model uses duty cycles from the AC load side controller. The control strategy is based on the principles of the SPWM, however instead of using PWM as in the case with the switching model, the reference sinusoidal waveform is compared with the measured sinusoidal value to generate the duty cycles and the AVEM uses the duty cycles to estimate the average phase voltage in each switching period.

6.2.1 Generator Side Average Voltage Estimation Model (AVEM) of AC/DC Voltage Source Converters

The AVEM for the PMSM drive has been described and developed in Chapter 3 and is the same as the AVEM for the PMSG side converter. As can be seen Figure 6-3, the configuration of the generator side AVEM same as the AVEM of PMSM drive shown in Figure 3-14 (b), the only difference is the mode of operation and the control parameters used to generate the duty cycles and the addition of the wind turbine. While the PMSM drive converts electrical power to mechanical power, the PMSG drive converts mechanical power (in this case from a wind turbine) to electrical power. In order to realise generating mode, the simple approach to this is to ensure that the reference current is at 180^0 out of phase with the back EMF and in the simulation model, this can be achieved by changing the polarity of the reference current. For the duty cycles, they are generated from the generator side control strategy which can be from current control, voltage control and MPPT control techniques.

6.2.2 AC load Side Average Voltage Estimation Model of DC/AC Voltage Source Inverters

Since in most cases the objective of the AC load/grid side is to maintain a constant DC link voltage, the AC load/grid side AVEM is developed to perform the same function of maintaining a constant DC link voltage. Therefore, the inputs to the AC load side AVEM are the duty cycles from the DC link voltage controller. It is important to state that though the AVEM was first developed for three phase PMSM drive system as described in section 3.2, it can be applied to any three phase system. With this being the case, the AVEM is applied to replace the three phase VSI at the AC load/grid side. However, modifications are made to apply the model to the AC load/grid side inverter. The duty cycles for the estimation of the AC load side is generated based on the control of the DC link voltage and this requires measurement of the AC load side currents which is different from that of the generator side. For the purpose of clarity, it is important to state that the designation used for the terminals of the AC load phases are: a, b, c and the three-phase AC load current as $i_a, i_b and\ i_c$.

6.3 Modelling of the DC Link Voltage

In section 3.2, the developed average voltage estimation model considers a constant DC link voltage which can be achieved from a battery source or a constant frequency rectified DC voltage and a value can be used for DC voltage in simulation. In the case of variable speed PMSG, as the speed varies the DC link voltage varies as speed varies and the control is required to ensure its maintained constant even when the wind speed varies. Therefore, modelling the DC link voltage is important in order to implement the generator and AC load side AVEM. The DC link model provides the required value of the DC link voltage and also establishes a 'Virtual' connection between the variable speed generator output and AC load/grid. The DC link voltage model is built based on the generator side DC link current and the AC load side DC link current as well as the DC link capacitance value. Whereas the generator side and the AC load side DC link current in the detailed switching model can be measured by simply using an ammeter, the DC Link current from the generator side and to the AC load side of the average voltage estimation model are calculated by the model.

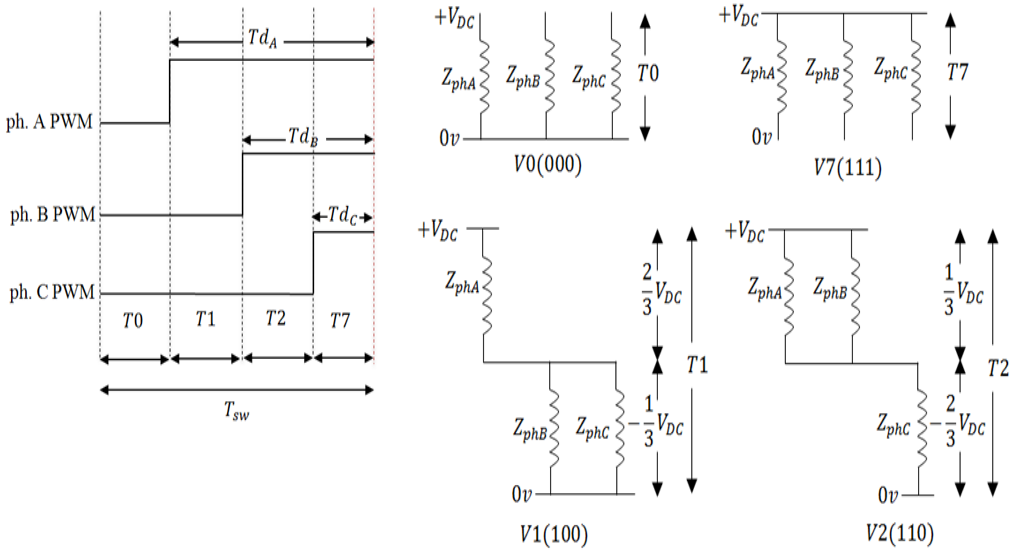

Figure 6-4: Commanded PWM output and equivalent circuit of three-phase AC load in sector 1

Figure 6-4 shows an example of a commanded PWM output and equivalent circuit of a three-phase load in sector 1. The PWM switching pattern, equivalent circuits and associated switch states shown in Figure 6-4 are used and an example of how the generator side DC link current is estimated is given. The sector is divided into four periods each having times T0, T1, T2 and T7 respectively. During the states T0 and T7 all the phase currents are circulating around the phases and therefore the DC Link current is zero during these times. During state T1 the DC Link current is equal to the phase A current and during state T2 the DC Link current is equal to the negative of phase C current, therefore the average DC Link current during this switching period in sector 1 is given as follows:

$$I_{DC\,gen} = \frac{T1}{Tsw} i_A - \frac{T2}{Tsw} i_C \tag{6.7}$$

The AC load side is modelled as a balanced three phase AC load consisting of a series combination of resistance and inductance. PWM outputs and equivalent circuits in sector 1 are similar to the one shown in Figure 6-4 and is used to derive the AC load side DC Link current. For ease in identification of the parameters used for the estimation, the three-phase designations used for the AC load side are a, b, c. Once again a similar approach is adopted on the load side to determine 'instantaneous' DC Link current supplied to the load given by

$$I_{DC_{load}} = \frac{T1}{Tsw} i_a - \frac{T2}{Tsw} i_c \tag{6.8}$$

The DC link currents in (6.7) and (6.8) are calculated in all the sectors in a switching period with consideration to the PM Machine equivalent circuits and commanded PWM output in each of the sectors and averaged over a period of time to obtain the actual DC link current. The final step is to determine the 'instantaneous' DC link voltage which is achieved through the relationship:

$$V_{DC} = \frac{1}{C} \int (\sum_{n=1}^{6} I_{DC_{gen}} - \sum_{n=1}^{6} I_{DC_{load}}) \tag{6.9}$$

Where n is the number of sector, C is the capacitance value

Two approaches are possible, either to model the DC link voltage as a parallel current sources separated by a DC link capacitor where the average DC current estimations are then input to a piecewise linear current source which then represents the 'instantaneous' DC Link current supplied by the generator, $I_{DC_{gen}}$ and that supplied to the AC load inverter, $I_{DC_{load}}$. Or by online estimation of the DC link voltage knowing the equivalent value of the DC link capacitor.

6.4 Implementation of Average Voltage Estimation Modelling of Back-Back VSI with Variable Speed PMSG Wind Energy Conversion System

The simulation of variable speed PMSG wind energy conversion system (WECS) requires models and modelling a wind energy conversion system in its completeness including all the dynamics and interactions of the components of the system such as the variable speed wind turbine, the mechanical drive, the PMSG, the power electronic converters, the AC load/grid and control technique. A good understanding of the functions of all the components of the wind energy conversion system is also important in order to achieve an accurate model. While the wind turbine extracts as much power as it can from the wind and converts it into mechanical power, the generator converts the mechanical power from the wind turbine into electrical power and the AC/DC/AC power electronic converters process and converts power for the AC load/grid. Hence, a complete model includes the wind turbine model, the PMSG model, the full scale back-

back VSC model or its equivalent (full scale average voltage estimation model) and the AC load or grid model.

6.4.1 Modelling of Wind Turbine

The model of the wind turbine is based on a fixed pitch five blade 1kW horizontal-axis wind turbine with a rotor diameter of 2m with the detailed parameters shown in Appendix A, Table 2. In order to model a Wind turbine the dynamics of the mechanical drive train must be adequately represented. The dynamics of the mechanical drive train can be represented either as a single rotating, two rotating mass or three-mass drive train. This is in consideration of the various mechanical effects acting on the wind turbine and generator such as the moment of inertia of the blade, hub and generator, the resistant torque in the wind turbine and generator bearing, the resistant torque in the hub, blades and generator due to the viscosity of the airflow, and the torque of torsional stiffness. When the mechanical drive train is represented by two rotating bodies, the inertias and resistant torques of the wind turbine and generator are separated [230][231]. For its implementation, detailed information of the resistant torques in wind turbine and generator bearing, resistant torques in the viscosity of the airflow on wind turbine and generator are required. This information is not easily available. In a more advanced case, a three mass model of the mechanical drive train is used for the study of the transient stability associated with the effect and bending of long flexible blade normally associated with large wind turbines [232][233].

In a small scale wind turbine of the range of 1kW -10kW considered in this thesis, where the turbine rotor is directly connected to the generator without a gearbox, a single-mass lumped model is adequate for the study of any characteristics and control strategies. The proposed model of the WEC is based on a single mass drive train where the wind turbine and the generator inertia are lumped together arriving at an equation which describes the wind turbine rotor dynamics.

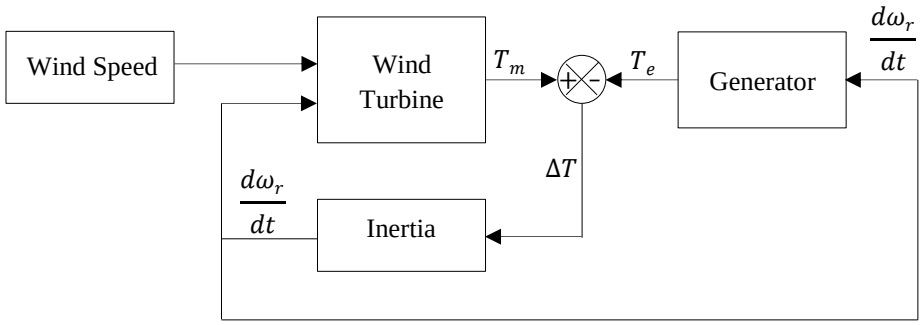

Figure 6-5: Block diagram of wind turbine and generator torque model

Figure 6-5 shows a block diagram of the wind turbine and generator torque model. The torque model represents the mechanical and electrical characteristics of the WECS whose rate of change of rotor angular speed can be calculated from the relationship between turbine mechanical torque, T_m and generator torque, T_e as follows;

$$\frac{d\omega_r}{dt} = \frac{1}{J}\left(T_m - T_e + C_v\omega_r\right) \tag{6.10}$$

Where J is the combined wind turbine rotor and generator inertia, ω_r is the turbine rotational speed (rad/sec), C_v is the viscous friction coefficient, and T_m and T_e are the turbine mechanical and generator electrical torque respectively.

The individual blocks in Figure 6-5 play important roles in wind energy conversion system and will be described in detail. The wind turbine extracts energy from the wind and converts it to mechanical power needed to produce the required mechanical torque to interact with the electrical torque from the generator to produce electrical power.

The mechanical power output of the wind turbine is calculated using the generic equation given as;

$$P_m = 0.5\rho A C_p(\lambda, \beta){V_w}^3 \tag{6.11}$$

Where: ρ is the air density (1.225kg/m^2), A is the swept area ($A = \pi R^2$) of the rotor blade, C_p is the power (performance) coefficient of the wind turbine, λ is the tip-speed ratio, β is the rotor blade pitch angle and V_w is the wind speed (m/s).

It can be seen that mechanical power of the wind turbine, P_m depends on the aerodynamic characteristics of the wind turbine defined by the efficiency of the wind turbine called the power coefficient, C_p. The power coefficient C_p is a nonlinear function of the tip speed ratio and the pitch angle with the maximum possible value set by Betz limit as $C_p = \frac{16}{27} = 0.593$ [231]. For fixed-pitch angle blade the actual mechanical power extracted from the wind by the fixed-pitch angle blade of the wind turbine can be calculated by

$$P_m = 0.5\rho\pi R^2 C_p(\lambda) {V_w}^3 \tag{6.12}$$

In this case, the power coefficient, C_p depends only on the tip-speed ratio and is given as

$$\lambda = \frac{\omega_r R}{\mathrm{V_w}} \tag{6.13}$$

Where: ω_r is the wind turbine rotor angular speed, R is the wind turbine blade radius

In order to generate electrical power, the mechanical power extracted from the wind turbine described (6.12) must generate mechanical torque and apply it on the generator. The mechanical torque is depicted by

$$T_m = \frac{P_m}{\omega_r} \tag{6.14}$$

Combining (6.12) and (6.13) and substituting into (6.14), the mechanical torque can be calculated using the expression

$$T_m = 0.5\rho\pi R^3 {V_w}^2 C_t \tag{6.15}$$

$$C_t = \frac{C_p(\lambda)}{\lambda} \tag{6.16}$$

Where: T_m is the mechanical torque (Nm) and C_t is the torque coefficient.

In order to implement the wind turbine model and emulator, the unique aerodynamic characteristics defined by the relationship between the power coefficient and tip speed ratio is required. Therefore, accurate representation of the C_p/λ curve is very important in the development of wind turbine model and emulator. There are methods available to develop the C_p/λ characteristics. Some of these methods are based on numerical approximations and polynomial expressions of $C_p vs\, \lambda$ as reported in [234][235]. The advantage of the polynomial approach is that the model and emulator

can emulate different turbines by simply changing the coefficients of the expression, the drawback being that the computation is complex and reduces performance. In fact much effort and computing time will be spent with considerable errors. An alternative approach to model C_p/λ curve is the look-up table approach. This approach requires a complete replacement of the table each time the turbine parameter is changed, but this is preferable and is used in the thesis because it represents a true C_p/λ as it's obtained directly from the wind turbine manufacturers or data sheet. Each C_p/λ curve has a maximium C_p and an optimium tip speed ratio at which maximium power can be extracted. The optimium tip speed ratio is based on the number of wind turbine blades and its value decreases as the number of blade increases given by [236]

$$\lambda_{opt} = \frac{4\pi}{n} \tag{6.17}$$

Where n is the number of wind turbine blades.

To operate at an optimium tip speed ratio higher than that defined by equation 6.17, most modern wind turbine blades are designed with highly efficient aerofoils which enable the wind turbine to operate at higher rotor rotational speeds and produce higher power. Figure 6-6 shows a typical C_p/λ used in modelling wind turbine in the thesis.

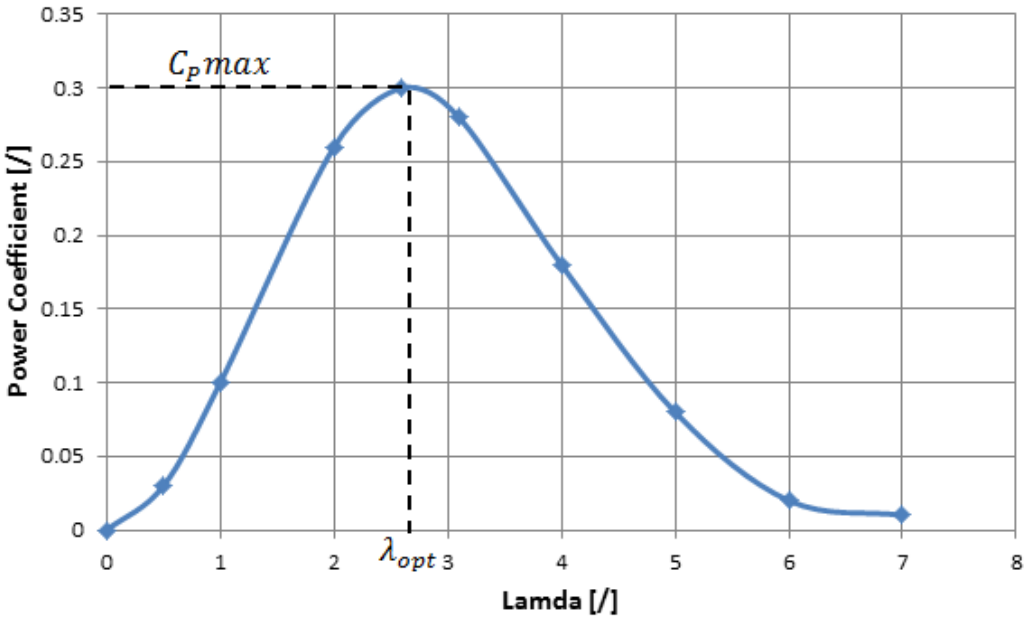

Figure 6-6: Power Coefficient versus tip speed ratio curve for the PMSG WECS

Figure 6-7 shows the block diagram of the model of wind turbine developed and implemented in PORTUNUS. The model is developed to calculate the mechanical power and torque that is applied to the rotor of the PMSG. This is achieved with wind speed and feedback rotational speed of the generator as inputs to the model. In a practical situation, this method involves the measurement of wind speed and rotational speed. Wind speed is measured using an anemometer and the rotational speed is measured with a speed sensor or an encoder mounted on the shaft of the generator. In addition in the simulation model, a wind speed profile can be developed and applied to the model.

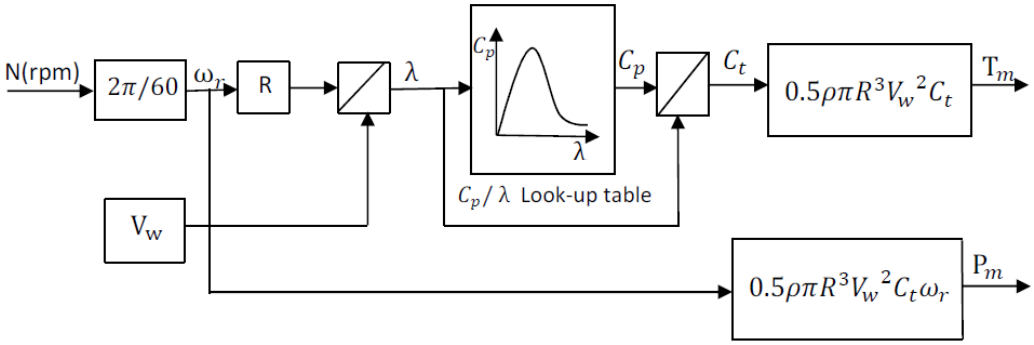

Figure 6-7: Block diagram of PORTUNUS wind turbine model

The next component model to consider is the permanent magnet synchronous generator model. As stated during the PMSM drive system modelling, the existing PM machine model in PORTUNUS simulation model is used, this is because much emphases on this thesis is placed on developing an alternative model for back-back voltage source inverter rather than improving the PM machine model.

6.5 Control Strategy

In order to implement the detailed switching and the average voltage estimation model of a voltage source inverter with variable speed PMSG wind turbine, a control strategy must be selected, developed and applied. It is obviously very important for any control strategy to take into account the variability of wind speed. The control techniques considered in this work is based on sinusoidal pulse width modulation (SPWM). SPWM is a well-established independent control technique in which each phase is controlled independent of the other. It is implemented with PI regulators. There are two controllers,

the generator side controller (GSC) and the AC load side controller (LSC). The generator side controller is designed to control the speed and the torque of the PMSG to track maximum power from the wind by controlling the stator current, and the AC load side controller controls the DC link voltage to the reference value, in order to control the power flow to the AC load. It is worth noting that future plans are to apply the proposed averaging technique to other control strategies such as vector control with the actual implementation of the AVEC block being essentially identical to the one for SPWM.

6.5.1 Generator Side Controller

The generator side control technique shown in Figure 6-8 consists of two main parts which are the outer speed control loop and the inner current (torque) control loop. The outer speed control loop controls the PMSG speed by controlling the generator stator current in a manner to track maximium power of the wind turbine at wind speeds below rated speed and limit power extraction to the rated power at higher wind speeds. The basic principle is that the generator side controller indirectly controls the electromagnetic torque by controlling the generator rotational speed to its optimum rotational speed at various wind speeds and in so doing maintains the tip speed ratio at the optimum value at all wind speeds.

For every wind speed there is an optimum rotational speed, ω_{opt} which corresponds to optimum tip speed ratio, λ_{opt} where the power of the turbine is maximum. In order to extract maximum power as wind speed varies, the turbine rotational speed is controlled to operate at the optimum tip speed ratio. This can be achieved by controlling the turbine rotational speed using a MPPT control technique given as

$$\omega_{opt} = \frac{\lambda_{opt} V_w}{R} \tag{6.18}$$

Where: ω_{opt} is the optimum rotational speed (rad/sec), λ_{opt} is the optimum tip speed ratio. From Figure 6-6, the optimum tip speed ratio at which maximum power can be extracted is 2.62 while the maximium coefficient of power, $C_{Pmax} = 0.3$.

The generator side uses the MPPT control to generate the optimum rotational speed (speed reference) which the outer speed control loop compares with the measured speed to generate a speed error signal. The speed error is fed into and processed by the PI

regulator to generate the reference current for the inner current control loop. However, for steady state performance tests of wind turbine emulator a variety of rotor rotational speed references are used to control the speed of PMSG to reproduce the power versus speed and torque versus speed of the wind energy conversion system.

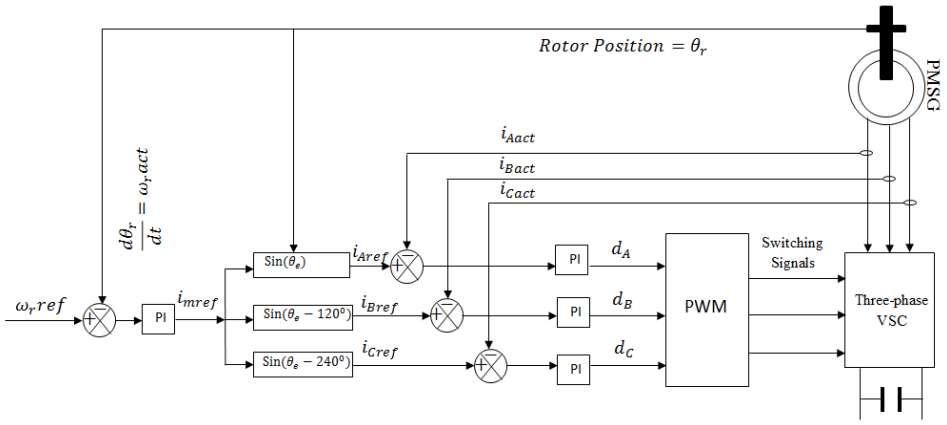

Figure 6-8: Generator side control technique structure

The current control loop compares the current reference with the measured current and ensures that the profile of the reference current is tracked by the actual current. Current sensors are used to measure the PMSG stator phase current per phase, i_{Aact}, i_{Bact}, i_{Cact} and compares with the sinusoidal reference, i_{Aref}, i_{Bref}, i_{Cref}. The result of each phase comparison is fed into the relevant PI regulator. For the switching model, the outputs of the PI regulators are compared with a triangular carrier signal and modulated at a high frequency (e.g. 20kHz as used in the models) to generates complementary gate drive signals in the relevant phase-leg while for the AVEM, the outputs of the PI regulators are used to estimate the average voltages per phase and applies the average voltages to voltage sources connected to the terminals of the PMSG.

6.5.2 AC Load Side Controller

The AC load side controller ensures that the DC Link voltage stabilizes at the desired reference value as the wind speed (and therefore power onto the DC Link) varies. Unlike the generator side controller, the AC load side outer control loop is the DC voltage control loop. The DC link voltage is measured and compared with the desired reference value, processed by the PI regulator. The output of the DC link voltage PI regulator as shown in Figure 6-9 is also passed through a sine wave generator to obtain the sinusoidal reference currents.

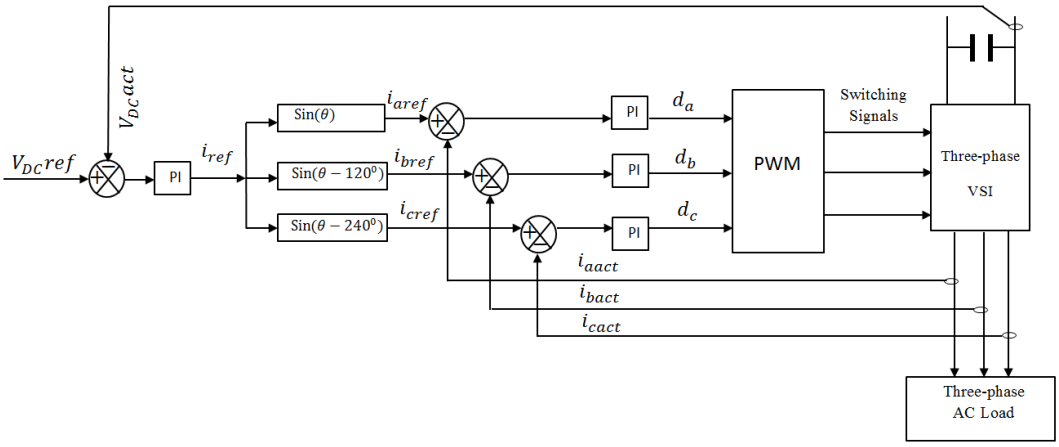

Figure 6-9: AC Load side control technique structure

Similarly the inner current control loop is responsible for the control of the currents. Current sensors are used to measure the AC load phase current per phase, i_{aact}, i_{bact}, i_{cact} and compared with the sinusoidal reference, i_{aref}, i_{bref}, i_{cref}. The result of each phase comparison is fed into its PI regulator. How the control strategy is applied differs in the models. In the detailed VSI switching modelling method, the output of the PI regulator (duty cycles) is compared with a triangular carrier signal and modulated at a high frequency (e.g. 20kHz as used in the models) to generates complementary gate drive signals in the relevant phase-leg. While, in the average voltage estimation model, the output of the PI regulator (duty cycles) serves as the input to estimate the average voltage in each switching period defined by the switching frequency.

6.5.3 Simulation and Validation of Average Voltage Estimation Model of Variable Speed PMSG Wind Energy Conversion System

The simulation studies were carried out using PORTUNUS system simulation software. The complete AVEM, switching simulation models and experimental setup of a fixed pitch small horse power (1kW) variable speed PMSG wind energy conversion system have been developed. The VSI loss model developed in section 3.3 was incorporated into the simulation models of PMSG WECS, one VSI loss model at the generator side and the other at the AC load side to account for the losses in the VSI. The control strategy is also implemented in the model and experimental setup. The PMSG model implemented in this simulation study is found in the PORTUNUS model library. The PMSG and wind turbine parameters are shown in Appendix A, Table 1 and Table 2. The step sizes were

chosen to reflect the requirements of each method. The limiting factor of the Average Voltage Estimation method is the minimum step size, which is restricted here to less than the PI loop run time of 50 microseconds on a typical DSP. For the PWM switching model, the limiting factor is minimum step size, which is set to the resolution of the PWM duty cycle, typically $<1000^{th}$ of PWM switching period.

The initial simulation was to determine the simulation steady state performance of the AVEM against the switching model of the WECS and then the steady state performance of the AVEM in comparison to the switching model and the laboratory wind energy conversion emulator in predicting the power versus speed characteristics of the WECS. It is important to state that the model is only used for steady state and the transient section of the simulation results is not considered in the analysis. A steady state test for the simulation models and laboratory WECS emulator over a range of wind speeds has been conducted. This is performed with only the inner current control loop at the generator side and the DC link voltage control at the AC load side. With the wind speed set to a fixed value each time, the reference current is varied to control the rotor rotational speed and the stator current, electromagnetic torque, voltage and power recorded and results are presented for 8m/s, 10m/s and 12m/s as follows. Currents and power flow from the Wind turbine to the AC load was investigated and compared.

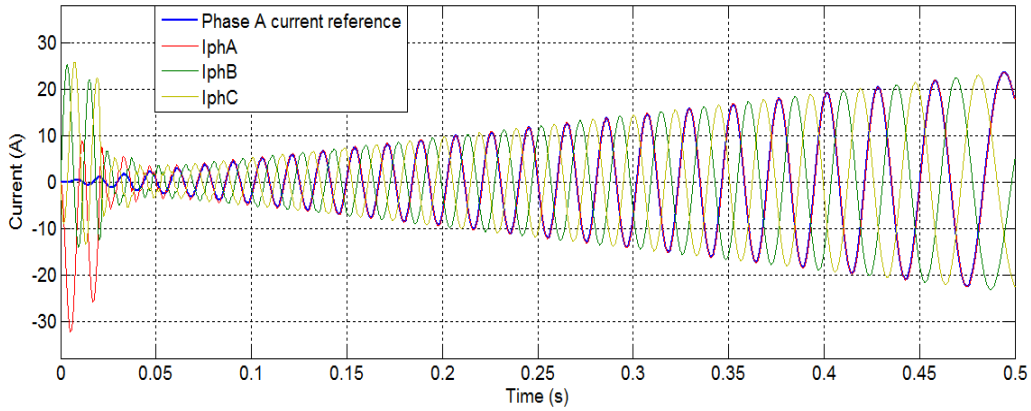

(a)

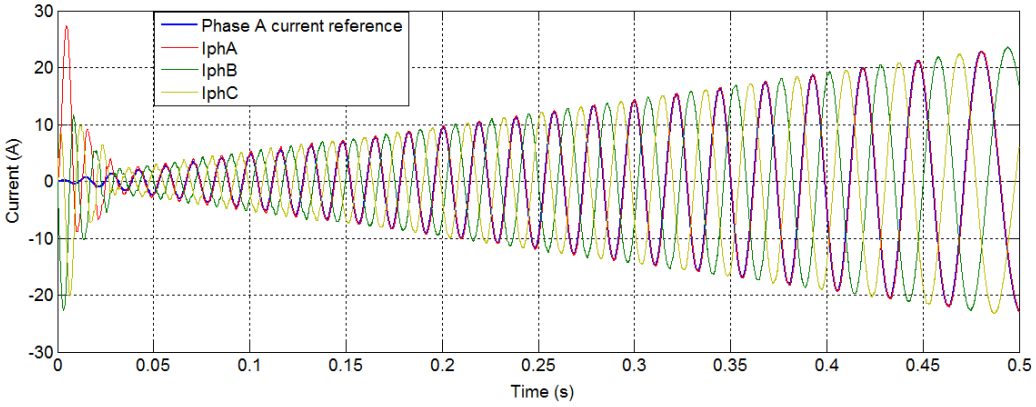

(b)

Figure 6-10: Simulation of PMSG stators current at variable current reference at 12m/s (a) AVEM (b) Switching model

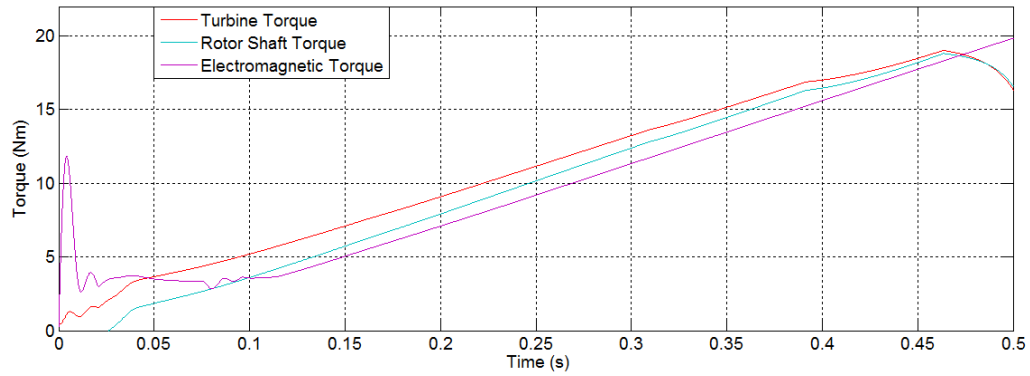

(a)

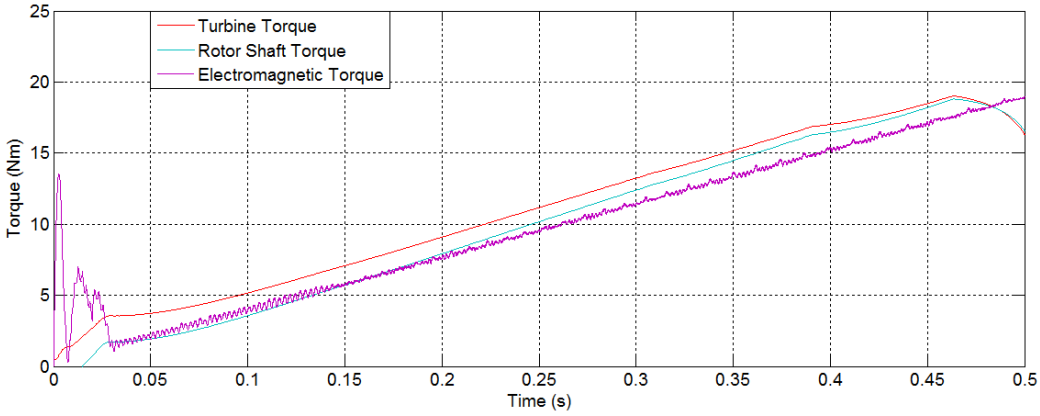

Figure 6-11: Simulation of WECS Torque at variable current reference at 12m/s (a) AVEM (b) Switching model

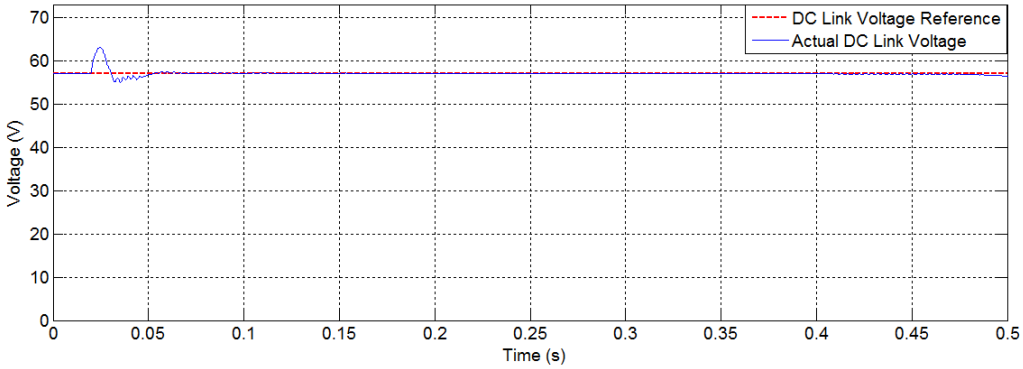

(a)

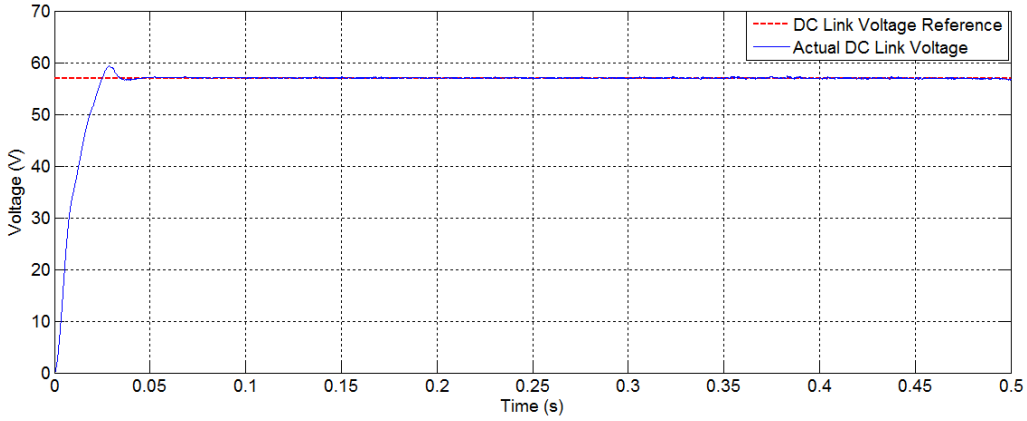

(b)

Figure 6-12: Simulation of WECS DC link Voltage at variable current reference at 12m/s (a) AVEM (b) Switching model

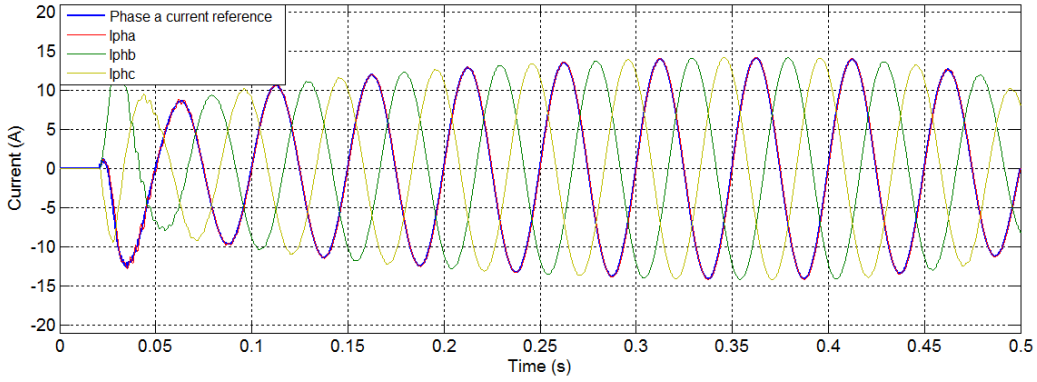

(a)

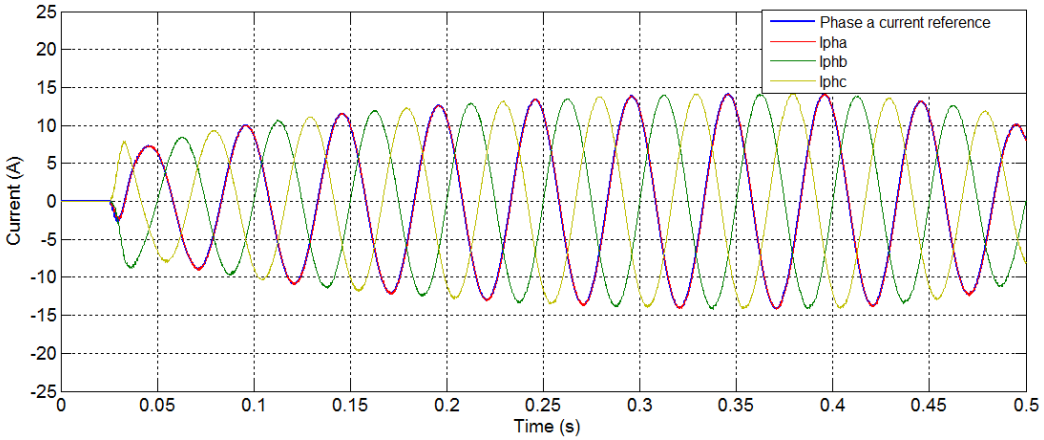

(b)

Figure 6-13: Simulation of WECS Load side phase current at PMSG stator variable current reference at 12m/s (a) AVEM (b) Switching model

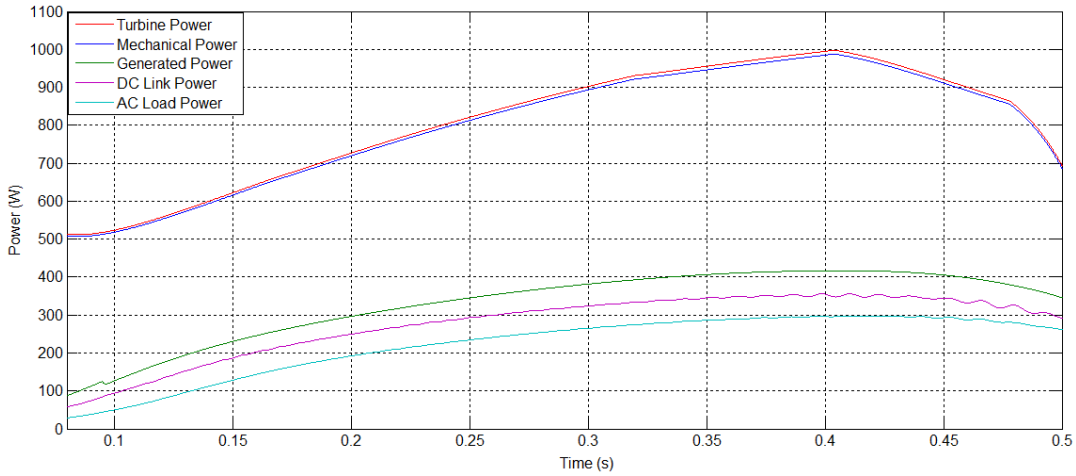

(a)

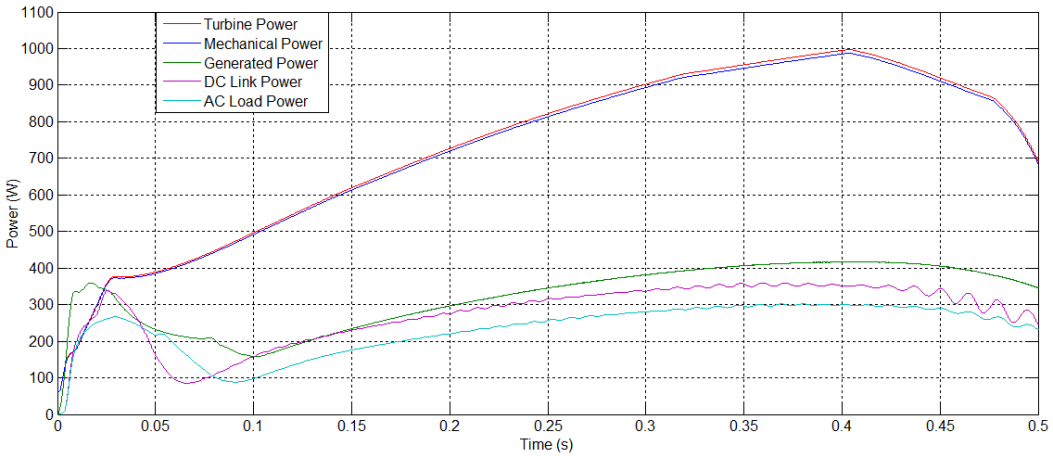

(b)

Figure 6-14: Simulation of WECS three-phase power with variable current reference at 12m/s (a) AVEM (b) Switching model

Figure 6-10 – Figure 6-14 show the PORTUNUS simulation of the AVEM and switching model of a complete PMSG WECS. This simulation result is necessary in order to validate the prediction of the AVEM against switching model before validation against experimental results. Note that analysis in this thesis is only based on steady state performance. At a fixed wind speed, the drive current reference is varied as the simulation is conducted. Figure 6-10 (a) shows the PMSG stator three phase current predictions using the AVEM and Figure 6-10 (b) shows the current prediction of the switching model. The result of the switching model validates the prediction of the

AVEM in waveform, tracking of the reference current magnitude, phase sequence and the frequency. The simulation results of the different torques such as turbine torque, the mechanical torque as well as the electromagnetic torque are simulated using the AVEM and the switching model of the WECS. It can be seen from Figure 6-11 that again the AVEM predict torque response results that are very close to the switching model in magnitude and distribution over time. However, differences can be seen between the electromagnetic torque predicted by the AVEM and the switching model. The switching model electromagnetic torque has ripples while that of the AVEM has not. This is due to the switching actions of the VSI switches and diodes which are totally eliminated in the AVEM. Similarly, the distribution and prediction of the DC link voltage, AC load current and power transfer of the AVEM have been shown in Figure 6-12- Figure 6-14. Apart from the reflection of ripples in the current on the power output of the switching model, the accuracy of the AVEM compares well with the switching model and validates the AVEM in simulating the input and output parameters and control technique of a typical WECS.

6.5.4 Performance Analysis and Validation of Average Voltage Estimation Model of Full Scale Back-Back Voltage Source Converter with Variable Speed PMSG Wind Energy Conversion System

The average voltage estimation model is validated against the switching model and experimental results of the wind turbine emulator to predict the power versus rotational speed and the torque versus rotor speed at different wind speeds. This consideration is necessary to determine how accurately the important characteristics such as the power versus speed and the torque versus speed of a wind energy conversion system can be reproduced using the AVEM. It is also based upon the ability of the AVEM to transfer power in the right direction and amount from the turbine to the AC load from which losses and efficiency can be evaluated.

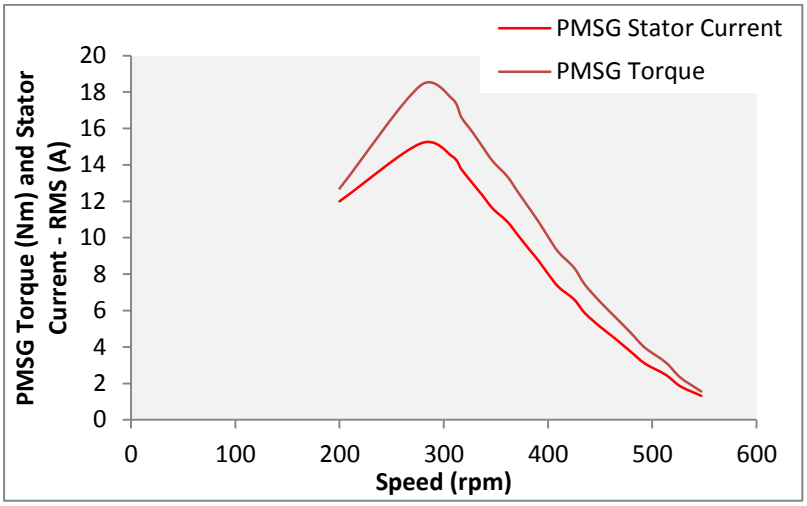

Figure 6-15: PMSG stator current and electromagnetic torque at 12m/s

Figure 6-15 shows the relationship between the generator current and electromagnetic torque control at 12m/s. It can be seen that, the stator current and electromagnetic torque have a linear relationship and an inverse relationship with speed and controlling the stator current, controls the electromagnetic torque. And by controlling the torque, the speed of the generator and turbine is controlled to track the C_p/λ curve to produce the characteristics of the WECS.

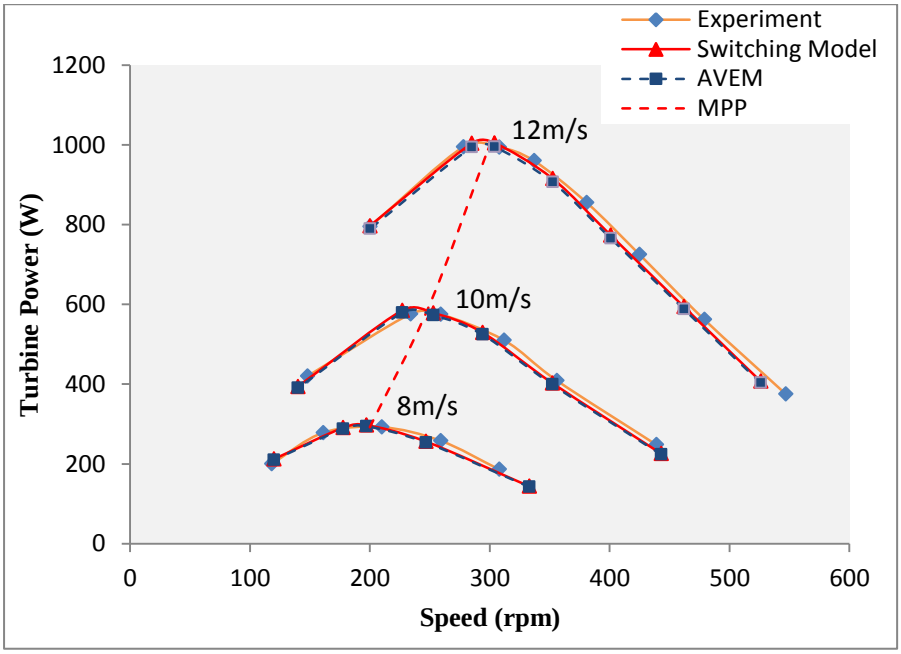

Figure 6-16: Comparison of wind turbine power versus rotor speed using AVEM, switching model and experiment

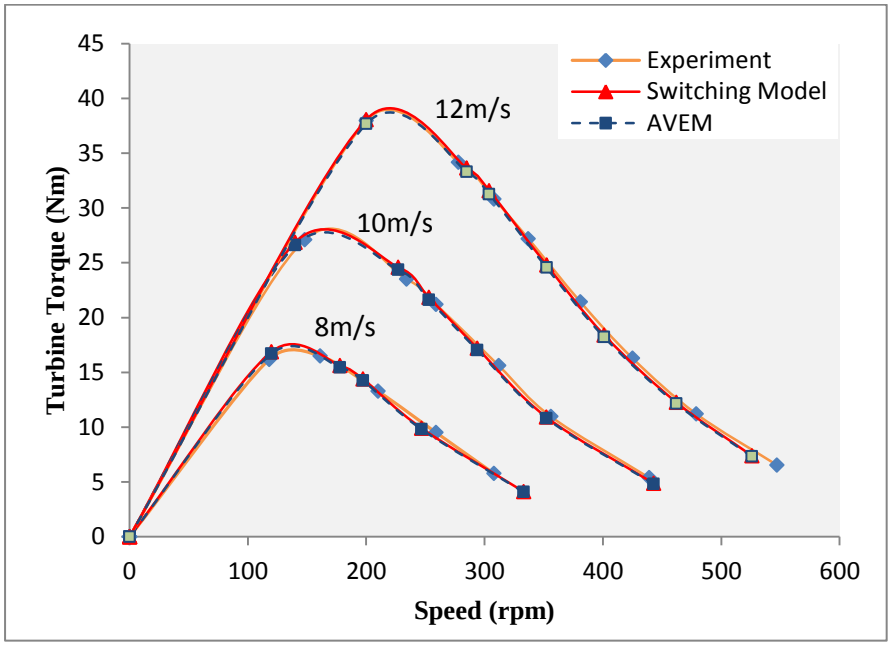

Figure 6-17: Comparison of wind turbine torque versus rotor speed using AVEM, switching model and experiment

Figure 6-16 and Figure 6-17 show the steady state performance comparison of the wind turbine power versus speed and torque versus speed curve predicted by AVEM against the switching model and experimental results at 8m/s, 10m/s and 12m/s. It can be seen that both the simulation models and the experiment reproduce the power versus speed and torque versus speed characteristics of the wind turbine at the lower and higher rotor rotational speed. As can be seen the AVEM results agrees closely with both the switching model and experimental results. The peak at each wind speed for the simulation models and experiment occurs at the same point and rotational speed which is very important in WECS. For example, at the rated wind speed of 12m/s with a rotor rotational speed of 300 rpm, both models and the experimental turbine predicted 1kW. The same trend can be seen at 8m/s and 10m/s. However, it is observed at higher rotor speed region that while the accuracy of both simulation models is maintained, there is some difference between the simulation models result and that of the experiment. Although, the difference is insignificant, this is due the difference in drive machine parameters between the simulation models and experiment such as the characteristics of the drive train materials which cannot be accurately established in the simulation models. On the whole this is an excellent performance by the AVEM considering that emphasis is on the lower speed region up to the rated speed of the wind turbine which in this case is

between 0rpm to 300rpm. This result verifies the performance of the AVEM in predicting the turbine power versus speed and torque versus speed characteristics of the wind turbine.

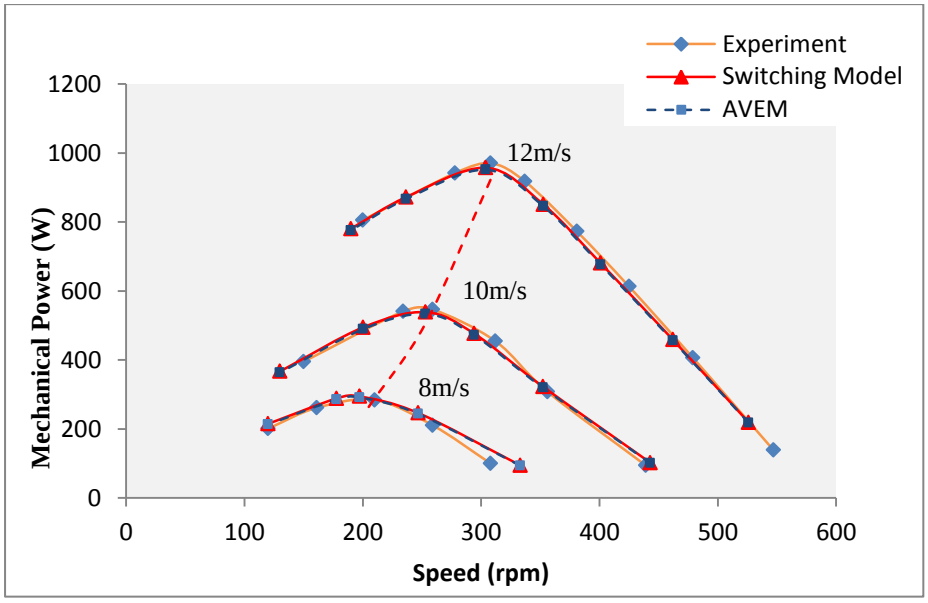

Figure 6-18: Comparison of PM machine mechanical power versus rotor speed using AVEM, switching model and experiment

Figure 6-18, shows the comparison of the mechanical power derived from the shaft of the developed PM machine wind turbine emulator at 8m/s, 10m/s and 12m/s with the AVEM and switching model. Comparing the results, the AVEM agrees well with the switching model and the experimental results in terms of variation with speed and current exhibiting the same profile. In addition the simulation results are reasonably close to experimental results, there are some differences between the results of the simulation models and the experimental results especially at higher rotor speed shown by the decrease in the predicted mechanical power by the experiment. This is more evident at the lower wind speed e.g. 8m/s and reduces as the wind speed increases towards 12m/s. This is due to under estimation of the shaft torque and the method of calculating the losses in the mechanical drive train. The test rig calculates the losses in the mechanical drive train based on machine parameters such as the friction in ball bearings, rotor and air, resistant torque in the drive which are all part of the test machine drive train but it difficult to be accurately calculated in the model. However, from the engineering simulation point of view, the AVEM has demonstrated good accuracy and performance in predicting the mechanical power versus rotor speed of a typical WECS. Further

considerations of losses available in the test rig will put the AVEM mechanical power closer to the experimental results.

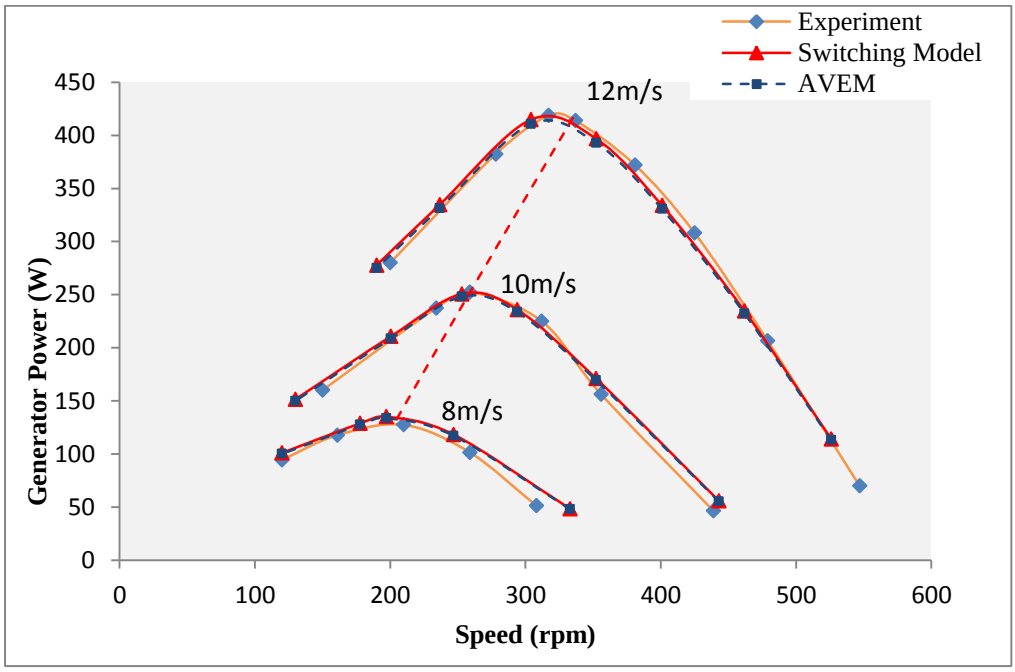

Figure 6-19: Comparison of the generated power using AVEM, switching model and experiment

Figure 6-19 shows the generated power/speed curve at 8m/s, 10m/s and 12m/s. it can be seen that the power generated using AVEM follows the power versus rotor rotational speed profile of the WECS and is in close agreement with the switching model and experimental results. At lower rotor rotational speed, a high level of accuracy is obtained with AVEM in tracking the prediction of the switching model and experiment. However, there is some difference between the simulation models and experimental results especially at higher rotor speed. Without doubt the impact of the difference in the prediction of the mechanical power by AVEM compared to the experiment will reflect in the generated power. This is due to difference in the method of calculation of the losses between simulation model and the experimental test rig. The experimental test rig has the entire losses components such as the resistant torque in the drive and generator bearing, the resistant torque in the generator due to the viscosity of the airflow, the torque of torsional stiffness and are difficult to be accurately calculated by the simulation models as such information are not readily available in manufacturer's datasheet. Again the

difference between the results is due to the difference in PM machine parameters such as the stator resistance value used in the simulation models and experimental test rig. The experimental test rig calculates resistance based on stator windings and material resistivity which varies with temperature while the simulation models uses the stator resistance measured from the machine. From the results, the power predicted by the simulation models at higher rotor speed is higher than the experimental results which suggest an under estimation of the stator resistance at higher rotor speed compared to experimental test rig. In addition, it can be seen that not all the mechanical power is converted by the generator. This is largely because the generator power output depends on the current demand and load on the generator and we were constrained by the limit of the measuring devices and applied load to operate at a maximum current of 15A rms. All analysis on WEC in this thesis is based on the 15A maximum current limit. Generally, the results validate the performance of the AVEM in predicting generated power versus speed profile and show that the numerical performance accuracy of the AVEM in predicting the generator power can further be enhanced by making much consideration to losses that are present in the actual test generator and drive train.

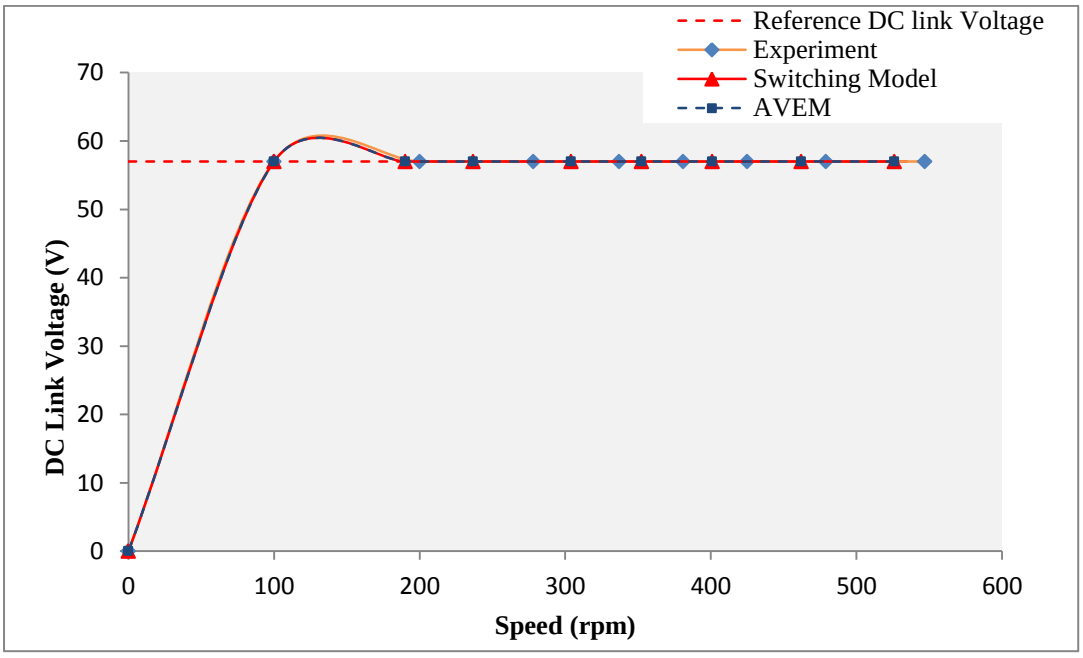

Figure 6-20: Comparison of DC link voltage control using AVEM, switching model and experiment

Figure 6-20 shows the DC link voltage predicted by the AVEM, switching model and experiment under the DC link voltage controller. This validation is a very important aspect of AVEM especially when the DC link and DC link capacitor were eliminated in the AVEM. In the switching model and experiment, the DC voltage can be measured at varying wind speeds, but in the AVEM the model calculates DC link voltage as described in section 6.3, it is important therefore to see how accurately the AVEM can predict the DC link voltage. Figure 6-20 shows how the AVEM DC voltage compares with the switching model and experimental results. It can be seen that at varying wind speed, the AVEM agrees well with the switching model and experiment results without loss of accuracy in controlling the DC voltage to the reference value of 57V. Having seen how the DC link voltage is effectively controlled the comparison of the DC power predicted different wind speed by AVEM against the switching model and experimental results are presented.

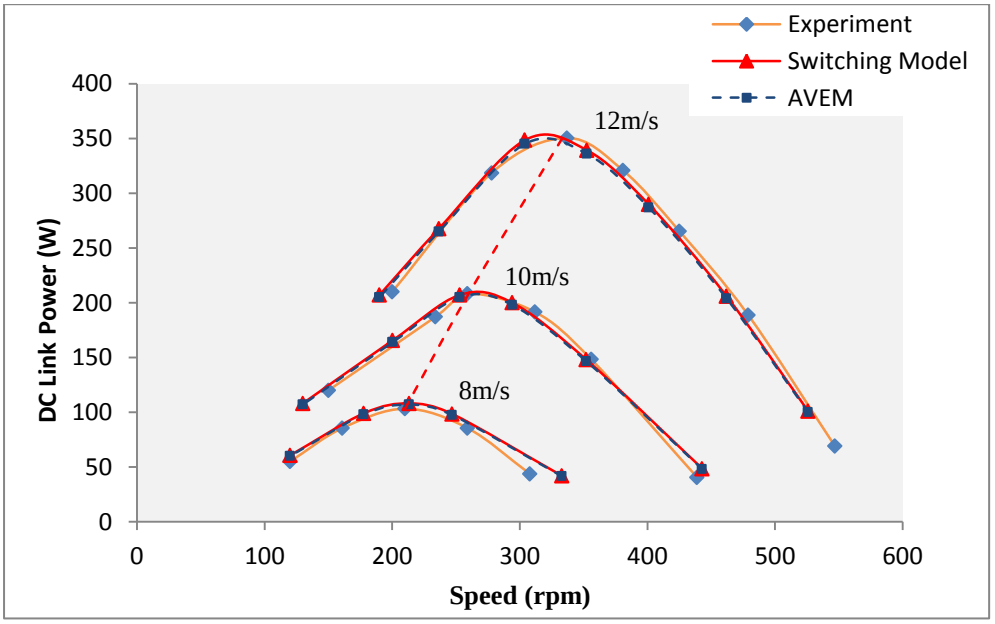

Figure 6-21: Comparison of DC link power using AVEM, switching model and experiment

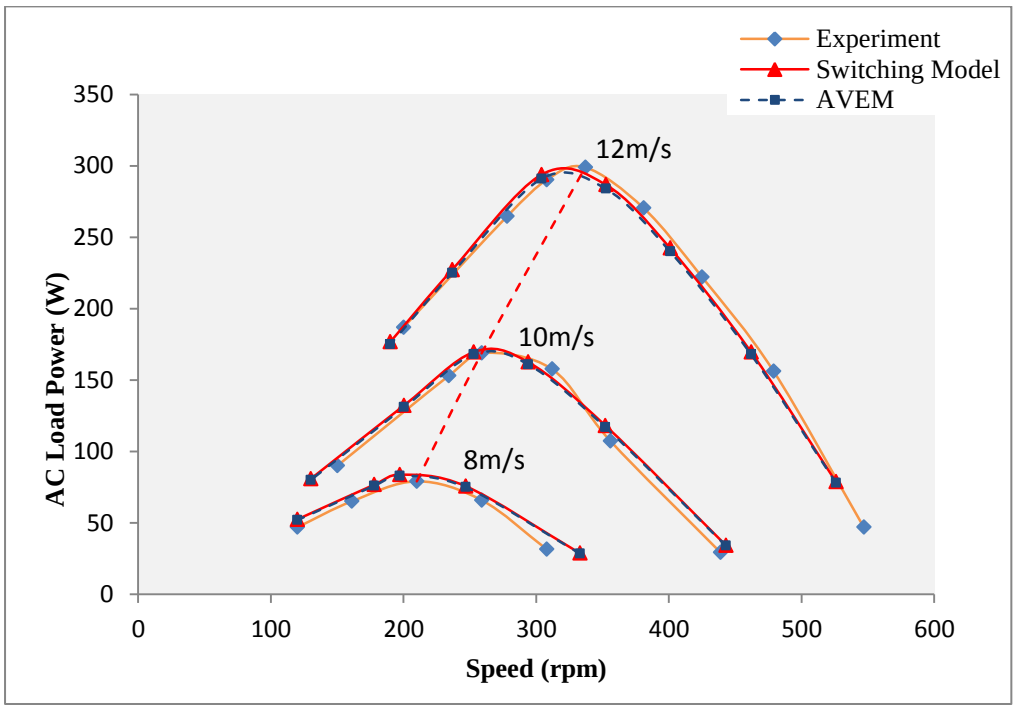

Figure 6-22: Comparison of AC load power using AVEM, switching model and experiment

Figure 6-21 and Figure 6-22 show the DC link power and the AC load power comparison between AVEM, switching model and experimental results. It can be seen that the AVEM and the switching model results are the same and are reasonably close to the experimental results. In both the DC link power and AC load power prediction comparison, it can be observed that there is noticeable difference at lower rotor rotational speed as well as higher rotor speed. The difference between the simulation models and experiments is due to the method of calculating the VSI losses. In the experimental test rig, the loss components of the VSI are part of the actual VSI while in the simulation models, the VSI losses are modelled using the information on the output characteristics of the IGBTs and diode supplied by the manufacturer's datasheet where the VSI conduction and switching losses are calculated. Generally, it is difficult to accurately calculate VSI conduction and switching losses. In addition, the difference at the higher rotor speed is a reflection of the difference in the prediction mechanical power by AVEM against the experiment. However, the error is insignificant; it can be improved on if much consideration is given to such losses in the simulation models. These results validate the performance of the AVEM in predicting the power versus speed profiles of the wind turbine as well as the right power flow direction from the turbine to the AC load.

6.5.5 Validation and Analysis of Losses and Efficiency of PMSG Wind Energy Conversion System

The challenge facing wind energy conversion systems designers and manufacturers is to effectively and efficiently utilise the energy extracted from the wind. For a given amount of power extracted from the wind, power electronic converters are design and controlled in a manner to utilise the energy in an efficient way. The most efficient way to utilise the energy from the generator is to know the losses in the generator and the power electronic converters. Knowing the losses helps in the right choice of power electronic converters, minimise losses and analysis of efficiency of WECS. To fully achieve the benefits of losses stated above, accurate and adequate VSI loss models are necessary. In order to accurately predict the losses, models must take into considerations the effect of varying wind speed, control strategies, the operating points as well as the complete interaction of the mechanical and electrical components of WECs. This is because to accurately predict the VSI losses, it requires the voltages, currents, phase angles and the PMSG factor and these depend on the variation of wind speed, control strategy and operating points. For the simulation analysis of the efficiency of the WECS, an expanded dynamic model of the WECS is applied which takes into consideration the VSI losses. The voltage source inverter loss models had been incorporated into the AVEM, it is important to validate the prediction of the losses and efficiency against experimental results.

This section presents a validation of the losses and efficiency predicted by the AVEM against experimental results and analyses of the efficiency of each component and overall system under PI current control at the generator side and the DC link voltage control at the AC load side and operating points. Although, the efficiency of wind energy conversion system is best calculated under MPPT control, it is presented here to demonstrate variation of efficiency and losses over the rotor operating speed.

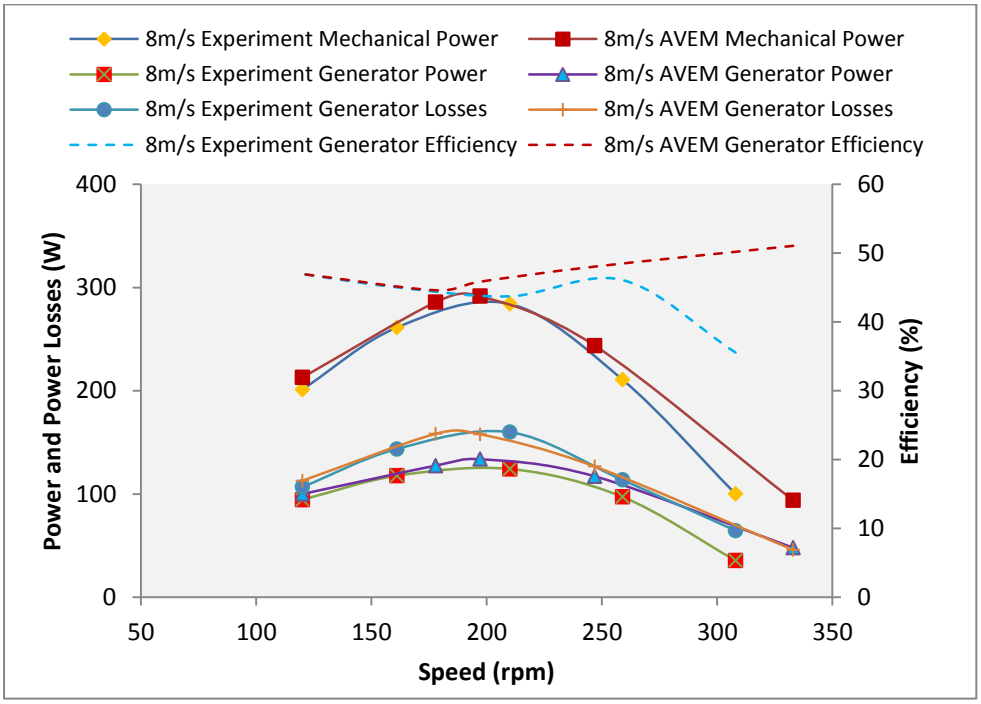

Figure 6-23: PMSG Losses and Efficiency at 8m/s

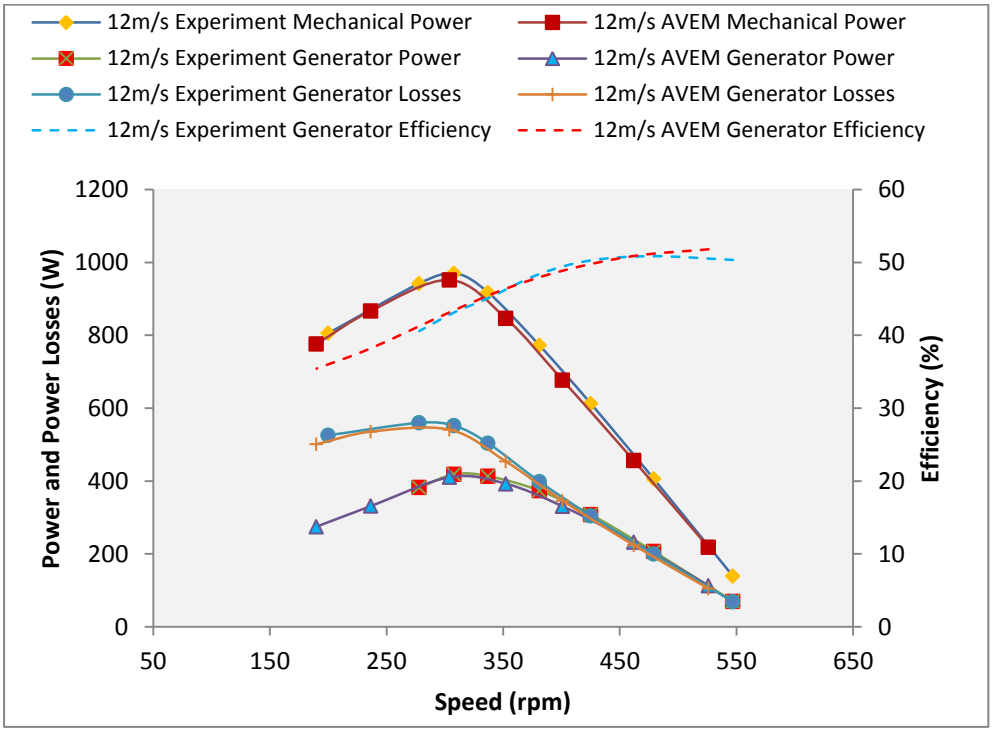

Figure 6-24: PMSG Losses and Efficiency at 12m/s

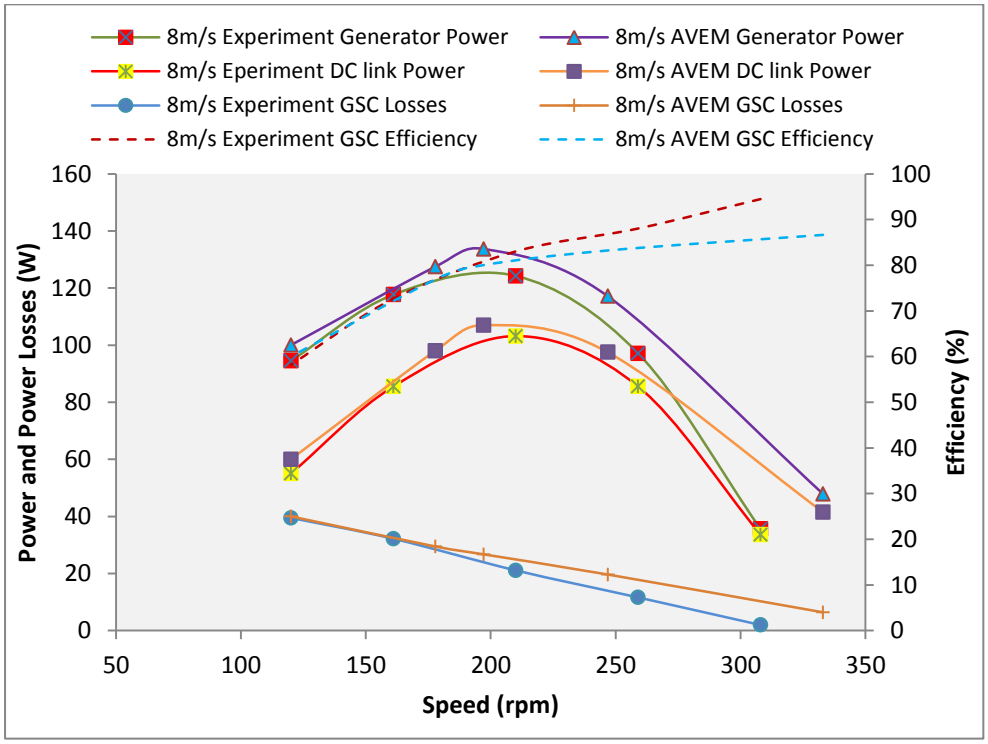

Figure 6-25: Generator Side Converter Losses and Efficiency at 8m/s

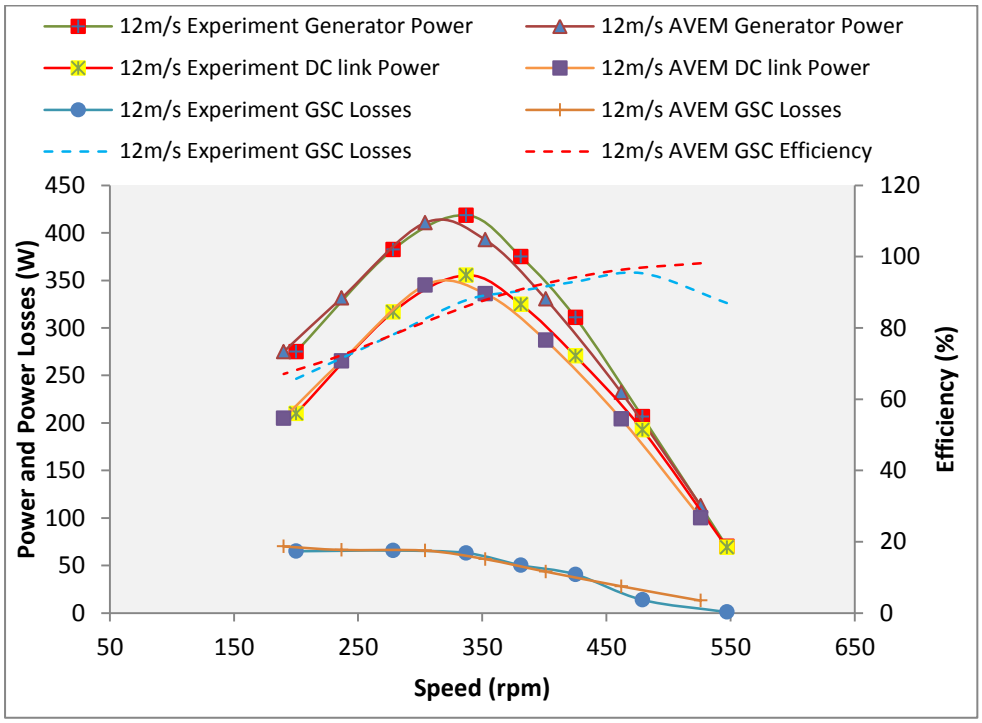

Figure 6-26: Generator Side Converter Losses and Efficiency at 12m/s

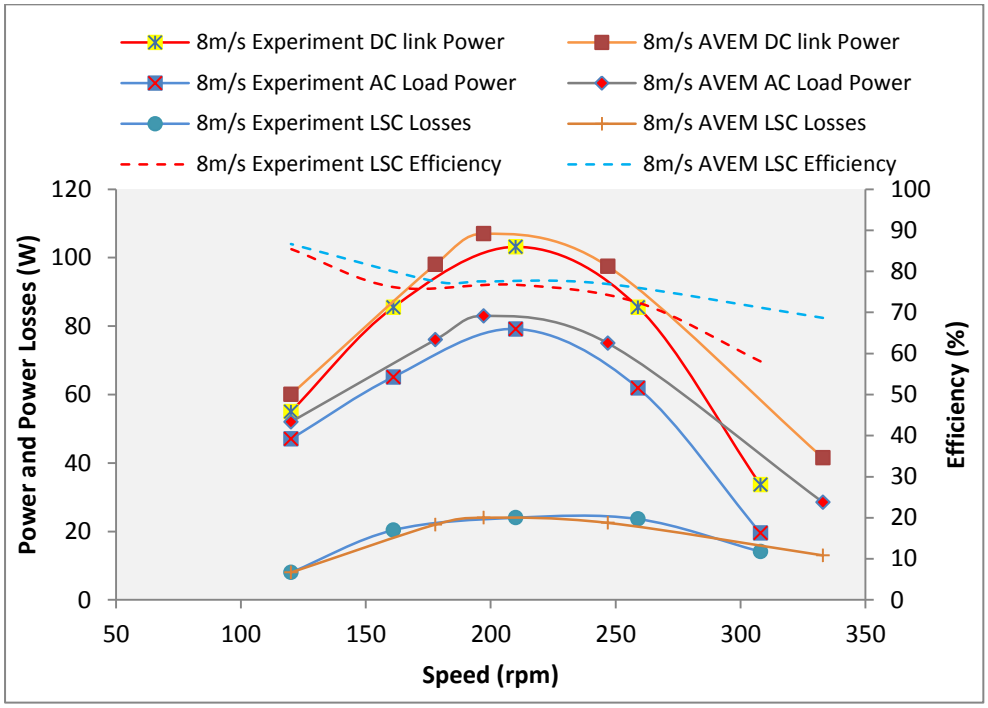

Figure 6-27: Load Side Converter Losses and Efficiency at 8m/s

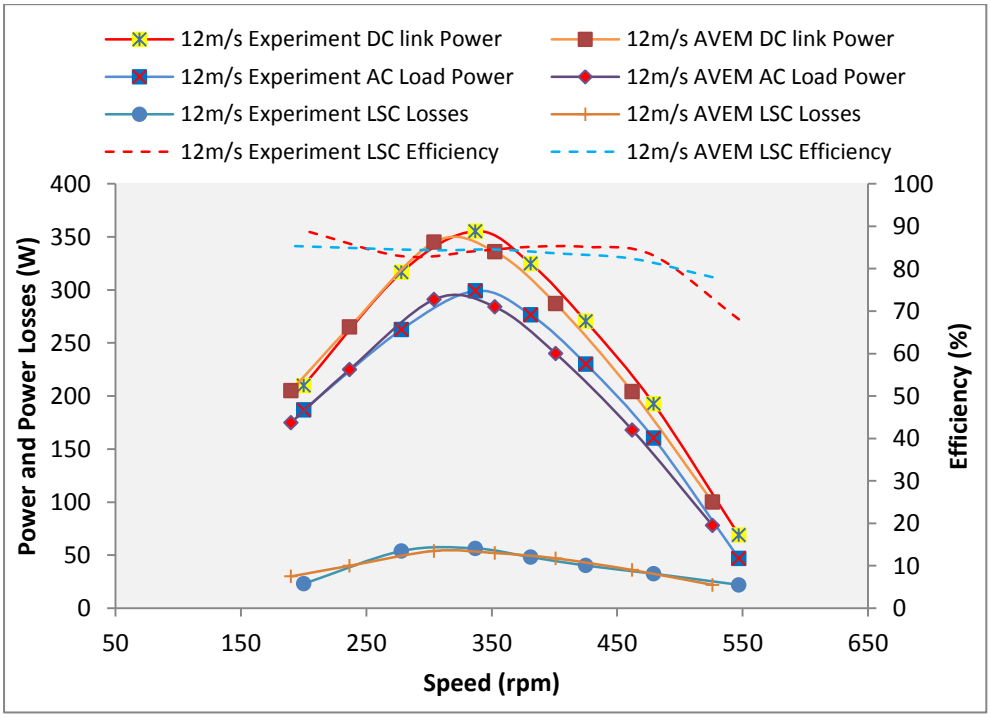

Figure 6-28: Load Side Converter Losses and Efficiency at 12m/s

Figure 6-23 – Figure 6-28 validate the losses and efficiency predicted using the AVEM against the experiments at 8m/s and 12m/s. Figure 6-23 and Figure 6-24 shows the PMSG losses and efficiency in which the Generator output power is compared with the

shaft mechanical power over the complete operating range. The results show that both the AVEM and experiment have the same profile versus the operating speed. At low rotor rotational speed region, the losses and efficiency predicted by the AVEM agree with the experimental results without loss of accuracy. However, at the higher rotor speed region when the wind speed is 8m/s, the losses predicted by the experimental test rig is observed to be higher which of course is due to differences in response of the PMSG parameters to changes in rotational speed and stator current between AVEM and experiment test rig. Comparing Figure 6-23 and Figure 6-24, it can be seen that the losses increase with increase in wind speed which is what is expected, as the wind speed changes, all the output quantities also changes. Also the accuracy of the prediction of losses and efficiency compared to experiment increases as the wind speed increases towards the rated wind speed of 12m/s. Generally, WECS performed well close to the rated wind speed, this again explains why the prediction of the AVEM and experiment follows the same profile. It can be seen from Figure 6-24 that both the AVEM and experiment traces the operating speed accurately, as the losses reduce, the efficiency increases. However, there is a difference in the prediction of the losses and efficiency at higher speed when operating at 8m/s as shown in Figure 6-23, the results of the AVEM at the rated wind speed validates the performance accuracy the AVEM in predicting the losses and efficiency of the PMSG.

Figure 6-25 and Figure 6-26 shows the generator side converter (GSC) losses and efficiency predicted by the AVEM compared with the experimental results at 8m/ and 12m/s. To calculate the GSC losses, the DC link power is compared with the generated power taking into consideration the wind speed and the control strategy and the efficiency determined by the ratio of the DC link power to the generated power. It can be seen from the results that the same trend as that obtained in Figure 6-23 and Figure 6-24 is obtained when considering the profile versus speed and variation of losses as the wind speed increases. At a wind speed of 8m/s, the lower rotor rotational speed region shows the same level of prediction accuracy by both the AVEM and experiment while at higher rotor rotational speed, a poorer prediction accuracy is shown at 8m/s. However, at the wind speed of 12m/s, a good level of accuracy is shown in the predicted GSC losses and efficiency by AVEM against the experimental results.

Figure 6-27 and Figure 6-28 show the comparison of the AC load side converter losses predicted by the AVEM and the experiment test rig. The results show the same profile over the rotor operating speed as the PMSG torque is controlled by varying the stator current. However, it is interesting to observe that, at low rotor rotational speed when the WECS operated at 8m/s, there is good accuracy in prediction of the load side converter losses and efficiency by AVEM against experimental results compared to that of the generator side converter. This is because the load side AVEM (load side converter) is decoupled from the generator and depends on the AC load supply frequency. In addition, it can be seen that, the LSC losses increases as the wind speed increases. For example, the maximum LSC losses predicted at 8m/s is 24W and that of 12m/s is 56W.

6.5.6 Comparison of Simulation Execution Time

In all the simulations in this chapter, the step sizes were chosen to reflect the requirements of each method. The limiting factor of the Average Voltage Estimation method is the minimum step size, which is restricted here to less than the PI loop run time of 50 microseconds on a typical DSP. For the PWM switching model, the limiting factor is minimum step size, which is set to the resolution of the PWM duty cycle, typically $<1000^{th}$ of PWM switching period.

Table 6-1: Comparison of simulation completion time between switching model and AVEM of PMSG WECS

Models	Time step	Simulation set time	Time taken to complete simulation
Switching model	$100e^{-9}$	0.5	4.5 hours
AVEM	$30e^{-6}$	0.5	5 minutes

Table 6-1 shows the comparison of the simulation completion time between switching model and AVEM. It can be seen that with the simulation set time of 0.5s, completion time for the switching model with a time step of $100e^{-9}$ is 4.5 hours while the simulation completion time for the AVEM with freedom of time step $30e^{-6}$ is 5 minutes which is 54 times faster than the switching model.

6.5.7 Wind Energy Conversion System Energy Output Estimation using AVEM Simulation and DSP-based AVEM Method

The amount of energy yield and methods to increase annual energy yield are important aspects of a wind energy conversion system. Most wind energy conversion system developers and customers are interested in knowing the amount of energy a particular WECS can generate annually and to know the savings they can make compared to the use of other forms of energy. Considering the importance attach to energy yield, it is important in WECS design process to analyse the potential quantity of energy yield.

This section introduces a wind energy conversion system energy estimation based on AVEM using simulation package and also implemented in the DSP controller. The DSP-based AVEM method of estimating energy of WECS is hard to find in literature. The proposed method provides an alternative through which energy of a three phase system can be estimated using the real time DSP controller which allows for a direct performance validation of the AVEM of full scale back-back VSI with variable speed PMSG WECS against measured energy. Generally, to estimate the output energy, the power output is taken over a certain period of time usually on an hourly basis over a day, a month or a year. In WECS, variable wind speed is applied to the wind energy conversion system and the energy from the generator and consumed by the load is determined by averaging the power generated and delivered to the AC load over a certain period of time taking wind speed data input into consideration. The power depends on the phase voltage and current. With the average phase voltage V_{avg} obtained as described in section 3.2 and measured instantaneous phase current, i three phase power output in one fundamental cycle is average over a period of time T to arrive at the three phase energy output as

$$E = 3\frac{1}{T}\int_0^T V_{avg}\, i\, dt \tag{6.19}$$

Where, V_{avg} is a phase average voltage calculated using the AVEM described in section 3.2, i is the instantaneous current and T is the period defined in this case by the simulation set time.

In the experimental test rig, DSP controller uses the duty cycles obtained from the control strategy to estimate the average phase voltage and with the measured

instantaneous phase current fed into the DSP controller calculates the average power. To estimate the energy output, the average power is accumulated over a period of time.

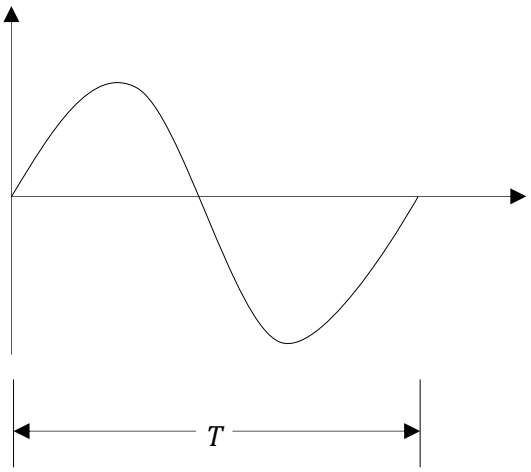

Figure 6-29: One cycle of a sinusoidal waveform

Figure 6-29 shows a sinusoidal waveform of output variables e.g. voltage and current over one fundamental cycle. In one fundamental cycle, there are series of samples which depend on control strategy switching cycle period, T_{sw} and the period of the fundamental waveform, T. This relationship between the switching period, the fundamental period and the number of samples allows a special technique for the DSP controller implementation of the AVEM-based energy estimation to use the number of samples, N instead of time. Hence the DSP controller calculates energy output from the accumulation of average power based on number of samples given by

$$E_{DSP} = 3 * \frac{1}{N} \sum_0^N V_{avg} * i \tag{6.20}$$

Where, V_{avg} is the average phase voltage estimated based on the AVEM, i is the measured phase instantaneous current, N is the number of samples and E_{DSP} is the three phase energy estimation using the DSP controller based on AVEM. The DSP first calculates the number of samples, N from the switching frequency and the period of the control strategy interrupt period and then uses equation 6.20 to calculate the three phase energy in one fundamental cycle and accumulate the energy as long as the test rig operates. Thus, the DSP uses equation 6.20 to calculate the energy produced by the PMSG and the energy available for use by the AC load which depends on wind speed, generator rotor speed and control strategy. The generator energy output estimation depends on duty cycles from the generator side controller while the load energy output

depends on duty cycles from the load side controller. Generally, as the wind speed varies, the wind turbine power, generator power, losses, AC load power and energy output also varies and the actual power and energy output from a wind energy conversion system depends on the ability of the control strategy to track maximum power points (MPPT) at each wind speed. Various MPPT control strategies have been reported in literature [237]-[245]. They are classified based on the use of sensors to measure wind speed and generator speed such as tip speed ratio (TSR) [246] and sensorless methods such as power signal feedback (PSF) [247] and the hill-climb searching (HCS) [248][249]. The sensorless methods reduce cost, improve the stability of the drive train but have the drawback of poor dynamic response to variation in wind speed. The optimum tip speed ratio method involves rotor speed and wind speed measurement and responds faster to variation in wind speed and reflects the dynamics of wind speed compared to other methods. However, this method has cost implications as it involved wind speed measurement but there is always a trade-off between accuracy and cost. This method is based on the fact that for a certain wind speed, power is maximum at a certain rotational speed known as optimum rotational speed and each optimum rotational speed has a matching optimum tip speed ratio. Thus maximum power can be obtained by controlling the wind turbine and generator speed to operate at the optimum rotational speed.

On the other hand, from Equations 6.10, 6.15 and 6.17, maximum power can be generated when the generator produces torque opposite to the mechanical torque given as

$$T_e = -(K_T {\omega_r}^2 - C_v \omega_r) \tag{6.21}$$

$$K_T = 0.5\rho\pi C_p max(\frac{R}{\lambda_{opt}})^3 \tag{6.22}$$

Using (6.21), the current reference for the generator side AVEM is obtained by

$$i_m = \frac{T_e}{K_t} \tag{6.23}$$

Where i_m is the peak value of the sinusoidal current reference, K_t is the torque constant of the PMSG given by $K_t = \frac{3}{2} p\phi_m$ and p is the number of pole pairs, ϕ_m is the magnetic flux.

To maximise the WECS energy output, the generator side controller controls the PMSG speed and torque by controlling the stator current to track maximum power point below

rated speed and above rated speed limit power to the rated value and the load side controller ensures that the DC link voltage is maintained constant as wind speed varies. For the generator side controller to control the PMSG stator current, a current reference is required. This is usually obtained by processing the error from the comparison of the actual rotor speed and reference rotor speed which is based on the fact that for every wind speed, there is an optimum (reference) rotor speed and stator current (torque) demand at which power generated is maximium. Therefore to simplify the control and energy output calculation, a passive maximium power point tracking control technique is developed in which the reference rotor speed can be set as a function of current reference for different wind speeds to track maximum power using a look-up table. As wind speed varies, the actual rotor speed is input into the look-up table and a matching current reference is selected and compared with the actual stator current to generate the three phase duty cycles.

6.5.8 DSP-based Implementation of AVEM WECS Energy Output Estimation

The DSP controller implementation of the proposed AVEM is an additional significant contribution of this thesis. The implementation of a DSP-based energy estimator using AVEM is based on SPWM control implemented with PI regulators. Since it is possible for software implementation of SPWM using a DSP controller, code was developed to use the three phase duty cycles from the control strategy to calculate the energy output. First the number of samples is calculated by the DSP controller from the switching period which depends on the choice of the switching frequency (which in this case is $50\mu s$) and the one cycle fundamental period of $20ms$. After this, considering the PWM pulse pattern for each phase changes over the switching cycle and calculation of average voltage is sector dependent, the DSP programing code is developed to identify the sector and calculate the timing variables, average voltage, power and energy. The details of the codes required to calculate the energy output by the DSP controller using AVEM is shown in Appendix E. The code for the energy estimator using AVEM runs in an interrupt routine and controls the accumulation of average power in one fundamental cycle over a given length of time (as long as the test rig operates). In the interrupt, the new average power is estimated and added to the previous average power. Therefore for the given length of time the total energy is calculated. This also allows energy to be

recorded at intervals of time depending on the choice of the user. Once, the PMSG operates, the energy estimated is held on and should be reset to zero before the next experiment (operation of the generator). Therefore, at the beginning of every experiment, a reset has to be made to clear the energy value from the previous experiment.

In order to verify the accuracy of the method, simulation and experiments were carried out. The simulation used the developed AVEM of wind energy conversion system with parameters of the PMSG and wind turbine stated in Appendix A, Table 1 and Table 2. A variable wind speed profile was applied to the WECS model and the experimental wind energy conversion emulation system.

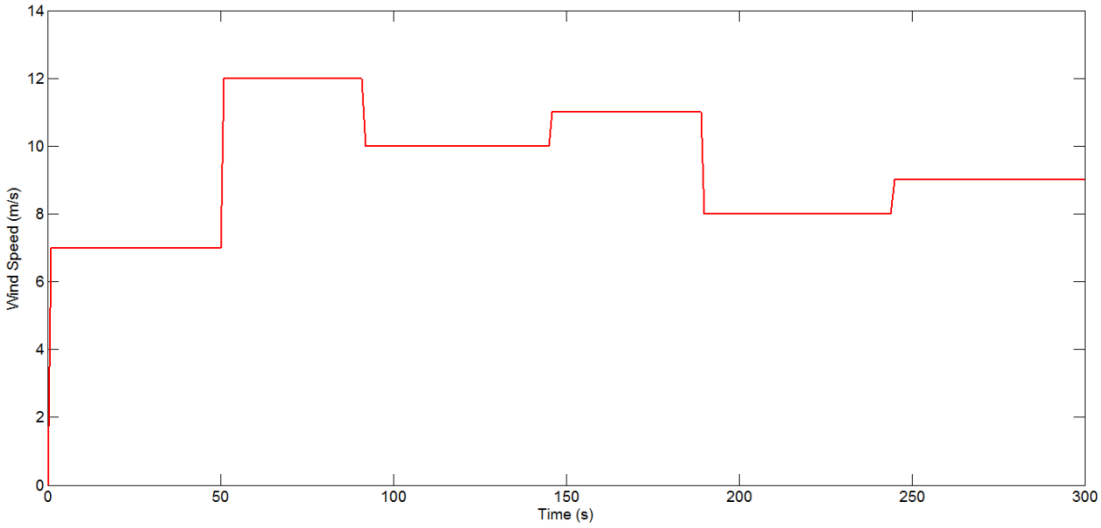

(a)

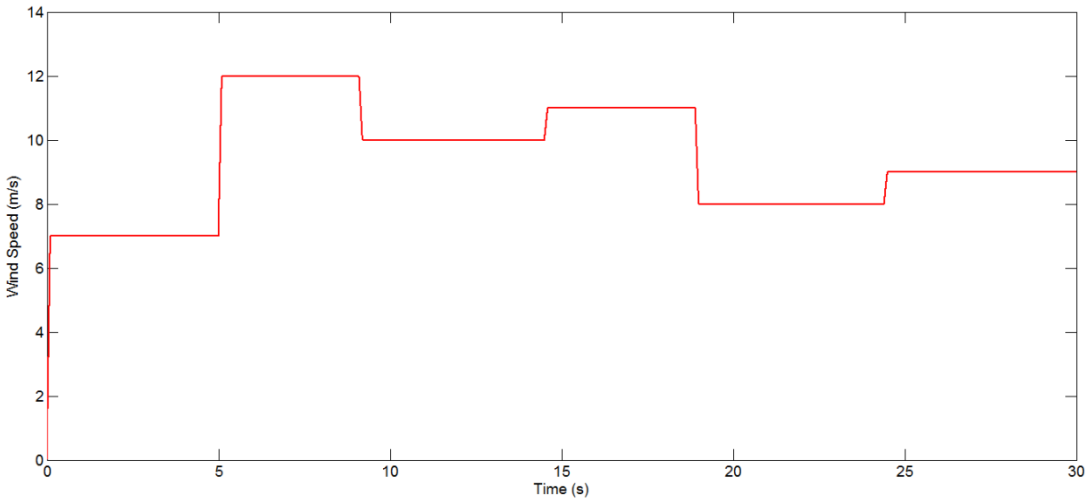

(b)

Figure 6-30: Wind speed profile (a) Actual for 5 minutes (300 seconds) (b) Scaled to 0.5 minutes (30 seconds)

A variable wind speed profile for a duration of 5 minutes shown in Figure 6-30 (a) was applied to both the AVEM and experimental wind turbine emulator. However, considering the difficulties of simulating a model for a long period, the time of the AVEM simulation wind speed profile is accelerated by a factor 10 as shown in Figure 6-30 (b). With this being the case, the AVEM is expected to predict energy output, when multiplied by 10, equivalent to the experimental results. In this performance test, the PMSG control is designed to ensure that each time the wind speed varies; a proportionate amount of current is demanded on the PMSG stator to ensure the torque and rotor speed are controlled to passively track maximum power points.

Figure 6-30 shows the wind speed profile applied to the AVEM during the simulation and experiment. It is a variable wind speed profile with a minimum value of about 7m/s and a maximum of 12m/s and serves as input to the wind turbine model. While Figure 6-30 (a) is applied to the experimental test rig, Figure 6-30 (b) is applied to the simulation model. The dynamic performance of the AVEM to track maximum power and estimate energy output was investigated.

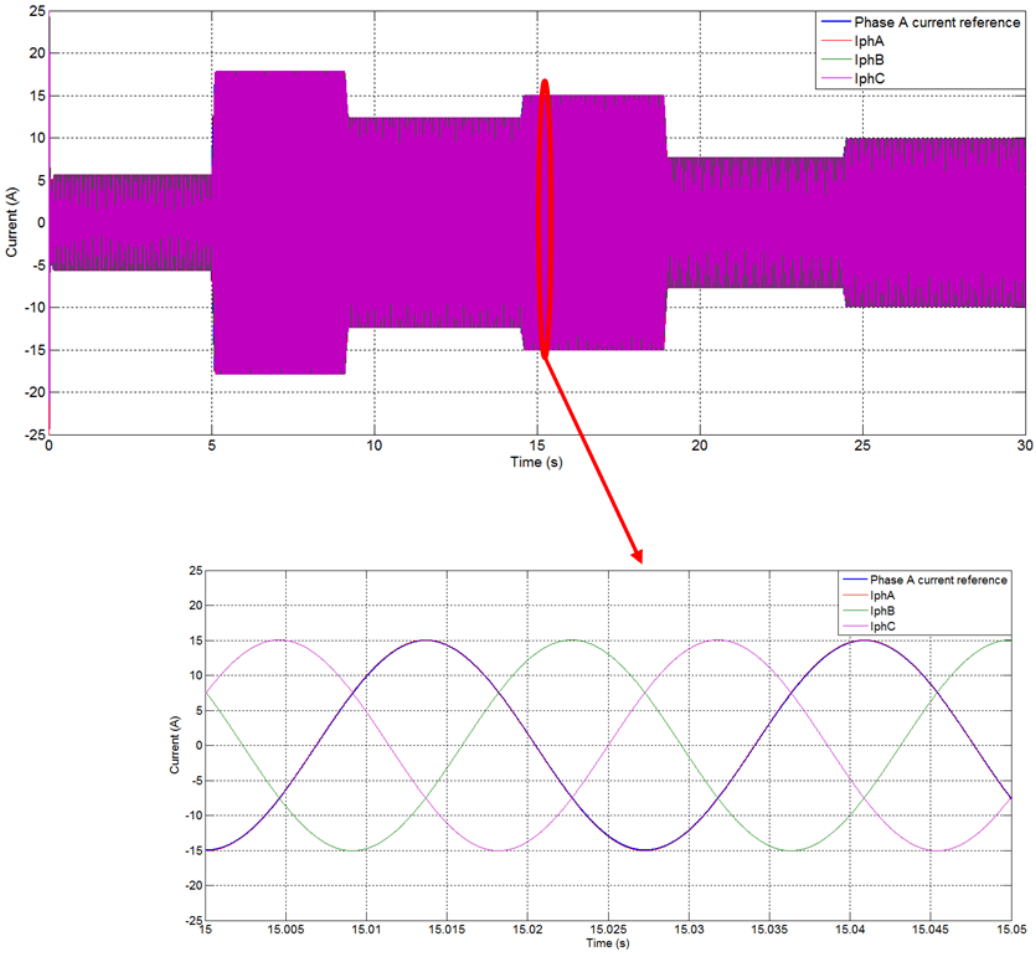

Figure 6-31: Simulation of PMSG stator current under the passive MPPT control using AVEM

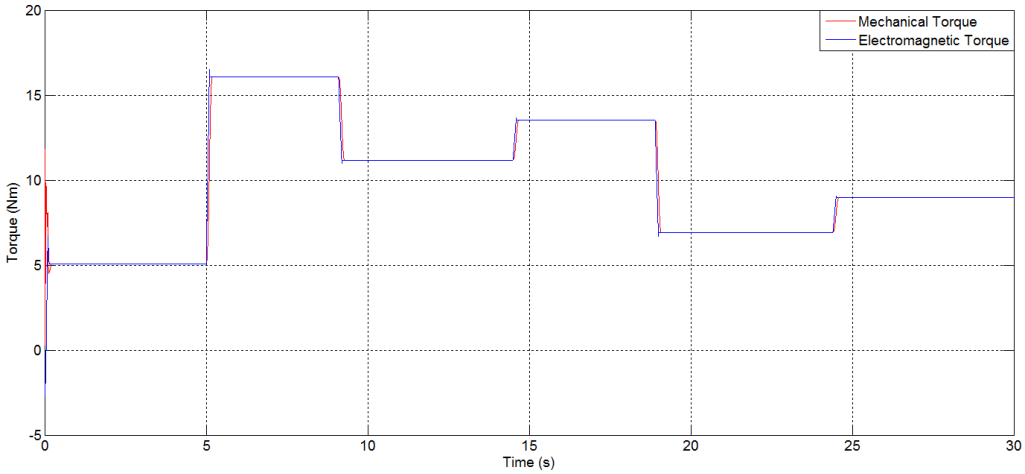

Figure 6-32: Simulation of mechanical and electromagnetic torque under the passive MPPT control using AVEM

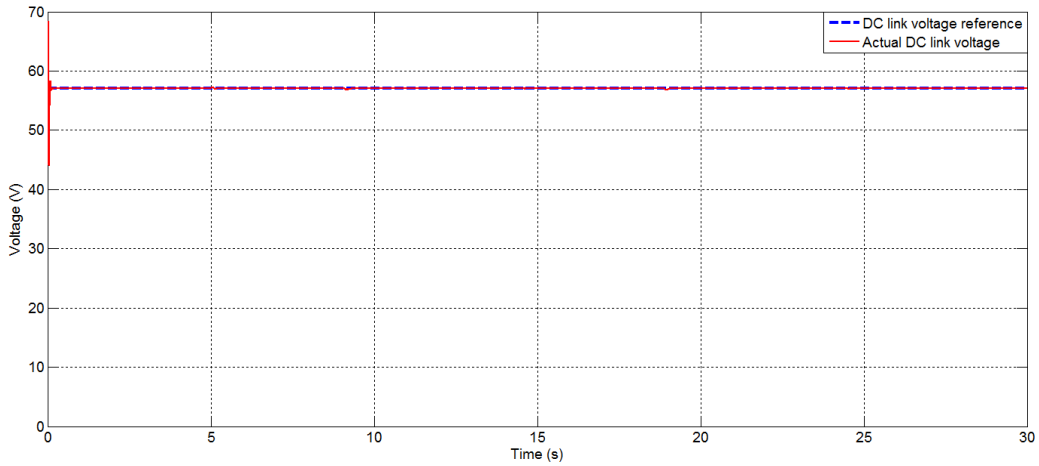

Figure 6-33: Simulation of DC link voltage under the passive MPPT using AVEM

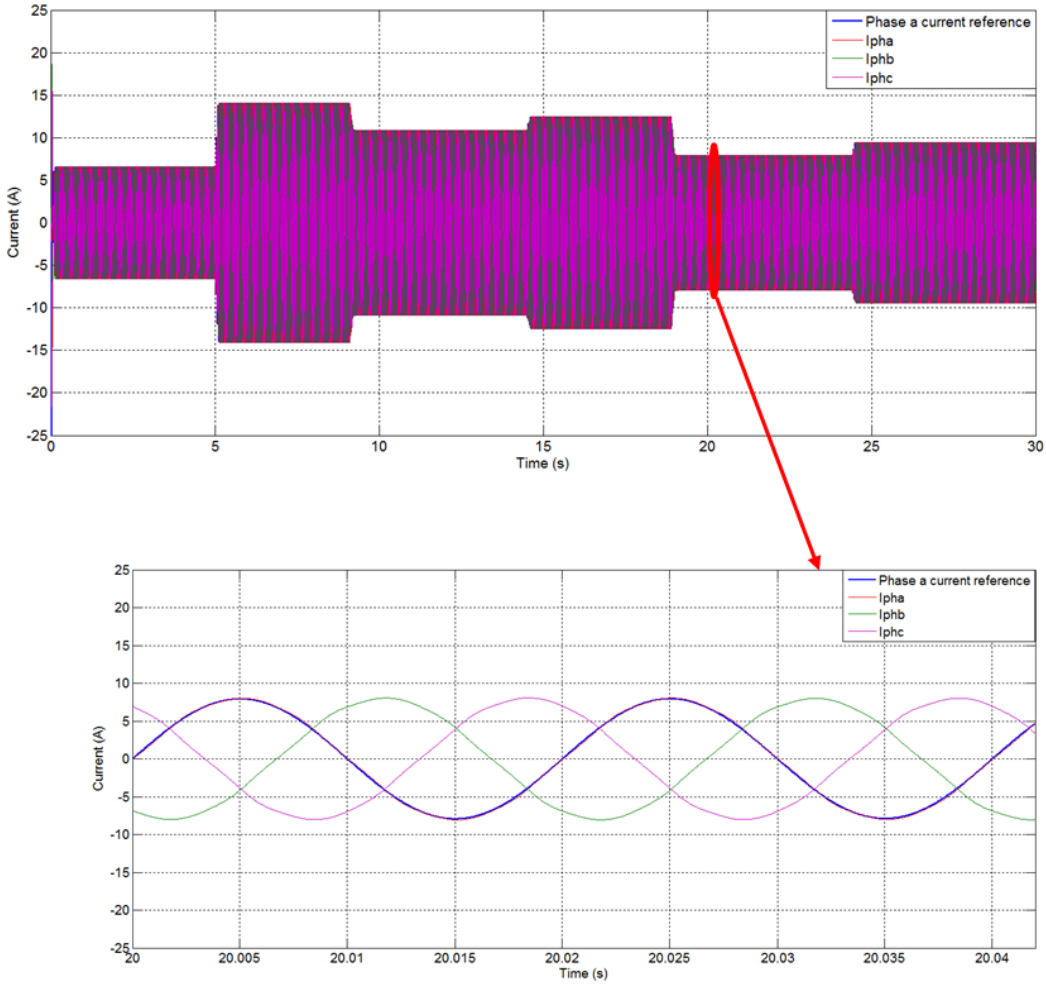

Figure 6-34: Simulation of AC Load side current under the passive MPPT using AVEM

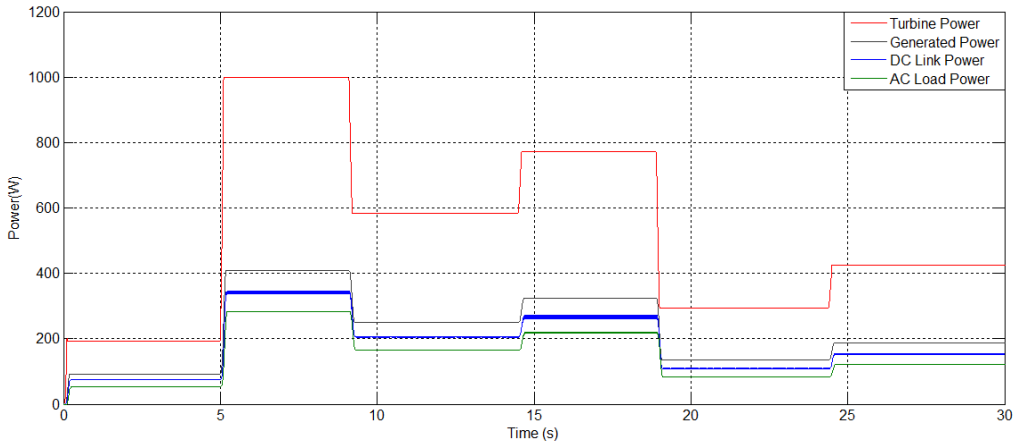

Figure 6-35: Simulation of the wind energy conversion system power under the passive MPPT

Figure 6-31 – Figure 6-35 show the simulation performance of the AVEM and the ability of the passive MPPT control technique to track maximum power as the wind speed varies. Figure 6-31 shows the prediction of the AVEM and the dynamic performance of the control technique in which the PMSG stator current is controlled to track the waveform and amplitude of the reference current in order to generate negative electromagnetic torque which balances the mechanical torque and generates maximum power. It can be seen that, the current demand of the generator varies as wind speed varies, for example, between the periods of 1-5s (1-50 seconds for experiment), when the wind speed is 7m/s, for maximum power to be extracted, the current demand on the generator was 5A peak. As soon as the wind speed changes from 7m/s to 12m/s between 5s and 9.1s (50-91seconds for experiments), the control technique responded and demanded a current of 19A peak from the generator track the maximum power as shown in Figure 6-31. The dynamic performance of the control technique in controlling the PMSG stator current to track the waveform of the reference current is shown in the electromagnetic torque as shown in Figure 6-32. The PMSG generates a negative electromagnetic torque equal in magnitude to the mechanical torque based on equation 6.21 due to current control establishing a point of equilibrium between the torques where maximum power is extracted. However, the electromagnetic torque so produced is negative; it is represented on the positive axis of Figure 6-32 for the purpose of clarity.

Figure 6-33 shows the DC link voltage as the wind speed varies. Irrespective of the variation in wind speed, for example from 7m/s to 12m/s between 1s to 5s, the DC voltage remains constant at the reference value of 57V generating a fixed frequency of 50Hz phase current to the AC load shown by the zoomed section of Figure 6-34. This is one important requirements of any wind energy conversion system which generated power is required to be utilise by conventional AC loads or connected to the grid (in addition it needs to be synchronised to the connecting grid as well).

Figure 6-35 shows the wind energy conversion system simulated amount of power that has been extracted from the turbine, generated by the generator and delivered to the AC load as the wind speed varies. The primary aim of the PMSG control technique of is to extract as much power as possible from the wind. It can be seen that the when the wind speed was 7m/s between 1s to 5s, the generator is controlled to track maximum turbine power of 190W, generated power of 91W, DC link power of 73W and the power delivered to the AC load of 54W while between the time interval of 5s to 9.1s when the wind speed changes to 12m/s the controller tracks the electromagnetic torque and produce maximum turbine power of 989W, generated power of 411W, DC link power of 345W and the power delivered to the AC load of 291W.

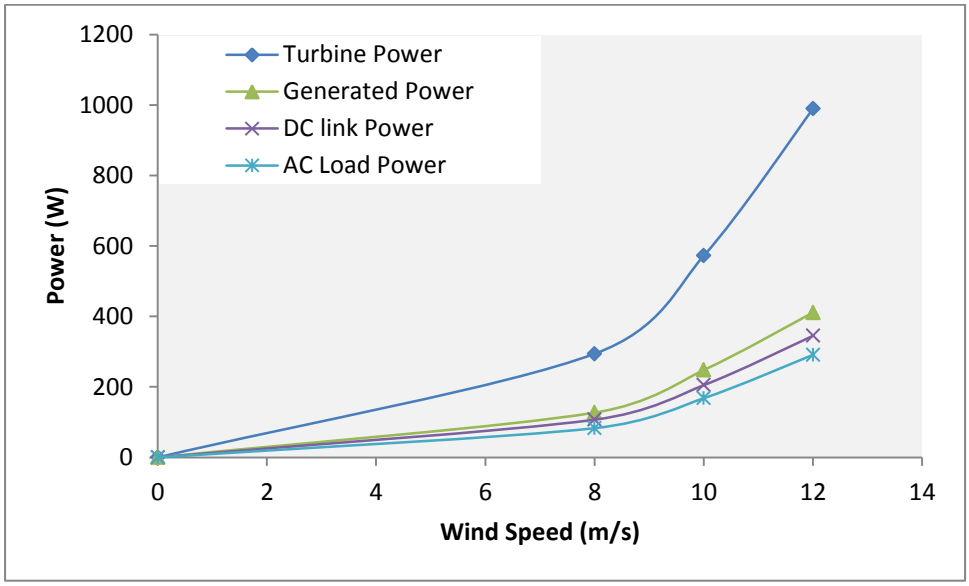

Figure 6-36: The wind energy conversion system power at different wind speeds under the passive MPPT control technique

Figure 6-36, shows the maximum power points obtained from the simulation of the AVEM under the MPPT control technique at various wind speeds. It can be seen that up to the rated wind speed of 12m/s, the maximum power points are tracked at each wind speed. From Figure 6-36, analysis of losses and efficiency of the wind energy conversions system under investigation can be obtained as shown in Figure 6-37. As the maximum power point is tracked so are the losses as the wind speed varies. It can be seen that for this particular WECS, the PMSG contributed the larger portion of the losses with a maximum value of 92W at 12m/s while the GSC generated maximum losses of 66W and the LSC generated 54W losses. It is also observed that the efficiency of each of the components and the total system vary as wind speed varies with the system's total efficiency at maximum value of 71% at 12m/s typical of small machines.

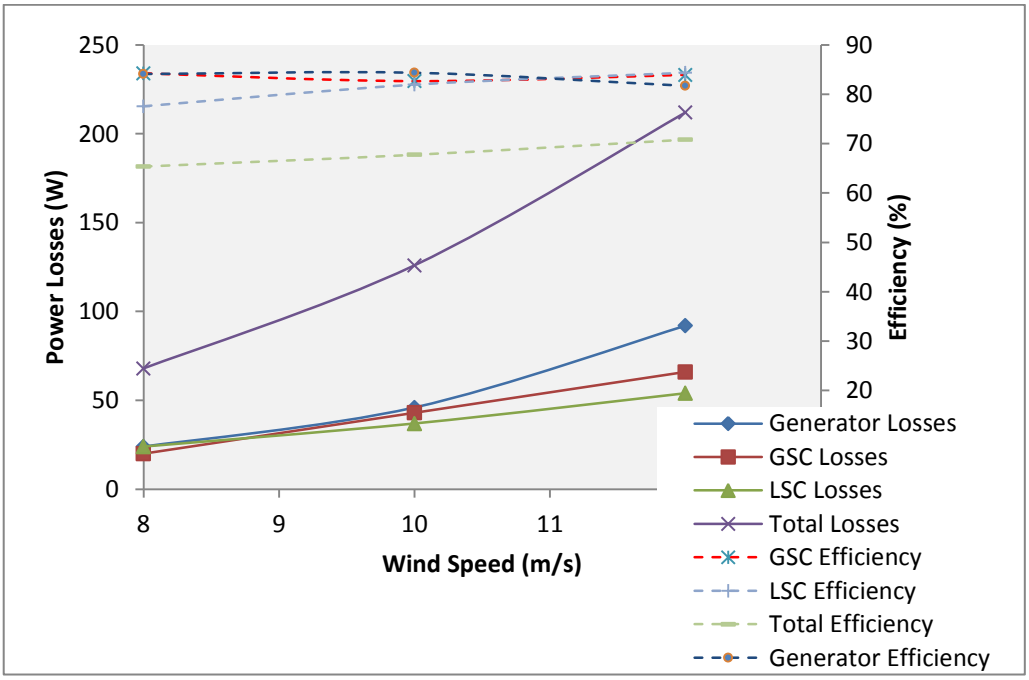

Figure 6-37: The wind energy conversion system power losses and efficiency at different wind speeds under the passive MPPT control technique

These results validate the performance accuracy of the control technique in tracking maximum power points and the ability of the proposed AVEM of WECS to implement the control technique. The conclusion being that it can be used in the simulation and analysis of a maximum power point tracking control technique, power, losses and efficiency of variable speed WECS.

6.5.9 Performance Comparison between WECS Energy Output Estimation using AVEM Simulation and DSP-based AVEM Method against Standard Calculation

In the performance analysis of WECS, accumulation of power over time (energy) is considered as the wind speed varies. Two case studies were investigated to validate the proposed DSP-based energy estimation method, the first one is when a constant torque is demanded from the PMSG as wind speed varies and the second is when different torque (current reference) under MPPT control technique is demanded from the PMSG as the wind speed varies. Figure 6-38, shows the simulation of the WECS energy output showing the amount of energy generated by the PMSG and fed to the AC load at various wind speeds and under the control technique capable of tracking maximum power. As stated earlier, the energy at each wind speed when multiplied by a factor of 10 equals the prediction of the calculated energy of the WECS. Such results obtained from the simulation are compared with the calculated and the DSP-based AVEM approach energy in Table 6-2 and Table 6-3.

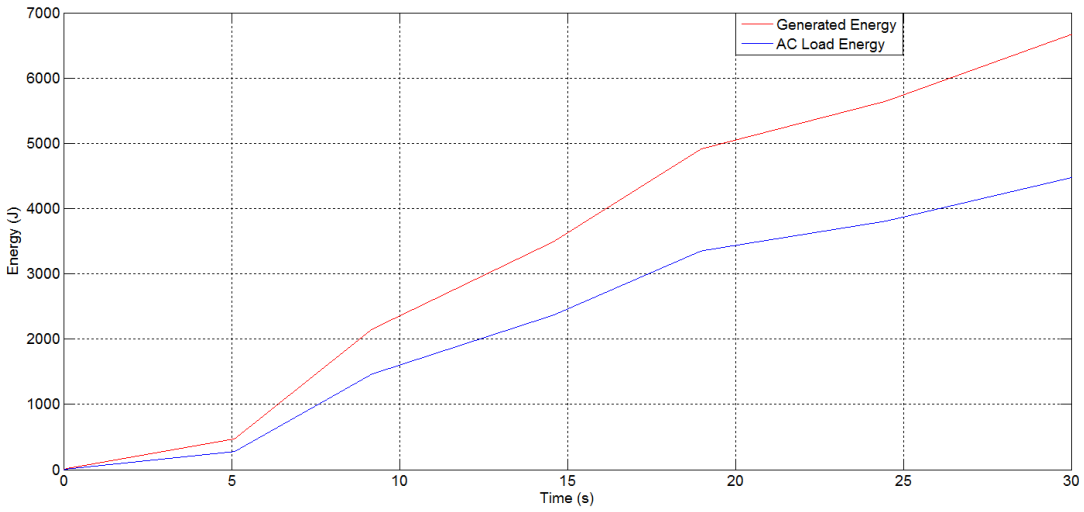

Figure 6-38: Simulation of PMSG wind energy conversion system Energy output using AVEM under the passive maximum power point tracking control technique

Table 6-2: Comparison between WECS Energy estimation using standard calculation, DSP-based AVEM method and AVEM simulation under variable wind speed and constant PMSG torque demand

Wind Speed (m/s)	Time Duration (s)	Generator				AC Load			
		Measured Power (W)	Calculated Energy (J)	DSP-based AVEM Energy Estimation (J)	AVEM Energy Estimation Simulation (J)	Measured Power (W)	Calculated Energy (J)	DSP-based AVEM Energy Estimation (J)	AVEM Energy Estimation Simulation (J)
0	0	0	0	0	0	0	0	0	0
7	50	77	3850	3700	4047	48	2400	2600	2642
12	41	207	8487	9000	9105	153	6273	6400	6532
10	54	164	8856	8900	8823	115	6210	6320	6063
11	44	189	8316	8500	8330	135	5940	6300	5858
8	55	107	5885	5600	6210	71	3905	4200	3952
9	56	134	7504	7500	7581	93	5208	5400	5046
Total	**300**		**42898**	**43200**	**44096**		**29936**	**31220**	**30093**

Table 6-3: Comparison between WECS Energy estimation using standard calculation, DSP-based AVEM method and AVEM simulation under variable wind speed and the passive MPPT control

Wind Speed (m/s)	Time Duration (s)	Generator				AC Load			
		Measured Power (W)	Calculated Energy (J)	DSP-based AVEM Energy Estimation (J)	AVEM Energy Estimation Simulation (J)	Measured Power (W)	Calculated Energy (J)	DSP-based AVEM Energy Estimation (J)	AVEM Energy Estimation Simulation (J)
0	0	0	0	0	0	0	0	0	0
7	50	78	3900	3900	4109	48	2400	2700	2642
12	41	425	17425	16100	16398	281	11521	12000	10608
10	54	244	13176	12100	12896	167	9018	9600	8533
11	44	332	14608	13300	14155	223	9812	10000	9771
8	55	121	6655	6200	7213	76	4180	4700	4539
9	56	181	10136	9200	10391	118	6608	7200	6750
Total	**300**		**65900**	**60800**	**65162**		**43539**	**46200**	**42843**

Table 6-2 and Table 6-3 show comparisons between the energy output of the WECS by the standard calculation method, the proposed DSP-based AVEM method and the energy output obtained by the simulation of the AVEM with variable wind speed from 7m/s to 12m/s for a) constant PMSG torque demand and b) the passive maximum power point tracking. In the standard calculation method, energy output is simply obtained by the product of the measured power and the length of time, while for the DSP-based AVEM method it is calculated based on the approach described in section 6.5.7 and section 6.5.8. Thus, energy output is compared at the same wind speed. From the tables, it can be

seen that the energy output variation with variable wind speed from 7m/s to 12m/s are similar to each other for the standard calculation method, DSP-based AVEM method and simulation with a maximum error of 8% which is within acceptable limits. From Table 6-2 and Table 6-3, a comparison is shown that variable speed with different PMSG torque demand during the passive MPPT control results in an increase in energy yield of about 45-50% in this case study compared to operating at constant PMSG torque demand. The results show that the AVEM can be implemented in practical situations using real time DSP controller and can be used as an alternative approach to estimating energy output of a WECS and any other three-phase system.

6.6 Conclusion

The average voltage estimation modelling of full scale back-back voltage source converter for variable speed PMSG wind energy conversion system has been developed as well as the detailed switching model. The average voltage estimation model eliminates the use of the back-back VSC and the switching actions of the transistors and diodes while the switching model considers the switching characteristics of the transistor and diodes. The detailed description of the generator side AVEM and the AC Load side AVEM have been presented along with the modelling of the DC link voltage considering that the DC link and capacitor have also been eliminated. The voltage source inverter losses were also modelled and incorporated into the AVEM to enable accurate prediction of power at each point of the WECS. In addition, methods to estimate the DC current at the generator side and AC load side from the control strategy duty cycles and instantaneous phase currents were described. This allows the DC link voltage to be accurately modelled. The chapter further presented a complete simulation of AVEM and switching model for a small scale wind turbine (1kW). The generator side and the AC load side control based on sinusoidal PWM PI current control strategy were also developed. The generator side controller controls the generator speed and torque while the AC load side controls the DC link voltage. Simulation of the models was carried out using the PORTUNUS package based on the requirements of each simulation modelling method and the results validated. The switching model and the experimental results were used as benchmarks against which the results of the AVEM were validated. The validation is first aimed at the steady state performance and ability of the model to

control the torque of the generator to reproduce the power and torque speed characteristics of the wind turbine at different wind speed. The turbine power predicted by simulation of AVEM was compared with the prediction of the switching model and results from the experimental test rig at different wind speeds such as 8m/s, 10m/s and 12m/s. The results validated the accuracy of the AVEM in reproducing the same power/speed and torque/speed curve of the wind turbine. However differences were observed at higher rotor rotational speed, where the experimental power speed curve shows an overestimated power which is due to the difference in the parameters and losses of the PM machine used in the simulation models and the experimental test rig.

The chapter also presented a detailed validation of the AVEM, where mechanical power, the generated power, DC link power and the power delivered to the AC load versus rotational speed at different wind speed were validated against the switching model and experiment. The aim is to verify the ability of the AVEM to accurately reproduce the power speed curve and ensure the correct direction of power flow. Again the results of the comparison validate the performance of AVEM reproducing the power versus speed curve and the right direction of power flow from the generator to the AC load. A consistent trend of overestimation of experimental power at high rotational speed is found with all the powers at each wind speed. Further to this, the validation of the losses in the PMSG, GSC and LSC predicted by the AVEM against the experimental are presented for 8m/s, 10m/s and 12m/s. the analysis of the results validates the AVEM in predicting the same profile of losses versus rotor speed against the experimental results with a very good level of accuracy at 12m/s. The chapter also presented the comparison of the simulation execution time between the AVEM and switching model where with the same simulation set time the AVEM completed a simulation approximately 50 times faster compared to the switching model.

In addition to the analysis and validation of powers, losses and efficiency versus rotor rotational speed of the WECS at different wind speed of the proposed AVEM, a passive MPPT control strategy to track maximum power was developed. The control technique based on controlling the electromagnetic torque of the PMSG to generate maximum power at various wind speeds is presented. Based on the variable wind profile input to the AVEM model, the performance of the control as well as complete analysis of the power, losses and efficiency was presented and results investigated. Also presented in

this Chapter is the practical implementation of AVEM, where the AVEM was applied to the estimation of energy yield of the complete WECS. A practical real time DSP controller based AVEM for a WECS energy estimator was also presented. A variable wind speed profile was applied to the model and simulation conducted on the AVEM. Simulation energy estimation results were presented and compared with experimental measured energy and DSP controller estimated energy. The results of the energy estimation using AVEM simulation agrees with the DSP controller AVEM energy estimation and the calculated energy, this again validates the effectiveness of the AVEM performance accuracy under dynamic conditions and its practical implementation using DSP controller providing an alternative approach to estimate energy output, hence it can be used to analyse different performance aspects of variable speed PMSG WECS and control strategy design process.

Chapter 7

7 Conclusion and Future Work

In this thesis alternative, faster simulation models for the analysis of voltage source inverter–fed PMSM drive systems, and variable speed PMSG wind energy conversion systems were developed and validated against the standard switching models using identical control strategies. The motivation for developing these models was to optimise, i.e. accelerate, the design process when incorporating PM machines into complete electromechanical system simulation models. The existing switching model and average value models were analysed in order to apply a different approach to modelling the VSI in PMSM drive where the slow dynamics of the mechanical system were taken into consideration.

A detailed description of all the components of a permanent magnet synchronous machine drive and the analysis of existing modelling methods of variable speed PMSM drive systems and PMSG wind energy conversion systems were presented in chapter 2. These are the detailed switching model and the average value model. The switching model is an established standard and accurate modelling approach which has been widely used, but its simulation is time consuming due to the restricted minimum time step requirement to achieve the necessary resolution of the PWM control. On the other hand, the existing average value model based on state space averaging guarantees fast simulation of VSI fed-PM machine drive systems. However, it is complicated and requires complex computation and transformation from three phase reference to rotating reference frame which in most cases requires additional circuitry such as filters, inductors and capacitors. In addition it requires transformation from rotating reference frame back to three phase reference if it must be applied to a three phase system. Another modelling approach, the mathematical equivalent also guarantees fast simulation but it is purely mathematical and does not consider the slow dynamic interaction of the machine and the voltage source inverter. Considering these drawbacks a new approach to modelling of the voltage source inverter that will totally eliminate the voltage source inverter switching actions and modulation was developed and integrated into the PMSM drive system. The modelling method is called the Average Voltage Estimation Model (AVEM). The model estimates the average voltage per phase based on the switching

function of three phase VSI, control strategy and DC link voltage over the switching period and uses the estimated voltage as a piece-wise linear function to drive voltage sources connected to the phases of the PMSM. The advantages are its simplicity, no complex computational transformation, no additional circuitry, it is fast and retains all the characteristics of the existing control strategy and it produces three phase sinusoidal current waveforms and accurate non sinusoidal waveforms at high speed.

The development of average voltage estimation model of PMSM drive system is presented in Chapter 3. The derivation of the switching modelling voltage and current equations based on switching functions and the proposed AVEM were given. This derivation contributes to the understanding of the principles of the switching model and exposes the simplicity in the derivation of the proposed AVEM. Another important part of the AVEM is the three phase voltage source inverter IGBT loss model. The VSI loss model was developed and incorporated in the AVEM enabling the AVEM to have additional advantages such as power input, power output and efficiency analysis as well as analysis of losses and characterisation of the voltage source inverter. The interesting part of the AVEM is the implementation of the PI current control and speed control strategy without the PWM modulators. The performance of the model was verified by comparison of the time domain simulation results with the switching model.

The AVEM of a PMSM drive, and a PMSG wind energy conversion system were verified against the associated switching models and experimental test. The complete experimental set up of a PMSM drive system and PMSG wind energy conversion system is achieved with one test rig described in chapter 4. The test platform was implemented with a small fractional horse power 1kW multi pole permanent magnet synchronous machine. The experimental results confirm the correct operation and emulation of wind energy conversion system and the results were used to validate the prediction of the AVEM through the switching model. A very important aspect of the experimental tests is the practical application of the AVEM to the estimation of the WECS energy yield which allows for direct validation of the AVEM with experimental results.

In Chapter 5 an expanded performance validation of the AVEM is presented against the switching model and experimental results over the operating speed range for the PM machine under investigation. This is based on the view that the best approach to determine the accuracy of a new model is to validate against existing standards such as

the detailed switching model and experimentation. Validation of performance characteristics include reproducing the torque versus speed curve, power, efficiency and losses associated with a typical drive system. The AVEM simulation model results were compared with the switching model and experimental results in constant torque and field weakening regions using PI current and speed control strategies. The results validate the performance accuracy of the AVEM in predicting the performance characteristics of the drive system. However, where there is loss of accuracy at higher speed, methods to enhance the accuracy of the models were outlined. Finally, chapter 5 presents a comparison of the simulation execution time of the AVEM against the switching model and the AVEM is found to be faster than the switching model by a factor of **50 to 70**.

Chapter 6 presents an extension and modification of the AVEM of single three phase voltage source inverter to a full scale back to back three-phase VSC incorporated in a variable speed PMSG wind energy conversion system. The details of the development of the average voltage estimation model and switching model with a variable speed PMSG wind energy conversion system have been presented. The complete model consists of the wind turbine model, the generator model, and the full scale back-back AVEM, the DC link model and the AC load model, the generator side control and the AC load side control. The generator side controller controls the speed and torque of the generator and the AC load side maintained a constant DC voltage and supplies a fixed frequency AC current to the AC load. The realisation of the AVEM in a complete WECS without the DC link capacitor but with the inclusion of a VSI loss model which guarantees accurate power prediction and power flow direction from the wind turbine to the AC load is a significant achievement. The inclusion of the loss model enables simulation, validation and analysis of the performance characteristics at different points of the WECS. The chapter presents a detailed comparison of the power versus speed curve, torque versus speed, efficiencies and losses predicted by the simulation models and the experimental wind turbine emulator. In addition, the simulation execution time of the AVEM was compared with the switching model. The results presented validate the steady state performance accuracy of the AVEM of variable speed WECS with simulation execution times in the region of **50 times** faster than the switching model. The analysis of the results had shown where accuracies are less and outlined methods to further enhanced the accuracy of the AVEM. Chapter 6 also presents the development of a passive MPPT control technique to track maximum power at various wind speeds and the practical

implementation of the AVEM in a WECS using a DSP controller and its application to calculate energy output of the wind energy conversion system. The DSP based AVEM and simulation of WECS energy yield prediction were compared with calculated energy at constant torque and different torque demand (MPPT) on the PMSG. The results of the DSP based AVEM and simulation of WECS energy output estimation is quiet close to the calculated energy with the energy yield of different torque demand higher than that of constant torque demand which is what is expected. This verifies the ability of the AVEM to implement MPPT control technique and provides an alternative method of calculating energy output of a three phase system using control strategy duty cycles.

Thus the thesis shows the process and development of the faster simulation model for voltage source inverter-fed permanent magnet synchronous motor and generator drive system where the VSI switching transistors and diodes and PWM modulators are totally eliminated. The AVEM has shown promise and can be used to rapidly simulate, analyse and investigate steady state performance of any electrical drive system and control strategies in the complete system design process. However, its application can be extended to transient analysis.

7.1 Future Work

The average voltage estimation model is a different approach to modelling and simulation of voltage source inverter-fed machine drive systems. Based on this, there is need to further develop and enhance the accuracy of the model. In addition, in the course of the research it is observed that there are some differences between the simulation models and the experimental tests where there is over estimation of torque, and power at higher operating speeds which suggest differences in loss considerations. In order to fully investigate these differences, future plans are to expand the scope of the validation of the AVEM to include different motors, generators and VSI devices in the model and experimental set up. Presently, the model is implemented with sinusoidal PI current controllers. There is a need to widen the application of the AVEM to analyse other control strategies such as space vector and direct torque control. Vector control provides independent control of permanent magnet synchronous machine torque and magnetic field. This is achieved with the popularly known field oriented control (FOC).

In FOC, the stator current is transforms into two components; the torque and magnetic flux producing components. By controlling the torque producing component of the stator current, the torque can be controlled to the desired value. The advantage of vector control is the elimination of the time and position dependencies associated with other types of controls and effective real time control of torque, generator speed and stator current with reduced torque ripple and better performance, especially in the region between constant torque and constant power.

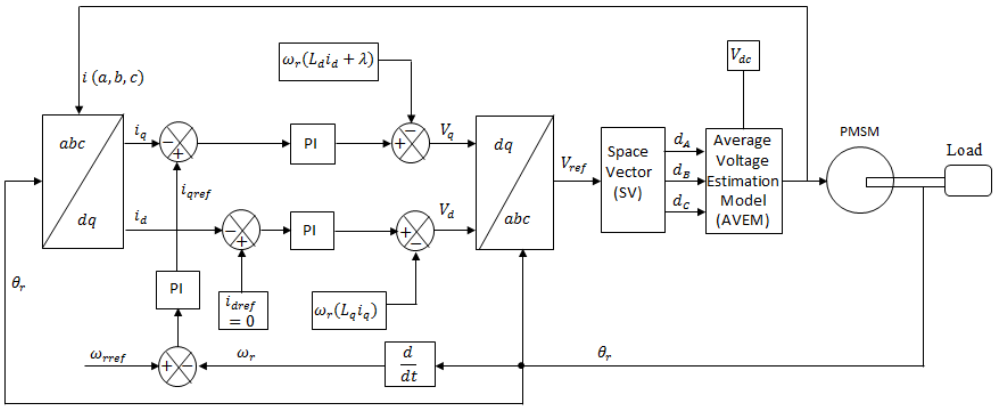

Figure 7-1: Block diagram of a typical Field Oriented (Vector) Control with proposed AVEM of PMSM drive system

Figure 7-1 shows a typical FOC of PMSM which can also be applied to the control of PMSG current and torque. The basic idea is to transform a non-rotating three-phase current into a two coordinate rotating system dq in order to eliminate the dependency of the torque on the position of the rotor flux using Park and Clark transformations. To achieve this, the dq coordinate rotate with the rotor flux electrical speed and the d-axis is aligned with the rotor flux electrical position. The torque is then controlled by the quadrature current, i_q. Since the permanent magnet continuously provides the excitation flux which is the role of the i_d, it is not necessary to control i_d and in most cases it equated to zero except when there is need for field weakening. In field weakening, where higher speed/power operation is required, allocating a value that is not zero to i_d will result in a magnet flux which opposes the flux generated by the permanent magnets thereby increasing the speed range of the PMSM. One of the disadvantages of field weakening using i_d is that it could result in demagnetisation of the rotor magnets (high heat generation). The implication therefore is that the torque producing capability and efficiency of the magnets will be reduced. As seen in Figure 7-1, the Clark and Park co-

ordinate transformation of the three-phase current realises the dq current in rotating frame. The dq currents are compared with the dq reference currents and regulated by PI current controllers. The torque is indirectly controlled by i_q with the outer speed control loop providing the i_q reference. The Inverse Park transforms the output of the current controllers and results to voltage vectors which are usually used to generate switching sequences and duty cycles by SVPWM which could then be used by a average voltage estimation model to estimate the average phase voltage in the three phases in each switching cycle in much the same manner as that implemented for the PI current controllers.

As a substitute for switching model, the application of the AVEM model requires to be widely tested. The AVEM will further be expanded and applied to different variable speed configurations such as one three phase VSI, dual parallel PMSM, two parallel three phase VSI, one PMSM and parallel back-back VSC with a single PMSG wind energy conversion system.

Finally, future plans are to apply the AVEM to other variable speed drive systems such as the induction motor, the doubly fed induction generator (DFIG), the switched reluctance motor, and other electrical machine variable speed drive systems.

References

[1] Mike Bilkey and Burt Judson, "Replacement of Mechanical PIV's by AC Drives Off Machine Coater Rebuild - Lineshaft to Sectional," Conference Record of the Annual Pulp and Paper Industry Technical Conference, pp 31-36, 27 June-1 July 2004.

[2] Robbie McELVEEN, Keith Lyles, Bill Martin and Wayne Wasserman, "Reliability of Cooling Tower Drives: Improving efficiency with New Motor Technology," IEEE Industry Applications Magazine, Vol. 18, No.6, pp 12-19, Nov. – Dec. 2012.

[3] Karl J. Strnat "Modern Permanent Magnets for Applications in Electro-Technology," Proceedings of the IEEE, Vol. 78, No. 6, pp 923-946, June 1990.

[4] Gianmario Pellegrino, Radu Iustin Bojoi and Paolo Guglielmi, "Unified Direct-Flux Vector Control for AC Motor Drives," IEEE transactions on industry applications, Vol. 47, Issue 5, pp 2093-2102, Sept.-Oct. 2011.

[5] Matthias Preindl and Silverio Bolognani, "Model Predictive Direct Speed Control with Finite Control Set of PMSM Drive Systems," IEEE Transactions on Power Electronics, vol 28, issue 2, pp. 1007-1015, September, 2012.

[6] Manu Jain1, Mukhtiar Singh, Ambrish Chandra, and Sheldon S. Williamson, "Sensorless Control of Permanent Magnet Synchronous Motor using ANFIS Based MRAS," IEEE International Electric machine & drives conference (IEMDC), Niagara Falls, ON, pp 599-606, 15-18 May 2011.

[7] Youssef. Errami, Mohamed Maaroufi and Mohammed. Quassaid, "Maximum Power Point Tracking Strategy and Direct Torque Control of Permanent Magnet Synchronous Generator Wind Farm," 2012 International Conference on Complex System (ICCS), pp 1-6, 5-6 Nov. 2012.

[8] Maitane Aguirre, Patxi Madina, Javier Poza, Aitor Aranburu, Txomin Nieva, "Analysis and Comparison of PWM Modulation Methods in VSI-Fed PMSM Drive Systems," XXth International Conference on Electrical Machines (ICEM), Marseille, pp 851-857, 2-5 Sept. 2012.

[9] Faa-Jeng Lin, Ying-Chih Hung, Jonq-Chin Hwang, and Meng-Ting Tsai, "Fault-Tolerant Control of a Six-Phase Motor Drive System Using a Takagi–Sugeno–Kang Type Fuzzy Neural Network With Asymmetric Membership Function," IEEE Transactions on Power Electronics vol 28, Issue 7, pp 3557-3572, 10 November, 2012.

[10] Anurag Singh Tomer and Satya Prakash Dubey, "Performance Analysis of Two Inverter Fed Six Phase PMSM Drive," Nirma University International Conference on Engineering (NUiCONE), Ahmedabad, pp 1-5, 28-30 Nov. 2013.

[11] Bimal K. Bose, "A high-performance Inverter-Fed Drive System of an Interior Permanent Magnet Synchronous Machine," IEE Transactions on Industry Applications, Vol. 24, No. 6, pp. 987-997, November, 1988.

[12] Pragasan Pillay and R. Krishnan, "Modeling of Permanent Magnet Motor Drives," IEEE Transactions on Industrial Electronics, Vol 35, No. 4, pp. 537-541, November 1988.

[13] Bernard Hebert, Yves Dube and Hoang Le-Huy, "Digital Simulation of a Smooth Positioning System with Parameter Estimation," IEEE Conference Records of the Industry Applications Society Annual Meeting, Pittsburgh, PA, USA, Vol. 1 pp. 562 – 565, 2-7 Oct. 1988.

[14] Araz Darba, Mohammad Esmalifalak and Ebrahim Sarbaz Barazandeh, "Implementing SVPWM technique to Axial Flux Permanent Magnet Synchronous Motor Drive with Internal Model Current Controller", The 4th International Power Engineering and Optimization Conference (PEOCO2010), Shah Alam, Selangor, MALAYSIA, pp. 126-131, 23-24 June 2010.

[15] Roberto Morales-Caporal, Edmundo Bonilla-Huerta, Marco A. Arjona and Concepción Hernández, "Sensorless Predictive DTC of a Surface-Mounted Permanent-Magnet Synchronous Machine Based on Its Magnetic Anisotropy" IEEE Transactions on Industrial Electronics, Vol. 60, No. 8, pp 3016-3024, August 2013.

[16] Wei Xie, Fengxiang Wang, Xiaocan Wang, Gurakuq Dajaku, Dieter Gerling and Ralph Kennel, "Analysis of High Efficiency and Low Cost Drive System of IPMSM by Using Two-Steps Model Predictive Torque Control", Proceedings of the 32nd Chinese control conference, X'an, China, pp 4114-4119, July 26-28, 2013.

[17] Fei Wang, Cheng Chang and Boqiang Liu, "Analysis of PMSM Control Performance Based on the Mathematical Model and Saturated Parameters," IEEE Conference and Expo Transportation Electrification Asia-Pacific (ITEC Asia-Pacific), Beijing, pp 1-5, August 30, 2014 –Sept 3, 2014.

[18] Selin Ozcira, Nur Bekiroglu and Ibrahim Senol, "Dynamic Performance and Analysis of Direct Torque Control Method Based on DSP for PMSM Drives," International Conference on Renewable Energy Research and Applications (ICRERA), Nagasaki, pp 1-5, 11-14 Nov. 2012.

[19] Narayan Prasad Gupta and Preeti Gupta, "Performance Analysis of Direct Torque Control of PMSM Drive using SVPWM – Inverter," International Conference on Communication Systems and Network Technologies (CSNT), Rajkot, pp. 825-829, 111-13 May, 2012.

[20] WANG Lei, HAO Shuanghui, HAO Minghui and SONG Baoyu, "A Hybrid PWM Strategy Combining Modified Space Vector and Sinusoidal Pulse Width Modulation Methods," Proceeding of the 11th World Congress on Intelligent Control and Automation, Shenyang, China, pp 4431-4434, June 29 - July 4 2014.

[21] Lijun He, Yongdong Li and Ronald G. Harley, "Adaptive Multi-mode Power Control of a Direct-Drive PM Wind Generation System in a Microgrid," IEEE Journal of Emerging and Selected Topics in Power Electronics, Vol. 1, No. 4, pp. 217-225, DECEMBER 2013.

[22] Jaswant Singh, Bindeshwar Singh, S. P. Singh and Mohd Naim, "Investigation of Performance Parameters of PMSM Drives using DTC-SVPWM Technique," Students Conference on Engineering Systems (SCES), Allahabad, Uttar Pradesh, pp 1-6, 16-18 March 2012.

[23] Luca Papini, Tsarafidy Raminosoa, David Gerada, and Chris Gerada, "A High-Speed Permanent-Magnet Machine for Fault-Tolerant Drivetrains," IEEE TRANSACTIONS ON INDUSTRIAL ELECTRONICS, VOL. 61, NO. 6, pp 3071 – 3080, JUNE 2014.

[24] Fabio Genduso, Rosario Miceli, Cosimo Rando, and Giuseppe Ricco Galluzzo, "Back EMF Sensorless-Control Algorithm for High-Dynamic Performance PMSM," IEEE Transactions on Industrial Electronics, Vol. 57, No. 6, pp 2092-2100, June 2010.

[25] Jorge O. Estima, and Antonio J. Marques Cardoso, "Efficiency Analysis of Drive Train Topologies Applied to Electric/Hybrid Vehicles," IEEE Transactions on Vehicular Technology, Vol. 61, No. 3, pp 1021-1031, March 2012.

[26] Kou Baoquan, Li Chunyan, and Cheng Shukang, "Flux-Weakening-Characteristic Analysis of a New Permanent-Magnet Synchronous Motor Used for Electric Vehicles," IEEE Transactions on Plasma Science, Volume: 39, Issue 1, pp 511-515, Jan. 2011.

[27] S. M. Muyeen, Rion Takahashi, Toshiaki Murata, and Junji Tamura, "A Variable Speed Wind Turbine Control Strategy to Meet Wind Farm Grid Code Requirements," Power Systems, IEEE Transactions on Volume: 25, Issue: 1, pp. 331 – 340, Feb. 2010.

[28] Hua Geng and Dewei Xu, "Stability Analysis and Improvements for Variable-Speed Multipole Permanent Magnet Synchronous Generator-Based Wind Energy Conversion System," IEEE Transactions on Sustainable Energy, Vol. 2, No. 4, pp. 459-467, October 2011.

[29] Shengwen Fan, Peng Wang and Chunxue Wen, "A New Sensorless Control Strategy used in Direct-drive PMSG Wind Power System," 2nd IEEE International Symposium on Power Electronics for Distributed Generation Systems (PEDG), Hefei, China, pp. 611-615, 16-18 June 2010.

[30] Deok-je Bang, Henk Polinder, Ghanshyam Shrestha and Jan Abraham Ferreira, "Comparative Design of Radial and Transverse Flux PM Generators for Direct-Drive Wind Turbines," 18th International Conference on Electrical Machines (ICEM), Vilamoura, pp 1-6, 6-9 Sept. 2008.

[31] Jiabin Wang, Weiya Wang, Kais Atallah, and David Howe, "Design Considerations for Tubular Flux-Switching Permanent Magnet Machines," IEEE Transactions on Magnetics, Vol. 44, No.11, pp 4026-4032, November 2008.

[32] Wei Hua, Ming Cheng, and Gan Zhang, "A Novel Hybrid Excitation Flux-Switching Motor for Hybrid Vehicles," IEEE Transactions on Magnetics, Vol. 45, No. 10, pp 4728-4731, October 2009.

[33] E. Sulaiman, T. Kosaka, and N. Matsui, "Design Optimization of 12Slot–10Pole Hybrid Excitation Flux Switching Synchronous Machine with 0.4kg Permanent Magnet for Hybrid Electric Vehicles," 8th International Conference on Power Electronics - ECCE Asia, (ICPE & ECCE) The Shilla Jeju, Korea, pp. 1913-1920, May 30-June 3, 2011.

[34] Jin Wang, Ronghai Qu, and Libing Zhou, "Dual-Rotor Multiphase Permanent Magnet Machine With Harmonic Injection to Enhance Torque Density," IEEE Transactions on Applied Superconductivity, Vol. 22, No. 3, ISSN: 1051-8223, June 2012.

[35] Adrian Augustin POP, Florin JURCA, Claudiu OPREA, Mihai CHIRCA, Stefan BREBAN and Mircea M. RADULESCU, "Axial-flux vs. radial-flux permanent-magnet synchronous generators for micro-wind turbine application," 15th European Conference on Power Electronics and Applications (EPE), Lille, pp 1-10, 2-6 Sept. 2013.

[36] Xubiao Wei, Kai Yang, Zhicheng Pan, Hongqin Xie, Cheng Zhu, Yingli Zhang, "Design of a Novel Axial-Radial Flux Permanent Magnet Motor," 2014 17th International Conference on Electrical Machines and Systems (ICEMS), Hangzhou, China, pp. 80-84, Oct. 22-25, 2014.

[37] Xiao Gong, Yanliang Xu, Wenxin Song, "Design of Novel Disc Transverse Flux Permanent Magnet Machine," 17th International Conference on Electrical Machines and Systems (ICEMS), Hangzhou, China, pp 1648-1651, Oct. 22-25, 2014.

[38] Bo Zhang, Torsten Epskamp, Martin Doppelbauer and Matthias Gregor, "A Comparison of the Transverse, Axial and Radial Flux PM Synchronous Motors for Electric Vehicle," IEEE International on Electric Vehicle Conference (IEVC), Florence, Italy, pp 1-6, 17-19 Dec. 2014 2014.

[39] Damien Bidart, Maria Pietrzak-David, Pascal Maussion and Maurice Fadel, "Mono Inverter dual parallel PMSM-Structure and Control," 34th Annual

Conference of IEEE Industrial Electronics, Orlando, FL, pp 268-273, 10-13 Nov. 2008.

[40] Ngoc Linh NGUYEN, Maurice FADEL, Ana LLOR, "A New Approach to Predictive Torque Control with Dual Parallel PMSM System," IEEE International Conference on Industrial Technology (ICIT), Cape Town, pp 1806-1811, 25-28 Feb. 2013.

[41] Zulkifilie Ibrahim, Jurifa Mat Lazi, Marizan Sulaiman, "Independent speed sensorless control of dual parallel PMSM based on Five-leg Inverter," 9th International Multi-conference on Systems, Signals and Devices (SSD), Chemnitz, pp 1-6, 20-23 March 2012.

[42] T V V S Lakshmi , Noby George, Umashankar S and Kothari D P, "Cascaded seven level inverter with reduced number of switches using level shifting PWM technique," International Conference on Power, Energy and Control (ICPEC), Sri Rangalatchum Dindigul, pp 676-680, 6-8 Feb. 2013.

[43] Ying Yan, Jianguo Zhu, Youguang Guo and Haiwei Lu, "Modeling and Simulation of Direct Torque Controlled PMSM Drive System Incorporating Structural and Saturation Saliencies," 41st IAS Annual Meeting, Industry Applications Conference, Tampa, FL, pp 76-83, 8-12 Oct 2006.

[44] Flah Aymen, Sbita Lassaad, "A new adaptive high speed control algorithm used for a FOC or a DTC PMSM drive strategies," 38th Annual Conference on IEEE Industrial Electronics Society (IECON), Montreal, QC, pp 4472-4476, 25-28 Oct. 2012.

[45] D.I Stroe, A.I Stan, I.Visa, I.Stroe, "Modeling and control of variable speed wind turbine equipped with PMSG," 13th world congress in mechanism and machine science, Guanajuato, mexico, 19-25 June 2011.

[46] Lakhdar Belhadji, Seddik Bacha, e tal.: Modeling and control of variable speed Micro-Hydropower plant based on Axial-flow Turbine and Permanent Magnet Synchronous Generator (MHPP-PMSG), 37th International Conference on IEEE Industrial Electronic Society (IECON), 2011, pp 896-901, (7-10 Nov; 2011).

[47] Zhipeng QIU, Keliang ZHOU, Yingtao LI, "Modelling and Control of Diode Rectifier Fed PMSG Based Wind Turbine," 4th International Conference on Electric Utility Deregulation and Restructuring and Power Technologies (DRPT), 2011, pp 1384-1388, (6-9 July, 2011)

[48] Youssef Errami, Mohamed Benchagra e tal, "Control Strategy for PMSG Wind Farm Based on MPPT and Direct Power Control," IEEE International Conference on Multimedia Computing and Systems (ICMCS), pp 1125-1130, (10-12 May, 2012).

[49] Bjarte Hoff and Waldemar Sulkowski, "Comprehensive Modeling and Practical Verification of Grid Connected VSI with LCL Filter," 15th International Power Electronics and Motion Control Conference (EPE-PEMC), ECCE Europe, Novi Sad, Serbia, pp. DS3f.7-1 – DS3f.7-7, 4-6 Sept. 2012.

[50] Sina Chiniforoosh, Hamid Atighechi and Juri Jatskevich, "Direct Interfacing of Dynamic Average Models of Line-Commutated Rectifier Circuits in Nodal Analysis EMTP-Type Solution," IEEE Transactions on Circuits and Systems 1: Regular Papers, Vol. 61, No. 6, pp 1892-1902, June 2014.

[51] Zhao Lin and Hao Ma, "Modeling and Analysis of Three-phase Inverter based on Generalized State Space Averaging Method," 39th IEEE Annual Conference on Industrial Electronics Society (IECON), Vienna, pp. 1007-1012, 10-13 November, 2013.

[52] H. Ouquelle, L-A. Dessaint and S.Casoria, "An Average Value Model-Based Design of a Deadbeat Controller for VSC-HVDC Transmission Link," IEEE Power & Energy Society General Meeting, (PES), Calgary, AB, pp. 1-6, 26-30 July, 2009

[53] N. Kroutikova, C.A. Hernandez-Aramburo and T.C. Green, "State-space model of grid-connected inverters under current control mode, Electric Power Applications, IET, pp. 329-338, May, 2007.

[54] Qiang Han, Nikolay Samoylenko and Juri Jatskevich, "Average-Value Modeling of Brushless DC Motors With 120◦ Voltage Source Inverter," IEEE Transaction on Energy Conversion, Vol. 23, No.2, pp. 423-432, June 2008.

[55] Masataka Miyamasu, Kan Akatsu, "Efficiency Comparison between Brushless DC Motor and Brushless AC Motor Considering Driving Method and Machine Design," 37th Annual conference on IEEE Industrial Electronics Society (IECON), Melbourne, VIC, pp 1830 – 1835, 7-10 Nov. 2011.

[56] Gaurang I. Vakil, and K. R. Rajagopal, "Performance Comparison of Sinusoidally-Fed PM BLDC Motors Having Different Rotor Topologies," Joint International Conference on Power Electronics, Drives and Energy Systems (PEDES) and Power India, New Delhi, pp 1-5, 20-23 Dec. 2010.

[57] Patel B. Reddy, Ayman M. El-Refaie, Kum-Kang Huh, Jagadeesh K. Tangudu, and Thomas M. Jahns, "Comparison of Interior and Surface PM Machines Equipped With Fractional-Slot Concentrated Windings for Hybrid Traction Applications," IEEE Transactions on Energy Conversion, Vol. 27, No. 3, pp 593-602, September, 2012.

[58] Hong Chen, Ronghai Qu, Jian Li and Bo Zhao, "Comparison of Interior and Surface Permanent Magnet Machines with Fractional Slot Concentrated Windings for Direct-Drive Wind Generators," 17th International Conference on Electrical Machines and Systems (ICEMS), Hangzhou, China, pp. 2612-2617, Oct. 22-25, 2014.

[59] Jingya Dai, Dewei Xu, Bin Wu, "A Novel Control Scheme for Current-Source-Converter-Based PMSG Wind Energy Conversion Systems," IEEE Transactions on Power Electronics, Vol. 24, Issue 4, pp 963-972, April 2009.

[60] Hak-Jun Lee, Sungho Jung, and Seung-Ki Sul, "A Current Controller Design for Current Source Inverter-fed PMSM Drive System," 8th International Conference on Power Electronics - ECCE Asia, The Shilla Jeju, Korea, pp. 1364-1370, May 30-June 3, 2011.

[61] Aaron VanderMeulen and John Maurin, "Current source inverter vs Voltage source inverter topology, "EATON Powering Business Worldwide, WP020001EN, EATON, www.eaton.com, August 2010.

[62] S.A.Azmi, K.H.Ahmed, S.J.Finney and B.W.Williams, Comparative analysis between voltage and current source inverters in Grid connected application," IET conference on Renewable Power Generation (RPG 2011), Edinburgh, pp. 1-6, 6-8 Sept. 2011.

[63] Long-Yun KANG, Zhi-Feng LU, Yoshida TAKESHI and Zhongqing YANG, "Study on Electric Vehicle In-Wheel PM SPWM Control Technology," 3rd International Conference on Power Electronics Systems and Applications, Hong Kong, pp 1-4, 20-22 May 2009.

[64] Jianlin LI, Ying ZHU, Hongyan XU and Honghua XU, "CPS-SPWM Flying Capacitor Three-Level Back-To-Back Converter Applicative Direct-Drive Wind Power Generator System," International Conference on Sustainable Power Generation and Supply (SUPERGEN), Nanjing, pp 1-6, 6-7 April 2009.

[65] Jaswant Singh, Bindeshwar Singh, S. P. Singh and Mohd Naim, "Investigation of Performance Parameters of PMSM Drives using DTC-SVPWM Technique," Students Conference on Engineering and Systems (SCES), Allahabad, Uttar Pradesh, pp 1-6, 16-18 March 2012.

[66] Cristian Busca, Ana-Irina Stan, Tiberiu Stanciu and Daniel Ioan Stroe, "Control of Permanent Magnet Synchronous Generator for Large Wind Turbines," IEEE International Symposium on Industrial Electronics (ISIE), Bari, pp. 3871-3876, 4-7 July, 2010.

[67] B. Neammanee, S. Sirisumranukul and S. Chatratana, "Control Performance Analysis of Feedforward and Maximum Peak Power Tracking for Small- and Medium-Sized Fixed Pitch Wind Turbines," 9th International Conference on Control, Automation, Robotics and Vision, (ICARCV), Singapore, pp 1-7, 5-8 Dec, 2006.

[68] Saeed Jahdi, Olayiwola Alatise and Phil Mawby, "Modeling of turn-OFF Transient Energy in IGBT Controlled Silicon PiN Diodes,"16th European Conference on Power electronics and applications (EPE'14-ECCE Europe), pp 1-9, 26-28 Aug, 2014.

[69] Toni Itkonen and Julius Luukko, "Switching-Function-Based Simulation Model for Three-Phase Voltage Source Inverter Taking Dead-Time Effects into Account," 34th IEEE Annual Conference of Industrial Electronics (IECON), Orlando, FL, pp. 992-997, 10-13 Nov 2008.

[70] Martin Jones, Emil Levi and Drazen Dujic, "The Impact of Inverter Dead Time on Performance of *n*-Motor Drives Supplied from (2*n*+1)-Leg VSI," IEEE 35th Annual Conference of Industrial Electronics, Porto, pp. 1350-1355, 3-5 Nov. 2009.

[71] Bu Ruofei, Zhao Rongxiang, YangHuan and Zeng Zhiyong, "Inductor Minimum Calculation Based on Analysis of AC Current Ripple for PWM Converter with Dead-time Effect," IEEE Industry Applications Society Annual Meeting, Lake Buena Vista, FL, pp 1-6, 6-11 Oct. 2013.

[72] Tomoyuki Mannen and Hideaki Fujita, "Performance of Dead Time Compensation Methods in Three-Phase Grid-Connection Converters," International Power electronic Conference (IPEC-Hiroshima 2014-ECCE-ASIA), Hiroshima, pp. 2042 – 2049, 18-21 May 2014.

[73] Zheng Zhao, Jih-Sheng Lai and Younghoon Cho, "Dual-Mode Double-Carrier-Based Sinusoidal Pulse Width Modulation Inverter With Adaptive Smooth Transition Control Between Modes," IEEE Transactions on Industrial Electronics, Vol 60, Issue 5, pp 2094-2103, May 2013.

[74] Amarendra Edpuganti, and Akshay K. Rathore, "Optimal Low-Switching Frequency Pulse width Modulation of Medium Voltage Seven-Level Cascade-5/3H Inverter," IEEE Transactions on Power Electronics, Vol. 30, Issue 1, pp 496-503, 25 Jan. 2015.

[75] Wonjin Cho, Edward J. Powers, and Surya Santoso, "Low and High Frequency Harmonic Reduction in a PWM Inverter using DiThered Sigma-Delta Modulation," 10th International Conference on Information Sciences Signal Processing and their Applications (ISSPA), Kuala Lumpur, pp 440-443, 10-13 May 2010.

[76] Gourisetti, S. N. G and Patangia, H., "A summary on modified carrier based real-time Selective Harmonic Eliminationt technique," IEEE 20th International Conference on Electronics, Circuits, and System (ICECS), Abu Dhabi, pp 78-79, 8-11 Dec. 2013.

[77] Amira Marzouki, Mahmoud Hamouda and Farhat Fnaiech, "Nonlinear Control of Three-Phase Active Rectifiers Based L and LCL Filters," International Conference on Electrical Engineering and Software Applications (ICEESA), Hammamet, pp 1-5, 21-23 March 2013.

[78] Fernando Rodriguez and Ali Emadi, "A Novel Digital Control Technique for Brushless DC Motor Drives," IEEE Transactions on Industrial Electronics, Vol. 54, No. 5, pp. 2365-2373, October, 2007.

[79] Satish Rajagopalan, Wiehan le Roux, Thomas G. Habetler and Ronald G. Harley, "Dynamic Eccentricity and Demagnetized Rotor Magnet Detection in Trapezoidal Flux (Brushless DC) Motors Operating Under Different Load Conditions," IEEE Transactions on Power Electronics, Vol. 22, No. 5, September, 2007.

[80] P. Damodharan and Krishna Vasudevan, "Sensorless Brushless DC Motor Drive Based on the Zero-Crossing Detection of Back Electromotive Force (EMF) From the Line Voltage Difference," IEEE Transactions on Energy Conversion, Vol. 25, No. 3, September, 2010.

[81] Salinamakki Ramabhatta Gurumurthy, Vivek Agarwal, Archana Sharma, "Optimal energy harvesting from a high-speed brushless DC generator-based flywheel energy storage system," IET Electric Power Applications, Vol. 7, No. 9, pp. 693-700, doi: 10.1049/iet-epa.2013.0134, November 2013.

[82] C. Olivieri, G. Fabri and M. Tursini, "Sensorless Control of Five-Phase Brushless DC Motors," First Symposium on Sensorless Control for Electric Drives (SLED), Padova, pp. 24-31, 9-10 July 2010.

[83] Yuanyuan Wu, Zhiquan Deng, Xiaolin Wang, Xing Ling, and Xin Cao, "Position Sensorless Control Based on Coordinate Transformation for Brushless DC Motor Drives," IEEE Transactions on Power Electronics, Vol. 25, No.9, pp. 2365-2371, September, 2010.

[84] Liviu Ioan Iepure, Ion Boldea and Frede Blaabjerg, "Hybrid I-f Starting and Observer-Based Sensorless Control of Single-Phase BLDC-PM Motor Drives," IEEE transactions on Industrial Electronics, Vol. 59, No. 9, pp. 3436-3444, September, 2012.

[85] Zahra Amjadi and Sheldon S. Williamson, "Power-Electronics-Based Solutions for Plug-in Hybrid Electric Vehicle Energy Storage and Management Systems," IEEE Transactions on Industrial Electronics, Vol. 57, Issue 2, pp 608-616, February 2010.

[86] Asano, J. -I. and Kondo, K. "A damping control method to enhance regenerative brake power under light consumption load conditions," 39th Annual conference of the IEEE Industrial Electronics Society (IECON), Vienna, pp 4516-4521, 10-13 Nov. 2013.

[87] Camocardi, P.; Battaiotto, P. and Mantz, R, "Autonomous water pumping system based on wind generation. Control by rotor frequency," IEEE International Conference on Industrial Technology (ICIT), Vi a del mar, pp. 903-908, 14-17 March 2010.

[88] Monica Chinchilla, Santiago Arnaltes, Juan Carlos Burgos, "Control of Permanent-Magnet Generators Applied to Variable-Speed Wind-Energy Systems Connected to the Grid," IEEE Transactions on Energy Conversion, Vol. 21, Issue. 1, pp 130-135, March 2006.

[89] Tarek Ahmed, Katsumi Nishida and Mutsuo Nakaoka, "Wind power grid integration of an IPMSG control for Grid-Side Inverters," Journal of power electronics, Vol. 10, No. 5, September 2010.

[90] M.G Molina, A.G Sanchez and A.M Rizzato Lede, "Dynamic Modeling of Wind Farms with Variable-Speed Direct-Driven PMSG Wind Turbines," IEEE/PES Transmission and Distribution Conference and Exposition (T&D-LA), Sao Paulo, Latin American, pp 816-823 8-10 Nov. 2010

[91] Maren Kuschke, Susanne Pertzsch, Kai Strunz, "Modeling of Tidal Energy Conversion Systems for Primary Response Testing," IEEE Power and Energy Society General Meeting San Diego, CA, pp 1-6, 22-26 July 2012.

[92] Vladimir Lazarov, Daniel Roye, Dimitar Spirov and Zahari Zarkov, "New Control Strategy for Variable Speed Wind Turbine with DC-DC converters," 14th International Power Electronics and Motion Control Conference, EPE-PEMC 2010, pp. T12-120 - T12-124, Ohrdi, 6-8 Sept. 2010.

[93] Mahmoud M. Hussein, Tomonobu Senjyu, Mohamed Orabi, Mohamed A. A. Wahab, and Mohamed M. Hamada, "Control of a Variable Speed Stand Alone Wind Energy Supply System," IEEE international conference on power and energy (PECon), Kota Kinabalu, Sabah, Malaysia, pp. 71-76, 2-5 December, 2012.

[94] Zhe Zhang, Yue Zhao, Wei Qiao and Liyan Qu, "A Space-Vector-Modulated Sensorless Direct-Torque Control for Direct-Drive PMSG Wind Turbines," IEEE Transactions on Industry Applications Vol. 50, Issue 4, pp 2331-2341, July/Aug. 2014

[95] Craig, L. M.; Saad-Saoud, Z. and Jenkins, N., "Electrodynamic braking of wind turbines," IEEE Proceedings on Electric Power Applications, Vol. 145, Issue 2, pp 140-146, March 1998

[96] Sugiarto, S.; Abu-Siada, A. and Islam, S. "Performance Enhancement of Grid-Connected Fixed Speed Wind Energy Conversion Systems (WECS)," Australasian Universities Power Engineering Conference (AUPEC), Adelaide, SA, pp 1-6, 27-30 Sept. 2009.

[97] Kedjar, B and Al-Haddad, K, "Optimal control of a grid connected variable speed wind energy conversion system based on squirrel cage induction generator," 38th Annual Conference on IEEE Industrial Electronics Society (IECON), Montreal, QC, pp 3560-3565, 25-28 Oct. 2012.

[98] Manaullah, M.; Sharma, A.K.; Ahuja, H.; Bhuvaneswari, G.; Balasubramanian, R., **"**Control and Dynamic Analysis of Grid Connected Variable Speed SCIG Based Wind Energy Conversion System," Fourth International Conference on Computational Intelligence and Communication Networks (CICN), Mathura, pp 588-593, 3-5 Nov. 2012.

[99] Nayar, C. V. and Bundell, J. H. "Output Power Controller for a Wind-Driven Induction Generator," IEEE Transactions on Aerospace and Electronic Systems, Vol: AES-23, Issue 3, pp. 388-401, May 1987.

[100] Helarisi Abeywardena, A. Atputharajah and J.B. Ekanayake, "Novel technique to smooth power output of a wound rotor induction generator based wind turbine," 6th IEEE International Conference on Industrial and information systems (ICIIS), Kandy, pp. 517-521, 16-19 Aug. 2011.

[101] Shahabi, M. Haghifam, M. -R.; Mohamadian, M. and Nabavi-Niaki, "Microgrid Dynamic Performance Improvement Using a Doubly Fed Induction Wind Generator," IEEE Transactions on Energy Conversion, vol. 24, Issue 1, pp 137-145, March 2009.

[102] da Costa, J. P.; Pinhiero, H.; Degner, T. and Arnold, G., "Robust Controller for DFIGs of Grid-Connected Wind Turbines," IEEE Transactions on Industrial Electronics, vol. 58, Issue 9, pp 4023-4038, Sept. 2011.

[103] Chang-Doo Cho, Soon-Ryul Nam, Sang-Hee Kang and Seon-Ju Ahn, "Modeling of DFIG Wind Turbines Considering Fault-ride-through Grid Code," International Conference on Advanced Power System Automation and Protection (APAP), Beijing, vol. 2, pp. 1024-1028, 16-20 Oct. 2011.

[104] Hassan H. EL-Tamaly, Hamdy M. Sultan, "Control and Simulation of a Crowbar Protection for DFIG Wind Turbine during Power Systems Disturbance," Recent Researches in Electrical Engineering, pp 239-245, ISBN: 978-960-474-392-6.

[105] Sava, G.N; Costinas, S.; Golovanov, N.; Leva, S. and Quan, D. M, "Comparison of active crowbar protection schemes for DFIGs wind turbines," 16th International Conference on Harmonics and Quality of Power (ICHQP), Bucharest, pp 669-673, 25-28 May 2014.

[106] Roberto Lacal Arántegui, "Technology, market and economic aspects of wind energy in Europe, European Commission JRC Scientific and Policy Report, 2013 JRC wind status report, Report EUR 26266 EN 2014

[107] Chowdhury, M.M; Haque, M. E.; Gargoom, A. and Negnevitsky, M., "Performance improvement of a grid connected direct drive wind turbine using super-capacitor energy storage," IEEE PES Innovative Smart Grid Technologies (ISGT), Washington, DC, pp 1-6, 24-27 Feb. 2013.

[108] Kazi Ahsanullah, Rukmi Dutta and M.F. Rahman, "Review of PM Generator Designs for Direct-Drive Wind Turbines," 22nd Australasian Universities Power Engineering Conference (AUPEC), Bali, pp.1-6, 26-29 Sept. 2012.

[109] Snitchler, G.; Gamble, B.; King, C. and Winn, P. "10 MW Class Superconductor Wind Turbine Generators," IEEE Transactions on Applied Superconductivity, Vol. 21, Issue 3, pp. 1089-1092, June 2011.

[110] Leban, K. Ritchie, E. and Argeseanu, A. "Design Preliminaries for Direct Drive under Water Wind Turbine Generator," XXth International Conference on Electrical Machines (ICEM), Marseille, pp. 190-195, 2-5 Sept. 2012.

[111] Muyeen, S.M; Takahashi, R.; Murata, T. and Tamura, J., "A Variable Speed Wind Turbine Control Strategy to Meet Wind Farm Grid Code Requirements," IEEE Transactions on Power Systems vol. Issue 1, pp 331-340, Feb 2010.

[112] Yonggao Zhang, Guangjian Kuang and Lizhong Long, "Research on Reduced Common-mode Voltage Nonzero Vector Pulse Width Modulation Technique for Three-phase Inverters," 7th International Power Electronics and Motion Control Conference (IPEMC), Harbin, China, vol.4, pp 2349-2352, 2-5 June 2012.

[113] Zhao Feng, Zhang Guangzhen, Wen Xuhui, Zhao Li and Guo qiujian, "A Novel Implementation of Harmonic Elimination Pulse Width Modulation Technique," IEEE Conference and Expo Transportation Electrification Asia-Pacific (ITEC Asia-Pacific), Beijing, pp 1-5, Aug. 31 2014-Sept. 3 2014.

[114] Amirhossein Moeini, Hossein Iman-Eini, Mohamadkazem Bakhshizadeh, "Selective harmonic mitigation-pulse-width modulation technique with variable DC-link voltages in single and three-phase cascaded H-bridge inverters," IET Power Electronics, vol. 7 No. 4, pp 924-932, April 2014

[115] Akimatsu, R. and Doki, S, "Improve torque response using the inverter overmodulation range in position sensorless control system of PMSM," 39th Annual Conference of the IEEE Industrial Electronics Society (IECON), Vienna, pp. 2911-2916, 10-13 Nov. 2013.

[116] Odavic, M; Zanchetta, P.; Clare, J. C, "A Theoretical Analysis of the Harmonic Content of PWM Waveforms for Multiple-Frequency Modulators," IEEE Transactions on Power Electronics, vol. 25, Issue 1, pp 131-141, Jan. 2010.

[117] K.T. Wong, "Harmonic analysis of PWM multi-level converters," IEEE proceedings on Electric Power Applications, Vol. 148, No. 1, pp 35-43, Jan 2001.

[118] William Dillard, Alec Leedy and R. Mark Nelms, "A Direct Method and Algorithm for Determining the Harmonic Content of Sinusoidal PWM Waveforms Suitable to Low-Level DSP and Microcontrollers," Fourtieth IAS Annual Meeting. Conference Record of the Industry Applications Conference, Vol. 2, pp. 1267 – 1271, 2 – 6 Oct. 2005.

[119] Dragutin J. Kostic, Zoran Z. Avramovic, and Ninoslav T. Ciric, "A New Approach to Theoretical Analysis of Harmonic Content of PWM Waveforms of Single- and Multiple-Frequency Modulators,"IEEE Transactions on Power Electronics, Vol. 28, No.10, pp. 4557 – 4567, October 2013.

[120] Ramesh, T. and Panda, A.K., "Direct flux and torque control of three phase induction motor drive using PI and fuzzy logic controllers for speed regulator and low torque ripple," Students Conference on Engineering and Systems (SCES), Allahabad, Uttar Pradesh, pp 1-6, 16-18 March 2012.

[121] Amit Vilas Sant , K. R. Rajagopal , and Nimit K. Sheth, "Permanent Magnet Synchronous Motor Drive Using Hybrid PI Speed Controller with Inherent and Noninherent Switching Functions," IEEE transactions on Magnetics, Vol. 47, Issue 10, pp. 4088-4091, Oct. 2011.

[122] Rajasekaran, V.; Merabet, A.; Ibrahim, H.; Beguenane, R. and Thongam, J.S, "Control system simulation for stand-alone hybrid wind diesel system," IEEE Electrical Power & Energy Conference (EPEC), Halifax, NS, pp1-5, 21-23 Aug. 2013.

[123] Kadri, R.; Gaubert, J. -P. and Champenois, G, "An Improved Maximum Power Point Tracking for Photovoltaic Grid-Connected Inverter Based on Voltage-Oriented Control," IEEE Transactions on Industrial Electronics, vol 58, Issue 1, pp 66-75, Jan. 2011.

[124] B. Zigmund, A. Terlizzi, X.T. Garcia, R.Pavlanin and L. Salvatore, "Experimental evaluation of PI tuning techniques for field oriented control of permanent magnet synchronous motors," Advances in Electrical and Electronic Engineering.

[125] Corradini, L.; Mattavelli, P.; Stefanutti, W. and Saggini, S., "Simplified Model Reference-Based Autotuningfor Digitally Controlled SMPS," IEEE Transactions on Power Electronics, vol. 23, Issue 4, pp1956-1963, July 2008.

[126] Filho, A. J. S. and Ruppert, E., "Tuning PI regulators for IM direct torque control using complex transfer function," 9th IEEE/IAS International Conference on Industry Applications (INDUSCON), Sao Paulo, pp 1-6, 8-10 Nov. 2010.

[127] Slimane Medjmadj, Demba Diallo, Mohammed Mostefai, Claude Delpha and Antoni Arias, "PMSM Drive Position Estimation: Contribution to the High-Frequency Injection Voltage Selection Issue," IEEE Transactions on Energy Conversion, Vol. PP, Issue 99, pp.1-10, 18 September 2014.

[128] Kashif, S. A. R.; Saqib, M. A. and ul Hassan, M. "Direct-Torque Control of a PMSM using Four-Switch Three-Phase Inverter," IEEE 23rd International Symposium on Industrial Electronics (ISIE), Istabul, pp. 795-799, 1-4 June 2014.

[129] Orlowska-Kowalska, T.; Dybkowski, M. and Szabat, K., "Adaptive Sliding-Mode Neuro-Fuzzy Control of the Two-Mass Induction Motor Drive without Mechanical Sensors," IEEE Transactions on Industrial Electronics, Vol. 57, Issue 2, pp. 553-564, Feb. 2010.

[130] Yongchang Zhang and Haitao Yang, "Torque ripple reduction of model predictive torque control of induction motor drives," IEEE Energy Conversion Congress and Exposition (ECCE) Denver, CO, pp. 1176-1183, 15-19 Sept. 2013.

[131] M. Farasat and E. Karaman, "Efficiency-Optimized Hybrid Field Oriented and Direct Torque Control of Induction Motor Drive," International Conference on Electrical Machines and systems (ICEMS), Beijing, pp. 1-4, 20-23 Aug. 2011.

[132] Farasat, M.; Rostami, N and Feyzi, M. R. "Speed sensorless hybrid field oriented and direct torque control of induction motor drive for wide speed range applications," 1st Power Electronic and Drive Systems & Technologies Conference (PEDSTC), Tehran, Iran, pp. 243-248, 17-18 Feb. 2010.

[133] Garg, R.; Mahajan, P.; Gupta, N. and Saroa, H., "A comparative study between field oriented control and direct torque control of AC traction motor," Recent Advances and Innovations in Engineering (ICRAIE), Jaipur, pp. 1-6, 9-11 May, 2014.

[134] Alvaro Luna, Francisco Kleber de Araujo Lima, David Santos, Pedro Rodríguez, Edson H. Watanabe, and Santiago Arnaltes, "Simplified Modeling of a DFIG for Transient Studies in Wind Power Applications," IEEE Transactions on Industrial Electronics, vol. 58, Issue 1, pp. 9-20, Jan. 2011.

[135] Yongchang Zhang and Jianguo Zho, "Direct torque control of cascaded brushless doubly fed induction generator for wind energy applications," IEEE International Electric Machines & Drives Conference (IEMDC), Niagara, Falls, ON, pp. 741-746, 15-18 May 2011.

[136] Fatma Hachichs, Lotfi Krichen, "Performance Analysis of a Wind Energy Conversion System Based On a Doubly-Fed Induction Generator," 8th International Multi-Conference on Systems, Signals and Devices (SSD), Sousse, pp. 1-6, 22-25 March 2011.

[137] Mohamed HILAL, Mohamed MAAROUFI and Mohamed OUASSAID, "Doubly Fed Induction Generator Wind Turbine Control for a maximum Power Extraction,"International Conference on Multimedia Computing and Systems (ICMCS), Quarzazate, pp. 1-7, 7-9 April 2011.

[138] Tommy A. Theubou, R. Wamkeue, and I. kamwa, "Control of Grid-Side Inverter for Isolated Wind-Diesel Power Plants using Variable Speed Squirrel Cage Induction Generator," 38th Annual Conference on IEEE Industrial Electronics Society (IECON), Montreal, QC, pp 4304-4309, 25-28 Oct. 2012.

[139] Gabriel O. Cimuca, Christophe Saudemont, Benoît Robyns and Mircea M. Radulescu, "Control and Performance Evaluation of a Flywheel Energy-Storage System Associated to a Variable-Speed Wind Generator," IEEE Transactions on Industrial Electronics, Vol. 53, No. 4, pp. 1074 – 1085, August 2006.

[140] Suvajit Mukherjee and Gautam Poddar, "Fast Control of Filter for Sensorless Vector Control SQIM Drive With Sinusoidal Motor Voltage," IEEE Transactions on Industrial Electronics, Vol. 54, No. 5, pp. 2435 – 2442, October 2007.

[141] S. A. Saleh and M. Azizur Rahman, "Development and Experimental Validation of Resolution-Level Controlled Wavelet-Modulated Inverters for Three-Phase Induction Motor Drives," IEEE Transactions on Industry Applications, Vol. 47, No. 4, pp. 1958-1970, July/August 2011.

[142] P. M. Menghal and Dr. A. Jaya Laxmi, "Adaptive Neuro Fuzzy Based Dynamic Simulation of Induction Motor Drives," IEEE International Conference on Fuzzy Systems (FUZZ), Hyderabad, pp. 1-8, 7-10 July, 2013.

[143] Ahmad Eid, Mostafa Dardeer and Roberto Caldon, "Control and Performance of Micro-Grids Under Extreme Gust Wind Scenarios," IEEE 16th International Conference on Harmonics and Quality of Power (ICHQP), Bucharest, pp. 684 - 688, 25-28 May 2014.

[144] Marian Gaiceanu and Cristian Nichita, "Regenerative AC Drive System with the Three-phase Induction Machine," International Conference on Applied and Theoretical Electricity (ICATE), Craiova, pp. 1-6, 23-25 Oct. 2014.

[145] Manaullah, Arvind Kumar Sharma and Hemant Ahuja, Arika Singh, "Performance Comparison of DFIG and SCIG based Wind Energy Conversion Systems," International Conference on Innovative Applications of Computational Intelligence on Power, Energy and Controls with their Impact on Humanity (CIPECH14), Ghaziabad, pp. 285 – 290, 28 - 29 November 2014.

[146] Mohammed Alnajjar and Dieter Gerling, "Control of Three-Source High Voltage Power Network for More Electric Aircraft," International Symposium on Power Electronics, Electrical Drives, Automation and Motion (SPEEDAM), Ischia, pp. 232-237, 18-20 June 2014.

[147] Xuanqin Wu, Guojun Tan, Qianqian Zhang and Wei Jing, "Research of Electrically Excited Synchronous Motor Vector Control System Based on Full-Order Closed-Loop Air Gap Flux Estimator," IEEE 6th International Power Electronics and Motion Control Conference (IPEMC), Wuhan, pp. 2054 – 2056, 17-20 May 2009.

[148] Loic Queval and Hiroyuki Ohsaki, "Back-to-back Converter Design and Control for Synchronous Generator-based Wind Turbines," International Conference on renewable energy Research and Applications (ICRERA), Nagasaki, pp 1-6, 11-14 Nov. 2012.

[149] Chi D. Nguyen and Wilfried Hofmann, "Self-Tuning Adaptive Copper-Losses Minimization Control of Externally Excited Synchronous Motors," International Conference on Electrical Machines (ICEM), Berlin, pp. 897 – 902, 2-5 Sept. 2014.

[150] Ying Yan, Jianguo Zhu, Youguang Guo and Haiwei Lu, "Modeling and simulation of direct Torque Controlled PMSM Drive System Incorporating Structural and Saturation Saliencies," 41st IAS annual Meeting and Conference on Industry Applications, Tampa, FL, Vol. 1, pp 76-83, 8-12 Oct. 2006.

[151] Ananthamoorthy, N.P. and Baskaran, K, "Simulation of PMSM based on current hysteresis PWM and Fed PI Controller," International Conference on Computer Communication and Informatics (ICCCI), Coimbatore, pp 1-5, 10-12 Jan. 2012.

[152] Yulong Huang, Jingjun Wang, Wenchao Zhang, Al-Dweikat, M., Dawei Li, Tao Yang, Shengnan Shao, "A Motor-Drive-Based Operating Mechanism for High-Voltage Circuit Breaker," IEEE Transactions on Power Delivery, Vol. 28, issue 4, pp 2602-2609, Oct 2013.

[153] Ranjini K.S., Sree, Jose Joel, Anuradha T., Prabhu V.Vasan and Sakthivel S., " Modeling and simulation of PMSM drive for remote inspection of steam generator tubes in PFBR, IEEE 2nd international conference on Electrical energy systems (ICEES), Chennai India, pp 116-121, 7-9 Jan. 2014.

[154] Pragasen Pillay and Ramu Krishnan, "Modeling, Simulation, and Analysis of Permanent-Magnet Motor Drives, Part I: The Permanent-Magnet Synchronous Motor Drive," IEEE Transactions on Industry Applications, Vol. 25, No. 2, pp 265-273, March/April 1989.

[155] Pragasen Pillay and Ramu Krishnan, "Modeling, simulation, and analysis of permanent-magnet motor drives. II. The brushless DC motor drive," IEEE Transactions on Industry Applications, Vol. 25, No. 2, pp 274-279, March/April 1989.

[156] Gole, A.M.; Keri, A.; Nwankpa, C. et al, "Guidelines for modeling power electronics in electric power engineering applications," IEEE Transactions on Power Delivery, Vol. **12,** No. 1, pp, 505-514, Jan. 1997.

[157] M. Azizur Rahman, Rasoul M. Milasi, Caro Lucas, Babak Nadjar Araabi and Tawfik S. Radwan, "Implementation of Emotional Controller for Interior Permanent-Magnet Synchronous Motor Drive," IEEE Transactions on Industry Applications, Vol. 44, Issue 5, pp 1466-1476, Sept – Oct. 2008.

[158] Liye Song and Jishen Peng, "The Study of Fuzzy- PI Controller of Permanent Magnet Synchronous Motor," IEEE 6th International Power Electronics and Motion Control Conference (IPEMC), Wuhan, pp 1863-1866, 17-20 May 2009.

[159] Yulong Huang, Dawei Li, Tao Yang, Jingjun Wang and Guozheng Xu, "Research on the control techniques of motor drive for SF6 high voltage circuit breaker," International Conference on Power System Technology (POWERCON), Hangzhou, pp 1-6, 24-28 Oct. 2010.

[160] A.N. Tiwari, P. Agarwal and S.P. Srivastava, "Performance investigation of modified hysteresis current controller with the permanent magnet synchronous motor drive," IET Electr. Power Appl., 2010, Vol. 4, Iss. 2, pp. 101–108.

[161] Sanjeet Dwivedi and Bhim Singh, "Vector Control Vs Direct Torque Control Comparative Evaluation for PMSM Drive,"Joint International Conference on Power Electronics, Drives and Energy Systems (PEDES), New Delhi, pp 1-8, 20-23 Dec, 2010.

[162] Jaswant Singh, B. Singh, and S.P. Singh, "Performance Evaluation of Direct Torque Control with Permanent Magnet Synchronous Motor," S-JPSET : ISSN : 2229-7111, Vol. 2, Issue 2 (c) samriddhi, 2011.

[163] Gupta, N. P. and Gupta, P. "Performance Analysis of Direct Torque Control of PMSM Drive using SVPWM – Inverter," 5th India International Conference on Power Electronics (IICPE), Delhi, pp 1-6, 6-8 Dec. 2012.

[164] Preindl, M. and Bolognani, S. "Model Predictive Direct Torque Control With Finite Control Set for PMSM Drive Systems, Part 2: Field Weakening Operation," IEEE Transactions On Industrial Informatics, Vol. 9, No. 2, pp 648-657, May 2013.

[165] Sharifian, M.B.B, Herizchi, T., Firouzjah, K.G., " Field oriented control of permanent magnet synchronous motor using predictive space vector modulation," IEEE symposium on industrial electronics & applications, (ISIEA 2009), Kuala Lumpur, vol. 2, pp 574-579, 4-6 Oct. 2009.

[166] Howlader, A.M, Urasaki, N, Yona, A, Senjyu, T, Saber, A.Y., "An online fuzzy adaptive pulse amplitude modulation control for a PMSM drive," 7th IEEE conference on industrial electronics and applications (ICIEA), Singapore, pp 40-45, 18-20 July 2012.

[167] Heekwang Lee, Junwoo Kim, Jinseok Hong and Kwanghee Nam, "Torque Control for IPMSM in the High Speed Range Based on Voltage Angle," Twenty-Ninth Annual IEEE Applied Power Electronics Conference and Exposition (APEC), Fort Worth, TX, pp 2500-2505, 16-20 March 2014.

[168] Munggonrit, S.; Konghirun M. and Tungpimolrut, K. "Implementation of Speed Controlled Permanent-Magnet Synchronous Motor Drive Using Low- Resolution Encoder for Low-Cost Applications," International Conference on Electrical Machines and Systems (ICEMS), Incheon, pp 700-705, 10-13 Oct. 2010.

[169] Wei, Qing, Kai Sun, Hongyan Ma and Lipei Huang, "Single Current Sensor Control for PWM Inverter fed AC Motor Drives under Over-modulation Mode," 35th Annual Conference of IEEE Industrial Electronics, Porto, pp 1304-1309, 3-5 Nov. 2009.

[170] Fei Ma, Yong Li, "Simulation research on speed sensorless control technique for PMSM in electric drive mining truck," International Conference on E-Product E-Service and E-Entertainment (ICEEE), Henan, pp 1-5, 7-9 Nov. 2010.

[171] J.S.V.Siva Kumar P. Sai Kumar M. Rambabu, "Model Reference Adaptive Controller-Based Speed and Q-axis Inductance Estimation for Permanent Magnet Synchronous Motor Drive by Utilizing Reactive Power," International Conference on Energy, Automation, and Signal (ICEAS), Bhubaneswar, Odisha, pp 1-6, 28-30 Dec. 2011.

[172] Singh, B. and Goyal, D. "Improved DSVM-DTC Based Current Sensorless Permanent Magnet Synchronous Motor Drive," 7th International Conference on Power Electronics and Drive Systems, Bangkok, pp 1354-1360, 27-30 Nov. 2007.

[173] Lazi, J. M.; Ibrahim, Z.; Sulaiman, M.; Jamaludin, I. W. and Lada, M. Y. "Performance Comparison of SVPWM and Hysteresis Current Control for Dual

Motor Drives," IEEE Applied Power Electronics Colloquium (IAPEC), Johor Bahru, pp 75-80, 18-19 April 2011.

[174] Ngoc Linh Nguyen, Fadel, M. and Llor, A. "Predictive Torque Control – A Solution for Mono Inverter-Dual Parallel PMSM System," IEEE International Symposium on Industrial Electronics (ISIE), Gdabsk, pp 697-702, 27-30 June 2011.

[175] Samat, A. A. A.; Ishak, D.; Saedin, P. and Iqbal, Shahid "Speed- Sensorless Control of Parallel- Connected PMSM fed by A Single Inverter Using MRAS, IEEE International Power Engineering and Optimization Conference (PEOCO), Melaka, Malaysia, pp 35-39, 6-7 June 2012.

[176] Bidart, D.; Pietrzak-David, M.; Maussion P. and Fadel, M. "Mono inverter dual parallel PMSM - Structure and Control strategy," 34th Annual Conference of IEEE industrial electronic (IECON 2008), Orlando FL, pp 268-273, 10-13 Nov. 2008.

[177] Jiangcheng Wang, Shanmei Cheng and Bo Gong, "Sensorless Vector Control for Permanent Magnet Synchronous Motor Fed by Three-Level Inverter," International Conference on Control, Automation and Systems (ICCAS), Gyeonggi-do, Korea, pp 1209-1213, 27-30 Oct, 2010.

[178] Quntao An, Guanglin Wang, and Li Sun, "A Fault-Tolerant Operation Method of PMSM Fed by Cascaded Two-Level Inverters," 7th International Power electronics and motion control conference (IPEMC), Harbin, China, pp. 1310-1313, 2-5 June 2012.

[179] Das, A.; Sivakumar, K.; Ramchand, R.; Patel, C. and Gopakumar, K, "A Combination of Hexagonal and 12-Sided Polygonal Voltage Space Vector PWM Control for IM Drives Using Cascaded Two-Level Inverters," IEEE Transactions on Industrial Electronics, Vol. 56, Issue 5, pp. 1657-1664, May 2009.

[180] Babu, N. N. V. S. and Fernandes, B. G., "Cascaded Two-Level Inverter-Based Multilevel STATCOM for High-Power Applications," IEEE Transactions on Power Delivery, Vol. 29, Issue 3, pp. 993-1001, June 2014.

[181] Abdul Kadir, M. N.; Mekhilef, S.; Hew Wooi Ping, "Direct Torque Control Permanent Magnet Synchronous Motor drive with asymmetrical multilevel inverter supply," 7th International Conference on Power Electronics (ICPE), Daegu, pp. 1196-1201, 22-26 Oct 2007.

[182] Hassan, W. and Bingsen Wang, "Efficiency Optimization of PMSM Based Drive System," IEEE 7th International Power Electronics and Motion Control Conference (IPEMC), Harbin, pp 1027-1033, 2-5 June 2012.

[183] Estima, J. O. and Marques Cardoso, A. J. "Efficiency Analysis of Drive Train Topologies Applied to Electric/Hybrid Vehicles," IEEE Transactions on Vehicular Technology, Vol. 61, No. 3, pp 1021-1031, March 2012.

[184] Anca D. Hansen and Gabriele Michalke, "Modelling and control of variable-speed multi-pole permanent magnet synchronous generator wind turbine," Wind Energy, Wind Energ. 2008;11: 537-554, DOI: 10.1002/we.278, 12 May 2008 in Wiley Interscience.

[185] Percis, E. S., Ramesh L., Nalini, A., Venmathi, M. and Sujatha, K., "Comparative Analysis of Variable Speed Wind Energy Conversion Systems," International Conference on Sustainable Energy and Intelligent Systems (SEISCON 2011), Chennai, pp 159-162, 20-22 July 2011.

[186] F. Kendouli, K. Abed, K. Nabti and H. Benalla and B. Azoui, "High Performance PWM Converter Control Based PMSG for Variable Speed Wind Turbine," First International Conference on Renewable Energies and Vehicular Technology (REVET), Hammamet, pp 502-507, 26-28 March 2012.

[187] D. I. Stroe, A. I. Stan, I. Visa and I. Stroe, "Modeling and control of variable speed wind turbine equipped with PMSG," 13th world congress in mechanism and machine science, Guanajuato, Mexico, pp 1-5, 19-25 June, 2011.

[188] Haque, M. E.; Muttaqi, K. M. and Negnevitsky, M. "Control of a standalone variable speed wind turbine with permanent magnet synchronous generator," IEEE Power and Energy Society General Meeting – Convention and Delivery of Electrical Energy in the 21st Century, Pittsburgh, PA, pp 1-9, 20-24 July 2008.

[189] Aziz Remli, Djamal Aouzellag and Kaci Ghedamsi, " Study and control of wind energy conversion system based permanent magnet synchronous generator connected to the grid," International journal of research and reviews in computing engineering, Vol. 1, No. 1, March 2011.

[190] Hui, J. and Jain, P.K, "Power management and control of a wind energy conversion system (WECS) with a fuzzy logic based maximum power point tracking (MPPT)," 38th Annual Conference on IEEE Industrial Electronics Society, Montreal, QC, pp 5966-5971, 25-28 Oct. 2012.

[191] Hui, Joanne, Bakhshai, Alireza and Jain, Praveen, "Power management supervisory control algorithm for standalone wind energy systems," IEEE 36th International Telecommunications Energy Conference (INTELEC), Vancouver, BC, Canada, pp 1-6, Sept. 28, 2014 – Oct. 2, 2014.

[192] Thongam, J. S.; Bouchard, P.; Ezzaidi, H. and Ouhrouche, M, "Wind speed sensorless maximum power point tracking control of variable speed wind energy conversion systems," IEEE International Electric Machines and Drives Conference, Miami, FL, pp 1832-1837, 3-6 May 2009.

[193] Thongam, J. S.; Bouchard, P.; Beguenane, R.; Okou, A.F. and Marabet, A., "Control of variable speed wind energy conversion system using a wind speed sensorless optimum speed MPPT control method," 37th Annual Conference on IEEE Industrial Electronics Society (IECON), Melbourne, VIC, pp 855- 860, 7-11 Nov. 2011.

[194] Shengwen Fan, Peng Wang and Chunxue Wen, "A new sensorless control strategy used in direct-drive PMSG wind power system," 2nd IEEE International Symposium on Power Electronics for Distributed Generation Systems (PEDG), Hefei, China, pp 611-615, 16-18 June 2010.

[195] Xu Yang, Xiang Gong and Wei Qiao, "Mechanical sensorless maximium power tracking control for direct drive PMSG wind turbine," IEEE Transactions on Energy Conversion Congress Exposition (ECCE), Atlanta, GA, pp 4091-4098, 12-16 Sept. 2010.

[196] Wei Qiao Xu Yang and Xiang Gong, "Wind Speed and Rotor Position Sensorless Control for Direct-Drive PMG Wind Turbines, IEEE Transactions on Industry Applications, vol 48, Issue 1, pp 3-11, Jan. –Feb. 2012.

[197] Zhe Zhang, Yue Zhao, Wei Qiao and Liyan Qu, "A space-vector modulated sensorless direct-torque control for direct-drive PMSG wind turbines," IEEE Industry Applications Society Annual Meeting (IAS), Las Vegas, NV, pp 1-7, 7-11 Oct. 2012.

[198] Mingxing Zhou, Guangqing Bao and Youmin Gong, "Maximum Power Point Tracking Strategy for Direct Driven PMSG," Asia-Pacific Power and Energy Engineering Conference (APPEEC), Wuhan, pp 1-4, 25-28 March 2011.

[199] Errami, Y.; Maaroufi, M. and Ouassaid, "Modelling and control strategy of PMSG based variable speed wind energy conversion system," International Conference on Multimedia Computing and Systems (ICMCS), Ouarzazate, pp 1-6, 7-9 April 2011.

[200] Errami, Y.; Benchagra, M.; Hilal, M.; Maaroufi, M. and Quassaid, M., "Control strategy for PMSG wind farm based on MPPT and direct power control," International Conference on Multimedia Computing and Systems (ICMCS), Tangier, pp 1125-1130, 10-12 May 2012.

[201] Abo-Elyousr, F. K. and Rim, G. H., "Performance evaluation of AC/DC PWM converter for 12-phase stand-alone PMSG with maximum power extraction," International Conference on Electrical Machines and systems (ICEMS), Incheon, pp 82-87, 10-13 Oct. 2010.

[202] Muyeen, S. M. and Al-Durra, A, "Modeling and control strategies of fuzzy logic controlled inverter system for grid interconnected variable speed wind generator," IEEE System Journal, vol. 7, No. 4, pp 817-824, Dec. 2013.

[203] G. W. Wester and R.D. Middlebrook, "Low-frequency Characterization of switched DC-to-DC Converters," Proceedings of the IEEE Power Processing and Electronic Specialist Conference, may 22-23, 1972, Atlantic city, NJ.

[204] R. D. Middlebrook and Slobodan Cuk, " A general unified approach to modelling switching-converter power stages," Proceedings of the IEEE Power Electronics Specialist Conference, June 8-10 1976, Cleveland, OH.

[205] V. Vorperian, "Simplified analysis of PWM converters using model of PWM switch. Continuous conduction mode," IEEE Transactions on Aerospace and Electronic Systems, Vol. 26, Issue 3, pp 490-496, May 1990.

[206] V. Vorperian, "Simplified analysis of PWM converters using model of PWM switch. II. Discontinuous conduction mode," IEEE Transactions on Aerospace and Electronic Systems, Vol. 26, Issue 3, pp 497-505, May 1990.

[207] Hiti, S.; Boroyevich, D. and Cuadros, C. "Small-Signal Modeling And Control of Three-Phase PWM Converters," Conference Record of the 1994 IEEE Industry Applications Society Annual Meeting, Denver, CO. Vol. 2 pp 1143-1150, 2-6 Oct 1994.

[208] Silva Hiti and Dushan Boroyevich, "Control of Front-End Three-phase Boost Rectifier," 9th Annual Applied Power Electronics Conference and Exposition (APEC '94), Orlando, FL, vol. 2, pp 927-933, 13-17 Feb 1994.

[209] Bina, M. T. "Switching Frequency Dependent Averaged Model for STATCOM," IEEE 2003. The Fifth International Conference on Power Electronics and drive Systems (PEDS), vol. 1, pp 136-140, 17-20 Nov 2003.

[210] Bina, M. T. and Bhat, A.K.S, "Averageing Technique for the modelling of STATCOM and active filters," IEEE Transactions on Power Electronics vol. 23, Issue 2, pp. 723-734, March 2008.

[211] Ahmed, S.; Boroyevich, D.; Wang, F. and Burgos, R. "Development of a new voltage source inverter (VSI) average model including low frequency harmonics," Twenty-Fifth Annual IEEE Applied Power Electronics Conference and Exposition (APEC), Palm Springs, CA, pp 881-886, 21-25th Feb. 2010.

[212] Han, Q.; Samoylenko, N. and Jatskevich, J. "Comparison of brushless DC motor drives with 180/120-degree inverter systems," Canadian Conference on Electrical and Computer Engineering (CCECE), Vancouver, BC, pp 111-114, 22-26 April 2007.

[213] Tabarraee, K.; Iyer, J.; Atighechi, H. and Jatskevich, J, "Dynamic Average-Value modelling of 120^0 VSI-commutated brudhless DC motors with trapezoidal back emf," IEEE Transactions on Energy Conversion, vol. 27, Issue 2, pp. 296-307, June 2012.

[214] Hoff, B. and Sulkowski, W, "Comprehensive modelling and practical verification of grid connected VSI with LCL Filters," 15th International Power Electronics and Motion Control Conference (EPE/PEMC), Novi Sad, DS3f.7-1-DS3f.7-7, 4-6 Sept. 2012.

[215] Junfei Chen, Hongbin Wu, Ming Sun, Weinan Jiang, Liang Cai and Caiyun Guo, " Modeling and simulation of directly driven wind turbine with permanent magnet synchronous generator," IEEE Innovative Smart Grid Technologies, Tianjin, pp. 1-5, 21-24 May 2012.

[216] Ohiero, P.O.; Cossar, C.; Melone, J. and Schofield, N. "A fast simulation model for permanent magnet synchronous motor (PMSM) based system," 7th International Conference on Power Electronics, machines and Drives (PEMD 2014), Manchester, pp 1-6, 8-10 April 2014.

[217] Yaohua Li, Dieter Gerling and Weiguo Liu, "A Simplified Voltage Vector Selection Strategy for the Permanent Magnet Synchronous Motor Direct Torque Control Drive with Low Torque Ripple and Fixed Switching Frequency," International Conference on Electrical Machines and Systems (ICEMS), Incheon, pp 674-679, 10-13 Oct. 2010

[218] J. Luomi C. Zwyssig, A. Looser, and J.W. Kolar, "Efficiency Optimization of a 100-W, 500 000-rpm Permanent-Magnet Machine Including Air Friction Losses," 42nd IAS Annual Meeting. Conference record of the Industry Applications Conference, New Orleans, LA, pp 861-868, 23-27 Sept. 2007

[219] Lukas Schwager, Arda Tüysüz, Ch ristof Zwyssig, Johann W. Kolar, "Modeling and Comparison of Machine and Converter Losses for PWM and PAM in High-Speed Drives," XXth International Conference on Electrical Machines (ICEM), Marseille, pp 2441-2447, 2-5 Sept. 2012

[220] Yang Liu, Liming Shi, Yaohua Li, "Comparison Analysis of Loss Calculation Methods and Measurement Techniques in Power Electronics and Motor Systems," International Conference on Electrical Machines and Systems (ICEMS), Bussan, pp 530-534, 26-29 Oct. 2013.

[221] Pasi Nuutinen, Aleksi Mattsson, Tero Kaipia, Pasi Peltoniemi, Antti Pinomaa, Andrey Lana, Janne Karppanen and Pertti Silventoinen, "Power Electronic Losses of a Customer-end Inverter in Low-Voltage Direct Current Distribution," 16th European Conference on Power Electronics and Applications (EPE'14-ECCE Europe), Lappeenranta, pp 1-10 26-28 Aug. 2014.

[222] Aguirre, M.; Calleja, C.; Lopez-de-Heredia, A.; Poza, J.; Aranburu, A. Nieva, T, "FOC and DTC comparison in PMSM for railway traction application," Proceedings of the 14th European Power Electronics and Applications (EPE 2011), Birmingham, pp 1-10, Aug. 30, 2011-Sept. 1, 2011

[223] Srikanth, V. and Dutt, A. A., "Performance analysis of a Permanent Magnet Synchronous Motor using a novel SVPWM," IEEE International Conference on Power Electronics, Drives and Energy Systems (PEDES), Bengaluru, pp 1-6, 16-19 Dec. 2012

[224] Ying Yan, Jianguo Zhu, Youguang Guo and Haiwei Lu, "Modeling and Simulation of Direct Torque Controlled PMSM Drive System Incorporating Structural and Saturation Saliencies," 42nd IAS Annual Meeting. Conference Record of the Industry Applications Conference, New Orleans, LA, pp 683-689, 23-27 Sept. 2007

[225] D. Staton, M. Popescu, T. Barucki, "Brushless Permanent Magnet Motor Modelling in Portunus: Inputs of Stator and Rotor Temperature and Outputs of Losses and link to reduced Node Thermal Imported from Motor-CAD," 2010.

[226] Vasilios C. Ilioudis, Nikolaos I. Margaris, "Flux Weakening Method for Sensorless PMSM Control Using Torque Decoupling Technique," First Symposium on Sensorless Control for Electrical Drives (SLED), Padova, pp 32-39, 9-10 July 2010.

[227] Moussa, M. F.; Helal, A.: Gaber, Y.; and Youssef, H. A., "Unity Power Factor Control of Permanent Magnet Motor Drive System," 12th International Middle-East Power System Conference, Aswan, pp 360-367, 12-15 March 2008.

[228] Shigeo Morimoto, Yukinori Inoue, Ting-Fei Weng, Masayuki Sanada, "Position Sensorless PMSM Drive System Including Square-wave Operation at High-speed," 42nd IAS Annual Meeting. Conference Records of the Industry Applications Conference, New Orleans, LA, pp 676-682, 23-27 Sept, 2007.

[229] Ohiero, P. O.; Cossar, C. and Melone, J., "A fast simulation model for a Permanent Magnet Synchronous Generator (PMSG) drive system," 16th European Conference on Power Electronics and Applications (EPE'14-ECCE Europe), Lappeenranta, pp 1-10, 26-28 Aug. 2014.

[230] Ziping Wu, Wenzhong Gao, Daye Yang, Yan Shi, "Comprehensive Modeling and Analysis of Permanent Magnet Synchronous Generator-Wind Turbine System with Enhanced Low Voltage Ride Through Capability," IEEE Energy Conversion Congress and Exposition (ECCE), Raleigh, NC, pp 2091-2098, 15-20 Sept. 2012.

[231] Daniel A. F. Collier and Marcelo L. Heldwein, "Modeling and design of a micro wind energy system with a variable-speed wind turbine connected to a permanent magnet synchronous generator and a PWM rectifier," Brazilian Power Electronics Conference (COBEP), Praiamar, pp 292-299, 11-15 Sept. 2011.

[232] Hany M. Hasanien, "Shuffled frog leaping algorithm-based static synchronous compensator for transient stability improvement of a grid-connected wind farm," Renewable Power Generation, IET, Vol. 8, Issue 6, pp 722-730, August 2014.

[233] Song Yongduan, Wang Rui and Cai Wenchuan, "Dynamic Modeling and Feature Analysis of Wind Turbine with Variable Ratio Gearbox," 33rd Chinese Control Conference (CCC), Nanjing, pp 7110-7115, 28-30 July 2014.

[234] M d Arifujjaman etal "Development of an Isolated Small wind Turbine Emulator" The open renewable energy journal 2011, 4, (Suppl 1-M2) 3-12, 1876-3871/11.

[235] Hsiang-Chun Lu, Le-Ren Chang-Chien "Use of Wind Turbine Emulator for the WECS Development" International Power Electronics Conference, Sapporo, pp 3188-3195, 21-24 June 2010.

[236] Agus Sunyoto, Frederikus Wenehenubun, Hadi Sutanto, "The Effect of Number of Blades on the Performance of H-Darrieus type Wind Turbine," International

Conference on QiR (Quality in Research), Yogyakarta, pp 192-196, 25-28 June 2013.

[237] Vladimir Lazarov, Daniel Roye, Dimitar Spirov and Zahari Zarkov, "New Control Strategy for Variable Speed Wind Turbine with DC-DC converters," 14th International Power Electronics and Motion Control Conference (EPE/PEMC), Ohrid, pp T12-120 – T12-124, 6-8 Sept. 2010.

[238] Dong Liu Zhensheng Wu Hui Wang Tianjian Wang, "MPPT Control Strategy for Off-grid Wind Power System," 2nd IEEE International Symposium on Power Electronics for Distributed Generation Systems (PEDG), Hefei, China, pp 759-764, 16-18 June 2010.

[239] Malini Sahu, Satyadharma Bharti, "An Intelligent Maximum Power Extraction Algorithm for Partial Scale Frequency Converter Wind Turbine System," IEEE Students' Conference on Electrical, Electronics and Computer Science (SCEECS), Bhopal, pp 1-6, 1-2 March 2014.

[240] Yuanye Xia, Khaled H. Ahmed, and Barry W. Williams, "Wind Turbine Power Coefficient Analysis of a New Maximum Power Point Tracking Technique," IEEE Transactions on Industrial Electronics, Vol. 60, Issue: 3, pp 1122-1132, March 2013.

[241] Chun Wei, Zhe Zhang, Wei Qiao, and Liyan Qu, "Intelligent Maximum Power Extraction Control for Wind Energy Conversion Systems Based on Online Q-learning with Function Approximation," IEEE Energy Conversion Congress and Exposition (ECCE), Pittsburgh, PA, pp 4911- 4916, 14-18 Sept. 2014.

[242] M.A. Abdullah, A.H.M. Yatim, C.W. Tan, A.S. Samosir, "Particle Swarm Optimization-Based Maximum Power Point Tracking Algorithm for Wind Energy Conversion System," IEEE International Conference on Power and Energy (PECon), Kota Kinabalu, pp 65-70, 2-5 Dec. 2012.

[243] N. Niassati1, M. Mohseni, H. Amiri, K. Seyedtabaei, A. Hajihosseinlu, "A New Maximum Power Point Tracking Technique for Wind Power Conversion Systems," 15th International Power Electronics and Motion Control Conference (EPE/PEMC), Novi Sad, DS2d.8-1-DS2d.8-6, 4-6 Sept. 2012.

[244] Syed Muhammad Raza Kazmi, Hiroki Goto, Hai-Jiao Guo and Osamu Ichinokura, "A Novel Algorithm for Fast and Efficient Speed-Sensorless Maximum Power Point Tracking in Wind Energy Conversion Systems," IEEE Transactions on Industrial Electronics, vol: 58, Issue 1, pp 29-36, Jan. 2011.

[245] Huynh Quang Minh, Nollet Frederic, Najib Essounbouli and Hamzaoui Abdelaziz, "A new MPPT method for stand-alone wind energy conversion system," 2nd International Symposium on Environment Friendly Energies and Applications (EFEA), Newcastle upon Tyne, pp 335-340, 25-27 June 2012.

[246] Jeroen D. M. De Kooning, Bart Meersman, Tine L. Vandoorn and Lieven Vandevelde, "Evaluation of the Maximum Power Point Tracking Performance in

Small Wind Turbines," IEEE Power and Energy Society General Meeting, San Diego, CA, pp 1-8, 22-26 July 2012.

[247] Geng Hua and Yang Geng, "A Novel Control Strategy of MPPT Taking Dynamics of Wind Turbine into Account," 37th IEEE Power Electronics Specialists Conference, Jeju, pp 1-6, 18-22 June 2006.

[248] Syed Muhammad Raza Kazmi, Hiroki Goto, Hai-Jiao Guo, and Osamu Ichinokura, "A Novel Algorithm for Fast and Efficient Speed-Sensorless Maximum Power Point Tracking in Wind Energy Conversion Systems," IEEE Transactions on Industrial Electronics, Vol. 58, Issue 1, pp 29-36, Jan. 2011.

[249] Rajin M. Linus and P. Damodharan, "Maximum Power Point Tracking and Grid feeding of Permanent Magnet Synchronous Generator based Wind Energy Conversion System Using Modified Hill Climb Searching Algorithm," 5th India International Conference on Power Electronics (IICPE), Delhi, pp 1-6, 6-8 Dec. 2012.

[250] Siemens BSM 100 GB 120 DN2K, www.datasheetcatalog.com

Appendix A: Permanent Magnet Synchronous Machine and Wind Turbine Specifications

Table A1 Parameters of PM machine

Rated power	1kW
No. of poles	16
Stator resistance	0.2 Ohms
D-axis Inductance	4mH
Q-axis Inductance	4mH
Flux linkage	0.075 Vs
Moment of inertia	0.1

Table A2 Parameters of wind turbine

Rated power	1kW
No. of rotor blade	5
Rotor diameter	2m
Rated wind speed	12m/s
Cut- in wind speed	2m/s

Table A3 Parameters of the thesis PI regulator Algorithm

Parameters	Motor control	Generator control	AC load control
K1	21	21	21
K2	17	17	17
Delay	$3ms$	$30\mu s$	$1ms$
Current scaling	200	200	200
Saturation limit (upper threshold) of current PI controller	1875	1875	1875
Saturation limit (lower threshold) of current PI controller	-1875	-1875	-1875
Offset of PI control output	1875+≥ 10%	1875+≥ 10%	1875+≥ 10%

Appendix B: Voltage Source Inverter Component Output Characteristics and Switching Energies

This appendix will show how the on-state parameters of the IGBTs and the diode are obtained for the VSI loss model. The power electronic devices used in this thesis are of the type BSM 100 GB 120 DN2K module [250].

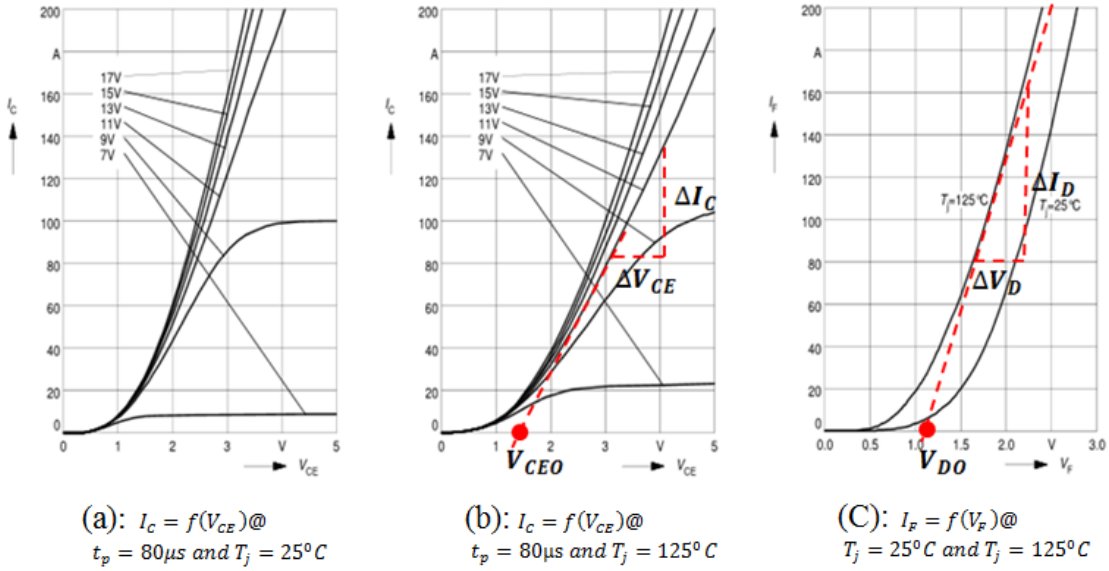

Figure 7-2: Output characteristics power electronic devices (a) IGBT at 25^0C (b) IGBT at 125^0C (c) Diode forward characteristics

Figure 7-2 (a) and (b) shows the output characteristics of the IGBTs and Figure 7-2 (c) shows the output characteristics of diodes. The on-state zero-current collector-emitter voltage, V_{CEO} is obtained when the tangent of the output characteristics of the IGBTs is extrapolated to the V_{CE} axis and the on-state collector-emitter voltage at zero collectors current is obtained. The same procedure applies to the on-state zero diode forward voltage, V_{DO}.

Collector on state resistance, r_C and on-state diode resistance, r_D are given as

$$r_C = \frac{\Delta V_{CE}}{\Delta I_C} \tag{B1}$$

$$r_D = \frac{\Delta V_D}{\Delta I_D} \tag{B2}$$

$$V_{CEO} = 1.2V$$

$$V_{CEO} = 1.1V$$

$$r_C = 0.02$$

$$r_D = 0.0071$$

$$0 \geq m_a \geq 1$$

$$0 \geq \cos \emptyset \geq 1$$

$$f_{sw} = 20kHz$$

$$Q_{rr} = 14$$

$V_{Drr} = 57V$ (DC link voltage, this depends on the design requirement and the user)

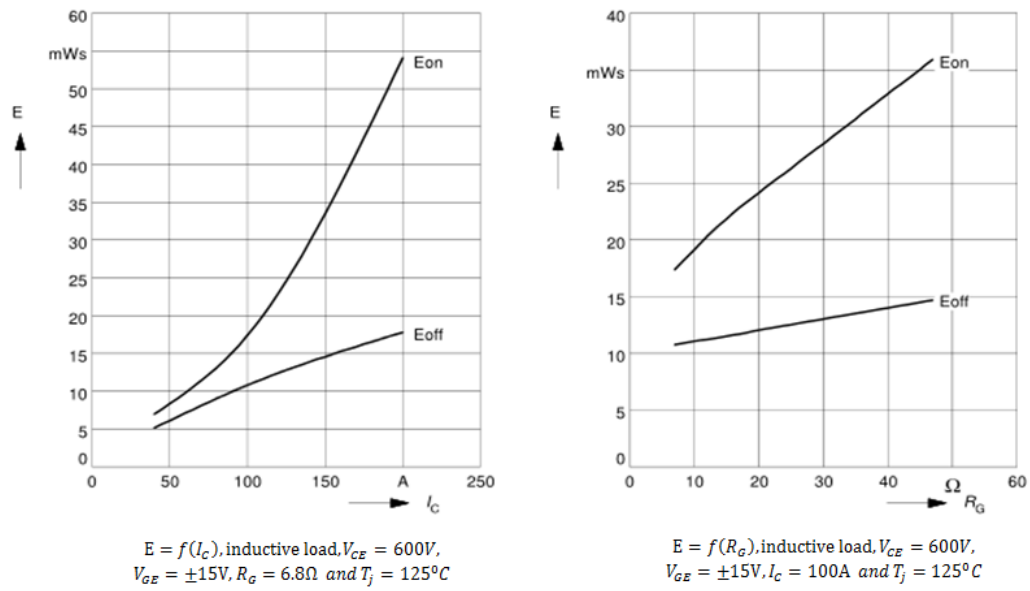

E = $f(I_C)$, inductive load, $V_{CE} = 600V$, $V_{GE} = \pm 15V$, $R_G = 6.8\Omega$ and $T_j = 125^0C$

E = $f(R_G)$, inductive load, $V_{CE} = 600V$, $V_{GE} = \pm 15V$, $I_C = 100A$ and $T_j = 125^0C$

Figure 7-3: Switching energies of the IGBTs

Figure 7-3 shows the turn-on and turn-off energy for the IGBTs and diode. Once the turn-on collector current and the turn-off diode forward current are known, the turn-on and turn-off energies of the IGBTs and diode can be determined from the curve and the switching losses calculated.

Appendix C: Measurements and Performance Calculations of PMSM Drive System

When the test rig operates on PMSM drive system, the DC power input is calculated from the DC voltage and DC current. The DC link voltage V_{DC} and DC current I_{DC} is recorded from display on the DC power supply hence DC power is calculated using

$$P_{DC} = I_{DC}V_{DC} \tag{C1}$$

AC current, voltage and power are measured using power Analyser. Power analyser receives instantaneous voltage and current and computes the RMS value of voltage and current from which power in single phase is measured and the three phase power calculated by multiplying the measured single phase power by a factor of 3 assuming a balanced three phase based on

$$P_{AC} = V_{RMS}I_{RMS} \tag{C2}$$

For three phase power

$$P_{AC(3-\emptyset)} = 3 * P_{AC} \tag{C3}$$

$$I_{pk} = \sqrt{2}I_{RMS} \tag{C4}$$

$$V_{pk} = \sqrt{2}V_{RMS} \tag{C5}$$

$V_{pk}\ and\ I_{pk}$, are the amplitude of the sinusoidal voltage and current waveform captured on the oscilloscope.

Mechanical power from the drive system is calculated by

$$P_m = \frac{2\pi N}{60} * T \tag{C6}$$

Where N is the speed in rpm and T is the torque in Nm measured using torque transducer and encoder.

The calculation for inverter losses in the simulation model is shown in section 3.3 and the method to obtain the parameters for the VSI simulation loss model is shown in Appendix B. For the experiment, the inverter, motor and overall drive losses and efficiency are obtained by calculation using the following

$$\text{Inverter losses } = P_{DC} - P_{AC(3-\emptyset)} \quad \text{(C7)}$$

$$\%\text{Inverter Efficiency} = \frac{P_{AC(3-\emptyset)}}{P_{DC}} * 100\% \quad \text{(C8)}$$

$$\text{PMSM Losses } = P_{AC} - P_m \quad \text{(C9)}$$

$$\%\text{PMSM Efficiency} = \frac{P_m}{P_{AC}} * 100\% \quad \text{(C10)}$$

$$\text{Overall drive system losses \%Inverter Efficiency} = P_{DC} - P_m \quad \text{(C11)}$$

$$\%\text{Drive system Efficiency} = \frac{P_m}{P_{DC}} * 100\% \quad \text{(C12)}$$

Appendix D: Measurements and Performance Calculations of PMSG Wind Energy Conversion Emulation System

When the test rig operates on variable PMSG wind energy conversion emulation system, the PMSG receives power from the PMSM drive emulating the wind turbine and the output of the generator is fed to the GSC and through the DC link and LSC connects the three phase AC load.

The calculation of the mechanical power on the shaft due to the operation of the wind turbine emulator is calculated using equation (C6) and the single phase generator power is given by

$$P_{gAC} = I_{gRMS} V_{gRMS} \quad \text{(D1)}$$

Where, P_{gAC} is the single power measured at the terminal of the PMSG using power analyser and then calculates the three phase power using

$$P_{gAC(3-\emptyset)} = 3 * P_{gAC} \quad \text{(D2)}$$

DC power is calculated using

$$P_{DC} = I_{DC} V_{DC} \quad \text{(D3)}$$

Where, V_{DC} and I_{DC} are the voltage and current measured at the DC link of the wind energy conversion emulation system.

The single phase AC Load Power is measured using power analyser based on

$$P_{LAC} = I_{LRMS}V_{LRMS} \tag{D4}$$

Where, P_{LAC} is the single power measured at the terminal of the three-phase AC load using power analyser and then calculates the three phase power using.

$$P_{LAC(3-\emptyset)} = 3 * P_{gAC} \tag{D5}$$

To calculate the losses and efficiency of the generator, inverters and the overall system taking into consideration the wind speed input, operating characteristics and control strategy the following equations were used.

$$\text{Generator losses} = P_m - P_{gAC(3-\emptyset)} \tag{D6}$$

$$\%\text{Generator Efficiency} = \frac{P_{gAC(3-\emptyset)}}{P_m} * 100\% \tag{D7}$$

$$\text{Generator side converter (GSC) losses } = P_{gAC(3-\emptyset)} - P_{DC} \tag{D8}$$

$$\%\text{GSC Efficiency} = \frac{P_{DC}}{P_{gAC(3-\emptyset)}} * 100\% \tag{D9}$$

$$\text{AC Load side converter (LSC) losses } = P_{DC} - P_{LAC(3-\emptyset)} \tag{D10}$$

$$\%\text{LSC Efficiency} = \frac{P_{LAC(3-\emptyset)}}{P_{DC}} * 100\% \tag{D11}$$

$$\text{Total back-back VSI losses} = P_{gAC(3-\emptyset)} - P_{LAC(3-\emptyset)} \tag{D12}$$

$$\%\text{Total VSI Efficiency} = \frac{P_{LAC(3-\emptyset)}}{P_{gAC(3-\emptyset)}} * 100\% \tag{D13}$$

The calculation of the overall drive system losses and efficiency is obtained based on power from the rotor shaft mechanical power, P_m as

$$\text{Overall WECS system losses} = P_m - P_{LAC(3-\emptyset)} \tag{D14}$$

$$\%\text{ Overall WECS Efficiency} = \frac{P_{LAC(3-\emptyset)}}{P_m} * 100\% \tag{D15}$$

Calculation of Error of Comparison between Simulation Model and Experiment

In all performance validation the experimental results is used as the benchmark to which the results of the simulation model are compared with. The error in the results predicted by the simulation model are calculated using

$$\%\text{error} = \frac{Q_{ept} - Q_{sim}}{Q_{ept}} * 100\% \quad \text{(D16)}$$

Where Q_{ept} is the quantity measured or calculated from experimental results such as current, torque, power, losses, and efficiency. While Q_{sim} is the quantity of the same parameters predicted by the simulation models.

Appendix E: Programming Codes to Calculate Energy Output of WECS based on AVEM using DSP-Controller

The programming codes for the estimation of energy output of wind energy conversion system based on AVEM using DSP controller is shown below. The duty cycles are calculated based on the control strategy and this section of the programming codes utilise the duty cycles and with the DC link voltage and measured phase current to calculate the energy yield thus;

// calculating the average voltage, power for one phase, three-phase and energy output of //WECS

```
if ((DutyC1>=DutyC2) & (DutyC2>=DutyC3))
{
DutyT1 = DutyC1 - DutyC2;
DutyT2 = DutyC2 - DutyC3;
Vavg = K*(2*DutyT1 + DutyT2);
}
else if ((DutyC2>=DutyC1) & (DutyC1>=DutyC3))
{
DutyT2 = DutyC2 - DutyC1;
DutyT3 = DutyC1 - DutyC3;
Vavg = K*(DutyT2 – DutyT3);
}
else if ((DutyC2>=DutyC3) & (DutyC3>=DutyC1))
{
DutyT3 = DutyC2 - DutyC3;
DutyT4 = DutyC3 - DutyC1;
Vavg = -K*(DutyT3 + 2*DutyT4);
}
else if ((DutyC3>=DutyC2) & (DutyC2>=DutyC1))
{
DutyT4 = DutyC3 - DutyC2;
DutyT5 = DutyC2 - DutyC1;
Vavg = -K*(2*DutyT4 + DutyT5);
}
else if ((DutyC3>=DutyC1) & (DutyC1>=DutyC2))
{
DutyT5 = DutyC3 - DutyC1;
```

```
DutyT6 = DutyC1 - DutyC2;
Vavg = - K*(DutyT5 + DutyT6);
}
else if ((DutyC1>=DutyC3) & (DutyC3>=DutyC2))
{
DutyT1 = DutyC1 - DutyC3;
DutyT6 = DutyC3 - DutyC2;
Vavg = K(2*DutyT1 + DutyT6);
}
Pavg = Vavg * Iph1_L2;
Ptotal = 3*Pavg;
Ptotal = Ptotal + Pavg;

if (Pcount > 1000)
{
EnergyT = Ptotal;
Ptotal = 0;
Pcount = 0;
 }

Pcount = Pcount + 1;
}
```

Where, K is factor representing the measured DC voltage and switching period and Iph1_L2 represents the phase current fed into the DSP controller.